Het schatten van kanaalparameters
voor coöperatieve systemen van het type 'Quantize and Forward'

Channel Parameter Estimation
for Quantize and Forward Cooperative Systems

Iancu Avram

Promotor: prof. dr. ir. M. Moeneclaey
Proefschrift ingediend tot het behalen van de graad van
Doctor in de Ingenieurswetenschappen: Elektrotechniek

Vakgroep Telecommunicatie en Informatieverwerking
Voorzitter: prof. dr. ir. H. Bruneel
Faculteit Ingenieurswetenschappen en Architectuur
Academiejaar 2015 - 2016

UNIVERSITEIT
GENT

ISBN 978-90-8578-864-5
NUR 959
Wettelijk depot: D/2015/10.500/108

Een woord van dank

Alvorens de wondere wereld van coöperatieve communicatiesystemen uit de doeken te doen, zou ik graag even de tijd willen nemen om een paar mensen te bedanken, zonder wie deze thesis nooit tot stand gekomen zou zijn. In de eerste plaats wil ik mijn promotor Marc Moeneclaey bedanken, en dit niet alleen omdat het zo hoort. Door zijn enthousiasme voor en kennis van het vak was Marc een promotor waar ik met elke vraag bij terecht kon. De keren dat ik om 17u een probleem aankaartte en dezelfde nacht nog een antwoord kreeg zijn niet zeldzaam; ik denk dat de promotoren die zo'n engagement aan hun studenten tonen dat wél zijn. Ook aan onze filosofische gesprekken aan de waterkoeler en op de Telin bieravonden hou ik goede herinneringen over.

Een tweede persoon die ik wil bedanken is mijn vriendin Helena, mijn steun en toeverlaat bij het schrijven van dit doctoraat. Zij heeft ervoor gezorgd dat ik elke dag graag thuiskwam na een dagje op kantoor. Verder wil ik natuurlijk ook mijn vader (Iancu) en mijn moeder (Nineta) bedanken, omdat zij mij altijd alle kansen hebben gegeven en er zo voor gezorgd hebben dat dit prachtwerk tot stand is kunnen komen. Hierbij wil ik ook Marc bedanken, onder andere voor het rijdende houden van mijn wrakken van auto's. Ook an-

dere familieleden, zoals Pavel, Andrei, Oana, Liviu, Cornelia, Nana en Bunicu Gheorghe mogen in dit lijstje niet ontbreken: Va multumesc pentru ca ati fost mereu alaturi de mine si pentru momentele frumoase din ultimii ani! Gerda en Freddy bedank ik voor de lekkere maaltijden op zondagavond en ook Stijn, Bert en Yoeri (met partners) voor de hulp bij zowat alle verbouwingswerken.

Naast mijn familie wil ik ook graag mijn vrienden bedanken, die de voorbije jaren voor de nodige ontspanning hebben gezorgd. Zo is er Nico, een vriend waar je op kan rekenen en waarmee je boeiende gesprekken kan voeren over de vreemdste onderwerpen, zoals over de slijmerigheid van slakken of de medische haalbaarheid van een menselijke duizendpoot. Ook Bram en Gijs, die samen hebben gezorgd voor een legendarische studententijd in Gent, wil ik in dit dankwoord vermelden, alsook de vrienden van OLVP Bornem, zoals er zijn: mijn vaste snooker-partners Jonas en Dimitri en ook Elke, Eva, Sabrina en Wim. Mijn vaste co-piloot Steven en zijn partner Tessa wil ik ook bedanken, voor alle bijna-overwinningen in de waterski-racing.

Last-but-not-least wil ik ook de collega's van Telin bedanken voor de leuke tijden op het werk. In het bijzonder wil ik hier Lennert vermelden, die 's middags in de Brug mee heeft geholpen om de kabeljauwpopulatie in toom te houden. Ook onze vakgroepvoorzitter Herwig wil ik bedanken, voor het scheppen van een licht-anarchistische, maar hierdoor juist uiterst aangename, werkomgeving.

Kortom: bedankt allemaal om mij gedurende deze periode te steunen en zo dit werk mogelijk te maken!

Iancu Avram - Augustus 2015

Contents

Abbreviations

AF	Amplify and Forward
BER	Bit Error Rate
BPSK	Binary Phase Shift Keying
CDF	Cumulative Distribution Function
CDMA	Code Division Multiple Access
CF	Compress and Forward
CRB	Cramer-Rao Bound
CSI	Channel State Information
DF	Decode and Forward
DSC	Distributive Source Coding
EM	Expectation Maximization
FDMA	Frequency Division Multiple Access
FIM	Fisher Information Matrix
IID	Independent and Identically Distributed
IS	Importance Sampling
LB	Lower Bound
LBC	Linear Block Code
LLR	Log-Likelihood Ratio
MAC	Medium Access Control

MAP	Maximum A-Posteriori
MARC	Multiple Access Relay Channel
MCRB	Modified Cramer-Rao Bound
MFIM	Modified Fisher Information Matrix
MIMO	Multiple-Input Multiple-Output
ML	Maximum Likelihood
MMSE	Minimum Mean Square Error
MSE	Mean Square Error
NMSE	Normalized Mean Square Error
PAM	Pulse Amplitude Modulation
PDF	Probability Density Function
PMF	Probability Mass Function
PSK	Phase Shift Keying
QAM	Quadrature Amplitude Modulation
QF	Quantize and Forward
QPSK	Quadrature Phase Shift Keying
SE	Squared Error
SNR	Signal to Noise Ratio
SRCC	Systematic Recursive Convolutional Code
STBC	Space-Time Block Code
TDMA	Time Division Multiple Access
ZMCSCG	Zero Mean Circular Symmetric Complex Gaussian

Notations

x	Variable
$\boldsymbol{x}$	Row vector
$\boldsymbol{X}$	Matrix
$\boldsymbol{X}^T$	Transpose of $\boldsymbol{X}$
$\boldsymbol{X}^H$	Hermitian transpose of $\boldsymbol{X}$
$x(k)$	k-th element of $\boldsymbol{x}$
$X(i,j)$	Element on the i-th row and j-th column of $\boldsymbol{X}$
$\lvert x \rvert$	Absolute value of x
$\arg(x) \in [0, 2\pi[$	Phase of x
x^*	Complex conjugate of x
$\mathbb{E}[x]$	Expectation of $\boldsymbol{x}$
$x \mod y$	Remainder after division of x by y
$\lfloor x \rfloor$	Mapping of x to the largest previous integer
$\lceil x \rceil$	Mapping of x to the smallest next integer
$\log(x)$	Natural logarithm of x
$\exp(x)$	Exponential of x
$\arg\max_x f(x)$	Value of x that yields the maximum value of $f(x)$
$d_H(\boldsymbol{x}, \boldsymbol{y})$	Hamming distance between $\boldsymbol{x}$ and $\boldsymbol{y}$

Samenvatting

De belangstelling voor draadloze communicatiesystemen heeft in de afgelopen dertig jaar een enorme boost ervaren, wat maakt dat draadloze toestellen een integraal deel uitmaken van ons dagelijks leven. Dit is grotendeels te danken aan de miniaturisatie van de draadloze apparaten. Terwijl dertig jaar geleden een draagbare telefoon een onpraktisch groot toestel was, die een autobatterij als energiebron nodig had om te werken, zijn er vandaag toestellen ter grootte van een muntstuk die dezelfde communicatietaken vervullen. Omdat de fysicawetten die de draadloze gegevensoverdracht beschrijven in die tijdspanne niet veranderd zijn, is de miniaturisatie bijna volledig te danken aan de toegenomen energie-efficiënte van de draadloze toestellen. Deze energie-efficiëntie is ook belangrijk vanuit een milieu en regelgevend oogpunt, aangezien de huidige regelgeving strikte beperkingen oplegt op het zendvermogen van draadloze communicatietoestellen.

Het is een bekend feit dat de betrouwbaarheid van draadloze gegevensoverdracht verbeterd kan worden door het zendvermogen te laten toenemen. Door de hierboven aangehaalde redenen is het eenvoudigweg verhogen van het zendvermogen echter in veel gevallen geen wenselijke oplossing. Boven-

dien is de betrouwbaarheid van draadloze communicatiesystemen, vooral in stedelijke omgevingen, grotendeels bepaald door het effect van *multipath propagation fading*. Dit effect wordt veroorzaakt doordat radiogolven op meerdere oppervlakken weerkaatsen en zowel constructief als destructief kunnen interfereren aan de antenne van de ontvanger. Het eenvoudigweg verhogen van het zendvermogen zal in het geval van *fading* slechts een kleine winst in betrouwbaarheid opleveren. In de literatuur zijn er daarom verschillende methoden voorgesteld om *multipath fading* te bestrijden. In bijna al deze technieken wordt er diversiteit geïntroduceerd door meerdere paden te creëren tussen de zender en de ontvanger. Een relatief nieuwe techniek om *multipath fading* tegen te gaan zijn coöperatieve communicatiesystemen. Deze introduceren diversiteit door gebruik te maken van de eigenschappen van het draadloos medium. Zo wordt een signaal dat uitgezonden is niet alleen ontvangen door de bestemming, maar ook door andere toestellen die zich in de buurt van de zender bevinden. In plaats van dit signaal te negeren zoals gebeurt in een klassiek communicatiesysteem, zullen deze naburige toestellen in een coöperatief systeem als relais optreden en dit signaal bewerken en doorsturen naar de bestemming. Zo ontstaan er verschillende paden tussen de zender en de bestemming en wordt er diversiteit geïntroduceerd. In tegenstelling tot andere diversiteitstechnieken vereisen coöperatieve communicatiesystemen geen gespecialiseerde hardware, zodat deze technologie gebruikt kan worden in combinatie met bestaande toestellen. Bovendien zijn er in de literatuur verschillende coöperatieve protocollen ontwikkeld die trachten de complexiteit aan de relais te beperken, zodat deze systemen kunnen gebruikt worden in sensor netwerken, waarin verschillende sensoren samenwerken om hun gegevens door te sturen naar een basisstation voor verwerking.

Wanneer een signaal zich voortplant door het draadloze medium, wordt het signaal door dit medium niet enkel geschaald, maar ook vervormd. Deze vervorming, die gemodelleerd wordt door een aantal kanaalparameters, moet door de ontvanger gekend zijn om de verzonden gegevens te kunnen achterhalen. In de meeste werken over coöperatieve systemen worden deze kanaalparameters als gekend verondersteld, zodat de wiskundige modellering eenvoudiger is. In een realistische situatie is deze veronderstelling echter fout, en zullen deze kanaalparameters geschat moeten worden. Daarom werd dit werk toegewijd aan het schatten van de onbekende kanaalparameters in coöperatieve systemen. Als uitgangspunt is een coöperatief protocol gekozen dat een lage relaiscomplexiteit vertoont, namelijk het *quantize and forward* QF protocol. In dit protocol zal de relais de inkomende gegevens kwantiseren en het resultaat van deze kwantisatiebewerking doorsturen naar de bestemming. Voor het gekozen protocol moeten er drie groepen kanaalparameters worden geschat, namelijk deze van het zender-bestemming kanaal, deze van het zender-relais kanaal en deze van het relais-bestemming kanaal. Van deze drie

kanalen die geschat moeten worden aan de bestemming is het zender-relais kanaal het moeilijkst te schatten, aangezien de bestemming niet rechtstreeks met dit kanaal verbonden is. Daarom hebben we in dit werk een aanpassing van het QF protocol voorgesteld, waarbij de relais zelf het zender-relais kanaal schat en vervolgens compenseert voor de vervormingen van dit kanaal. Hierdoor moet het zender-relais kanaal niet langer aan de bestemming worden geschat. De prestaties van het voorgestelde protocol en de schattingsalgoritmen zijn geanalyseerd met numerieke simulaties waaruit gebleken is dat beiden naar behoren presteren. Een nadeel van het voorgestelde protocol is dat de schatting van het zender-relais kanaal aan de relais berekend moet worden. Hierdoor neemt de complexiteit van de relais toe, wat in sommige situaties niet wenselijk is. Als antwoord op dit probleem hebben we schattingsalgoritmen ontwikkeld die alle kanalen, inclusief het zender-relais kanaal, aan de bestemming schatten, waardoor de complexiteit van de relais laag blijft. Een bijkomend voordeel van deze aanpak is dat de schatting van het zender-relais kanaal nu aan de bestemming verfijnd kan worden met behulp van het EM-algoritme, waardoor de nauwkeurigheid van deze schatting toeneemt. Verder beschouwen we in dit werk ook de situatie waarin er een frequentiefout optreedt tussen de draaggolf van het ontvangen signaal en de interne oscillator van de ontvanger. Ook voor deze situatie hebben we nauwkeurige schattingsalgoritmen ontwikkeld die toelaten om alle kanaalparameters, inclusief de frequentiefouten, aan de bestemming te schatten.

Door hun verbeterde spectrale efficiëntie winnen *two-way relaying* kanalen en *multiple access relay channels* (MARC) steeds meer aan populariteit in de onderzoekswereld. In een *two-way relaying* systeem zal een relais tegelijkertijd twee toestellen helpen die informatie sturen naar elkaar, terwijl in de MARC één relais meerdere toestellen tegelijk assisteert om te communiceren met één enkele bestemming. In dit werk hebben we een nieuw QF protocol ontworpen voor het *two-way relaying* kanaal. Het voorgesteld protocol vertoont een lage complexiteit aan de relais en laat toe om alle kanaalparameters aan de bestemming te schatten. Met behulp van numerieke simulaties hebben we bepaald dat het ontworpen protocol even goed presteert als vergelijkbare protocollen, maar tegelijk een veel lagere complexiteit aan de relais vertoont. Ook voor de MARC werd in dit werk een QF protocol voorgesteld. Hoewel we hebben aangetoond dat het voorgesteld protocol goede foutkarakteristieken vertoont, blijft het ontwerpen van schattingsalgoritmen voor dit protocol een open onderzoeksthema. Samengevat heeft dit proefschrift nauwkeurige schattingsalgoritmen opgeleverd voor verschillende uitvoeringen van het QF protocol. Deze algoritmen brengen praktische toepassingen die gebruik maken van het QF protocol een stap dichterbij.

Summary

The interest in wireless communication systems has experienced a huge boost in the last thirty years, making wireless devices an integral part of our daily lives. This is in part due to the miniaturization of the wireless communication devices. While thirty years ago a mobile phone was an impractical large device needing a car battery to operate, today we have devices the size of a coin performing the same communication tasks. Because the laws of physics that govern wireless transmission have not changed during that period, the miniaturization wave was made possible by the design of energy efficient communication devices. This energy efficiency is also important from an environmental and regulatory point of view, as the current regulations impose strict limits on the transmit power a wireless communication device can emit.

It is an easily understood fact that the more transmit power is used, the better the signal is received at the other end. However, due to the reasons mentioned above, simply increasing the transmit power is not an option in most cases. Especially because, in urban environments, the reliability of communication greatly suffers from multipath propagation fading. The latter is caused by the waves from the transmitter reflecting on multiple surfaces and interfering constructively or destructively at the receiving antenna. Simply in-

creasing the transmit power does not solve the fading problem, and will yield only a small increase in reliability, at a great cost. Therefore, different techniques have been proposed to combat multipath propagation fading. Almost all these techniques rely on introducing diversity by creating multiple signal paths between the transmitter and the destination terminal, be it in time, space or frequency. An elegant answer to the fading problem is provided by cooperative communication systems. The latter introduce diversity by using the broadcast nature of the wireless propagation medium. Indeed, the signal sent by the transmitter is not only received by the intended destination, but also by other terminals nearby. Instead of ignoring this signal, these nearby terminals can forward an edited copy of this signal to the destination, thus creating different signal paths between the source and the destination and introducing diversity. As opposed to other diversity techniques, cooperative communication systems require no specialized hardware to be present in the cooperating devices. Furthermore, cooperative protocols have been developed which try to minimize the computational complexity at the relay, making them suitable for cooperative sensor networks, where many small sensors cooperate to transmit their data to a base station for processing.

A signal propagating through the wireless medium is distorted by the latter, so that the signal reaching the receiver is not merely a scaled version of the one sent by the transmitter. This distortion, modelled by a certain number of channel parameters, needs to be known the destination in order to be able to decode the information sent. In most works on cooperative systems, these channel parameters are assumed to be known to the destination. In a real-life scenario however, these parameters are not known and will need to be estimated. Therefore, in this work, we have focussed on the channel parameter estimation in cooperative communication systems. As a starting point, we have selected a cooperative protocol which has a low complexity at the relay, namely the quantize and forward (QF) protocol. In this protocol, the relay performs a coarse quantization operation on the data received from the source, before forwarding it to the destination. In the selected protocol, three sets of parameters need to be estimated at the destination, namely those of the source-destination channel, those of the source-relay channel and those of the relay-destination channel. Of these three parameter sets, the channel parameters of the source-relay channel are the most difficult to estimate, because the destination is not directly connected to the aforementioned channel. Therefore, we have proposed a modification to the QF protocol, in which the relay makes its own estimate of the source-relay channel, and compensates for the distortion caused by this channel. In doing so, the source-relay channel no longer needs to be known to the destination. The performance of the proposed protocol and estimation algorithms was evaluated using numerical simulations and was deemed satisfactory. A drawback of the aforementioned

protocol is the fact that the relay needs to calculate an estimate of the source-relay channel. This operations adds to the complexity of the latter, which can be undesirable in some situations. Therefore, we developed a novel estimation algorithm which makes it possible to estimate all channel parameters, including those of the source-relay channel, at the destination. In addition to lowering the complexity of the relay terminal, the proposed estimation method also improves the estimation accuracy as compared to the case in which the source-relay channel is estimated at the relay. This is because at the destination, the obtained estimates, including those of the source-relay channel, can be refined using the expectation-maximization (EM) algorithm. Further driven by the motivation of using more realistic channel models, we also considered the situation in which there is a frequency mismatch between the carrier of the signal received at a terminal and the internal oscillator of the latter. We have used the system in which all channel parameters are estimated at the destination as a starting point, and proposed modifications to the estimation algorithms in order to make them able to function in the presence of a carrier frequency mismatch.

Due to their improved spectral efficiency, two-way relaying channels and multiple-access relay channels (MARC) are gaining interest in the research world. In a two-way relaying system, a relay simultaneously assists two terminals communicating with each other, while in the MARC, a relay simultaneously assists multiple source terminals communicating to one destination terminal. In this work, we have developed a novel QF protocol for the two-way relaying channel. The proposed protocol features a low relay-side complexity and allows the destination to easily estimate all channel parameters involved. Using numerical simulations, we have verified the efficiency of the proposed protocol and estimation algorithms. It was shown that, while the proposed protocol has a much lower relay-side complexity, its error performance is on par with that of other two-way relaying protocols. A QF protocol was also designed for the MARC. It was shown that the proposed protocol yields a good error performance, however, the design of estimation algorithms for the aforementioned protocol remains a topic of future work. All in all, this thesis has yielded accurate estimation algorithms for various implementation of the QF protocol, paving the way for the mainstream implementation of QF cooperative systems.

Part I

Introductory Matter

1

Introduction

As the title of this dissertation hints, various methods for the channel parameter estimation in quantize and forward (QF) cooperative systems are presented in this thesis. For those who feel overwhelmed by technical terms, the aforementioned phrase is explained in section 1.1, whereafter the motivation for writing this thesis is outlined in section 1.2. Finally, the outline of this work is presented in section 1.3.

1.1 Background

The ability to communicate is one of the key factors that allowed the human species to thrive and shape the present day society. While a few centuries ago almost all communication took place face-to-face or using written letters, today we can talk to friends and relatives across oceans as if we were standing next to them. Furthermore, with the advent of smart devices which are connected to the internet, we have access to information anytime anywhere. This

is all made possible by digital communication systems.

The basic model of a digital communication system consists of a transmitter and a receiver. At the transmitter, the information to be transmitted, which can be speech, a photograph or data from a web browser, is first converted into binary digits, called bits. The main advantage of this approach is that, by designing a system that can transmit bits from one terminal to another, this system can be used to transmit all kinds of information, without needing to design a separate system for each information type. After converting the information to bits, the transmitter outputs these bits to a channel, to which the receiver is also connected. After receiving the data from the channel, the receiver will try to reconstruct the information which was sent by the transmitter. The main difficulty herein lies in the fact that the channel distorts the transmitted information and introduces noise, so that the signal received by the receiver is not identical to the signal sent by the transmitter. The nature and magnitude of this distortion depend on the properties of the channel.

The channel can either be a wired channel or a wireless channel, or a cascade of both types. Examples of wired channels include twisted-pair telephone cable and copper on-chip interconnections, while examples of wireless channels are terrestrial broadcast channels and satellite links. An example of a cascade is the communication between two mobile phones, where there is a wireless channel between the mobile phones and their respective base stations and a wired channel between the base stations. Historically, most of the communication systems were wired communication systems, taking advantage of the relative simple modelling of wired channels. Due to the ever changing nature of the wireless propagation medium, caused not only by the motion of the communicating terminals themselves but also by moving objects and weather influences, communication over wireless channels is much more involved, especially in urban environments where there is no line-of-sight path between the transmitter and the receiver. For the end user however, wireless systems are much more convenient to use, as they offer the freedom of mobility. The design of reliable wireless communication systems is therefore of great importance.

One phenomenon that considerably affects the performance of wireless communication systems is multipath propagation fading. Especially in urban environments with a large number of buildings, the waves broadcast by the transmitter reflect on different surfaces before they arrive at the antenna of the receiver. Because the reflected waves arrive at the receiver antenna at slightly different times, they interfere with one another and can even cancel each other out. When there is too much destructive interference, it is very difficult to reliably transmit information over the wireless channel, and the channel is said

to be in fading. Different diversity techniques, like adding more antennas to the transmitter and/or receiver terminal, have been proposed to tackle the problem of multipath propagation fading, each having their advantages and disadvantages, as explained more in depth in section 4.1. One particularly attractive solution is offered by cooperative communication systems.

Cooperative communication systems take advantage of the broadcast nature of the wireless propagation medium, meaning that a signal sent by a transmitter is not only received by the intended destination, but also by other terminals nearby. When the channel between the source and the destination is in fading, the terminals nearby can act as relays and convey the information from the transmitter to the destination. In doing so, cooperative communication systems offer an increased communication reliability without having to increase the transmit power, yielding a longer battery life and a lower impact on the environment. Furthermore, no special hardware is required, making cooperative systems easy and cheap to deploy using existing devices.

1.2 Motivation

When a signal propagates through the wireless medium, the latter distorts the signal, so that the signal received at the destination terminal is not the same as the signal sent by the transmitter. For the destination to retrieve the information sent by the transmitter, the former needs to know the nature and magnitude of the distortion introduced by the channel, in order to compensate for its effects. This effort is further complicated by the fact that the wireless propagation medium changes constantly due to the motion of objects and weather effects, so that the different channels, which are a mathematical abstraction of the propagation medium, are also in a state of constant change.

In literature, different strategies for cooperative communication have been proposed and analyzed from an information theoretical point of view. In most of these works, the different channels are assumed to be known to the destination terminal, in order to provide a simple mathematical model to work on. In real-life systems however, the assumption of known channels does not hold, and the latter need to be estimated. This work aims to provide a bridge between the theoretical work on cooperative communication systems and their implementation in real-life systems. Special attention is given to cooperative systems which have a low relay-side complexity. This low relay-side complexity is of great importance when deploying cooperative systems in sensor networks, which are networks consisting of many small, typically battery-powered sensors which all transmit data to a base station for processing. If the sensor devices are to implement a cooperative protocol and relay messages for one another, it is important that this relaying operation does not

significantly deplete the power source.

A cooperative relaying protocol suitable to be used in sensor networks is the quantize and forward (QF) protocol. The latter features a low relay-side complexity and can be implemented in half-duplex devices, which cannot send and receive information at the same time. Owing to these properties, the QF protocol is selected as a starting point for this work. After briefly discussing the available literature on the QF protocol, efficient estimation algorithms are developed for all relevant channel parameters. Alterations of the QF protocol that facilitate the channel parameter estimation process are also proposed, together with a novel QF protocol which can be used in two-way relaying systems.

1.3 Outline

The outline of this thesis is as follows:

• In **chapter 2**, the basic notions of the probability theory are outlined. Several methods for obtaining estimates of unknown parameters are discussed, together with some of the more important performance metrics that can be used to benchmark these estimates.

• Afterwards, in **chapter 3**, the reader is introduced to the world of digital communication. A general description of a digital communication system is first introduced, whereafter the different building blocks are discussed in more detail.

• Cooperative communication systems are discussed in **chapter 4**, where important notions such as diversity are also introduced.

• The cooperative protocol used throughout this work, namely the QF protocol, is presented in **chapter 5**.

• In **chapter 6**, an algorithm is proposed which estimates the channel between the source and the relay at the relay itself. Because the relay can directly observe this channel, mathematical expressions for the various estimators are obtained relatively easy.

• An important drawback of estimating the source-relay channel at the relay, is the increased complexity at the latter due to the estimation burden. This problem is tackled in **chapter 7**, where an algorithm is presented which estimates all channels, including the source-relay channel, at the destination.

While the resulting algorithm is mathematically more complex, it features a reduced relay-side complexity, making it especially suitable to be used in sensor networks.

• In the previous two chapters, it was assumed that there is no frequency mismatch between the carrier of the received wireless signal and the oscillator at the receiver. This assumption is lifted in **chapter 8**, where in addition to the various channel parameters, the carrier frequency mismatch is also estimated.

• In **chapter 9**, a novel two-way relaying system using the QF protocol is discussed. Unlike the one-way cooperative systems, in which a source communicates to a destination with the aid of a relay, in two-way relaying systems, two terminals communicate with one another, and the relay simultaneously assists both terminals.

• Topics for future work are discussed in **chapter 10**. These include the calculation of the Cramer-Rao bound for the estimates obtained in this work, and the development of a low complexity QF protocol for a multiple access relay channel (MARC) system.

• Finally, conclusions are drawn in **chapter 11**

2

Probability Theory

Probability theory is the branch in mathematics dedicated to the analysis of random events. Consider the variable X, whose value results from an experiment with an outcome determined by chance. When X is a discrete variable, we can characterize X by the probability mass function (PMF) $p_X(x) = \Pr[X = x]$, denoting the probability of X assuming a certain value x. When X is a continuous variable, we can characterize x by the cumulative distribution function (CDF) $F_X(x) = \Pr[X < x]$. Taking the derivative of this CDF with respect to x yields the probability density function (PDF) of X, defined as $p_X(x) = \frac{\partial}{\partial x} F_X(x)$. Multiple variables $(X_1, X_2, ..., X_n)$ can be derived from the same experiment, being fully characterized by their joint PMF, defined as $p_{X_1,...,X_n}(x_1, ..., x_n) = \Pr[X_1 = x_1, ..., X_n = x_n]$ in the case of discrete valued variables or their joint CDF (and PDF), defined as $F_{X_1,...,X_n}(x_1, ..., x_n) = \Pr[X_1 < x_1, ..., X_n < x_n]$, in the case of continuous valued variables.

In an experiment with two continuous random variables X and Y, with

joint PDF $p_{X,Y}(x,y)$, we define the marginal PDF of X as

$$p_X(x) = \int_y p_{X,Y}(x,y)\mathrm{d}y, \tag{2.1}$$

and similarly for the marginal PDF of Y. We further define the conditional PDF of Y given X, as

$$p_{Y|X}(y|x) = \frac{p_{X,Y}(x,y)}{p_X(x)}. \tag{2.2}$$

Similar definitions hold for discrete random variables. In the remainder of this work, we will not explicitly state the variables in the subscript of the density and mass functions, as these can be derived implicitly from the function arguments.

2.1 Estimation

There are many instances in which we want to estimate an unknown parameter vector $\boldsymbol{x}$, based on an observation vector $\boldsymbol{r}$, which is not only affected by $\boldsymbol{x}$, but also by (unknown) noise. This problem is the research topic of the estimation and detection theory, which is discussed in great detail in [1–4]. Before discussing some widely used estimation methods in section 2.1.2, we first introduce a few performance metrics in section 2.1.1.

2.1.1 Performance Metrics

2.1.1.1 Biased Versus Unbiased Estimates

With $\hat{\boldsymbol{x}}$ being an estimate of $\boldsymbol{x}$, we designate $\hat{\boldsymbol{x}}$ as being an unbiased estimate if

$$\mathbb{E}\left[\hat{\boldsymbol{x}}\right] = \boldsymbol{x}. \tag{2.3}$$

If (2.3) is not fulfilled, the estimate is said to be biased.

2.1.1.2 Mean Square Error

The mean square error (MSE) is a popular metric used to evaluate the accuracy of a given estimate. With $\hat{\boldsymbol{x}}$ being an estimate of $\boldsymbol{x}$, we define the mean square error (MSE) of $\hat{\boldsymbol{x}}$ as

$$\mathrm{MSE} = \mathbb{E}\left[\left(\hat{\boldsymbol{x}} - \boldsymbol{x}\right)\left(\hat{\boldsymbol{x}} - \boldsymbol{x}\right)^H\right]. \tag{2.4}$$

2.1.1.3 Cramer-Rao Bound

The Cramer-Rao bound (CRB) is a fundamental lower bound on the MSE of an unbiased estimate; it is impossible to find an unbiased estimate of a parameter vector $\boldsymbol{x}$ which has an MSE that is lower than the CRB. As a result, the CRB can be used to benchmark the MSE performance of a certain estimation method. If the computed estimate $\hat{\boldsymbol{x}}$ has a MSE that is close to the CRB, one can conclude that the given estimation method performs well and that it will be difficult to find a more accurate unbiased estimate of $\boldsymbol{x}$. The Cramer-Rao bound is discussed in more detail in section 10.1.

2.1.2 Estimation Methods

In the next subsections, we will briefly discuss a few methods for obtaining an estimate of $\boldsymbol{x}$, denoted $\hat{\boldsymbol{x}}$, given the observation vector $\boldsymbol{r}$. The reader is referred to [1,2] for a more in-depth analysis.

2.1.2.1 Maximum Likelihood Estimation

The likelihood of the observation $\boldsymbol{r}$ given the unknown variable $\boldsymbol{x}$ is defined as $p(\boldsymbol{r} \mid \boldsymbol{x})$. The maximum likelihood (ML) estimator calculates from $\boldsymbol{r}$ an estimate $\hat{\boldsymbol{x}}_{\text{ML}}$ of $\boldsymbol{x}$ by selecting the value of $\boldsymbol{x}$ that maximizes the aforementioned likelihood:

$$\hat{\boldsymbol{x}}_{\text{ML}} = \arg\max_{\boldsymbol{x}} p(\boldsymbol{r} \mid \boldsymbol{x}). \tag{2.5}$$

2.1.2.2 Maximum A Posteriori Estimation

Another widely used estimator is the maximum a posteriori (MAP) estimator, which exploits not only the observation $\boldsymbol{r}$, but also the a priori knowledge that the estimating terminal has on $\boldsymbol{x}$. A MAP estimate $\hat{\boldsymbol{x}}_{\text{MAP}}$ of $\boldsymbol{x}$, given the observation $\boldsymbol{r}$, is given by:

$$\hat{\boldsymbol{x}}_{\text{MAP}} = \arg\max_{\boldsymbol{x}} p(\boldsymbol{x} \mid \boldsymbol{r}) = \arg\max_{\boldsymbol{x}} p(\boldsymbol{r} \mid \boldsymbol{x}) p(\boldsymbol{x}). \tag{2.6}$$

Note that when the estimating terminal does not possess any a priori information on $\boldsymbol{x}$ (i.e. $p(\boldsymbol{x})$ is a uniform distribution not depending on $\boldsymbol{x}$), the MAP estimator coincides with the ML estimator.

2.1.2.3 Minimum Mean Square Error Estimation

The minimum mean square error (MMSE) estimate is an estimate that minimizes the MSE. It can be shown [1] that the MMSE estimate $\hat{\boldsymbol{x}}_{\text{MMSE}}$ of $\boldsymbol{x}$ can be expressed as

$$\hat{\boldsymbol{x}}_{\text{MMSE}} = \mathbb{E}\left[\boldsymbol{x} \mid \boldsymbol{r}\right] = \int \boldsymbol{x}\, p(\boldsymbol{x} \mid \boldsymbol{r}) \mathrm{d}\mathbf{x}. \tag{2.7}$$

Note that in order to calculate the MMSE estimate, averaging over the a posteriori distribution of $\boldsymbol{x}$ conditioned on $\boldsymbol{r}$ is needed. This makes the calculation of the MMSE estimate more involved as compared to the MAP estimate, as the latter only requires the location of the maximum of the a posteriori distribution of $\boldsymbol{x}$.

2.1.3 Estimation in the Presence of Nuisance Parameters

In many real-life estimation problems, the observation $\boldsymbol{r}$ is not only influenced by a parameter vector $\boldsymbol{x}$ which we want to estimate, but also by other unknown parameters, which we group in the vector $\boldsymbol{z}$. These parameters, also referred to as nuisance parameters, affect the observation $\boldsymbol{r}$, but cannot be directly observed by the device performing the estimation. In order to be able to calculate an estimate of $\boldsymbol{x}$, we need to integrate over the nuisance parameter vector $\boldsymbol{z}$, so that

$$p(\boldsymbol{r} \mid \boldsymbol{x}) = \int_{\boldsymbol{z}} p(\boldsymbol{r} \mid \boldsymbol{x}, \boldsymbol{z}) p(\boldsymbol{z} \mid \boldsymbol{x}) \mathrm{d}\boldsymbol{z}. \tag{2.8}$$

Subsequently, (2.8) can be used in (2.5) and (2.6) to obtain an ML or MAP estimate of $\boldsymbol{x}$. The problem is that, in many practical cases, the integral in (2.8) is difficult to evaluate analytically.

A solution to this problem is given by the expectation-maximization (EM) algorithm [5], which is an iterative approximation algorithm that can converge to the exact ML or MAP estimate when it is properly initialized. The EM algorithm consists of two steps: an expectation step and a maximization step. When trying to obtain an ML estimate of $\boldsymbol{x}$, given an observation $\boldsymbol{r}$, in the presence of the nuisance parameter vector $\boldsymbol{z}$, the expectation step of the i-th iteration consists of calculating the function

$$Q\left(\boldsymbol{x}, \hat{\boldsymbol{x}}^{(i-1)}\right) = \mathbb{E}_{\boldsymbol{z}}\left[\ln p(\boldsymbol{r}, \boldsymbol{z} \mid \boldsymbol{x}) \,\middle|\, \boldsymbol{r}, \hat{\boldsymbol{x}}^{(i-1)}\right]. \tag{2.9}$$

The vector $\hat{\boldsymbol{x}}^{(i-1)}$ represents an estimate of $\boldsymbol{x}$ which was obtained in the $(i-1)$-th iteration. In the maximization step, the expression from (2.9) is maximized with respect to $\boldsymbol{x}$ in order to obtain a new estimate of $\boldsymbol{x}$:

$$\hat{\boldsymbol{x}}^{(i)} = \arg\max_{\boldsymbol{x}} Q\left(\boldsymbol{x}, \hat{\boldsymbol{x}}^{(i-1)}\right). \tag{2.10}$$

This iterative process is usually stopped after a fixed number of iterations. Note that due to its iterative nature, the EM algorithm needs to initialized by selecting a value for $\hat{x}^{(0)}$. A proper initialization is important in order for the EM algorithm to converge to the true ML estimate, instead of a local extremum. Similar expressions are obtained for calculating an MAP estimate in the presence of nuisance parameters; the reader is referred to [1,5] for more information on this topic.

3
Digital Communication Model

3.1 Overview

The purpose of a digital communication system is to convey information from a transmitter to a receiver. The basic layout of a such a system using a discrete-time channel is displayed in Fig. 3.1. In the next subsections, the individual components that make up a digital communication system are discussed separately.

3.1.1 Source Coding

Information can take up many forms, for example speech, video and text. To rid us from the burden of having to design a communication system for each information type, source coding is used to convert analog information into digital information, consisting of bits. These bits are subsequently presented

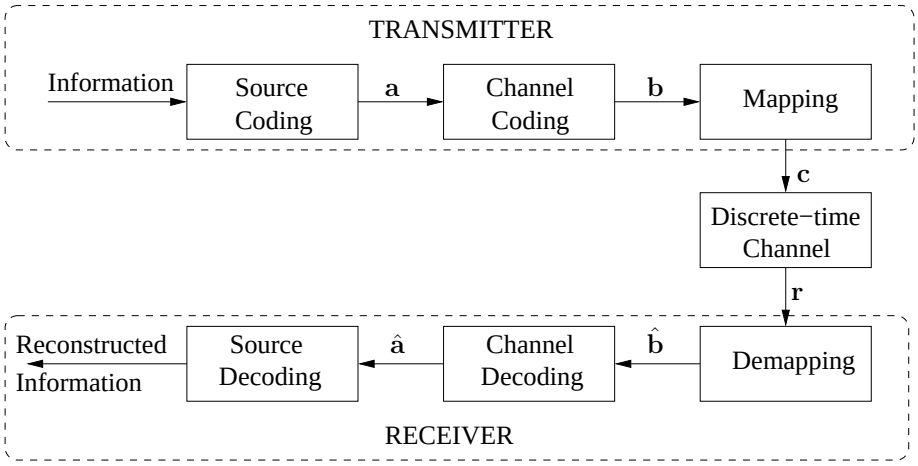

Figure 3.1: Basic layout of a digital communications system.

to a digital communication system that transfers them from the source to their destination.

At the source, an analog signal is made digital by sampling it at fixed intervals. In order to avoid aliasing, the sample frequency needs to be at least twice the bandwidth of the analog signal [6]. The real-valued samples are subsequently quantized. The number of bits used to quantize each sample, as well as the quantization scheme (linear / non-linear), are chosen according to the distortion requirements [7, 8]. In addition to digitizing analog signals, the source coding system can also compress the data before transmission by removing redundancy [9].

At the destination side, the bits that are output by the channel decoder are presented to the source decoder. The latter decompresses the received information by re-introducing redundancy. In the case of analog information, waveform reconstruction is performed by the source decoder, yielding an analog signal. In the remainder of this dissertation, we will only consider digital communication systems. Analog inputs will be assumed to have been passed through a source coding system for digitization.

3.1.2 Channel coding

When digital information is transported over a physical communications channel, the channel induces noise, which can make the bits at the output of the channel differ from the bits at its input. The purpose of channel encoding is to add redundancy to a stream of information bits, in order to make them

more resilient to errors induced by the channel [10]. Consider the vector $\boldsymbol{a}$, consisting of A information bits, which is output by the source encoder. By adding redundancy, $\boldsymbol{a}$ is transformed into the vector $\boldsymbol{b}$ using a channel coding function: $\boldsymbol{b} = \varrho(\boldsymbol{a})$. The vector $\boldsymbol{b}$ contains B coded bits, with $B \geq A$. The ratio A/B is called the code rate. At the receiver side, the coded bits are decoded by the channel decoder in order to obtain an estimate of the sent information bits. Due to the added redundancy, the channel decoder can detect and sometimes even correct transmission errors caused by the noisy channel. Some widely used channel codes are described in the next subsections.

3.1.2.1 Linear Block Codes

In a linear block code (LBC), the information bit sequence $\boldsymbol{a}$ is split into blocks of N_a bits: $\boldsymbol{a} = (\boldsymbol{a}_0, \boldsymbol{a}_1, ..., \boldsymbol{a}_{L-1})$, with $L = A/N_a$. Trailing zeroes are added to $\boldsymbol{a}$ to make its length a multiple of N_a. Each block is subsequently multiplied by a $N_a \times N_b$ generator matrix $\boldsymbol{G}$, with $N_b \geq N_a$, yielding blocks of coded bits:

$$\boldsymbol{b}_0 = \boldsymbol{a}_0 \boldsymbol{G}. \tag{3.1}$$

The code rate is given by N_a/N_b. The properties of the channel code are determined by the generator matrix $\boldsymbol{G}$. The reader is referred to [10–13] for more information on linear block codes.

3.1.2.2 Convolutional Codes

In contrast to a LBC, in which a coded block $\boldsymbol{b}_k$ only depends on the corresponding block of information symbols $\boldsymbol{a}_k$, in a convolutional code, a coded block also depends on the previous L blocks $\boldsymbol{a}_{k-1}$, $\boldsymbol{a}_{k-2}$, ..., $\boldsymbol{a}_{k-L}$. In the remainder of this work, we will assume that the size of a block is equal to 1 (i.e. $N_a = 1$). The block diagram of a simple convolutional code is shown in Fig. 3.2. At each step k, a new information bit $a(k)$ is presented to the convolutional encoder. This bit is used, together with the bits stored in the memory blocks of the encoder, to calculate the parity bits $p_1(k)$ and $p_2(k)$, using modulo-2 addition operations. After this computation, the memory blocks update by storing the bit presented at their input, and the process repeats for the next information bit until all elements of $\boldsymbol{a}$ have been processed. Finally, the vectors $\boldsymbol{p}_1$ and $\boldsymbol{p}_2$ are serialized bit-wise into the vector $\boldsymbol{b}$. A convenient way to specify the characteristics of a convolutional code is the octal notation, in which, for each modulo-2 adder, the memory blocks connected to this adder are specified in octal format, where the most significant bit corresponds to the memory block containing the most recent information bit. For example, the octal representation of the code shown in Fig. 3.2 is $(6,5)_8$. Efficient algorithms, such as the Viterbi [14,15] algorithm, have been proposed in literature for decoding convolutional codes.

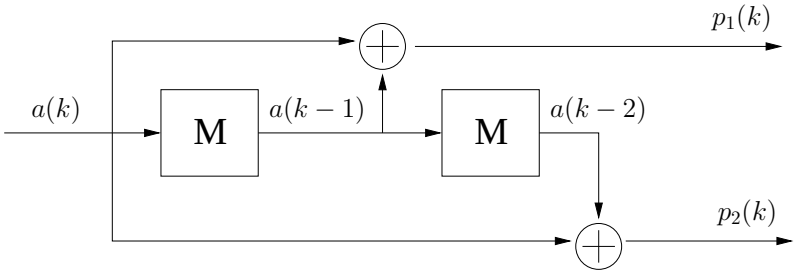

Figure 3.2: A $(6,5)_8$ non-recursive, non-systematic convolutional code.

Systematic versus Non-Systematic In a systematic convolutional code, the input bits are transmitted unaltered, together with added parity bits. The output of a non systematic convolutional code does not include the input data and only contains parity bits which are derived from the input bits.

Recursive versus Non-Recursive A recursive convolutional code contains a feedback loop, in which the output of a modulo-2 adding block is added to the input bits as they enter the system. A non-recursive convolutional code does not contain this feedback loop. Recursive codes are typically systematic while non-recursive codes are typically non-systematic. The octal representation of a systematic, rate $1/2$ recursive convolutional code is of the form $(1, x/y)_8$, where x is the octal representation of the positions used to calculate the parity bit and y is the octal representation of the positions used in the feedback loop.

3.1.2.3 Turbo Codes

A turbo code consists of two convolutional codes merged together by an interleaver. The turbo codes used throughout this work make use of two systematic, recursive convolutional codes (SRCC) that are concatenated in parallel using an interleaver. The input bits $\boldsymbol{a}$ are presented to the first SRCC encoder, which calculates the parity bits $\boldsymbol{p}_1 = \boldsymbol{a}$ and $\boldsymbol{p}_2$. The input bits $\boldsymbol{a}$ are also presented to an interleaver, which outputs a vector $\boldsymbol{a}'$ containing the information bits from $\boldsymbol{a}$ in a different order. The output of this interleaver is presented to the second SRCC encoder, which uses them to compute the parity bits $\boldsymbol{p}'_1 = \boldsymbol{a}'$ and $\boldsymbol{p}'_2$. The coded bits $\boldsymbol{b}$ are obtained by serializing the vectors $\boldsymbol{a}$, $\boldsymbol{p}_2$ and $\boldsymbol{p_2}'$, resulting in a rate $1/3$ code. The decoding of a turbo code proceeds iteratively and is discussed in [16]. A more elegant decoding approach using factor graphs is proposed in [17]. More information on factor graphs can be found in [18, 19].

Merging of Decoder Iterations with EM Iterations As shown in section 2.1.3, the EM algorithm can be used to obtain an estimate of an unknown parameter vector in the presence of nuisance parameters. In almost all estimation problems studied in this work, the symbols sent by the source are considered to be nuisance parameters, so that the a posteriori probabilities of these symbols are needed in each EM iteration, in order to update the considered estimates. These a posteriori probabilities are provided by the channel decoder, requiring the channel code to be fully decoded. When an iteratively decoded channel code is used, such as a turbo code, multiple code iterations need to be performed per EM iteration in order to obtain the required a posteriori probabilities.

In order to reduce the computational complexity arising from the use of the EM algorithm in combination with iteratively decoded channel codes, we can execute only one decoder iteration for each EM iteration, without resetting the decoder. The a posteriori symbol probabilities obtained this way will only be an approximation of the true a posteriori symbol probabilities. However, with successive EM-code iterations, the channel decoder converges and the approximated symbol probabilities will approach the real a posteriori probabilities. As shown in [32], this approach does not have a considerable effect on error performance, while it significantly decreases the computational complexity.

3.1.2.4 Hard and Soft Decision Decoding

The output of a channel decoder can either be a hard decision or a soft decision. A hard decision only consists of the decoded bits, while a soft decision also contains information on the reliability of the decoded bits, in the form of the a posteriori bit probabilities, defined as $p(\hat{a}(k) \mid \boldsymbol{r})$. A soft decision can be transformed into a hard decision by selecting for each information bit the value with the highest a posteriori probability:

$$\hat{a}(k) = \arg\max_{a(k)} p(a(k) \mid \boldsymbol{r}). \tag{3.2}$$

3.1.3 Mapping

The mapping operation transforms a codeword $\boldsymbol{b}$ consisting of B coded bits into a sequence $\boldsymbol{c}$ consisting of K complex symbols, called a frame. To this purpose, the vector $\boldsymbol{b}$ is split into blocks of $\log_2 M$ bits: $\boldsymbol{b} = (\boldsymbol{b}_0, \boldsymbol{b}_1, ..., \boldsymbol{b}_K)$, with $K = B/\log_2 M$. Each such block is transformed by the mapper function χ into a coded symbol $c(k) = \chi(\boldsymbol{b}_k)$. The set of all possible outputs of χ is called the mapper constellation and its cardinality, equal to M, is called the constellation size, which in all practical cases is an integer power of 2. In this work, we will assume that the average energy per symbols at the output of

the mapper is equal to one, i.e.

$$\mathbb{E}[\boldsymbol{c}\boldsymbol{c}^H] = K. \tag{3.3}$$

For mapping constellations with $M > 2$, a gray code is typically used to assign a certain bit sequence to a constellation point [20]. Popular mapping schemes include pulse amplitude modulation (PAM), phase shift keying (PSK) and quadrature amplitude modulation (QAM) mapping. The first two are briefly discussed below.

3.1.3.1 PAM Mapping

In PAM mapping, each block of $\log_2 M$ coded bits is mapped to a real number. The mapper constellation is given by the set

$$\{c \mid c = d(2l - M + 1), l = 0, 1, ..., M - 1\}. \tag{3.4}$$

The variable d denotes half the minimum distance between constellation points. It is chosen to satisfy the normalization constraint (3.3) and is equal to

$$d = \frac{1}{\sqrt{\frac{1}{M}\sum_{l=0}^{M-1} |(2l - M + 1)|^2}} = \sqrt{\frac{3}{M^2 - 1}}. \tag{3.5}$$

3.1.3.2 PSK Mapping

In a PSK mapping scheme, each block of $\log_2 M$ coded bits is mapped to a complex number having an amplitude equal to 1 and a phase that depends on the bits of the considered block. The mapping constellation is given by the set

$$\left\{ c \;\middle|\; c = \exp\left(\frac{j2\pi l}{M}\right), l = 0, 1, ..., M - 1 \right\}. \tag{3.6}$$

Because each member of the constellation has an amplitude equal to 1, the normalization constraint (3.3) is automatically satisfied.

3.1.4 Channel Modeling

Through this work, a discrete time memoryless channel model is used, in which the complex symbols $\boldsymbol{c}$ at the output of the mapper are amplified by a factor $\sqrt{E_0}$ and are subsequently presented to the channel at a rate R_s. The output of the channel also consists of discrete symbols, at the same symbol rate R_s. Because real-life channels work with real-valued continuous waveforms, the discrete time memoryless channel model is a mathematical abstraction of the cascade of a modulator, a waveform channel and a demodulator,

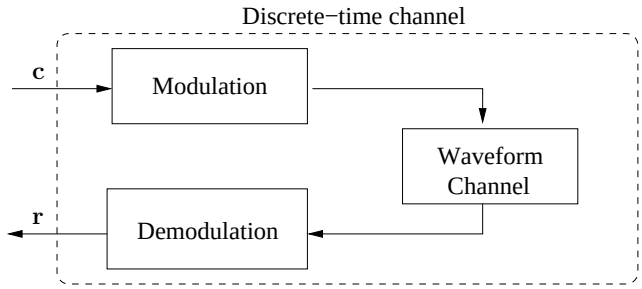

Figure 3.3: Discrete-time channel abstraction.

as shown in Fig. 3.3. The modulator assigns a transmit pulse to each symbol, shifts the baseband signal to the desired frequency band and presents it to the waveform channel. The demodulator in turn converts the output of the channel back into a baseband signal, which is subsequently sampled at fixed intervals to obtain a sequence of complex symbols. If the sampling interval, the waveform channel and the receiver filter are such that the inter symbol interference can be neglected, the cascade shown in Fig. 3.3 can be modeled as a discrete time memoryless channel. For such a channel, the relation between the input symbols, contained in $\boldsymbol{c}$ and the output symbols, contained in $\boldsymbol{r}$, can be written as

$$r(k) = \sqrt{E_0}h(k)\exp(j2\pi\nu k)c(k) + n(k). \tag{3.7}$$

The elements of $\boldsymbol{h}$ model the physical propagation environment. In the remainder of this work, we will assume a slow-fading channel model, meaning that the channel coherence time is much larger than the time it takes to transmit a frame (= K/R_s). Therefore, it can be assumed that $h(1) = h(2) = ... = h(K) = h$, so that (3.7) can be written as

$$r(k) = \sqrt{E_0}h\exp(j2\pi\nu k)c(k) + n(k). \tag{3.8}$$

The factor $\exp(j2\pi k\nu)$ represents a frequency mismatch between the carrier frequency of the received signal and the oscillator at the receiver. This mismatch can be the result of the oscillators at the source and receiver operating at slightly different frequencies, or it can be caused by Doppler shift, which occurs when the transmitter and receiver are moving relative to each other. The vector $\boldsymbol{n}$ represents random noise introduced by the environment and the receiver circuitry. Its elements are modeled as independent and identically distributed (IID) random variables having a zero mean circular symmetric complex Gaussian (ZMCSCG) distribution with variance N. The statistics of the channel coefficient h depend on the chosen fading model. A few widely used fading models are discussed below.

3.1.4.1 AWGN Channel

The AWGN channel is a convenient channel model for scenarios where there is only one dominant propagation path between the transmitter and the receiver, such as line-of-sight communication between a satellite and a base station. In the AWGN channel, h is assumed to be equal to $Ae^{j\theta}$, with A being a deterministic variable.

3.1.4.2 Rayleigh Fading

In urban environments with a large number of tall buildings, typically there is no line-of-sight path between the transmitter and the receiver terminals. Instead, there are multiple indirect paths between the former two terminals, created by the reflection of radio waves on different surfaces, giving rise to a phenomenon called multipath fading. The waves propagating along these different paths can interfere either destructively or constructively at the receiver antenna, yielding a signal whose strength varies in time due to the motion of the receiver and changes in the propagation environment (moving objects, effects of wind, ...). Because we assumed that the channel coherence time is much longer than the time it takes to transmit a frame, we can assume the channel coefficient to remain constant within one frame. However, due to the time-varying nature of the channel, different frames will have different channel coefficients. It can be shown that in such a scenario, the channel coefficient can be modeled as having a ZMCSCG distribution [21], i.e.

$$p(h) = \frac{1}{\pi N_h} \exp\left(-\frac{|h|^2}{N_h}\right). \tag{3.9}$$

Under these conditions, the squared magnitude of h, denoted $A_h^2 = |h|^2$ has a Chi-squared distribution and the magnitude of h is described by a Rayleigh distribution:

$$p(A_h) = \frac{2A_h}{N_h} exp\left(\frac{-A_h^2}{N_h}\right). \tag{3.10}$$

3.1.4.3 Other Fading Models

Many other fading models have been described in literature to model different wireless propagation environments, such as Rice fading, describing the scenario in which there is both a direct path and many interfering indirect paths between the transmitter and the receiver terminal, and Nakagami fading, a versatile fading model that can fit many wireless channels [22–27]. Their discussion however falls outside the scope of this work and the reader is referred to the presented literature for more information.

3.2 Performance Metrics

In this section, some performance metrics and definitions that are used throughout this work will be introduced.

3.2.1 Bit Error Rate and Word Error Rate

Ideally, the bits at the output of the channel decoder at the receiver terminal are the same as the ones presented to the channel encoder at the transmitting terminal, i.e. $\hat{\boldsymbol{a}} = \boldsymbol{a}$. However, due to the noise present on the channel, this is not always the case. The average ratio of erroneously decoded bits to the total number of bits is called the bit error rate (BER) and is defined by

$$\text{BER} = \frac{\mathbb{E}[d_H(\hat{\boldsymbol{a}}, \boldsymbol{a})]}{A}, \tag{3.11}$$

with A being the size of $\boldsymbol{a}$ and d_H representing the Hamming distance between $\hat{\boldsymbol{a}}$ and $\boldsymbol{a}$, defined as the number of positions at which the latter two differ. In order to have a reliable communication link between the transmitter and the receiver, the BER needs to be as low as possible. Because fading conditions and noise vary from frame to frame, the BER is typically averaged over a large number of frames.

In most practical cases, applications that make use of digital communication links have a system in place to detect transmission errors. This can be achieved for example by checking the validity of a checksum of the received bits. If the checksum turns out invalid, a retransmission is requested. The performance of such a system depends on the probability that a frame contains at least one erroneously decoded bit. A quantitative measure for this performance is the word error rate (WER), denoting the average ratio of codewords containing at least one bit error to the total number of codewords received.

3.2.2 Signal to Noise Ratio

An indicator of the quality of a signal is its signal to noise ratio (SNR). It is expressed as the ratio between the power of the useful part of the signal to that of the noise. In fading environments, it is convenient to distinguish between the instantaneous SNR and the average SNR. The former is defined as the SNR for one particular frame, while the latter is defined as the SNR averaged over different frames. For example, for the Rayleigh fading channel from section 3.1.4.2, the instantaneous SNR is given by

$$\text{SNR}_{\text{inst}} = \frac{E_s |h|^2}{N}, \tag{3.12}$$

while the average SNR is equal to

$$\mathrm{SNR}_{\mathrm{av}} = \frac{E_s N_h}{N}. \tag{3.13}$$

A widely used performance metric is obtained by expressing the average BER (or WER) as function of the average SNR.

3.3 Channel State Information

When studying digital communication systems, different assumptions can be made concerning the channel state information (CSI) that the different terminals possess:

• **Full CSI**: Both the transmitter and the receiver are assumed to perfectly know the state of the channels involved. This is the ideal situation, as the transmitter can adjust its transmit signal based on the channel conditions in order to optimize certain performance criteria. At the receiver, the CSI is used to decode the received information. While this scenario yields the best performance, it is not a realistic assumption: in a real-life situation, the different channels are not known and will need to be estimated (see below).

• **Receiver CSI**: Only the receiver is assumed to known the state of the channels. In case this information also needs to be known to the transmitter, it needs to be fed back to the latter by the receiver.

• **No CSI**: This is the most realistic scenario, in which neither the receiver nor the transmitter know the state of the channel. The receiver needs to make an estimate of the various channel parameters in order to decode the received information. In case the transmitter also needs to dispose of CSI, the estimates calculated by the receiver need to be fed back to the transmitter.

3.4 Medium Access Control

In a typical real-life situation, multiple users want the access the same medium at the same time. In order to avoid high levels of inter-user interference, a medium access control (MAC) protocol needs to be enforced, dictating how users should regulate their transmissions. A few popular MAC protocols are described below:

• **Time Division Multiple Access (TDMA)**: In a TDMA scheme, the available transmission time is divided into different slots called time slots. During each time slot, only one transmitter is active [28].

• **Frequency Division Multiple Access (FDMA)**: In a FDMA scheme, each transmitter makes use of a specific frequency band to transmit its information. The frequency bands are spaced sufficiently apart to avoid interference [29].

• **Code Division Multiple Access (CDMA)**: CDMA is a spread-spectrum technique, in which multiple users transmit at the same time using the same central frequency. Each transmitter modulates the information to be transmitted using a personal code which has a higher bandwidth as compared to the original information-bearing signal. At the receiver, the original signal is retrieved using signal correlation techniques [30, 31].

4

Cooperative Communication

4.1 Diversity

In order to discuss the notion of diversity, we first define the channel capacity, which was introduced by Shannon in 1948 to develop the noisy channel coding theorem [33]. The theorem states that, by using a suitable channel code, the probability of a decoding error occurring during transmission over a noisy channel can be made arbitrary small by increasing the codeword length, only if the information bitrate is lower than the channel capacity. The theorem however does not outline how to construct such a capacity-achieving channel code. For the AWGN channel discussed in section 3.1.4.1, it can be shown that the channel capacity is an increasing function of the instantaneous SNR [34]. The same result applies to the Rayleigh fading channel discussed in section 3.1.4.2. However, in the Rayleigh fading model the instantaneous SNR is a probabilistic quantity, as it depends on the squared magnitude of the channel

coefficient h, and thus occasionally assumes arbitrarily small values. Therefore, strictly speaking, the capacity of a Rayleigh fading channel is equal to 0, as no positive rate can be found that always allows error-free communication according to Shannon's theorem [35, 36].

For us to be able to describe the quality of fading channels, the concept of outage is introduced. Given a selected information bitrate, an outage event is said to occur during the transmission of a frame if the capacity of the fading channel is smaller as compared to the selected rate. When this is the case, the channel is said to be in deep fading and error-free transmission of the considered frame cannot be achieved. We further define the outage probability as the probability of an outage event occurring during a particular frame; the outage probability is a lower bound on the decoding error probability of practical channel codes on the fading channel. For the Rayleigh fading channel discussed in section 3.1.4.2, it can be shown that for high values of the average SNR, denoted SNR_{av}, the outage probability P_{out} behaves as [37]

$$P_{\text{out}} = \kappa \left(\frac{1}{\text{SNR}_{\text{av}}} \right)^{D}, \tag{4.1}$$

with κ being a factor that depends on the selected information bitrate. The exponent D represents the diversity gain, and is equal to 1 for the channel model described in section 3.1.4.2. Large gains in communication reliability can be made by increasing the diversity gain D. This can be achieved using several methods:

• **Spatial diversity**: Spatial diversity can be achieved by installing multiple antennas at the transmitter and/or receiver terminal, creating a multiple input, multiple output (MIMO) system. In a Rayleigh fading environment, the instantaneous signal strength depends on the specific location of the transmitting and receiving terminals. By equipping (one of) the terminals with more than one antenna, different paths in space are created between the transmitter and the receiver. If the antennas on a same terminal are spaced far enough apart, the fading coefficients of the different paths become uncorrelated, and the diversity gain D increases, as multiple signal paths now need to be simultaneously in a deep fading state for an outage event to occur [38–41]. A drawback of MIMO systems is the increased cost associated with the extra hardware needed to support a multiple antenna system. Furthermore, in case of small devices, it is not always possible to achieve sufficient spacing between the different antennas.

• **Time diversity**: As mentioned in section 3.1.4.2, the signal strength on a fading channel varies over time. The diversity gain can be increased by transmitting the same information more than once at different points in time. If

the time between retransmissions is larger than the channel coherence time, the different retransmissions will experience a different fading state, thus increasing the system's diversity.

• **Frequency diversity**: On frequency-selective channels, where different frequencies experience different fading conditions, diversity can be introduced by transmitting the information over different frequency bands. In OFDM systems, the data is encoded into different subcarriers, each having a slightly different central frequency [42]. Using the right coding techniques, OFDM systems can be used to mitigate the effects of frequency selective fading. However, when the channel coherence bandwidth is so large that all subcarriers within the channel bandwidth are in fading simultaneously, OFDM systems fail to offer an increased diversity.

• **Cooperative diversity**: Cooperative diversity schemes make use of the broadcast nature of the wireless medium. A signal sent by a transmitter is not only received by the intended destination, but also by other terminals nearby. In a non-cooperative system, these terminals will ignore this signal, as it is not destined to them. In a cooperative system however, the terminals nearby will act as a relay and forward (a modified version of) the received information to the destination. This creates additional signal paths between the transmitter and the destination. If the relay operation is chosen carefully, an increased diversty gain can be achieved [43–47]. As compared to MIMO techniques, no additional hardware is required, making cooperative systems cheap to implement. Furthermore, very small devices can be used, as multiple antennas are not required. Cooperative systems are discussed in more detail in the sections below.

4.2 Single-Relay Channel Model

A cooperative system in which one source communicates to one destination with the aid of only one relay is shown in Fig. 4.1. The channels are modelled as flat Rayleigh fading channels with AWGN and no frequency mismatch, so that the complex samples obtained at the output of the source-destination, source-relay and relay-destination channels, denoted by the vectors $\boldsymbol{r}_0$, $\boldsymbol{r}_1$ and $\boldsymbol{r}_2$, respectively, can be written as

$$\begin{aligned} \boldsymbol{r}_0 &= \sqrt{E_0} h_0 \boldsymbol{c}_0 + \boldsymbol{n}_0 \\ \boldsymbol{r}_1 &= \sqrt{E_0} h_1 \boldsymbol{c}_0 + \boldsymbol{n}_1 \\ \boldsymbol{r}_2 &= \sqrt{E_r} h_2 \boldsymbol{c}_r + \boldsymbol{n}_2. \end{aligned} \tag{4.2}$$

The variables h_0, h_1 and h_2 represent the complex channel coefficients of the source-destination, source-relay and relay-destination channels, respectively.

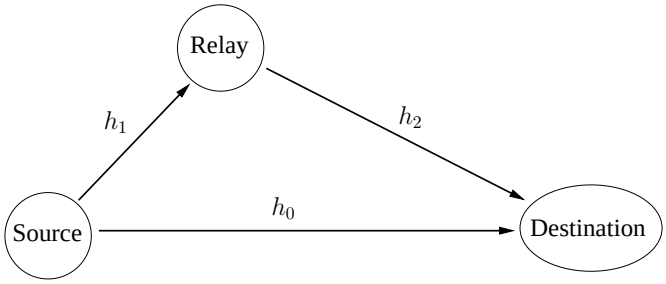

Figure 4.1: One-way relay channel model.

The vectors $\boldsymbol{n}_0$, $\boldsymbol{n_1}$ and $\boldsymbol{n}_2$ represent the AWGN noise, with respective variances equal to N_0, N_1 and N_2. The vectors $\boldsymbol{c}_0$ and $\boldsymbol{c}_r$ represent the symbols transmitted by the source and relay, respectively. Assuming the normalization of $\boldsymbol{c}_0$ and $\boldsymbol{c}_r$ (i.e. $\mathbb{E}[|\boldsymbol{c}_0|^2] = \mathbb{E}[|\boldsymbol{c}_r|^2] = K$, with K denoting the number of symbols per codeword), the variables E_0 and E_r represent the energy of the symbols transmitted by the source and relay, respectively.

The communication process is initiated by the source broadcasting its information, which is received by both the relay and the destination terminals. The signal received by the relay is processed and forwarded to the destination, creating two different signal paths between the source and the destination: one direct path, consisting of the information propagating directly from the source to the destination, and one relay path, consisting of the information forwarded by the relay to the destination. As a result, a single channel being affected by deep fading does not necessarily cause an outage event, as the information can be retrieved from the signal path which does not contain the affected channel.

The relay terminals can either be full-duplex or half-duplex terminals. A full-duplex terminal can send and receive information at the same time. This can be achieved by using a different frequency band for the incoming and outgoing signals, or by using a self-interference cancellation scheme. A half-duplex terminal cannot achieve this feature: it is either receiving or transmitting. A full-duplex relay can simultaneously receive information from the source and forward it to the destination. A half-duplex relay requires a TDMA scheme to be in place, where the available transmission time is divided into two time slots. The first time slot is used by the source to transmit its information to the relay and the destination, while the second time slot is used by the relay to forward the received information to the destination. The relay thus needs to store the information received in the first time slot before it can be forwarded to the destination in the second time slot. Besides storing the

information received from the source, the relay can also perform an operation on the received signal. This operation determines the symbol vector $\boldsymbol{c}_r$, which is transmitted by the relay to the destination, and considerably affects the performance of the cooperative system and the diversity gain it achieves. A few widely used operations, called relaying protocols, are briefly presented in the next subsections. Methods to estimate the various channel parameters involved are also discussed for each protocol.

4.2.1 Amplify and Forward

Perhaps one of the most documented relaying protocols is the amplify and forward (AF) protocol. In an AF system, the relay transmits to the destination an amplified version of the signal it receives from the source [43]. The AF protocol is characterized by the relationship

$$\boldsymbol{c}_r = \beta \boldsymbol{r}_1 = \beta \sqrt{E_0} h_1 \boldsymbol{c}_0 + \beta \boldsymbol{n}_1. \tag{4.3}$$

Two strategies are commonly used to select a value for the gain β. In the first, β is chosen so that the average (over multiple frames) transmit energy per symbol of the relay is equal to E_r, yielding

$$\beta = \frac{1}{\sqrt{E_0 N_{h_1} + N_1}}, \tag{4.4}$$

with $N_{h_1} = \mathbb{E}\left[|h_1|^2\right]$. In the second strategy, β is chosen so that the average (over a single frame) transmit energy per symbol of each frame is equal to E_r, yielding

$$\beta = \frac{1}{\sqrt{E_0 |h_1|^2 + N_1}}. \tag{4.5}$$

The second method has the advantage of a more constant transmit power in time, as it takes into account the exact value of the fading coefficient h_1. This however requires the relay to calculate an estimate of h_1 to be used in (4.5). When using the first method, the relay does not need to estimate h_1, as only the expected value of $|h_1|^2$ is used in (4.4).

Channel parameter estimation for the AF protocol is discussed in [48–54]. In [48,49], a distinction is made between estimating the source-relay and relay-destination channels separately, and estimating the cascade of the two channels at the destination terminal, without estimating the channels separately. It is shown that the second approach is favorable in terms of BER performance and also in terms of relay complexity, as the first approach requires the relay to send an estimate of the source-relay channel to the destination. The estimation of the various channel parameters using pilot symbols is discussed

in [50, 51], while a code-aided approach is outlined in [52–54]. The impact of imperfect channel estimates on the error performance of an AF system is discussed in [55, 56]. Finally, in [57], the CRB is obtained for the various channel parameter estimates.

4.2.2 Decode and Forward

Another popular cooperative protocol is the decode and forward (DF) protocol, in which the relay decodes the information sent by the source. After decoding, the relay will re-encode the decoded bits with its own channel code and transmit the result to the destination. It is shown in [43] that a system in which the relay is strictly required to correctly decode the source message does not achieve an increased diversity gain. In order to increase the systems diversity, different approaches have been proposed. In [43], an adaptive DF protocol that achieves cooperative diversity is proposed, in which the relay only transmits when the SNR on the source-relay link is sufficiently high. When multiple relay terminals are present, power allocation schemes have also been proven to achieve cooperative diversity [58–60]. In [61], a closed-form expression is obtained for the outage behavior of a DF cooperative system consisting of multiple relay terminals that only transmit if they can successfully decode the information received from the source. An analytical expression for the BER of such a system is obtained in [62]. Hybrid AF/DF algorithms, in which the relay either selects the AF or DF protocol depending on the channel conditions, have been proposed in [63–65]. Channel estimation algorithms for the DF protocol are discussed in [66–68].

4.2.3 Compress and Forward

The DF protocol discussed in the previous subsection suffers from the limitation that the relay terminals are required to correctly decode the information from the source in order to be able to participate in the cooperative process. Typically, a frame that is not correctly decoded by the relay only differs from the correct frame by a limited number of bits. The large majority of the information bits present in the frame are correctly decoded, but, because the frame contains errors, it will not be used by relays implementing the DF protocol. This shortcoming is addressed by the compress and forward (CF) protocol, which also utilizes the incorrectly decoded frames to provide to the destination more information on the message sent by the source.

In [69], the ideas from the distributive source coding (DSC) theory are applied to a cooperative system consisting of a source, a relay and a destination. DSC was first investigated by Slepian and Wolf in [70], where it is shown that when two sources transmit correlated information to the same destination, the latter can jointly decode the two information streams. In doing so, higher

rates can be achieved as compared to the situation in which the correlation of the sources is not exploited. In the CF system from [69], the source transmits a frame which is received by both the relay and the destination. After decoding, the relay obtains a frame that is either correcly decoded or one that contains decoding errors, and transmits the obtained frame to the destination. Because the Hamming distance between an incorrectly decoded frame and the original frame is typically small, there is a high degree of correlation between the information forwarded by the relay and the information transmitted by the source, so that DSC techniques can be used at the destination to provide an increased diversity gain. An improvement on [69] is discussed in [71], where the relay uses Wyner-Ziv encoding [72] to transmit soft decoding decisions to the destination, providing information on the reliability of the decoded data. Different compression schemes are discussed in [73]. Finally, in [74], the performance differences between DF and CF are studied.

4.2.4 Quantize and Forward

While the DF and CF protocols discussed in the previous subsections have been shown to yield an increased diversity gain, they require the relay to decode (and re-encode) the information received from the source. This places a significant burden on the relay terminals, as they need to be equipped with powerful hardware to be able to perform the decoding and encoding operations. Especially in sensor networks, consisting of many low complexity and battery powered sensors cooperating with one another, this increased complexity can be deemed unacceptable [75]. A solution is to use the AF protocol instead, which does not require the relay to decode the received information. While having a seemingly low complexity, the AF protocol, when used with half-duplex devices, requires a large memory at the relay for storing with high precision the signal received during the first slot, awaiting transmission to the destination during a later slot. Implementing a full-duplex relay terminal is not always an option, as it requires specialized hardware to be able to transmit and receive on different frequency bands.

A viable solution for implementing low-complexity relay terminals is the quantize and forward (QF) protocol, which is the main topic of this dissertation. In the QF protocol, the relay does not decode the channel code of the source, but instead quantizes the received symbols, whereafter it performs an operation on the quantization values and forwards the result to the destination. In [76], a QF protocol is described in which the source transmits 16-QAM symbols, and the relay uniformly quantizes the received samples. The quantized values are subsequently source coded using a Huffman code [77] and the result is channel coded using a turbo code and transmitted to the destination. While this approach does not require a decoding operation to be performed

at the relay, it does require the latter to perform a source coding and a channel coding operation. An approach not requiring the aforementioned operations is presented in [78], where a QF system is described in which the relay coarsely quantizes the symbols received from the source and transmits the quantized samples to the destination, without performing any additional operations on the quantized values; because of the coarse quantization, the storage requirements at the relay are considerably relaxed, compared to the AF protocol. This QF system is discussed more in depth in chapter 5. Methods to estimate the various channel parameters in such a system are investigated in chapters 6, 7 and 8.

Part II

Quantize and Forward Cooperative Communication

5

The Quantize and Forward protocol

In this chapter, a low-complexity Quantize and Forward (QF) protocol is introduced. This protocol has been proposed in [78] and features a low relay-side complexity by limiting the number of operations that need to be performed by the relay. This reduced complexity makes the protocol ideally suited for battery-powered relay terminals with limited computing power. Compared to the Amplify and Forward (AF) protocol described in section 4.2.1, the bulk of the computational burdon is shifted to the destination, where typically more resources are available. The outline of this chapter is as follows: In section 5.2 the reader is introduced to the QF protocol and the quantization at the relay is discussed. In section 5.3, the detection at the destination terminal is outlined, whereafter the WER performance is discussed in section 5.4.

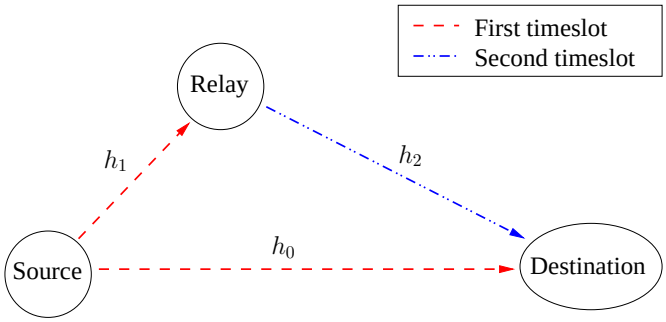

Figure 5.1: One-way relay channel model.

5.1 Channel Model

Consider the one-relay channel model from section 4.2, repeated for clarity in Fig. 5.1. The relay operates in half-duplex mode, meaning that it cannot simultaneously receive and transmit information. The channels are modelled as flat Rayleigh fading channels with AWGN and no frequency mismatch. The medium access mode is TDMA. Throughout this chapter, the complex channel coefficient and noise variances are assumed to be known to the destination terminal.

In the first timeslot, a frame consisting of A information bits is applied to the channel encoder which transforms it into a frame of $B = N/\lambda$ coded bits, with λ representing the code rate. These coded bits are then mapped on M_1-PSK symbols, with M_1 an integer power of 2, yielding a frame of $K = B/\log_2 M_1$ symbols, represented by the vector $\boldsymbol{c}_0$. A PSK constellation is used in order to be able to exploit circular symmetry at the relay and at the receiver side. The mapped symbols are broadcast by the source in the first timeslot. These symbols are received by both the destination and the relay. At the relay, the received samples are quantized using the quantization scheme to be discussed in the next section, and the output of the quantizer is broadcast to the destination in the second timeslot. The destination subsequently combines the signal received from the source and the signal received from the relay in order to retrieve the information sent by the source.

Using the definitions from section 4.2, the channel outputs can be written as

$$\begin{aligned} \boldsymbol{r}_0 &= \sqrt{E_0} h_0 \boldsymbol{c}_0 + \boldsymbol{n}_0 \\ \boldsymbol{r}_1 &= \sqrt{E_0} h_1 \boldsymbol{c}_0 + \boldsymbol{n}_1 \\ \boldsymbol{r}_2 &= \sqrt{E_r} h_2 \boldsymbol{c}_r + \boldsymbol{n}_2. \end{aligned} \tag{5.1}$$

All channel coefficients have a Zero Mean Circular Symmetric Complex Gaussian (ZMCSCG) distribution with variance $N_{h_i} = 1/{d_i}^n$, with d_i the distance between the two terminals involved ($i \in \{0, 1, 2\}$) and n the path-loss exponent; this implies a channel gain normalization yielding $\mathbb{E}[|h_i|^2] = 1$ for $d_i = 1$. The elements of the vector $\boldsymbol{n}_i$ are also ZMCSCG distributed with variance N_i ($i \in \{0, 1, 2\}$). The vector $\boldsymbol{c}_r$ represents the symbols transmitted by the relay, which depend on the output of the quantizer, as explained in the next section. The total energy needed to transmit one information bit from the source to the destination, denoted as E_b, is proportional to E_0 and E_r, and is given by:

$$E_b = \frac{(E_0 + E_r)}{\lambda \log_2(M_1)}. \tag{5.2}$$

5.2 Quantization Scheme

At the relay, the phase of the signal received from the source is quantized uniformly using $\log_2 M_2$ bits. In order to be able to exploit circular symmetry at the relay, we impose that M_2 is a multiple of M_1. We first introduce the quantization function $f_Q(x) \in \{0, 1, ..., M_2 - 1\}$, defined as

$$f_Q(x) = \left\lfloor 0.5 + \frac{M_2}{2\pi} \arg(x) \right\rfloor \bmod M_2, \tag{5.3}$$

so that $f_Q(x) = q$ when $\frac{2\pi}{M_2}(q - \frac{1}{2}) \leq \arg(x) < \frac{2\pi}{M_2}(q + \frac{1}{2})$ for $q = 1, 2, ..., M_2 - 1$, and $f_Q(x) = 0$ when $0 \leq \arg(x) < \frac{\pi}{M_2}$ or $2\pi - \frac{\pi}{M_2} \leq \arg(x) < 2\pi$. This is represented graphically in Fig. 5.2 for $M_2 = 4$.

Using (5.3), the quantizer output $q_1(k)$ corresponding to the k-th element of $\boldsymbol{r}_1$ is equal to

$$q_1(k) = f_q(r_1(k)). \tag{5.4}$$

This quantizer output is then mapped on M_2-PSK symbols using the mapping function $\chi_{M_x}(y)$, defined as

$$\chi_{M_x}(y) = \exp\left(\frac{j2\pi y}{M_x}\right), \tag{5.5}$$

yielding the symbols $\boldsymbol{c}_r$ transmitted by the relay in the second timeslot:

$$c_r(k) = \chi_{M_2}(q_1(k)). \tag{5.6}$$

5.3 Detection

At the destination, two signals related to the information from the source are received, one from the source terminal itself and one from the relay terminal.

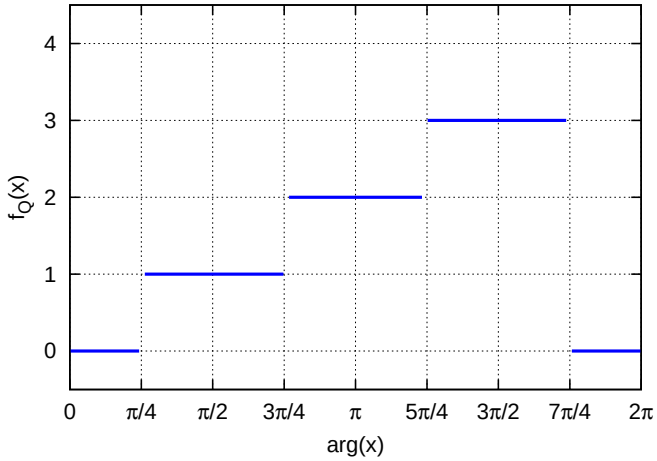

Figure 5.2: Graphic representation of the quantization function $f_Q(x)$.

By calculating the likelihood of the symbols sent by the source, the received information can be decoded at the destination using factor graph based MAP decoding. Taking into consideration that the noise contributions $\boldsymbol{n}_0$ and $\boldsymbol{n}_2$ in 5.1 are statistically independent, this likelihood is equal to

$$p(\boldsymbol{r}_0, \boldsymbol{r}_2 \mid \boldsymbol{c}_0) = p(\boldsymbol{r}_0 \mid \boldsymbol{c}_0) p(\boldsymbol{r}_2 \mid \boldsymbol{c}_0). \tag{5.7}$$

The dependence of symbol likelihoods on the channel parameters is not explicitly noted, as the latter are considered to be known to the destination. Evaluating (5.7) on a symbol-by-symbol basis and conditioning on the symbols sent by the relay yields

$$p(\boldsymbol{r}_0, \boldsymbol{r}_2 \mid \boldsymbol{c}_0) = \prod_{k=1}^{K} p(r_0(k) \mid c_0(k)) \sum_{c_r(k)} p(r_2(k) \mid c_r(k)) p(c_r(k) \mid c_0(k)), \tag{5.8}$$

where the summation runs over all M_2-PSK values $c_r(k)$ can adopt. Taking into consideration the flat Rayleigh fading channel model, $p(r_0(k) \mid c_0(k))$ and $p(r_2(k) \mid c_r(k))$ can be written as

$$p(r_0(k) \mid c_0(k)) = \frac{1}{\pi N_0} \exp\left(-\frac{|r_0(k) - \sqrt{E_0} h_0 c_0(k)|^2}{N_0} \right) \tag{5.9}$$

$$p(r_2(k) \mid c_r(k)) = \frac{1}{\pi N_2} \exp\left(-\frac{|r_2(k) - \sqrt{E_0} h_2 c_r(k)|^2}{N_2} \right). \tag{5.10}$$

The discrete probabilities $P\left[c_r(k) = \chi_{M_2}(q) \mid c_0(k)\right]$ from (5.8), further on referred to as the transition probabilities, are calculated by noting that $c_r(k) = \chi_{M_2}(q)$ only if $f_Q(r_1(k)) = q$ so that

$$P\left[c_r(k) = \chi_{M_2}(q) \mid c_0(k)\right] = P\left[q_1(k) = q \mid c_0(k)\right]. \tag{5.11}$$

An expression for $P\left[q_1(k) = q \mid c_0(k)\right]$ is found using the phase density function $f_\Theta(\theta, \gamma)$, defined as [78]

$$f_\Theta(\theta;\gamma) = \frac{1}{2\pi}\left[e^{-\gamma} + \sqrt{\pi\gamma}\cos(\theta)e^{-\gamma\sin^2(\theta)}\text{erfc}(-\sqrt{\gamma}\cos(\theta))\right]. \tag{5.12}$$

This function describes the distribution of the received phase when a symbol with phase 0 is sent over an AWGN channel. The variable γ is the instantaneous SNR ratio at the receiving terminal, in this case the relay, yielding $\gamma = \frac{E_0|h_1|^2}{N_1}$. Centering $f_\Theta(\theta, \gamma)$ around $\arg(h_1 c_0(k))$ and integrating between the quantization borders corresponding to the quantization interval q yields

$$P\left[q_1(k) = q \mid c_0(k)\right] = \int_{\frac{2\pi q - \frac{1}{2}}{M_2}}^{\frac{2\pi q + \frac{1}{2}}{M_2}} f_\Theta\left(\theta - \arg(h_1 c_0(k)); \frac{E_0|h_1|^2}{N_1}\right) \mathrm{d}\theta, \tag{5.13}$$

concluding the calculation of the symbol likelihoods.

5.4 Performance Evaluation

The performance of the QF protocol described is analyzed by studying the word error rate (WER) for various E_b/N_0 ratios using Monte Carlo [96] simulations. At the source, frames consisting of 1024 information bits are coded by means of a $(1, 13/15)_8$ recursive systematic convolutional turbo code punctured to rate 2/3, whereafter the coded bits are mapped on BPSK ($M_1 = 2$) symbols that are broadcast by the source in the first timeslot. The distance between the source and the destination is considered unity, and the relay is located halfway on a line connecting the source and destination terminals. The path-loss exponent n is equal to 4 and the symbol transmit energy of the source and relay are both equal to 1 ($E_0 = E_r = 1$). All noise variances are considered to be equal ($N_0 = N_1 = N_2$).

By analyzing QF systems with different M_2 values, the impact of the number of quantization bits on the WER performance is determined. The QF system is also compared to an AF system, in which there is no quantization at the relay. By choosing the gain β in (4.3) equal to $\frac{1}{\sqrt{E_0|h_1|^2+N_1}}$, the behavior of the AF system at high SNR corresponds to that of a QF system in which $M_2 = \infty$. Therefore, the WER of this AF system is a lower bound on the WER of the considered QF protocol.

Fig. 5.3 displays the WER performance of the QF system with $M_2 = 2$, $M_2 = 4$ and $M_2 = 8$. The performance of the AF system is also plotted, together with that of a non-cooperative system. In order to obtain a fair comparison between the non-cooperative and cooperative systems, in the non-cooperative system the second time slot is used to transmit extra parity bits.

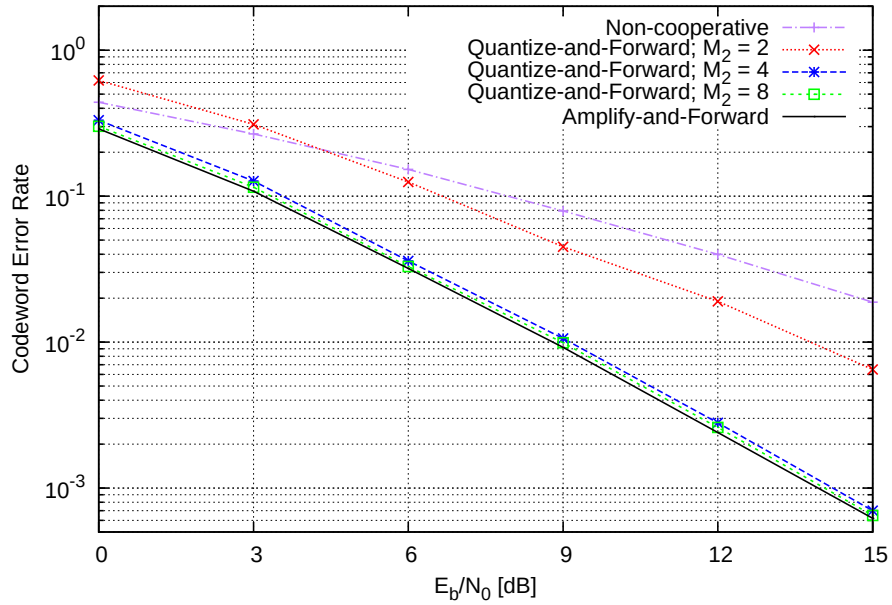

Figure 5.3: WER performance as function of the E_b/N_0 ratio for various configurations of the QF protocol.

To this purpose, the turbo code is not punctured, yielding a code rate of $1/3$. The figure shows that in order to achieve a WER performance that is close to that of AF, a minimum of 2 quantization bits ($M_2 = 4$) are needed at the relay to quantize the data received from the source. Using more than 2 quantization bits yields only a marginal gain in WER performance, which does not outweigh the increase in relay complexity. The reader is referred to [78] for WER results pertaining to PSK constellations with $M_1 > 2$. As a general rule, WER results close to those of the AF protocol are achieved if $M_2 \geq 2M_1$. Due to their increased diversity, all cooperative systems outperform the non-cooperative system at high E_b/N_0 ratios.

6

Relay-side Estimation of the Source-Relay Channel Gain

In the previous chapter, the QF protocol has been introduced and its performance analyzed under the assumption that all channel parameters are known to the destination terminal. In a real-life situation, these parameters are not known and need to be estimated. At the destination, estimates of the source-destination, relay-destination and source-relay channels are needed, in order to be able to decode the received symbols. However, because the destination is not connected to the source-relay channel, obtaining an accurate estimate of this channel is difficult. This problem is solved by introducing a novel quantization scheme, which greatly facilitates channel parameter estimation, without introducing a too large increase in computational complexity at the relay.

In the proposed quantization scheme, the relay first makes a coarse estimate of the source-relay channel gain based on pilot symbols received from

the source. This estimate is used to compensate for the channel rotation caused by this channel, before quantizing the received signal. As will be shown, the proposed protocol requires only $\log_2 M_1$ bits for the quantization of each symbol (as opposed to $\log_2 M_1 + 1$ bits required by the QF system described in chapter 5) to achieve a performance similar to that of an AF system. In addition to estimating and compensating for the source-relay channel rotation, the relay also makes an estimate of the SNR on the source-relay channel and forwards this estimate to the destination using a limited number of symbols. The latter uses this information in order to properly combine the signals received from the source and relay terminals.

At the destination, pilot-based estimates of the source-relay and relay-destination channel coefficients and noise variances are obtained using the received pilot symbols. These pilot-based estimates are then refined using the expectation maximization (EM) algorithm, introduced in section 2.1. Using the refined estimates and the information on the source-relay channel SNR, the received symbols can be decoded in order to retrieve the information bits sent by the source.

The outline of this chapter is as follows: In section 6.1 the system model is introduced and the structure of the relay is discussed, including the novel quantization scheme. The decoder structure at the destination is presented in section 6.2. In section 6.3, the estimation of the unknown channel parameters is tackled, whereafter the performance of the obtained estimation algorithms is studied using Monte Carlo [96] simulations in section 6.4.

6.1 System Model

The cooperative model used throughout this chapter consists of a source transmitting information to a destination, assisted by a single relay operating in half-duplex mode as shown in Fig. 5.1 of the previous chapter. At the source, blocks of A information bits are encoded into blocks of B coded bits which are then mapped on K M_1-PSK symbols, with M_1 an integer power of 2. In a first timeslot, the source transmits K_p pilot symbols along with the K coded data symbols, which are received by both the relay and the destination. These pilot symbols are used for estimating the source-destination channel state (at the destination) and the source-relay channel state (at the relay). In a second timeslot, the relay sends to the destination K_p pilot symbols followed by K M_2-PSK symbols corresponding to a quantized version of the noisy K coded symbols received from the source. The pilot symbols sent by the relay are used at the destination to estimate the relay-destination channel state. The relay also sends to the destination an estimate of the instantaneous signal-to-noise ratio (SNR) on the source-relay channel, using K_γ M_2-PSK coded

symbols. This SNR ratio is needed at the destination for properly combining the signals received from the relay and from the source. The destination combines the data symbols received during both timeslots in order to detect the information bits sent by the source.

6.1.1 Communication Channels

The communication channels involved are modelled as independent flat Rayleigh fading channels with AWGN. No frequency mismatch is present. The source-destination, source-relay and relay-destination channel coefficients are denoted h_0, h_1 and h_2, respectively. Considering the channel model, the output of the different channels can be written as

$$\begin{aligned} \boldsymbol{r}_0 &= \sqrt{E_0} h_0 \boldsymbol{c}_0 + \boldsymbol{n}_0 \\ \boldsymbol{r}_1 &= \sqrt{E_0} h_1 \boldsymbol{c}_0 + \boldsymbol{n}_1 \\ \boldsymbol{r}_2 &= \sqrt{E_r} h_2 \boldsymbol{c}_r + \boldsymbol{n}_2. \end{aligned} \tag{6.1}$$

All channel coefficients have a ZMCSCG distribution with variance $N_{h_i} = 1/{d_i}^n$, with d_i the distance between the two terminals involved ($i = 0, 1, 2$) and n the path loss exponent. The elements of the vector $\boldsymbol{n}_i$ are also ZMCSCG distributed with variance N_i ($i = 0, 1, 2$). In the remainder of this chapter, the suffix p in the subscript of a vector will be used to denote the part of that vector that corresponds to the pilot symbol positions.

Because the pilot symbols transmitted by the source and relay need to be known by the destination, they cannot be used to transfer useful data from the source to the destination. Together with the K_γ symbols used to forward the SNR estimate of the source-relay channel to the destination, they are considered estimation overhead. At the source and relay, K_p and $K_p + K_\gamma$ overhead symbols are added, respectively. Using E_b to denote the total energy needed to transmit one bit of information from the source to the destination, we obtain the following expression for E_b expressed in terms of E_0 and E_r:

$$E_b = \frac{1}{\lambda \log_2(M_1)} \left(E_0 \frac{(K + K_p)}{K} + E_r \frac{(K + K_p + K_\gamma)}{K} \right). \tag{6.2}$$

For a fixed E_b value, less energy is available for the transmission of the data symbols compared to the situation in which no estimation overhead is present. Indeed, comparing (6.2) to (5.2) under the assumption that $E_0 = E_r$, it can be seen that for a fixed value of E_b, the symbol transmit energy is reduced by a factor ζ_{loss} equal to

$$\zeta_{\text{loss}} = \frac{2K}{2K + 2K_p + K_\gamma} < 1, \tag{6.3}$$

due to the addition of the estimation overhead symbols.

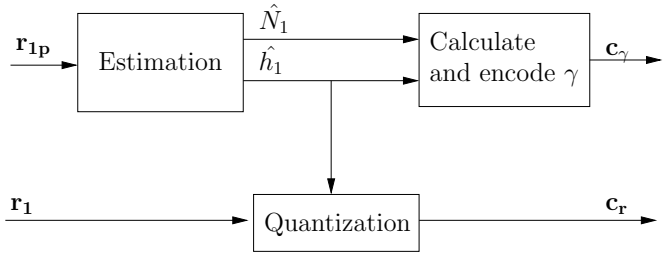

Figure 6.1: Schematic representation of the operations performed by the relay terminal.

6.1.2 Structure of the Relay Terminal

We propose a relay that compensates for the channel rotation caused by the source-relay channel, before quantizing the received signal. In order to perform this compensation, the source-relay channel first needs to be estimated using the pilot symbols sent by the source. Using the notation $\hat{h_1}$ to denote an estimate of the source-relay channel coefficient, the k-th data symbol transmitted by the relay can be written as

$$c_r(k) = \chi_{M_2}(q_1(k)), \tag{6.4}$$

with

$$q_1(k) = f_q\left(r_1(k)\hat{h_1}^*\right) \tag{6.5}$$

and the functions f_q and χ_{M_2} defined in (5.3) and (5.5), respectively.

Using this quantization scheme, the destination will only be required to know the instantaneous SNR on the source-relay channel, given by

$$\gamma = E_0|h_1|^2/N_1, \tag{6.6}$$

rather than h_1 and N_1 individually, as will be proven in the next subsection. This instantaneous SNR is estimated by the relay, quantized, encoded, mapped to M_2-PSK symbols and forwarded to the destination. The resulting structure of the relay terminal is represented schematically in Fig. 6.1.

Instead of compensating for the channel rotation caused by the source-relay channel, an estimate of it could be sent to the destination, along with the estimate of the SNR on the source-relay channel. However, the quantization of the channel rotation is more complex than the quantization of the instantaneous SNR. While a coarse quantization is sufficient for the latter, a much more accurate quantization is required for the former. Even though this could be achieved by quantizing the channel rotation estimate using a large number

of bits or by using a logarithmic quantization scheme, it would significantly increase the complexity of the relay terminal. Therefore, it is beneficial to compensate for the channel rotation of the source-relay channel at the relay, instead of forwarding its estimate to the destination.

Furthermore, when compensating for the channel rotation at the relay, we will show that the data symbols can be quantized with $\log_2 M_2 = \log_2 M_1$ bits, which is one bit less as compared to when no compensation is used. This further lowers the complexity of the relay terminal.

6.1.3 Calculation and Encoding of the Instantaneous SNR

As stated in section 6.1.2, the relay needs to forward to the destination an estimate of the instantaneous SNR on the source-relay channel, denoted as $\hat{\gamma}$. This estimate is calculated at the relay using the estimates of h_1 and N_1:

$$\hat{\gamma} = \frac{E_0 |\hat{h_1}|^2}{\hat{N_1}}. \tag{6.7}$$

In a Rayleigh fading environment, $\hat{\gamma}$ has a large dynamic range. In order to efficiently quantize $\hat{\gamma}$, its dynamic range is first clipped to the interval $[\gamma_{\min}, \gamma_{\max}]$. The optimal values of $\gamma_{\min}$ and $\gamma_{\max}$ are determined in section 6.4.2.2. After clipping, the base-10 logarithm of $\hat{\gamma}$ is quantized uniformly using γ_q bits. These bits are subsequently encoded with a simple $(1, 3)_8$ convolutional code, mapped on M_2-PSK symbols and sent to the destination in the second timeslot.

6.2 Detection

In order to retrieve the information sent by the source, the destination needs to calculate the likelihood of the symbols received in the first and second timeslot. This was outlined in section 5.3 for a system in which all parameters are known to the destination. This section will discuss the calculation of the symbol likelihoods for the system at hand with an emphasis on the specific aspects caused by the assumption of unknown channel parameters. The reader is encouraged to first consult section 5.3 for a better understanding of the results presented here.

Introducing $\boldsymbol{h} = \{h_0, h_1, h_2\}$ and $\boldsymbol{N} = \{N_0, N_1, N_2\}$, the likelihoods of the symbols sent by the source are equal to

$$p\left(\boldsymbol{r}_0, \boldsymbol{r}_2 \mid \boldsymbol{c}_0, \boldsymbol{h}, \boldsymbol{N}\right) = p\left(\boldsymbol{r}_0 \mid c_0, h_0, N_0\right) p\left(\boldsymbol{r}_2 \mid c_0, h_1, h_2, N_1, N_2\right). \tag{6.8}$$

The first factor of (6.8) can be written as

$$p\left(\boldsymbol{r}_0 \mid c_0, h_0, N_0\right) = \prod_{k=1}^{K} p\left(r_0(k) \mid c_0(k), h_0, N_0\right), \tag{6.9}$$

with

$$p(r_0(k) \mid c_0(k), h_0, N_0) = \frac{1}{\pi N_0} \exp\left(\frac{-|r_0(k) - \sqrt{E_0} h_0 c_0(k)|^2}{N_0}\right). \tag{6.10}$$

The second factor from (6.8) is obtained by conditioning on the symbol vector $\boldsymbol{c}_r$, transmitted by the relay, and by noting that the latter depends on the estimate $\hat{h_1}$, that is used at the relay to compensate for the channel rotation of the source-relay channel, yielding

$$\begin{aligned} p\left(\boldsymbol{r}_2 \mid c_0, h_1, h_2, N_1, N_2\right) &= \sum_{\boldsymbol{c}_r} p\left(\boldsymbol{r}_2 \mid \boldsymbol{c}_r, h_2, N_2\right) p\left(\boldsymbol{c}_r \mid \boldsymbol{c}_0, h_1, N_1\right) \\ &= \sum_{\boldsymbol{c}_r} p\left(\boldsymbol{r}_2 \mid \boldsymbol{c}_r, h_2, N_2\right) \int p\left(\boldsymbol{c}_r, \hat{h_1} \mid \boldsymbol{c}_0, h_1, N_1\right) \mathrm{d}\hat{h_1} \\ &= \sum_{\boldsymbol{c}_r} p\left(\boldsymbol{r}_2 \mid \boldsymbol{c}_r, h_2, N_2\right) \int p\left(\boldsymbol{c}_r \mid \hat{h_1}, \boldsymbol{c}_0, h_1, N_1\right) p\left(\hat{h_1} \mid \boldsymbol{c}_0, h_1, N_1\right) \mathrm{d}\hat{h_1}. \end{aligned} \tag{6.11}$$

where the summation runs over all values $\boldsymbol{c}_r$ can adopt. The first factor from (6.11) can be written as

$$p\left(\boldsymbol{r}_2 \mid \boldsymbol{c}_r, h_2, N_2\right) = \prod_{k=1}^{K} p\left(r_2(k) \mid c_r(k), h_2, N_2\right), \tag{6.12}$$

with

$$p(r_2(k) \mid c_r(k), h_2, N_2) = \frac{1}{\pi N_2} \exp\left(\frac{-|r_2(k) - \sqrt{E_0} h_2 c_r(k)|^2}{N_2}\right). \tag{6.13}$$

Taking into account that $p\left(\boldsymbol{c}_r \mid \hat{h_1}, \boldsymbol{c}_0, h_1, N_1\right)$ from (6.11) can be written as

$$p\left(\boldsymbol{c}_r \mid \hat{h_1}, \boldsymbol{c}_0, h_1, N_1\right) = \prod_{k=1}^{K} p\left(c_r(k) \mid \hat{h_1}, c_0(k), h_1, N_1\right), \tag{6.14}$$

and taking into consideration (6.12), (6.11) can be expressed as

$$\begin{aligned} &p\left(\boldsymbol{r}_2 \mid c_0, h_1, h_2, N_1, N_2\right) \\ &= \int \prod_{k=1}^{K} \left(\sum_{c_r(k)} p(r_2(k) \mid c_r(k), h_2, N_2) p\left(c_r(k) \mid \hat{h_1}, c_0(k), h_1, N_1\right) \right) \\ &\qquad .p\left(\hat{h_1} \mid \boldsymbol{c}_0, h_1, N_1\right) \mathrm{d}\hat{h_1}. \end{aligned} \tag{6.15}$$

The factor $p\left(c_r(k) \mid \hat{h_1}, c_0(k), h_1, N_1\right)$ from (6.15) is found using the phase density function $f_\Theta(\theta, \gamma)$ from (5.12) yielding

$$P\left[c_r(k) = \chi_{M_2}(q) \mid \hat{h_1}, c_0(k), h_1, N_1\right] = \int_{\frac{2\pi q - \frac{1}{2}}{M_2}}^{\frac{2\pi q + \frac{1}{2}}{M_2}} f_\Theta\left(\theta - \arg(c_0(k) h_1 \hat{h_1}^*); \gamma\right) \mathrm{d}\theta, \tag{6.16}$$

while the factor $p\left(\hat{h_1} \mid \boldsymbol{c}_0, h_1, N_1\right)$ from (6.15) depends on the criterion for estimating h_1 at the relay.

The destination knows the estimation criterion for calculating $\hat{h}_1$, making it possible to calculate the density function $p\left(\hat{h_1} \mid c_0(k), h_1, N_1\right)$ and evaluate (6.15) by means of numerical integration. After integrating out $\hat{h_1}$, the resulting likelihood of $\boldsymbol{r}_2$ from (6.15) still contains the channel parameters h_1, h_2, γ and N_2, while the likelihood of $\boldsymbol{r}_0$ from (6.9) contains the channel parameters h_0 and N_0. As these parameters are not known at the destination, the likelihoods will be computed at the destination with the true channel parameters replaced by estimates. The channel gains h_0 and h_2 and noise variances N_0 and N_2 are estimated at the destination, while estimates of h_1 and γ, computed by the relay, could be sent from the relay to the destination to be used by the latter instead of the actual values of h_1 and γ. While this approach is theoretically possible, it considerably increases the complexity of the destination, compared to the case where the channels are known to the destination.

To avoid these difficulties, the destination will use the simplifying assumption that the relay makes a perfect estimate of h_1, so that

$$p(\hat{h_1} \mid \boldsymbol{c}_0, h_1, N_1) \approx \delta(\hat{h_1} - h_1). \tag{6.17}$$

Using (6.17), (6.15) can be written as

$$\begin{aligned} &p\left(\boldsymbol{r}_2 \mid c_0, h_1, h_2, N_1, N_2\right) \\ &\quad \approx \prod_{k=1}^{K} \sum_{c_r(k)} p(r_2(k) \mid c_r(k), h_2, N_2) p\left(c_r(k) \mid \hat{h_1} = h_1, h_1, c_0(k), N_1\right). \end{aligned} \tag{6.18}$$

The second factor from (6.18) can further be simplified, yielding

$$p\left(c_r(k) \mid \hat{h_1} = h_1, h_1, c_0(k), N_1\right) = P\left[c_r(k) = \chi_{M_2}(q) \mid \hat{h_1} = h_1, h_1, c_0(k), N_1\right] \quad \text{with } q \in \{0, 1, ..., M_2 - 1\}$$

$$= \int_{\frac{2\pi q - \frac{1}{2}}{M_2}}^{\frac{2\pi q + \frac{1}{2}}{M_2}} f_\Theta\left(\theta - \arg(c_0(k) h_1 h_1^*); \gamma\right) \mathrm{d}\theta$$

$$= \int_{\frac{2\pi q - \frac{1}{2}}{M_2}}^{\frac{2\pi q + \frac{1}{2}}{M_2}} f_\Theta\left(\theta - \arg(c_0(k)); \gamma\right) \mathrm{d}\theta$$

$$= P\left[c_r(k) = \chi_{M_2}(q) \mid c_0(k), \gamma\right]. \tag{6.19}$$

As a result, as far as the source-relay channel is concerned, only the value γ now needs to be known by the destination; a coarse estimate of γ is sent from the relay to the destination.

It is shown in Appendix 6.6 that the approximation made in (6.17) holds for high instantaneous SNR values on the source-relay channel. Although a significant error is made at low instantaneous SNR values, it does not significantly affect the error performance. As the value of γ approaches zero, $P\left[c_r(k) = \chi_{M_2}(q) \mid c_0(k), \gamma\right]$ from (6.19) approaches a uniform distribution, reducing (6.8) to

$$p\left(\boldsymbol{r}_0, \boldsymbol{r}_2 \mid \boldsymbol{c}_0, \boldsymbol{h}, \boldsymbol{N}\right) = \prod_{k=1}^{K} p\left(r_0(k) \mid c_0(k), h_0, N_0\right) \sum_{c_r(k)} p\left(r_2(k) \mid c_r(k), h_2, N_2\right) \frac{1}{M_2}. \tag{6.20}$$

Because the summation from (6.20) no longer depends on $c_0(k)$, it can be discarded. The likelihood of the k-th received source symbol is now calculated using only the source-destination path and is thus not influenced by the invalid approximation (6.17) regarding the channel coefficient estimate of the source-relay channel. This results in a very robust system: with decreasing values of γ, the error caused by the assumption made in (6.17) increases, but the impact this approximation has on the error performance decreases. This will also be verified in section 6.4.3.1 using Monte Carlo simulations.

6.3 Channel Parameter Estimation

In order to be able to transmit information from the source to the destination, the unknown channel parameters first need to be estimated at the relay and at the destination. At the relay, the source-relay channel gain and

noise variance need to be estimated in order compensate for the source-relay channel rotation and to calculate an estimate of the instantaneous SNR γ. At the destination, the source-destination and relay-destination channel gain and noise variances need to be estimated in order to be able to calculate the symbol likelihoods from section 6.2.

To initiate the estimation process, both the source and the relay transmit a limited number of pilot symbols. These pilot symbols are transmitted along with the data symbols and are known to the receiving terminals, allowing the latter to calculate initial estimates of the unknown channel parameters. The quality of these pilot-based estimates improves as the number of pilot symbols is increased. However, as shown by (6.2), adding pilot symbols to a frame reduces the amount of energy available for the data symbols, so that the number of pilot symbols should be limited to a small fraction of the number of data symbols. This contradiction can be overcome with the use of the EM algorithm discussed in section 2.1, which also exploits the presence of the unknown data symbols when calculating an estimate of an unknown parameter. This allows improving the pilot-based estimates without transmitting additional pilot symbols.

As will be shown later on, each EM iteration requires the knowledge of the a posteriori symbol expectation of the data symbols conditioned on the estimates obtained in the previous iteration, requiring a decoding operation for each EM iteration. This would significantly increase the complexity of the relay terminal, should the EM algorithm be used to refine the pilot-based estimates of the source-relay channel parameters. Furthermore, it would also require the relay to store the unquantized samples of the signal received from the source, in order to be able to quantize it with the refined channel gain estimate, thus defeating the purpose of using the QF protocol in the first place. Therefore, the pilot-based estimates calculated at the relay will not be refined using the EM algorithm. It will be shown in section 6.4.3.1 that this approach has only a small impact on the error performance.

6.3.1 Pilot-based Estimation

6.3.1.1 Relay-side Estimation of h_1 and N_1

At the relay, the unknown parameters of the source-relay channel need to be estimated. This estimation is performed using pilot symbols sent by the source. The ML estimate of the source-relay channel parameters satisfies the following relationship:

$$(\hat{h_1}, \hat{N_1}) = \arg \max_{(h_1, N_1)} p(\boldsymbol{r}_{1p} \mid \boldsymbol{c}_{0p}, h_1, N_1), \tag{6.21}$$

with

$$p(\boldsymbol{r}_{1p}(k) \mid \boldsymbol{c}_{0p}(k), h_1, N_1) = \frac{1}{(\pi N_1)^{K_p}} \exp\left(\frac{-|\boldsymbol{r}_{1p} - \sqrt{E_0} h_1 \boldsymbol{c}_{0p}|^2}{N_1}\right). \quad (6.22)$$

It is shown in Appendix 6.7 that the following expressions for $\hat{h_1}$ and N_1 satisfy (6.22):

$$\hat{h}_1 = \frac{\boldsymbol{r}_{1p}\boldsymbol{c}_{0p}^H}{\sqrt{E_0}K_p} \quad (6.23)$$

$$\hat{N_1} = \frac{|\boldsymbol{r}_{1p} - \sqrt{E_0}\hat{h}_1\boldsymbol{c}_{0p}|^2}{K_p}. \quad (6.24)$$

The relay uses the estimate $\hat{h}_1$ to compensate for the channel rotation of the source-relay channel, while the estimate of N_1 is used together with $\hat{h}_1$ in (6.7) to compute an estimate of the instantaneous SNR on the source-relay channel.

6.3.1.2 Destination-side Estimation of h_0,N_0,h_2 and N_2

Pilot-based estimates of the channel gains h_0 and h_2 and of the noise variances N_0 and N_2 are obtained at the destination terminal. The pilot symbols transmitted by the source are used to calculate an estimate of h_0 and N_0, while the pilot symbols transmitted by the relay are used to calculate an estimate of h_2 and N_2:

$$(\hat{h_0}, \hat{N_0}) = \arg\max_{h_0, N_0} p(\boldsymbol{r}_{0p} \mid \boldsymbol{c}_{0p}, h_0, N_0) \quad (6.25)$$

$$(\hat{h_2}, \hat{N_2}) = \arg\max_{h_2, N_2} p(\boldsymbol{r}_{2p} \mid \boldsymbol{c}_{rp}, h_2, N_2). \quad (6.26)$$

Considering the similarity between (6.25), (6.26) and (6.21), the results from Appendix 6.7 can be used to solve (6.25) and (6.26), yielding

$$\hat{h}_0 = \frac{\boldsymbol{r}_{0p}\boldsymbol{c}_{0p}^H}{\sqrt{E_0}K_p} \quad (6.27)$$

$$\hat{N_0} = \frac{|\boldsymbol{r}_{0p} - \sqrt{E_0}\hat{h}_0\boldsymbol{c}_{0p}|^2}{K_p} \quad (6.28)$$

and

$$\hat{h}_2 = \frac{\boldsymbol{r}_{2p}\boldsymbol{c}_{rp}^H}{\sqrt{E_r}K_p} \quad (6.29)$$

$$\hat{N_2} = \frac{|\boldsymbol{r}_{2p} - \sqrt{E_r}\hat{h}_2\boldsymbol{c}_{rp}|^2}{K_p}, \quad (6.30)$$

respectively.

6.3.1.3 Remarks Concerning the Noise Variance Estimation

When calculating a noise variance estimate using (6.24), (6.28) or (6.30), the obtained estimate is biased by a factor $(K_p - 1)/K_p$, as shown in Appendix 6.8 for $\hat{N}_0$. Especially when using a small number of pilot symbols, it is important to compensate for this bias by multiplying the estimate with $K_p/(K_p - 1)$, yielding an unbiased estimated denoted $\hat{\hat{N}}_i$:

$$\hat{\hat{N}}_i = \hat{N}_i \frac{K_p}{K_p - 1} \quad , i \in \{0, 1, 2\}. \tag{6.31}$$

Further, it can be advantageous to average the noise variance estimates over consecutive frames, because the noise variance tends to fluctuate much more slowly than the channel gain. This can be achieved by storing a running average, denoted $N_{i,\text{avg}}$, that is updated each time a new noise variance estimate is available:

$$N_{i,\text{avg}} = \xi N_{i,\text{avg}} + (1 - \xi)\hat{\hat{N}}_i \quad , i \in \{0, 1, 2\}. \tag{6.32}$$

The averaged estimates are subsequently used in (6.7) for the calculation of $\hat{\gamma}$ and at the destination for the calculation of the symbol likelihoods. The weighting factor ξ lies between 0 and 1 and depends on the expected speed of fluctuation of the noise variance.

6.3.1.4 Remarks Concerning the Channel Gain Estimation

The pilot-based estimates of the channel coefficients h_0, h_1 and h_2 are unbiased, as shown below for h_0:

$$\mathbb{E}\left[\hat{h}_0\right] = \mathbb{E}\left[\frac{\boldsymbol{r}_{0p}\boldsymbol{c}_{0p}^H}{\sqrt{E_0}K_p}\right] = \mathbb{E}\left[h_0 + \frac{\boldsymbol{n}_{0p}\boldsymbol{c}_{0p}^H}{\sqrt{E_0}K_p}\right] = h_0 \tag{6.33}$$

A similar reasoning holds for h_1 and h_2.

Likewise, the MSE of $\hat{h_0}$ is also easily obtained:

$$\mathbb{E}\left[|\hat{h_0} - h_0|^2\right] = \mathbb{E}\left[\left|\frac{\boldsymbol{r}_{0p}\boldsymbol{c}_{0p}^H}{\sqrt{E_0}K_p} - h_0\right|^2\right] = \mathbb{E}\left[\left|\frac{\boldsymbol{n}_{0p}\boldsymbol{c}_{0p}^H}{\sqrt{E_0}K_p}\right|^2\right] = \frac{N_0}{E_0 K_p}, \tag{6.34}$$

where in the last step the statistical independence of the noise samples, described in (6.63), was used. A similar result is obtained for the estimates of h_1 and h_2.

6.3.2 Code-aided Estimation at the Destination Terminal

The channel coefficient estimates discussed in the previous section are solely based on the pilot symbols which represent only a small part of the received signal energy. In order to improve these estimates, the EM algorithm is used. The EM algorithm is an iterative algorithm that alternates between an estimation step and a maximization step and is described in section 2.1.3. It allows calculating a ML estimate of a set of parameters from an observation that is also influenced by other unknown variables, named nuisance parameters. In this specific case, the source-destination channel coefficient (h_0) and the relay-destination channel coefficient (h_2) are the parameters that need to be estimated, while the symbols sent by the source and relay, denoted $\boldsymbol{c}_0$ and $\boldsymbol{c}_r$, respectively, are considered nuisance parameters. As shown in section 6.4.3.3, there is little to gain in refining the pilot-based estimates of N_0 and N_2. Therefore, only the estimates of h_0 and h_2 will be updated using the EM algorithm.

Introducing $\boldsymbol{r}_d = (\boldsymbol{r}_0, \boldsymbol{r}_2)$, $\boldsymbol{c}_d = (\boldsymbol{c}_0, \boldsymbol{c}_r)$, and $\boldsymbol{h}_d = (h_0, h_2)$, the estimation step during iteration i involves calculating the function

$$Q\left(\boldsymbol{h}_d, \hat{\boldsymbol{h}_d}^{(i-1)}\right) = \mathbb{E}_{\boldsymbol{c}_d}\left[\ln p(\boldsymbol{r}_d, \boldsymbol{c}_d \mid \boldsymbol{h}_d) \mid \boldsymbol{r}_d, \hat{\boldsymbol{h}_d}^{(i-1)}\right]. \tag{6.35}$$

In order not to overload the notation, the dependency of the distributions on the noise variance is not noted explicitly. The maximization step involves determining a value for h_0 and h_2 that maximizes the Q function from (6.35), so the new estimates calculated at iteration k are equal to

$$\hat{\boldsymbol{h}_d}^{(i)} = \arg\max_{\boldsymbol{h}_d} Q\left(\boldsymbol{h}_d, \hat{\boldsymbol{h}_d}^{(i-1)}\right), \tag{6.36}$$

where $\hat{\boldsymbol{h}_d}^{(0)}$ contains the estimate of (h_0, h_2) obtained from the pilot symbols only. As shown in Appendix 6.9, the values of h_0 and h_2 that maximize (6.36) are equal to:

$$\hat{h_0}^{(i)} = \frac{\boldsymbol{r}_0\left(\boldsymbol{u}_0^{(i)}\right)^H}{(K_p + K)\sqrt{E_0}} \tag{6.37}$$

$$\hat{h_2}^{(i)} = \frac{\boldsymbol{r}_2\left(\boldsymbol{u}_r^{(i)}\right)^H}{(K_p + K)\sqrt{E_r}}, \tag{6.38}$$

with $\boldsymbol{u}_0^{(i)}$ and $\boldsymbol{u}_r^{(i)}$ denoting the a posteriori expectations (conditioned on $\boldsymbol{r}_d$ and $\hat{\boldsymbol{h}_d}^{(i-1)}$) of the symbol vectors $\boldsymbol{c}_0$ and $\boldsymbol{c}_r$, respectively.

The components of $\boldsymbol{u}_0^{(i)}$ and $\boldsymbol{u}_r^{(i)}$ that correspond to the pilot symbols are equal to these pilot symbols. The computation of the components of $\boldsymbol{u}_0^{(i)}$ and

$\boldsymbol{u}_r^{(i)}$ that correspond to the data symbols is outlined below. The k-th elements of the vectors $\boldsymbol{u}_0^{(i)}$ and $\boldsymbol{u}_r^{(i)}$ are equal to

$$\begin{aligned} u_0^{(i)}(k) &= \sum_{c_0(k)} \sum_{c_r(k)} c_0(k) p\left(c_0(k), c_r(k) \mid \boldsymbol{r}_d, \hat{\boldsymbol{h}_d}^{(i-1)}\right) \\ &= \sum_{c_0(k)} c_0(k) p\left(c_0(k) \mid \boldsymbol{r}_d, \hat{\boldsymbol{h}_d}^{(i-1)}\right) \end{aligned} \tag{6.39}$$

and

$$\begin{aligned} u_r^{(i)}(k) &= \sum_{c_0(k)} \sum_{c_r(k)} c_r(k) p\left(c_0(k), c_r(k) \mid \boldsymbol{r}_d, \hat{\boldsymbol{h}_d}^{(i-1)}\right) \\ &= \sum_{c_0(k)} \sum_{c_r(k)} c_r(k) p\left(c_r(k) \mid c_0(k), \boldsymbol{r}_d, \hat{\boldsymbol{h}_d}^{(i-1)}\right) p\left(c_0(k) \mid \boldsymbol{r}_d, \hat{\boldsymbol{h}_d}^{(i-1)}\right). \end{aligned} \tag{6.40}$$

The summations in (6.39) and (6.40) run over all values that $c_0(k)$ and/or $c_r(k)$ can adopt. The conditional distribution of $c_r(k)$ in (6.40) can be expressed as

$$\begin{aligned} p\left(c_r(k) \mid c_0(k), \boldsymbol{r}_d, \hat{\boldsymbol{h}_d}^{(i-1)}\right) &= \frac{p\left(c_r(k), r_2(k) \mid c_0(k), \hat{\boldsymbol{h}_d}^{(i-1)}\right)}{p\left(r_2(k) \mid c_0(k), \hat{\boldsymbol{h}_d}^{(i-1)}\right)} \\ &= \frac{p\left(r_2(k) \mid c_r(k), \hat{h_2}^{(i-1)}\right) p\left(c_r(k) \mid c_0(k)\right)}{\sum_{\tilde{c}_r(k)} p\left(r_2(k) \mid \tilde{c}_r(k), \hat{h_2}^{(i-1)}\right) p\left(\tilde{c}_r(k) \mid c_0(k)\right)}. \end{aligned} \tag{6.41}$$

The destination computes $p(c_r(k) \mid c_0(k))$ under the simplifying assumption that the relay makes a perfect estimate of h_1, so that $p(c_r(k) \mid c_0(k))$ is given by (6.19). When evaluating (6.19), the destination substitutes γ by the estimate $\hat{\gamma}$, forwarded by the relay. The marginal a posteriori probabilities of the data symbols $c_0(k)$ can be calculated by the decoder at the destination, therefore, this EM approach is referred to as code-aided.

6.3.2.1 Remarks Concerning the EM Channel Gain Estimation

A simple lower bound on the MSE related to the code-aided estimation of h_0 and h_2 is obtained by assuming that the data symbols transmitted by the source and the relay are known to the destination (i.e., $\boldsymbol{u}_0 = \boldsymbol{c}_0$, $\boldsymbol{u}_r = \boldsymbol{c}_r$). A same reasoning as was used for the pilot-based estimates in (6.34) yields

$$\mathbb{E}[|\hat{h_0} - h_0|^2] \geq \mathbb{E}[|\hat{h_0} - h_0|^2]\Big|_{\boldsymbol{u}_0 = \boldsymbol{c}_0} = \frac{N_0}{(K_p + K)E_0}, \tag{6.42}$$

and similarly for $\mathbb{E}[|\hat{h_2} - h_2|^2]$.

6.4 Performance Evaluation.

In this section, the performance of the QF system discussed is analyzed using different performance metrics. Because it is nearly impossible to obtain closed-form expressions for most performance metrics, numerical simulation techniques are used.

6.4.1 Simulation Parameters

We consider a source that encodes frames of 1024 information bits by means of an $(1, 13/15)_8$ RSCC turbo code that is punctured to a rate of 2/3. After encoding, the coded bits are mapped on M_1-PSK symbols. At the decoder side, 8 iterations are used to decode the turbo code. The code-aided refining is executed using 8 EM iterations. In the code-aided refinement, the EM iterations and turbo decoding iterations are merged as explained in section 3.1.2.3. Using this technique, the increase in complexity introduced by the code-aided estimation process is minimal.

The relay is located halfway between the source and the destination. The path loss exponent equals 4 and the distance between the source and the destination is considered unity. For a given E_b/N_0 ratio, the symbol energy transmitted by the source and relay is computed using (6.2), assuming that $E_0 = E_r$. All noise variances are assumed to be equal ($N_0 = N_1 = N_2$) but will be estimated separately. A factor ξ equal to 0.95 is used in (6.32) for averaging the noise variance estimates. For $M_1 = 2$, $M_1 = 4$ and $M_1 = 8$, 12, 6 and 4 pilot symbols, respectively, are added to the data symbol frames. This approach yields a constant ζ_{loss} in (6.3) and ensures that the estimation overhead uses the same percentage of the total transmit energy, independent of the constellation size. No pilot symbols are transmitted when determining the performance of the reference system, in which the channel parameters are considered to be known.

For the transmission of $\hat{\gamma}$ from the relay to the destination, a total of 3 bits are used to quantize the base-10 logarithm of $\hat{\gamma}$ at the relay, yielding 8 quantization intervals. As explained in section 6.1.3, these bits are subsequently encoded with a simple $(1, 3)_8$ convolutional code and mapped on M_2-PSK symbols.

6.4.2 Known Channel Parameters

In this subsection, the WER performance of the proposed QF protocol is studied under the assumption that the relay and the destination know all relevant channel parameters. While this is an unrealistic assumption, it allows us to

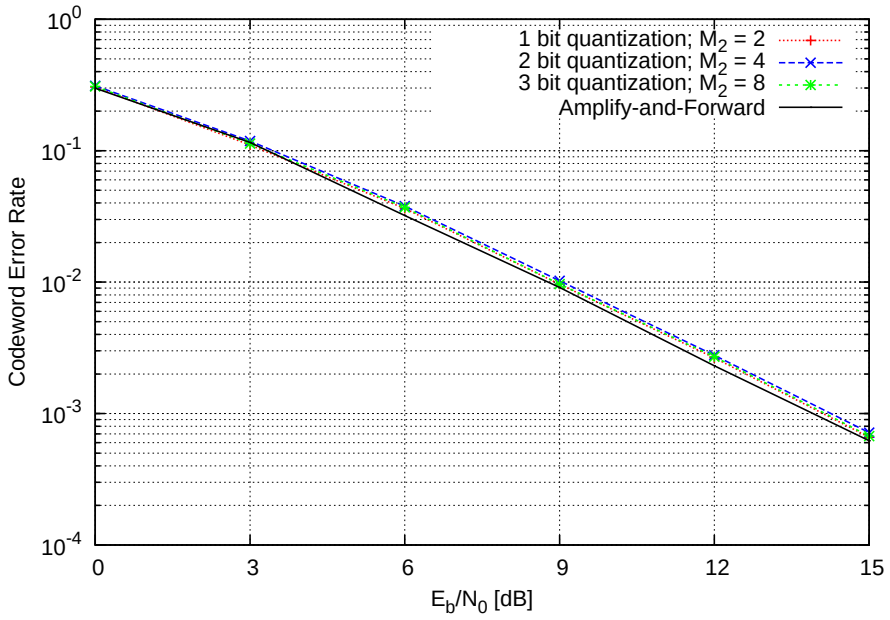

Figure 6.2: WER performance as function of the E_b/N_0 ratio for various number of quantization bits at the relay, using BPSK mapping at the source. The WER performance of the AF protocol is provided for reference.

establish a benchmark for the evaluation of the WER performance of the estimation algorithms.

6.4.2.1 Optimal Number of Quantization Bits

In Fig. 6.2, the number of quantization bits the relay uses to quantize the incoming symbols is varied and the resulting WER performance plotted. A BPSK mapping constellation is used at the source ($M_1 = 2$). Note that the proposed QF protocol closely approaches the performance of AF using only 1 quantization bit ($M_2 = M_1 = 2$).

A careful examination of Fig. 6.2 shows that the best results are obtained when only 1 quantization bit is used. When going from 1 to 2 quantization bits, the WER performance deteriorates, only to improve again when using 3 quantization bits. This is explained by noting that due to the symmetry of

$f_\Theta(\theta;\gamma)$ from (6.19) around $\theta = 0$, the following relationship holds:

$$P\left[c_r(k) = \chi_{M_2}(q) \,|\, c_0(k) = \chi_{M_1}(0), h_1, N_1\right] = P\left[c_r(k) = \chi_{M_2}\left((M_2 - q) \mod M_2\right) \,|\, c_0(k) = \chi_{M_1}(0), h_1, N_1\right], \tag{6.43}$$

for $q \in \{0, 1, ..., M_2 - 1\}$. Additionally, circular symmetry at the relay implies that

$$P\left[c_r(k) = \chi_{M_2}(q) \,|\, c_0(k) = \chi_{M_1}(0), h_1, N_1\right] = P\left[c_r(k) = \chi_{M_2}\left(\left(q + \frac{mM_2}{M_1}\right) \mod M_2\right) \,\middle|\, c_0(k) = \chi_{M_1}(m), h_1, N_1\right], \tag{6.44}$$

for $q \in \{0, 1, ..., M_2 - 1\}$ and $m \in \{0, 1, ..., M_1 - 1\}$. Combining (6.43) and (6.44) and assuming BPSK mapping at the source ($M_1 = 2$) yields

$$P\left[c_r(k) = \chi_{M_2}\left(\frac{M_2}{4}\right) \,\middle|\, c_0(k) = \chi_{M_1}(0), h_1, N_1\right] = P\left[c_r(k) = \chi_{M_2}\left(\frac{M_2}{4}\right) \,\middle|\, c_0(k) = \chi_{M_1}(1), h_1, N_1\right] \tag{6.45}$$

and

$$P\left[c_r(k) = \chi_{M_2}\left(\frac{3M_2}{4}\right) \,\middle|\, c_0(k) = \chi_{M_1}(0), h_1, N_1\right] = P\left[c_r(k) = \chi_{M_2}\left(\frac{3M_2}{4}\right) \,\middle|\, c_0(k) = \chi_{M_1}(1), h_1, N_1\right]. \tag{6.46}$$

This means that for all M_2 values ≥ 4, there are two quantization intervals which do not provide any information on the symbol sent by the source; a symbol that is quantized to one of those intervals has an equal probability to originate from either source constellation point. The size of these quantization intervals decreases with increasing value of M_2, explaining why this effect is less pronounced for $M_2 = 8$ as compared to $M_2 = 4$.

When using QPSK and 8-PSK mapping, we have verified (results not displayed) that quantization with 2 and 3 bits, respectively, is again optimal and yields a WER performance close to that of a pure AF system using the same constellation. Therefore, in the remainder of this chapter, the relay and source will use the same constellation size ($M_2 = M_1$).

6.4.2.2 Optimization of the Dynamic Range of γ

The optimal dynamic range of γ is determined by keeping the E_b/N_0 ratio constant, and varying the values of $\gamma_{\min}$ and $\gamma_{\max}$. A 2-dimensional search is avoided by imposing that $\gamma_{\min} = \frac{1}{\gamma_{\max}}$. In Fig. 6.3, the WER performance of a QF system using BPSK mapping at the source is analyzed for different values of $\gamma_{\max}$ for an E_b/N_0 ratio of 3 and 12 dB.

Considering the y-axis scale, the figure shows that the WER performance of the system is very insensitive to the selected value of $\gamma_{\max}$ (and $\gamma_{\min}$). As is to be expected, a higher E_b/N_0 ratio requires a larger $\gamma_{\max}$ value. However, due to the low sensitivity, a $\gamma_{\max}$ value of 20 dB is selected and will be used in the remainder of this chapter, independently of the E_b/N_0 ratio.

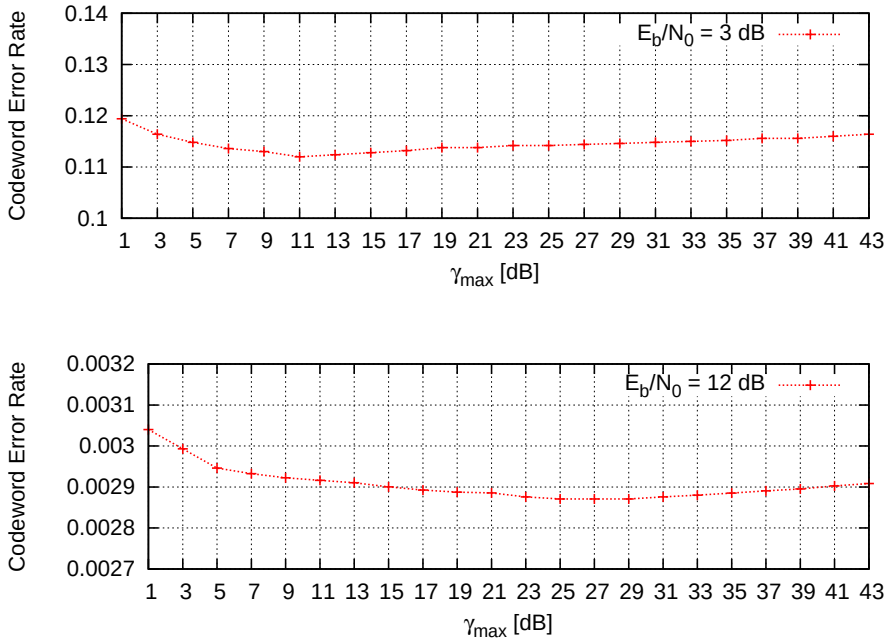

Figure 6.3: WER performance as function of $\gamma_{\max}$ for various E_b/N_0 ratios.

6.4.3 Estimated Channel Parameters

In this subsection, the different channel parameters are no longer assumed to be known and will need to be estimated. First, the impact of an imperfect source-relay channel estimate will be analyzed, in order to evaluate the consequences of the approximation made in (6.17). Thereafter, the WER and

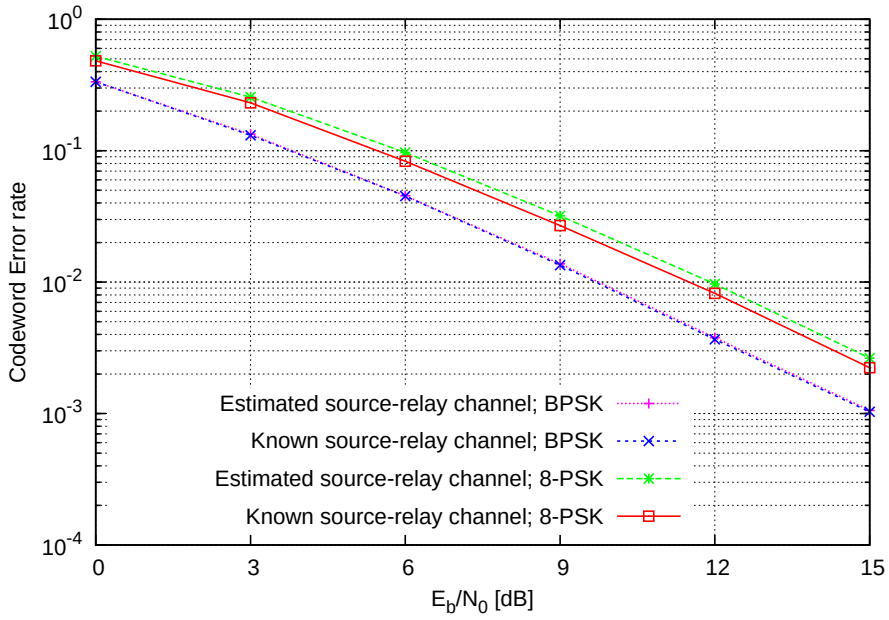

Figure 6.4: WER performance of a system in which the source-relay channel is assumed to be known, compared to that of a system in which the source-relay channel is estimated.

MSE performance of a system with estimated channel parameters is studied. Finally, the approach involving no further refining of the noise variance estimates using a code-aided approach is justified.

6.4.3.1 Impact of an Imperfect Source-Relay Channel Estimate

In order to simplify the calculation of the symbol likelihoods in section 6.2, the destination assumed that the relay makes a perfect estimate of the source-relay channel. In a real-life system however, the source-relay channel estimate will not be perfect. In order to investigate the impact of this assumption, the WER performance of a system in which the relay knows the source-relay channel is compared to that of a system in which the source-relay channel is estimated by the relay (but is assumed to be known to the relay when calculating the symbol likelihoods at the destination). The remaining channel parameters are assumed to be known to the destination. The results are shown in Fig. 6.4 for BPSK and 8PSK source mapping.

The figure shows that for BPSK mapping both WER curves virtually coincide, which indicates that the approximation made in (6.17) has only a neg-

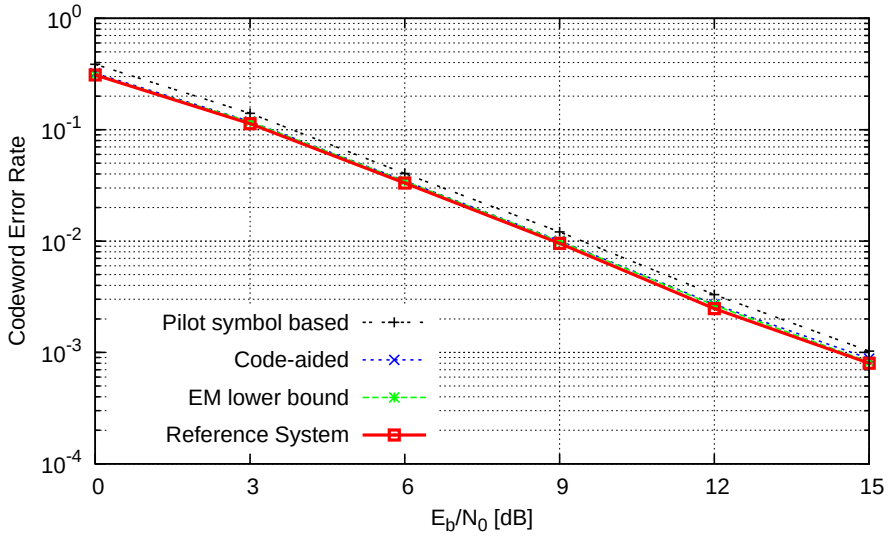

Figure 6.5: WER performance resulting from the different estimation techniques as function the E_b/N_0 ratio for BPSK mapping at the source.

ligible impact on the WER performance of the system. When using 8-PSK mapping however, there is a clear difference between both WER curves. This is due to the finer quantization at the relay, which yields smaller quantization intervals as compared to the situation in which BPSK mapping is used. An estimation error in the phase of h_1 thus has a greater probability to induce quantization errors.

6.4.3.2 WER Analysis Using Estimated Channel Parameters

The WER performance of a system using estimated channel parameters is analyzed in this subsection. Three different scenarios are being considered: pilot-based only, code-aided EM and an EM lower bound. The pilot-based approach uses only the received pilot symbols for calculating an estimate of the different channel parameters, without running the EM algorithm. In the code-aided EM method, the a posteriori symbol probabilities needed to calculate $\boldsymbol{u}_0$ and $\boldsymbol{u}_r$ from (6.39) and (6.40), respectively, are provided by the channel decoder. When calculating the EM lower bound, the symbols transmitted by the source and relay are considered to be known to the destination when calculating the estimates of h_0 and h_2. This corresponds to a situation in which $\boldsymbol{u}_0 = \boldsymbol{c}_0$ and $\boldsymbol{u}_r = \boldsymbol{c}_r$. All three scenarios are also compared to a reference system, in which all channel parameters are assumed to be known and no pilot symbols are transmitted.

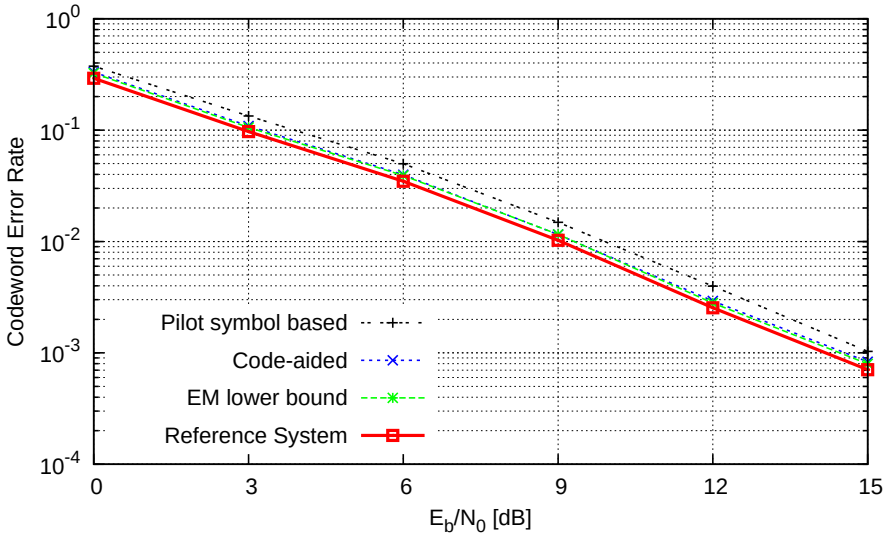

Figure 6.6: WER performance resulting from the different estimation techniques as function the E_b/N_0 ratio for QPSK mapping at the source.

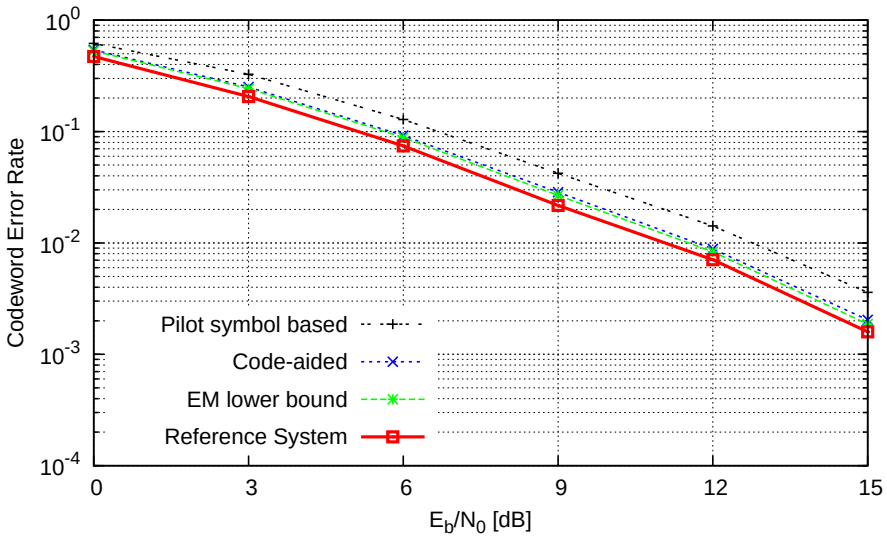

Figure 6.7: WER performance resulting from the different estimation techniques as function the E_b/N_0 ratio for 8-PSK mapping at the source.

BPSK	E_b/N_0 (dB)	Difference (dB)
Reference system	8.92	0
EM lower bound	9.04	+ 0.12
EM code-aided	9.04	+ 0.12
Pilot-based only	9.52	+ 0.60

QPSK	E_b/N_0 (dB)	Difference (dB)
Reference system	9.03	0
EM lower bound	9.29	+ 0.26
EM code-aided	9.32	+ 0.29
Pilot-based only	9.91	+ 0.88

8-PSK	E_b/N_0 (dB)	Difference (dB)
Reference system	11.10	0
EM lower bound	11.52	+ 0.42
EM code-aided	11.67	+ 0.57
Pilot-based only	12.78	+ 1.68

Table 6.1: E_b/N_0 ratio needed to achieve a WER of 0.01.

The results for BPSK, QPSK and 8-PSK mapping are shown in Fig. 6.5, Fig. 6.6 and Fig. 6.7, respectively. The results are also summarized in Table 6.1, where it is determined which E_b/N_0 ratio is needed to obtain a WER of 0.01. The results show that the effect of channel estimation errors on the WER becomes more severe as the number of bits per symbol increases (and the minimum distance between 2 constellation points decreases). The simulation results also show that by using a code-aided approach to refine the pilot-based estimates, a WER performance close to that of the reference system is obtainable. When the code-aided approach is not used, there is a significant performance degradation as compared to the reference system.

Within the displayed E_b/N_0 range, the code-aided approach practically coincides with the EM lower bound, indicating that the a posteriori probabilities available from the channel decoder are sufficiently accurate, even at low E_b/N_0 ratios. As compared to the reference system with known channel parameters and no pilot symbols transmitted, this EM lower bound has a worse WER performance due to channel estimation errors. Especially the pilot-based estimation of the source-relay channel yields a performance degradation when using higher mapping constellations, as also shown in section 6.4.3.1. Additionally, the WER performance of the EM lower bound is also degraded by the smaller E_0 and E_r from (6.2), due to the presence of the pilot symbols. This degradation is however minimal, as the number of pilot symbols (12) is very limited as compared to the number of data symbols (1536), reducing the

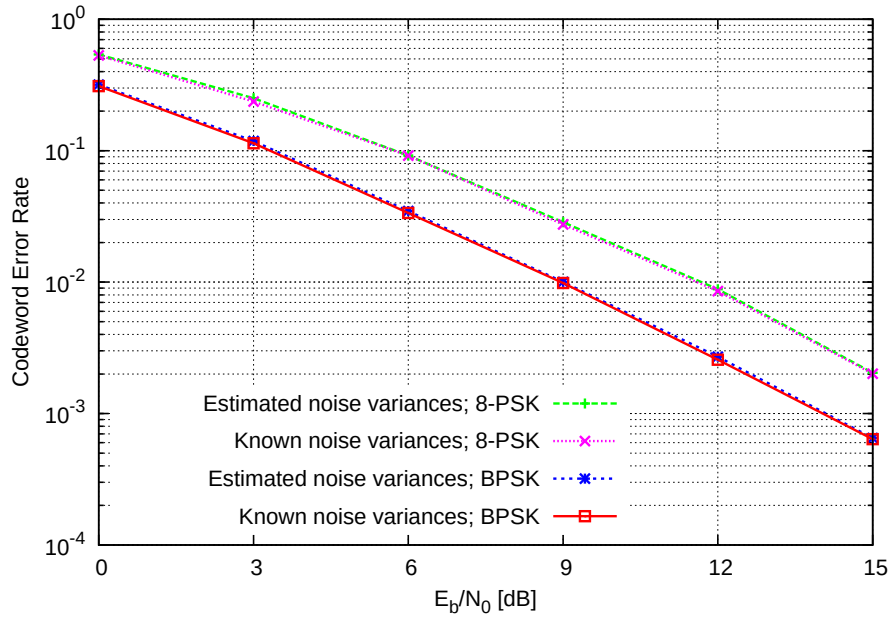

Figure 6.8: WER of a system with estimated noise variances, compared to a system with known noise variances, for both BPSK and 8-PSK mapping.

symbol energy in (6.2) by a factor of 0.989 (= 0.048 dB) due to the estimation overhead symbols.

6.4.3.3 Noise Estimation Performance

In this section, the performance loss resulting from the noise variance estimation is analyzed. This is done by comparing a system with estimated noise variances to a system where the noise variances are assumed to be known to the destination. The noise variance estimates are based only on pilot symbols as described in section 6.3.1.3, while the other channel parameters are estimated using a code-aided EM approach. The WER performance of both systems is displayed in Fig. 6.8 in the case of BPSK and 8-PSK mapping. As shown in the aforementioned figure, the WER performance of the system with estimated noise variances is very close to that of the system in which the noise variances are assumed to be known. This shows that there is little to be gained in refining the noise variance estimates, as the potential improvement in WER performance is very small.

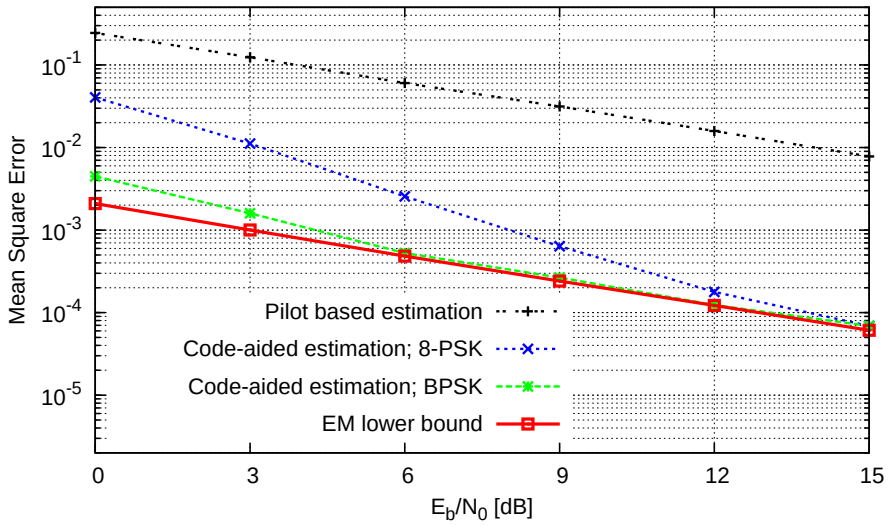

Figure 6.9: Mean Square Error values for the estimate of h_0.

6.4.3.4 MSE Analysis

The effect of the constellation size on the WER performance degradation can be explained by investigating the MSE values resulting from the different estimations, shown in Fig. 6.9 (for h_0) and Fig. 6.10 (for h_2). The curves related to pilot based estimation and to the EM lower bound coincide with (6.34) and with the lower bound in (6.42), respectively.

The deterioration in WER performance for larger constellations is also reflected in the larger MSE of the estimates of h_0 and h_2. As the SNR on the source-destination and relay-destination links increases, the number of erroneously decoded frames decreases. This yields a posteriori symbol probabilities in (6.39) and (6.40) that provide more reliable information on the symbols actually transmitted, accounting for the decrease in the MSE gap between the code-aided estimates and the EM lower bound. At high E_b/N_0 ratios, the a posteriori symbol expectations $u_0(k)$ and $u_r(k)$ converge to the symbols actually transmitted, making the MSE of the code-aided estimation coincide with the EM lower bound. Due to the higher number of decoding errors when using 8-PSK mapping, the code-aided estimation requires a higher E_b/N_0 ratio to approach the EM lower bound when using 8-PSK mapping as compared to BPSK mapping. From (6.39) and (6.40), one notices that the a posteriori expectation of the symbol vectors sent by both source and relay is conditioned on the observation $\boldsymbol{r}_d = (\boldsymbol{r}_0, \boldsymbol{r}_2)$ of both communication channel outputs (direct link and relaypath). This cooperative nature accounts for the very accurate

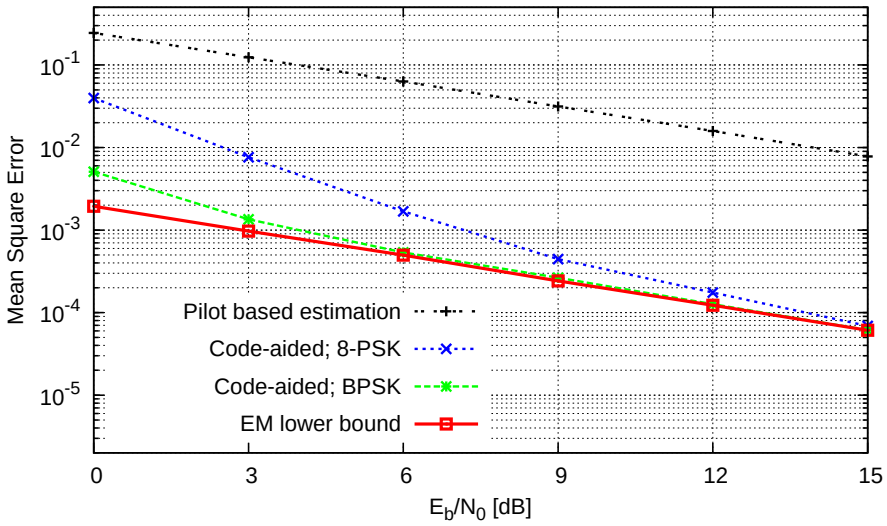

Figure 6.10: Mean Square Error values for the estimate of h_2.

estimate of the source-destination and relay-destination channel.

The normalized MSE (NMSE) of the noise variance estimate of the source-destination channel is shown in Fig. 6.11. This NMSE is obtained by dividing the MSE by the squared expected value of the noise variance. The noise variance is estimated using (6.27), whereafter different scenarios are considered:

1. No averaging or unbiasing is used.
2. The noise variance estimate is made true using (6.31). No averaging is used.
3. The noise variance estimate is averaged over consecutive frames using (6.32), with $\xi = 0.95$. No unbiasing is used.
4. The noise variance estimate is made true, whereafter it is averaged over consecutive frames.

The figure shows that the noise variance estimation NMSE is very weakly coupled with the E_b/N_0 ratio. The coupling that exists is attributed to the increasing quality of the source-destination channel gain estimate at higher E_b/N_0 ratios, which in turn is used in (6.28) for calculating the noise variance estimate. The figure also shows that there is much to gain when averaging the noise variance estimate over consecutive frames, especially in a system in which the noise variance is expected to be more or less constant over time.

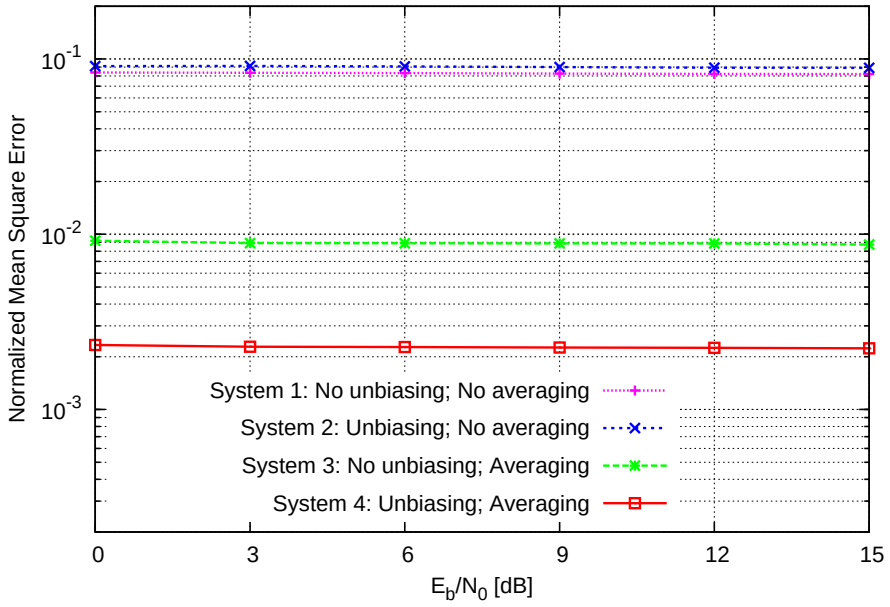

Figure 6.11: Mean Square Error values for the estimate of N_0.

When no averaging is used, no NMSE performance gain is obtained from unbiasing the noise variance estimate using (6.31). On the contrary, the NMSE of the unbiased estimate is slightly worse as compared to the biased estimate. However, when the noise variances estimates are averaged over consecutive frames, using the unbiased estimate yields a significant performance benefit. This is explained by noting that the unbiased estimate will converge to the actual value of the noise variance when being averaged, while the biased estimate will not.

6.5 Conclusions

In this chapter, an alternative QF protocol has been introduced, which involves the relay making a coarse estimate of the source-relay channel, using only the received pilot symbols. Doing so, it is shown that quantization with only $\log_2 M_1$ bits, with M_1 being the source constellation size, is sufficient to approach the performance of an AF system, while respecting the half-duplex constraint at the relay terminals. Furthermore, the structure of the destination terminal is simplified, as the latter no longer needs to make an estimate of the source-relay channel.

At the destination, a code-aided EM algorithm allows improving the pilot-based estimates of the source-destination and relay-destination channel coefficients. The code-aided approach yields a very good WER and MSE performance, but it also increases the computational complexity, as each EM iteration in principle requires the decoder to fully decode. This complexity can partly be reduced when using iterative decoding by changing the way the EM iterations and the decoder iterations are executed, as explained in section 3.1.2.3.

6.6 Appendix: Assumption of a Perfect Source-Relay Channel Estimate

In section 6.2, it was assumed in (6.17) that the relay makes a perfect estimate of h_1. We will now prove that this assumption holds for high SNR values on the source-relay channel. It is shown in section 6.3 that a pilot-based ML estimate of the source-relay channel gain is given by

$$\hat{h_1} = \frac{\boldsymbol{r}_{1p}\boldsymbol{c}_{0p}^H}{K_p\sqrt{E_0}} \tag{6.47}$$

By using (6.1), this can be written as

$$\hat{h_1} = \frac{\sqrt{E_0}h_1\boldsymbol{c}_{0p}\boldsymbol{c}_{0p}^H}{K_p\sqrt{E_0}} + \frac{\boldsymbol{n}_1\boldsymbol{c}_{0p}^H}{K_p\sqrt{E_0}}. \tag{6.48}$$

In a normalized M-PSK constellation $\boldsymbol{c}_{0p}\boldsymbol{c}_{0p}^H$ equals K_p, yielding

$$\hat{h_1} = h_1 + \frac{\boldsymbol{n}_1\boldsymbol{c}_{0p}^H}{K_p\sqrt{E_0}}. \tag{6.49}$$

By taking into account the ZMCSCG noise distribution, one obtains the following expression for the distribution of $\hat{h_1}$ conditioned on h_1 and N_1:

$$p(\hat{h_1} \mid h_1, N_1) = \frac{1}{\pi\frac{N_1}{K_pE_0}}\exp\left(\frac{-|\hat{h_1} - h_1|^2}{\frac{N_1}{K_pE_0}}\right). \tag{6.50}$$

When the number of pilot symbols and the SNR on the source-relay link is sufficiently high ($K_pE_0 \gg N_1$), (6.50) will approach a Dirac distribution:

$$p(\hat{h_1} \mid h_1, N_1) \approx \delta(\hat{h_1} - h_1). \tag{6.51}$$

6.7 Appendix: Pilot-based Estimation at the Relay Terminal

At the relay, ML estimates for the source-relay channel parameter $\hat{h_1}$ and $\hat{N_1}$ are obtained by solving the following optimization:

$$(\hat{h_1}, \hat{N_1}) = \arg\max_{(h_1,N_1)} p(\boldsymbol{r}_{1p} \mid \boldsymbol{c}_{0p}, h_1, N_1), \tag{6.52}$$

with

$$p(\boldsymbol{r}_{1p} \mid h_1, N_1, \boldsymbol{c}_{0p}) = \frac{1}{(\pi N_1)^{K_p}}\exp\left(\frac{-|\boldsymbol{r}_{1p} - \sqrt{E_0}h_1\boldsymbol{c}_{0p}|^2}{N_1}\right). \tag{6.53}$$

This 2-dimensional optimization is solved in two steps. In the first step, (6.53) is maximized w.r.t. h_1 for a given N_1:

$$\hat{h_1}(N_1) = \arg\max_{h_1} \left(\frac{1}{(\pi N_1)^{K_p}} \exp\left(\frac{-|\boldsymbol{r}_{1p} - \sqrt{E_0} h_1 \boldsymbol{c}_{0p}|^2}{N_1} \right) \right). \tag{6.54}$$

Taking into account that $\ln(.)$ is a monotonically increasing function and that factors and terms that do not depend on h_1 can be omitted in the minimization operation, (6.54) can be written as

$$\hat{h_1}(N_1) = \arg\min_{h_1} |\boldsymbol{r}_{1p} - \sqrt{E_0} h_1 \boldsymbol{c}_{0p}|^2. \tag{6.55}$$

This can be further written as

$$\begin{aligned} \hat{h_1}(N_1) &= \arg\min_{h_1} \left(-\sqrt{E_0} \boldsymbol{r}_{1p} h_1^* \boldsymbol{c}_{0p}^H - \sqrt{E_0} \boldsymbol{r}_{1p}^H h_1 \boldsymbol{c}_{0p} + E_0 h_1 h_1^* \boldsymbol{c}_{0p} \boldsymbol{c}_{0p}^H \right) \\ &= \arg\min_{h_1} \left(K_p E_0 \left| h_1 - \frac{\boldsymbol{r}_{1p} \boldsymbol{c}_{0p}^H}{\sqrt{E_0} K_p} \right|^2 \right) \\ &= \frac{\boldsymbol{r}_{1p} \boldsymbol{c}_{0p}^H}{\sqrt{E_0} K_p}, \end{aligned} \tag{6.56}$$

yielding the ML estimate of h_1, which is independent of N_1.

In the second step, the estimate of h_1 from (6.56) is used in (6.52) to obtain an estimate of the noise variance:

$$\begin{aligned} \hat{N_1} &= \arg\max_{N_1} \left(\frac{1}{(\pi N_1)^{K_p}} \exp\left(\frac{-|\boldsymbol{r}_{1p} - \sqrt{E_0} \hat{h_1} \boldsymbol{c}_{0p}|^2}{N_1} \right) \right) \\ &= \arg\min_{N_1} \left(K_p \ln(\pi N_1) + \frac{|\boldsymbol{r}_{1p} - \sqrt{E_0} \hat{h_1} \boldsymbol{c}_{0p}|^2}{N_1} \right). \end{aligned} \tag{6.57}$$

The noise variance estimate is found by searching the root of the derivative with respect to N_1, yielding

$$K_p \frac{1}{N_1} - \frac{1}{N_1^2} |\boldsymbol{r}_{1p} - \sqrt{E_0} \hat{h_1} \boldsymbol{c}_{0p}|^2 = 0. \tag{6.58}$$

Solving (6.58) yields

$$\hat{N_1} = \frac{|\boldsymbol{r}_{1p} - \sqrt{E_0} \hat{h_1} \boldsymbol{c}_{0p}|^2}{K_p}. \tag{6.59}$$

6.8 Appendix: Noise Variance Estimation Bias

An ML estimate of the noise variance is given by

$$\hat{N_0} = \frac{|\boldsymbol{r}_{0p} - \sqrt{E_0}\hat{h}_0\boldsymbol{c}_{0p}|^2}{K_p},. \tag{6.60}$$

Inserting (6.23) and (6.1) into (6.60) yields

$$\begin{aligned}
\hat{N_0} &= \frac{\left|\sqrt{E_0}h_0\boldsymbol{c}_{0p} + \boldsymbol{n}_{0p} - \sqrt{E_0}h_0\boldsymbol{c}_{0p} - \frac{\boldsymbol{n}_{0p}\boldsymbol{c}_{0p}^H\boldsymbol{c}_{0p}}{K_p}\right|^2}{K_p} \\
&= \frac{1}{K_p}\left|\boldsymbol{n}_{0p} - \frac{\boldsymbol{n}_{0p}\boldsymbol{c}_{0p}^H\boldsymbol{c}_{0p}}{K_p}\right|^2 \\
&= \frac{1}{K_p}\left(\boldsymbol{n}_{0p}\boldsymbol{n}_{0p}^H - \frac{\boldsymbol{n}_{0p}\boldsymbol{c}_{0p}^H\boldsymbol{c}_{0p}\boldsymbol{n}_{0p}^H}{K_p} - \frac{\boldsymbol{n}_{0p}\boldsymbol{c}_{0p}^H\boldsymbol{c}_{0p}\boldsymbol{n}_{0p}^H}{K_p} + \frac{\boldsymbol{n}_{0p}\boldsymbol{c}_{0p}^H\boldsymbol{c}_{0p}\boldsymbol{c}_{0p}^H\boldsymbol{c}_{0p}\boldsymbol{n}_{0p}^H}{{K_p}^2}\right) \\
&= \frac{1}{K_p}\left(\boldsymbol{n}_{0p}\boldsymbol{n}_{0p}^H - \frac{\boldsymbol{n}_{0p}\boldsymbol{c}_{0p}^H\boldsymbol{c}_{0p}\boldsymbol{n}_{0p}^H}{K_p}\right).
\end{aligned} \tag{6.61}$$

Taking the expected value of (6.61) yields

$$\mathbb{E}\left[\hat{N_0}\right] = \frac{1}{K_p}\left(\mathbb{E}\left[\boldsymbol{n}_{0p}\boldsymbol{n}_{0p}^H\right] - \mathbb{E}\left[\frac{\boldsymbol{n}_{0p}\boldsymbol{c}_{0p}^H\boldsymbol{c}_{0p}\boldsymbol{n}_{0p}^H}{K_p}\right]\right). \tag{6.62}$$

The statistical independence of the noise samples can be expressed as

$$\mathbb{E}[n_{0p}(i)n_{0p}(j)^*] = \begin{cases} 0 & \text{if } i \neq j \\ N_0 & \text{if } i = j \end{cases}. \tag{6.63}$$

Taking (6.63) into consideration, (6.62) can be rewritten as

$$\mathbb{E}\left[\hat{N_0}\right] = N_0 - \frac{N_0}{K_p} = N_0\left(\frac{K_p - 1}{K_p}\right). \tag{6.64}$$

The expression above shows that the estimate of the noise variance is biased by a factor equal to $(K_p - 1)/K_p$. This bias can be removed by multiplying the estimate (6.60) with $K_p/(K_p - 1)$.

6.9 Appendix: Maximization of $Q\left(\boldsymbol{h}_d, \hat{\boldsymbol{h}_d}^{(i-1)}\right)$

Each EM iteration i, new estimates of the channel coefficients h_0 and h_2 are calculated by selecting the value of those parameters that maximizes the function

$Q\left(\boldsymbol{h}_d, \hat{\boldsymbol{h}_d}^{(i-1)}\right)$. Using factorization (5.7), this function can be written as

$$Q\left(\boldsymbol{h}_d, \hat{\boldsymbol{h}_d}^{(i-1)}\right) = \mathbb{E}_{\boldsymbol{c}_d}\left[\ln p(\boldsymbol{r}_0 \mid \boldsymbol{c}_0, h_0) \mid \boldsymbol{r}_d, \hat{\boldsymbol{h}_d}^{(i-1)}\right] + \mathbb{E}_{\boldsymbol{c}_d}\left[\ln p(\boldsymbol{r}_2 \mid \boldsymbol{c}_r, h_2) \mid \boldsymbol{r}_d, \hat{\boldsymbol{h}_d}^{(i-1)}\right]. \tag{6.65}$$

The new estimate of h_0 should maximize the first term in (6.65), while the new estimate of h_2 should maximize the second term in (6.65):

$$\hat{h_0}^{(i)} = \arg\max_{h_0} \mathbb{E}_{\boldsymbol{c}_d}\left[\ln p(\boldsymbol{r}_0 \mid \boldsymbol{c}_0, h_0) \mid \boldsymbol{r}_d, \hat{\boldsymbol{h}_d}^{(i-1)}\right] \tag{6.66}$$

$$\hat{h_2}^{(i)} = \arg\max_{h_2} \mathbb{E}_{\boldsymbol{c}_d}\left[\ln p(\boldsymbol{r}_2 \mid \boldsymbol{c}_r, h_2) \mid \boldsymbol{r}_d, \hat{\boldsymbol{h}_d}^{(i-1)}\right]. \tag{6.67}$$

Using (6.10), (6.66) can be written as

$$\begin{aligned}\hat{h_0}^{(i)} &= \arg\min_{h_0} \mathbb{E}_{\boldsymbol{c}_d}\left[|\boldsymbol{r}_0 - \sqrt{E_0} h_0 \boldsymbol{c}_0|^2 \mid \boldsymbol{r}_d, \hat{\boldsymbol{h}_d}^{(i-1)}\right] \\ &= \arg\min_{h_0} \mathbb{E}_{\boldsymbol{c}_d}\left[E_0 h_0 h_0^* \boldsymbol{c}_0 \boldsymbol{c}_0^H - \sqrt{E_0}\boldsymbol{r}_0 h_0^* \boldsymbol{c}_0^H - \sqrt{E_0} h_0 \boldsymbol{c}_0 \boldsymbol{r}_0^H \mid \boldsymbol{r}_d, \hat{\boldsymbol{h}_d}^{(i-1)}\right].\end{aligned} \tag{6.68}$$

By introducing the vector $\boldsymbol{u}_0^{(i)}$ defined as

$$\boldsymbol{u}_0^{(i)} = \mathbb{E}_{\boldsymbol{c}_d}\left[\boldsymbol{c}_0 \mid \boldsymbol{r}_d, \hat{\boldsymbol{h}_d}^{(i-1)}\right] = \sum_{\boldsymbol{c}_d} \boldsymbol{c}_0 p\left(\boldsymbol{c}_d \mid \boldsymbol{r}_d, \hat{\boldsymbol{h}_d}^{(i-1)}\right), \tag{6.69}$$

(6.68) can be written as

$$\hat{h_0}^{(i)} = \arg\min_{h_0}\left(h_0 h_0^*(K_p + K)E_0 - \sqrt{E_0}\boldsymbol{r}_0 h_0^*\left(\boldsymbol{u}_0^{(i)}\right)^H - \sqrt{E_0} h_0 \boldsymbol{u}_0^{(i)} \boldsymbol{r}_0^H\right). \tag{6.70}$$

This minimization problem is very similar to (6.56), yielding the following solution for $\hat{h_0}^{(i)}$:

$$\hat{h_0}^{(i)} = \frac{\boldsymbol{r}_0\left(\boldsymbol{u}_0^{(i)}\right)^H}{(K_p + K)\sqrt{E_0}}. \tag{6.71}$$

A similar method can be used to solve (6.67), in order to obtain an estimate $\hat{h_2}^{(i)}$ of the relay-destination channel coefficient, yielding

$$\hat{h_2}^{(i)} = \frac{\boldsymbol{r}_2\left(\boldsymbol{u}_r^{(i)}\right)^H}{(K_p + K)E_r}, \tag{6.72}$$

with

$$\boldsymbol{u}_r^{(i)} = \sum_{\boldsymbol{c}_d} \boldsymbol{c}_r p\left(\boldsymbol{c}_d \mid \boldsymbol{r}_d, \hat{\boldsymbol{h}_d}^{(i-1)}\right). \tag{6.73}$$

7

Destination-side Estimation of the Source-Relay Channel

In the previous chapter, a QF system was introduced in which the source-relay channel is estimated at the relay. This estimate is used by the relay to compensate for the channel rotation of the source-relay channel, before quantizing the information received from the source. In doing so, it is shown that the system can achieve a WER performance close to that of the AF protocol. Furthermore, by estimating the source-relay channel at the relay, it no longer needs to be estimated at the destination.

The main drawback of the QF protocol proposed in the previous chapter is the complexity associated with the relay-side estimation of the source-relay channel. In applications requiring a low relay-side complexity, the additional burdon the estimation process places on the relay can be undesirable. Therefore, in this chapter, a method is proposed to estimate the source-relay channel at the destination. This approach lowers the relay-side complexity at the

expense of an increased destination-side complexity. However, in most applications, there is more computing power available at the destination, where it is needed to decode the channel code and perform various other tasks. Additionally, when estimating the source-relay channel at the destination, it is possible to use code-aided refinement in order to improve the source-relay channel estimate, yielding an improved WER performance as compared to a system in which the source-relay channel is estimated at the relay using only pilot symbols.

The starting point for the discussion in this chapter is the QF system described in chapter 5. In the aforementioned chapter, a QF protocol is described in which the relay quantizes the phase of the received M_1-PSK symbols, without knowing the source-relay channel. When the number of quantization intervals is at least twice as large as the source constellation size, a WER performance similar to that of AF is achieved. The results presented in chapter 5 are obtained under the assumption that the destination knows all relevant channel parameters. This assumption is removed in the present chapter by developing estimation algorithms for all channel parameters involved. Furthermore, a novel low complexity algorithm is introduced for the estimation of the source-relay channel at the destination.

The outline of this chapter is as follows. In section 7.1, the system model is introduced, whereafter the detection at the destination terminal is discussed in section 7.2. The estimation of the different parameters is discussed in section 7.3. In section 7.3.4, a new estimation method is proposed, reducing the computational complexity at the destination while maintaining a good WER performance. The proposed algorithms are tested using computer simulations in section 7.4, whereafter conclusions are drawn in section 7.5.

7.1 System Model

The QF system described in chapter 5 is used as a starting point in this chapter. The reader is referred to section 5.1 for a description of the employed channel model and relay quantization scheme. In order to facilitate the estimation process, K_p pilot symbols are added to the K M_1-PSK data symbols, with M_1 an integer power of 2, that are broadcast by the source in the first timeslot and are received by both the relay and the destination. At the relay, the phases of the received samples are quantized using $\log_2(M_2)$ bits and without knowing the state of the source-relay channel. After completing the quantization operation, the relay utilizes the second timeslot to send to the destination the quantized version of the samples that correspond to the K_d data symbols and to $\lceil \alpha K_p \rceil$ of the K_p pilot symbols sent by the source, where $0 \leq \alpha \leq 1$. In addition, the relay also sends to the destination $\lfloor (1-\alpha) K_p \rfloor$ pilot symbols of

its own, randomly selected from an M-PSK constellation. Hence, during the second timeslot, a total of $K + K_p$ samples are transmitted from the relay to the destination.

When decoding the received data symbols, the destination needs to know the state of the different communication channels involved. An estimate of the source-destination, relay-destination and source-relay channels is computed using the K_p pilot symbols sent by the source, the $\lfloor (1-\alpha)K_p \rfloor$ pilot symbols sent by the relay, and the $\lceil \alpha K_p \rceil$ pilot symbols from the source that have been quantized by the relay, respectively.

After obtaining an initial estimate of all the channel parameters involved, the signals received during both timeslots are combined in order to compute the a posteriori symbol expectations by means of the channel decoder. These expectations are used to iteratively refine the channel estimates using the EM algorithm. After convergence of the channel estimates, the channel decoder provides (its decision on) the information bits sent by the source.

7.1.1 Symbol Energy

Due to the addition of pilot symbols which do not carry any information from the source to the destination, less energy is available for the transmission of the data symbols. This yields the following expression for E_b, the energy per information bit, expressed in terms of E_0 and E_r, the symbol energies transmitted by the source and relay, respectively:

$$E_b = \frac{1}{\lambda \log_2(M_1)} \left(E_0 \frac{(K+K_p)}{K} + E_r \frac{(K+K_p)}{K} \right). \tag{7.1}$$

Comparing (7.1) to (6.2) from the previous chapter, one notices that in the system at hand, less energy is wasted on estimation overhead as compared to the system described in chapter 6. Indeed, because the source-relay channel is estimated at the destination, information about its SNR no longer needs to be forwarded from the relay to the destination.

7.2 Detection

The reader is referred to section 5.3 for a detailed description on how the symbol likelihoods needed to decode the received information are calculated. Only the particularities arising from the channel estimation methods used in this chapter will be discussed here. Introducing $\boldsymbol{h} = (h_0, h_1, h_2)$ and $\boldsymbol{N} = (N_0,$

N_1, N_2), the likelihood of the source symbols can be written as

$$p(\boldsymbol{r}_0, \boldsymbol{r}_2 \mid \boldsymbol{c}, \boldsymbol{h}, \boldsymbol{N}) = \prod_{k=1}^{K} p(r_0(k) \mid c_0(k), h_0, N_0). \sum_{c_r(k)} p(r_2(k) \mid c_r(k), h_2, N_2) p(c_r(k) \mid c_0(k), h_1, N_1), \tag{7.2}$$

with

$$p(r_0(k) \mid c_0(k), h_0, N_0) = \frac{1}{\pi N_0} \exp\left(-\frac{|r_0(k) - h_0 c_0(k)|^2}{N_0}\right) \tag{7.3}$$

$$p(r_2(k) \mid c_r(k), h_2, N_2) = \frac{1}{\pi N_2} \exp\left(-\frac{|r_2(k) - h_2 c_r(k)|^2}{N_2}\right) \tag{7.4}$$

$$p(c_r(k) \mid c_0(k), h_1, N_1) = \int_{\phi^l_{c_r(k)}}^{\phi^u_{c_r(k)}} f_\Theta\left(\theta - \arg(c_0(k) h_1); \frac{E_0 |h_1|^2}{N_1}\right) \mathrm{d}\theta. \tag{7.5}$$

The summation in (7.2) runs over all values that $c_r(k)$ can adopt. In (7.5), $\phi^l_{c_r(k)}$ and $\phi^u_{c_r(k)}$ represent the upper and lower bound, respectively, of the quantization interval corresponding to $c_r(k)$, i.e. $\phi^l_{c_r(k)} = \frac{2\pi q - \frac{1}{2}}{M_2}$ and $\phi^u_{c_r(k)} = \frac{2\pi q + \frac{1}{2}}{M_2}$ for $c_r(k) = \chi_{M_2}(q)$. The function $f_\Theta(\theta, \gamma)$ is defined in (5.12).

Noting that (7.5) depends only on the instantaneous SNR $\gamma = E_0 |h_1|^2 / N_1$ and on the phase $\phi_{h_1} = \arg(h_1)$ of the source-relay channel, (7.5) can be written as

$$p(c_r(k) \mid c_0(k), \phi_{h_1}, \gamma) = \int_{\phi^l_{c_r(k)}}^{\phi^u_{c_r(k)}} f_\Theta(\theta - (\arg(c_0(k)) + \phi_{h_1}); \gamma) \mathrm{d}\theta. \tag{7.6}$$

The probability of $c_r(k)$ conditioned on $c_0(k)$, as defined by (7.6), is the transition probability of the equivalent channel with $c_0(k)$ as input and $c_r(k)$ as output.

7.3 Estimation

The likelihoods obtained in the previous section are conditioned on the channel parameters h_0, N_0, γ, ϕ_{h_1}, h_2 and N_2. In order to limit the complexity at the relay, these unknown channel parameters will all be estimated at the destination. As will be shown in section 7.3.2.2, it is not possible to obtain a closed form estimate of the source-relay channel parameters γ and ϕ_{h_1}, requiring numerical maximization. Therefore, an alternative estimation algorithm is proposed for the estimation of the source-relay channel parameters, which yields a closed-form expression.

The necessary estimates are calculated in two phases. In the first phase, the pilot symbols transmitted by the source and relay are used to calculate pilot-based estimates. Due to the limited number of pilot symbols, these estimates are of limited accuracy. This is improved in the second phase, where a code-aided approach allows using the unknown data symbols in the estimation process, drastically improving the estimation quality.

In the remainder of this section, the structure of the relay terminal will be discussed in section 7.3.1, whereafter pilot-based estimates will be obtained for the different parameters in section 7.3.2. Subsequently, in section 7.3.3, a code-aided EM algorithm approach will be used to refine the pilot-based estimates. Finally, an alternative estimation algorithm not requiring numerical maximization is presented in section 7.3.4, whereafter some closing remarks are made in section 7.3.5.

7.3.1 Structure of the Relay Terminal

At the destination, the direct path observation $\boldsymbol{r}_0$ is used to calculate an estimate of the source-destination channel parameters, while the relay path observation $\boldsymbol{r}_2$ is used to estimate the source-relay and relay-destination channel parameters. Initial estimates of the source-destination channel parameters are derived using K_p pilot symbols sent by the source, denoted $\boldsymbol{c}_{0p}$. Similarly, the relay sends $\lfloor(1-\alpha)K_p\rfloor$ pilot symbols, denoted $\boldsymbol{c}_{rp^\diamond}$, which are observed at the destination as $\boldsymbol{r}_{2p^\diamond}$ and are used by the latter for obtaining initial estimates of the relay-destination channel parameters.

Making an initial estimate of the source-relay channel is more involved, as the destination is not directly connected to this channel. We assume that the relay not only quantizes the portion of the received signal containing the data symbols received from the source, denoted $\boldsymbol{r}_{1d}$, but also the portion of the received signal that corresponds to the pilot symbols transmitted by the source, denoted $\boldsymbol{r}_{1p}$, in order to allow the destination to compute an initial estimate of the source-relay channel. A number $\lceil\alpha K_p\rceil$ of these quantized samples, denoted $\boldsymbol{c}_{rp^\dagger}$ and observed at the destination as $\boldsymbol{r}_{2p^\dagger}$, are sent to the destination together with the quantized data symbols, denoted $\boldsymbol{c}_{rd}$, and the relay-generated pilot symbols, denoted $\boldsymbol{c}_{rp^\diamond}$. The vector encompassing all pilot symbol transmitted by the relay is denoted $\boldsymbol{c}_{rp} = (\boldsymbol{c}_{rp^\dagger}, \boldsymbol{c}_{rp^\diamond})$, which is received as $\boldsymbol{r}_{2p} = (\boldsymbol{r}_{2p^\dagger}, \boldsymbol{r}_{2p^\diamond})$ at the destination. This results in a low complexity relay structure, which is represented schematically in Fig. 7.1.

7.3.2 Pilot-based Estimation

Before a code-aided approach can be used to refine the channel estimates, pilot-based estimates need to be obtained. These are obtained as the solution

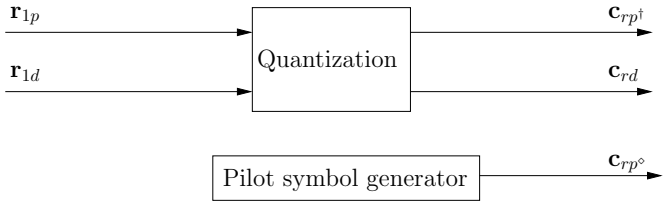

Figure 7.1: Schematic representation of the relay structure.

to the following maximization problem:

$$(\hat{\boldsymbol{h}}, \hat{\boldsymbol{N}}) = \arg\max_{\boldsymbol{h},\boldsymbol{N}} p(\boldsymbol{r}_{0p}, \boldsymbol{r}_{2p} \mid \boldsymbol{c}_{0p}, \boldsymbol{c}_{rp}, \boldsymbol{h}, \boldsymbol{N}). \tag{7.7}$$

Using (7.2), the maximization problem (7.7) can be split up as

$$(\hat{h_0}, \hat{N_0}) = \arg\max_{h_0,N_0} p(\boldsymbol{r}_{0p} \mid \boldsymbol{c}_{0p}, h_0, N_0) \tag{7.8}$$

$$(\hat{h_1}, \hat{N_1}, \hat{h_2}, \hat{N_2}) = \arg\max_{h_1,N_1,h_2,N_2} p(\boldsymbol{r}_{2p} \mid \boldsymbol{c}_{0p}, \boldsymbol{c}_{rp}, h_1, N_1, h_2, N_2), \tag{7.9}$$

where (7.8) corresponds to the estimation of the direct path and (7.9) corresponds to the estimation of the relay path. These two subproblems will now be discussed separately in the following subsections.

7.3.2.1 Direct Path

The channel coefficient and noise variance estimates of the source-destination channel are found as a solution to (7.8). Considering the similarities between (7.8) and (6.25) from chapter 6, and taking into account that the system described in the aforementioned chapter uses the the same channel model for the source-destination channel, the following expressions are obtained for the pilot-based estimates of h_0 and N_0:

$$\hat{h}_0 = \frac{\boldsymbol{r}_{0p}\boldsymbol{c}_{0p}^H}{\sqrt{E_0}K_p} \tag{7.10}$$

$$\hat{N}_0 = \frac{|\boldsymbol{r}_{0p} - \sqrt{E_0}\hat{h}_0\boldsymbol{c}_{0p}|^2}{K_p}. \tag{7.11}$$

As explained in section 6.3.1.3, the noise variance estimate is biased by a factor $(K_p - 1)/K_p$ and is made unbiased by multiplying it with $K_p/(K_p - 1)$.

7.3.2.2 Relay Path

The state of the relay path is characterized by the source-relay channel h_1 and noise variance N_1, and by the the relay-destination channel coefficient h_2 and

noise variance N_2. As shown in (7.6), the state of the source-relay channel can also be characterized by the phase ϕ_{h_1} and SNR γ. Using this second approach will yield a less complex estimation problem.

Introducing $\boldsymbol{h}_r = (\phi_{h_1}, \gamma, h_2, N_2)$, an ML estimate of $\boldsymbol{h}_r$ is computed at the destination using the received pilot symbols $\boldsymbol{r}_{2p}$, consisting of $\boldsymbol{r}_{2p^\dagger}$ and $\boldsymbol{r}_{2p^\diamond}$, yielding

$$\hat{\boldsymbol{h}}_r = \arg\max_{\boldsymbol{h}_r} p(\boldsymbol{r}_{2p^\diamond}, \boldsymbol{r}_{2p^\dagger} \mid \boldsymbol{c}_{0p}, \boldsymbol{c}_{rp}, \boldsymbol{h}_r). \tag{7.12}$$

In the equation above, the observation vector $\boldsymbol{r}_{2p^\diamond}$ depends on the relay pilot symbols $\boldsymbol{c}_{rp^\diamond}$, while the observation vector $\boldsymbol{r}_{2p^\dagger}$ not only depends on $\boldsymbol{c}_{0p}$, but also on $\boldsymbol{c}_{rp^\dagger}$, the quantized version of $\lceil \alpha K_p \rceil$ elements of $\boldsymbol{r}_{1p}$. Taking this dependency into consideration yields

$$\hat{\boldsymbol{h}}_r = \arg\max_{\boldsymbol{h}_r} \sum_{\boldsymbol{c}_{rp^\dagger}} p(\boldsymbol{r}_{2p} \mid \boldsymbol{c}_{0p}, \boldsymbol{c}_{rp^\diamond}, \boldsymbol{c}_{rp^\dagger}, \boldsymbol{h}_r) p(\boldsymbol{c}_{rp^\dagger} \mid \boldsymbol{c}_{0p}, \boldsymbol{h}_r). \tag{7.13}$$

Because it is difficult to solve (7.13) analytically, (7.12) is solved instead using the EM algorithm, in which the forwarded pilot symbols $\boldsymbol{c}_{rp^\dagger}$ are considered to be nuisance parameters, yielding the following Q-function

$$Q\left(\boldsymbol{h}_r, \hat{\boldsymbol{h}}_r^{(i-1)}\right) = \mathbb{E}_{\boldsymbol{c}_{rp^\dagger}}\left[\ln p(\boldsymbol{r}_{2p}, \boldsymbol{c}_{rp^\dagger} \mid \boldsymbol{c}_{rp^\diamond}, \boldsymbol{c}_{0p}, \boldsymbol{h}_r) \,\middle|\, \boldsymbol{r}_{2p}, \hat{\boldsymbol{h}}_r^{(i-1)}\right] \tag{7.14}$$

The M-step of the i-th iteration consists of the maximization of (7.14), with respect to $\boldsymbol{h}_r$, yielding

$$\hat{\boldsymbol{h}}_r^{(i)} = \arg\max_{\boldsymbol{h}_r} Q\left(\boldsymbol{h}_r, \hat{\boldsymbol{h}}_r^{(i-1)}\right). \tag{7.15}$$

As shown in Appendix 7.6, this maximization problem can be split into a part corresponding to the source-relay channel parameters and a part corresponding to the relay-destination channel parameters, yielding

$$(\hat{h_2}^{(i)}, \hat{N_2}^{(i)}) = \arg\max_{(h_2, N_2)} \mathbb{E}_{\boldsymbol{c}_{rp^\dagger}}\left[\ln p(\boldsymbol{r}_{2p} \mid \boldsymbol{c}_{rp}, h_2, N_2) \,\middle|\, \boldsymbol{r}_{2p}, \hat{\boldsymbol{h}}_r^{(i-1)}\right] \tag{7.16}$$

and

$$\left(\hat{\phi_{h_1}}^{(i)}, \hat{\gamma}^{(i)}\right) = \arg\max_{(\phi_{h_1}, \gamma)} \mathbb{E}_{\boldsymbol{c}_{rp^\dagger}}\left[\ln p(\boldsymbol{c}_{rp^\dagger} \mid \boldsymbol{c}_{0p}, \phi_{h_1}, \gamma) \,\middle|\, \boldsymbol{r}_{2p}, \hat{\boldsymbol{h}}_r^{(i-1)}\right]. \tag{7.17}$$

Solving the maximization problem in (7.16) yields the following solution for

$\hat{h_2}^{(i)}$ and $\hat{N_2}^{(i)}$:

$$\hat{h_2}^{(i)} = \frac{\boldsymbol{r}_{2p}\left(\boldsymbol{c}_{rp^\diamond}, \boldsymbol{u}_{rp^\dagger}^{(i)}\right)^H}{K_p\sqrt{E_r}} \tag{7.18}$$

$$\hat{N_2}^{(i)} = \frac{\left|\boldsymbol{r}_{2p} - \sqrt{E_r}\hat{h_2}^{(i)}\left(\boldsymbol{c}_{rp^\diamond}, \boldsymbol{u}_{rp^\dagger}^{(i)}\right)\right|^2 + E_r\left|\hat{h_2}^{(i)}\right|^2\left(\lceil \alpha K_p \rceil - \boldsymbol{u}_{rp^\dagger}^{(i)}\left(\boldsymbol{u}_{rp^\dagger}^{(i)}\right)^H\right)}{K_p} \tag{7.19}$$

with $\boldsymbol{u}_{rp^\dagger}^{(i)}$ defined by (7.51).

As also shown in Appendix 7.6, (7.17) can be written as

$$\left(\hat{\phi_{h_1}}^{(i)}, \hat{\gamma}^{(i)}\right) = \arg\max_{(\phi_{h_1},\gamma)} \sum_{q=0}^{M_2-1} \ln P\left[c_{rp^\dagger} = \chi_{M_2}(q) \mid c_{0p} = 1, \phi_{h_1}, \gamma\right] \Gamma^{(i)}(q), \tag{7.20}$$

with $\Gamma^{(i)}(q)$ defined by (7.58). Due to the complicated structure of $f_\Theta(\theta;\gamma)$ from (5.12) used in (7.6) to calculate the source-relay transition probabilities, it is not possible to obtain a closed-form estimate for ϕ_{h_1} and γ. After the elements of the vector $\boldsymbol{\Gamma}^{(i)}$ have been calculated, a 2-dimensional numerical search is used to find the values of ϕ_{h_1} and γ that maximize (7.20). This search is simplified by noting that the transition probabilities, for a given ϕ_{h_1} and γ, do not depend on the symbol position k and are the same for each frame. As a result, the value of $\ln P\left[c_{rp^\dagger} = \chi_{M_2}(q) \mid c_{0p} = 1, \phi_{h_1}, \gamma\right], q \in \{0, 1, ..., M_2 - 1\}$ can be pre-calculated for different ϕ_{h_1} and γ values and stored in a table. The numerical search thus consists of finding the table entry that maximizes (7.20) and selecting the corresponding ϕ_{h_1} and γ values.

The expressions (7.51) and (7.58) for $\boldsymbol{u}_{rp^\dagger}^{(i)}$ and $\Gamma^{(i)}(q)$ both contain the conditional distribution $p\left(\boldsymbol{c}_{rp^\dagger}(k) \mid \boldsymbol{r}_{2p^\dagger}, \hat{\boldsymbol{h}}_r^{(i-1)}\right)$, which can be written as

$$p\left(c_{rp^\dagger}(k) \,\middle|\, \boldsymbol{r}_{2p^\dagger}, \hat{\boldsymbol{h}}_r^{(i-1)}\right) = p\left(c_{rp^\dagger}(k) \,\middle|\, r_{2p^\dagger}(k), \hat{\boldsymbol{h}}_r^{(i-1)}\right) = \frac{p\left(r_{2p^\dagger}(k) \,\middle|\, c_{rp^\dagger}(k), \hat{h_2}^{(i-1)}, \hat{N_2}^{(i-1)}\right) p\left(c_{rp^\dagger}(k) \,\middle|\, c_{0p}(k), \hat{\phi_{h_1}}^{(i-1)}, \hat{\gamma}^{(i-1)}\right)}{\sum_{\tilde{c}_{rp^\dagger}(k)} p\left(r_{2p^\dagger}(k) \,\middle|\, \tilde{c}_{rp^\dagger}(k), \hat{h_2}^{(i-1)}, \hat{N_2}^{(i-1)}\right) p\left(\tilde{c}_{rp^\dagger}(k) \,\middle|\, c_{0p}(k), \hat{\phi_{h_1}}^{(i-1)}, \hat{\gamma}^{(i-1)}\right)}, \tag{7.21}$$

where the summation in the denominator runs over all points in a M_2-PSK constellation. The factors of (7.21) can be evaluated using the expressions

from section 7.2.

As the algorithm presented for the estimation of the relay path channel parameters is iterative, it needs to be initialized. This is achieved by assuming in the first iteration that all the source-relay channel transition probabilities are equal:

$$P[c_{rp^\dagger}(k) = \chi_{M_2}(q) \mid c_{0p}(k) = 1, \phi_{h_1}, \gamma) = \frac{1}{M_2} \qquad , \forall q \in \{0, 1, ..., M_2 - 1\}, \tag{7.22}$$

and by calculating the estimates of h_2 and N_2 using only the pilot symbols sent by the relay, yielding

$$\hat{h_2}^{(0)} = \frac{\boldsymbol{r}_{2p^\diamond} \boldsymbol{c}_{rp^\diamond}^H}{\lfloor (1-\alpha) K_p \rfloor \sqrt{E_r}} \tag{7.23}$$

$$\hat{N_2}^{(0)} = \frac{\left| \boldsymbol{r}_{2p^\diamond} - \hat{h_2}^{(0)} \boldsymbol{c}_{rp^\diamond} \right|^2}{\lfloor (1-\alpha) K_p \rfloor}. \tag{7.24}$$

After the pilot-based EM iterations have been performed, the noise variance estimate $\hat{N_2}$ is made unbiased by multiplying it with $K_p/(K_p - 1)$, whereafter it is used together with the other pilot-based estimates for the initialization of the code-aided EM algorithm discussed in the next subsection.

7.3.3 Code-aided Estimation

The pilot-based channel estimates obtained in the previous subsection can be refined by using not only the part of the observation that corresponds to the received pilot symbols, but the whole observation vector. This is achieved using a code-aided EM algorithm, in which the data symbols sent by the source and relay are considered to be nuisance parameters. In the case at hand, the estimates of the channels parameters h_0, ϕ_{h_1}, γ and h_2 are refined using the EM algorithm. As the error performance is not very sensitive to noise variance estimation errors, as is shown in section 6.4.3.3, the pilot-based estimates of N_0 and N_2 will not be refined and, in order not to overload the notation, the dependency of the probability density functions on these noise variances will not be noted explicitly.

Introducing $\boldsymbol{r}_d = (\boldsymbol{r}_0, \boldsymbol{r}_2)$ and $\boldsymbol{h} = (h_0, \phi_{h_1}, \gamma, h_2)$, the expectation step during iteration i consists of calculating the Q-function

$$Q\left(\boldsymbol{h}, \hat{\boldsymbol{h}}^{(i-1)}\right) = \mathbb{E}_{\boldsymbol{c}_0, \boldsymbol{c}_r}\left[\ln p(\boldsymbol{r}_d, \boldsymbol{c}_0, \boldsymbol{c}_r | \boldsymbol{h}) \,\middle|\, \boldsymbol{r}_d, \hat{\boldsymbol{h}}^{(i-1)} \right]. \tag{7.25}$$

The maximization step involves finding the value of $\boldsymbol{h}$ that maximizes the Q function from (7.25):

$$\hat{\boldsymbol{h}}^{(i)} = \arg\max_{\boldsymbol{h}} Q\left(\boldsymbol{h}, \hat{\boldsymbol{h}}^{(i-1)}\right). \tag{7.26}$$

As shown in Appendix 7.7, the elements of $\hat{\boldsymbol{h}}^{(i)}$ are equal to

$$\hat{h_0}^{(i)} = \frac{\boldsymbol{r}_0 \left(\boldsymbol{u}_0^{(i)}\right)^H}{(K_p + K)\sqrt{E_0}} \tag{7.27}$$

$$\hat{h_2}^{(i)} = \frac{\boldsymbol{r}_2 \left(\boldsymbol{u}_r^{(i)}\right)^H}{(K_p + K)\sqrt{E_r}}, \tag{7.28}$$

$$\left(\hat{\phi_{h_1}}^{(i)}, \hat{\gamma}^{(i)}\right) = \arg\max_{(\phi_{h_1}, \gamma)} \sum_{q=0}^{M_2-1} \ln P\left[c_r = \chi_{M_2}(q) \,\middle|\, c_0 = 1, \phi_{h_1}, \gamma\right] \Gamma_c^{(i)}(q), \tag{7.29}$$

with $\boldsymbol{u}_0^{(i)}$, $\boldsymbol{u}_r^{(i)}$ and $\Gamma_c^{(i)}(q)$ defined in (7.66), (7.67) and (7.72), respectively. Once the elements of the vector $\boldsymbol{\Gamma_c}^{(i)}$ have been calculated, the estimates of ϕ_{h_1} and γ that satisfy (7.29) can be obtained using numerical maximization. According to (7.66), (7.67) and (7.72), the elements of $\boldsymbol{u}_0^{(i)}$, $\boldsymbol{u}_r^{(i)}$ and $\boldsymbol{\Gamma}_c^{(i)}$ can be expressed in terms of the probabilities $p\left(c_0(k) \,\middle|\, \boldsymbol{r}_d, \hat{\boldsymbol{h}^{(i-1)}}\right)$ and $p\left(c_r(k) \,\middle|\, c_0(k), \boldsymbol{r}_d, \hat{\boldsymbol{h}^{(i-1)}}\right)$.

The marginal a posteriori symbol probabilities $p\left(c_0(k) \,\middle|\, \boldsymbol{r}_d, \hat{\boldsymbol{h}}^{(i-1)}\right)$ of the data symbols $c_0(k)$ can be calculated by the decoder at the destination, as explained in section 3.1.2.3. The probabilities $p\left(c_r(k) \,\middle|\, c_0(k), \boldsymbol{r}_d, \hat{\boldsymbol{h}^{(i-1)}}\right)$ are obtained as

$$\begin{aligned} p\left(c_r(k) \,\middle|\, \boldsymbol{c}_0, \boldsymbol{r}_d, \hat{\boldsymbol{h}}^{(i-1)}\right) &= p\left(c_r(k) \,\middle|\, \boldsymbol{c}_0, r_2(k), \hat{\boldsymbol{h}}^{(i-1)}\right) \\ &= \frac{p\left(r_2(k) \,\middle|\, c_r(k), \hat{h_2}^{(i-1)}\right) p\left(c_r(k) \,\middle|\, c_0(k), \hat{\phi_{h_1}}^{(i-1)}, \hat{\gamma}^{(i-1)}\right)}{\sum_{\tilde{c}_r(k)} p\left(r_2(k) \,\middle|\, \tilde{c}_r(k), \hat{h_2}^{(i-1)}\right) p\left(\tilde{c}_r(k) \,\middle|\, c_0(k), \hat{\phi_{h_1}}^{(i-1)}, \hat{\gamma}^{(i-1)}\right)}. \end{aligned} \tag{7.30}$$

The distribution $p\left(c_r(k) \,\middle|\, c_0(k), \hat{\phi_{h_1}}^{(i-1)}, \hat{\gamma}^{(i-1)}\right)$ used in (7.30) follows from (7.6).

7.3.3.1 Initialization

In order to initialize the code-aided EM algorithm, the pilot-based estimates obtained in section 7.3.2 are used. These are also obtained iteratively using the EM algorithm, which is initialized using (7.23), (7.24) and (7.22). Instead of

performing pilot-based EM iterations and using the resulting estimates to initialize the code-aided EM algorithm, the initial values (7.23), (7.24) and (7.22) could be used to directly initialize the code-aided EM algorithm, without first performing the pilot-based EM iterations. While this is a valid possibility, it will be shown in section 7.4.2.3 that this approach yields a poor error performance.

7.3.4 Direct Estimation of the Transition Probabilities

For obtaining estimates of the source-relay channel parameters ϕ_{h_1} and γ, a numerical maximization step is required for obtaining both the pilot-based estimates using (7.20) and the code-aided estimates using (7.29). These estimates are then used to compute the corresponding transition probabilities, according to (7.6). The computational complexity of this search can be avoided by directly estimating the transition probabilities, in which case the estimation of the actual channel parameters ϕ_{h_1} and γ is no longer needed. In this approach, the cascade of the source-relay channel and the quantization operation is abstracted to be a discrete channel with M_1 inputs and M_2 outputs, which is fully characterized by the probabilities $\overline{\Phi}(q,m)$, given by

$$\overline{\Phi}(q,m) = P\left[c_r = \chi_{M_2}(q) \,\middle|\, c_0 = \chi_{M_1}(m)\right] \\ ,\forall q \in \{0,1,...,M_2-1\} \quad \text{and} \quad \forall m \in \{0,1,...,M_1-1\}. \quad (7.31)$$

Using the circular symmetry at the relay given by (7.56), the elements of the matrix $\overline{\mathbf{\Phi}}$ can be written as function of the one-dimensional vector $\mathbf{\Phi}$:

$$\begin{aligned}\overline{\Phi}(q,m) &= P\left[c_r = \chi_{M_2}(q) \,\middle|\, c_0 = \chi_{M_1}(m)\right] \\ &= P\left[c_r = \chi_{M_2}\left(q + \frac{M_2 m}{M_1}\right) \,\middle|\, c_0 = 1\right] = \Phi\left(q + \frac{M_2 m}{M_1}\right). \end{aligned} \quad (7.32)$$

By estimating the elements of the vector $\mathbf{\Phi}$, we no longer need to know the value of ϕ_{h_1} and γ, as the elements of $\mathbf{\Phi}$ can directly be used to calculate the source-relay transition probabilities using (7.31) and (7.32). In the remainder of this chapter, this estimation strategy will be referred to as direct estimation.

7.3.4.1 Pilot-based Estimates

When using the direct estimation method, the pilot-based estimates of the relay path channel parameters are obtained iteratively using the EM algorithm:

$$(\hat{h_2}^{(i)}, \hat{N_2}^{(i)}, \hat{\mathbf{\Phi}}^{(i)}) = \arg\max_{h_2,N_2,\mathbf{\Phi}} \\ \mathbb{E}_{\boldsymbol{c}_{rp^\dagger}}\left[\ln p(\boldsymbol{r}_{2p}, \boldsymbol{c}_{rp^\dagger} \mid \boldsymbol{c}_{rp^\diamond}, \boldsymbol{c}_{0p}, h_2, N_2, \mathbf{\Phi}) \,\middle|\, \boldsymbol{r}_{2p}, \hat{h_2}^{(i-1)}, \hat{N_2}^{(i-1)}, \hat{\mathbf{\Phi}}^{(i-1)}\right]. \quad (7.33)$$

As explained in section 7.3.2.2, (7.33) can be split into a part corresponding to the source-relay channel parameters and a part corresponding to the relay-destination channel parameters, yielding (7.18) and (7.19) as an estimate for h_2 and N_2, respectively.

The value of $\widehat{\mathbf{\Phi}}^{(i)}$ is obtained by solving the following equation

$$\widehat{\mathbf{\Phi}}^{(i)} = \arg\max_{\mathbf{\Phi}} \sum_{q=0}^{M_2-1} \ln P\left[c_{rp^\dagger} = \chi_{M_2}(q) \mid c_{0p} = 1, \mathbf{\Phi}\right] \Gamma^{(i)}(q), \tag{7.34}$$

with $\Gamma^{(i)}(q)$ defined by (7.58). As shown in Appendix 7.8, this yields the following closed-form solution for the source-relay transition probabilities estimate

$$\widehat{\Phi}^{(i)}(q) = \frac{\Gamma^{(i)}(q)}{\sum_{\tilde{q}=0}^{M_2-1} \Gamma^{(i)}(\tilde{q})}. \tag{7.35}$$

The evaluation of (7.58) is performed using (7.21), in which the factor $p\left(c_{rp^\dagger}(k) \,\middle|\, c_{0p}(k), \hat{\phi}_{h_1}^{(i-1)}, \hat{\gamma}^{(i-1)}\right)$ is replaced by $p\left(c_{rp^\dagger}(k) \,\middle|\, c_{0p}(k); \widehat{\mathbf{\Phi}}^{(i-1)}\right)$.

7.3.4.2 Code-aided Refinement

The same approach that was used for the pilot-based estimates in section 7.3.4.1, can be used to obtain code-aided channel estimates using the direct estimation technique. Each code-aided EM-iteration i, the estimates of h_0 and h_2 are given by (7.27) and (7.28), respectively, while the estimate of $\mathbf{\Phi}$ is given by

$$\widehat{\Phi}^{(i)}(q) = \frac{\Gamma_c^{(i)}(q)}{\sum_{\tilde{q}=0}^{M_2-1} \Gamma_c^{(i)}(\tilde{q})}, \tag{7.36}$$

with $\Gamma_c^{(i)}(q)$ defined by (7.72).

7.3.5 Remarks

7.3.5.1 Concerning the Pilot-Based Estimation of the Source-Relay Channel

Decoding the received information using the pilot-based estimates obtained in section 7.3.2.2 and section 7.3.4.1 yields a poor error performance, as will be shown in section 7.4.2.2 and 7.4.2.3. When adding only a small number of pilot symbols, some source-relay transition probabilities can be falsely estimated to be equal to zero. When this happens, it is very difficult to correctly decode the information received, even in the presence of a strong source-destination

link, as explained in more detail in Appendix 7.9. This problem can be solved by adding a small offset to the transition probabilities, after completing the pilot-based EM iterations. The updated transition probabilities, denoted by the conditional distribution P_{comp} are defined as

$$P_{\text{comp}}\left[c_{rp^\dagger} = \chi_{M_2}(q) \,\middle|\, c_{0p} = 1\right] = \frac{P\left[c_{rp^\dagger} = \chi_{M_2}(q) \,\middle|\, c_{0p} = 1\right] + \frac{\beta}{M_2}}{1+\beta}, \quad (7.37)$$

where β/M_2 is the offset term and $1+\beta$ is the resulting normalization factor. The transition probabilities $P\left[c_r = \chi_{M_2}(q) \,\middle|\, c_{rp^\dagger} = 1\right]$ are to be determined using either (7.20) or (7.35). When adding an offset, the error performance drastically improves. A suitable value of β is determined in section 7.4.2.2.

7.3.5.2 MSE Lower Bound

A simple lower bound on the MSE related to the code-aided estimation of the channel coefficients h_0 and h_2 is obtained by assuming that the data symbols transmitted by the source and the relay are known to the destination (i.e., $\boldsymbol{u}_0 = \boldsymbol{c}_0$, $\boldsymbol{u}_r = \boldsymbol{c}_r$) when estimating h_0 and h_2, yielding

$$\mathbb{E}[|\hat{h_0} - h_0|^2] \geq \mathbb{E}[|\hat{h_0} - h_0|^2]\Big|_{\boldsymbol{u}_0=\boldsymbol{c}_0} = \frac{N_0}{(K_p+K)E_0} \quad (7.38)$$

$$\mathbb{E}[|\hat{h_2} - h_2|^2] \geq \mathbb{E}[|\hat{h_2} - h_2|^2]\Big|_{\boldsymbol{u}_r=\boldsymbol{c}_r} = \frac{N_2}{(K_p+K)E_r} \quad (7.39)$$

for the MSEs related to estimating h_0 and h_2, respectively.

7.4 Performance Evaluation.

In this section, the WER and MSE performances of the different estimation techniques discussed in section 7.3 are analyzed using computer simulations. First, the performance of the pilot-based estimates obtained in sections 7.3.2 and 7.3.4.1 is studied. This includes optimizing the number of pilot symbols quantized by the relay, determined by α, and the value of the offset β used in (7.37). Next, the code-aided EM algorithm is used to iteratively refine these pilot-based estimates, and the WER and MSE performance of the resulting estimates is investigated. Finally, the WER performance is compared to that from the system described in chapter 6, in which the source-relay channel is estimated at the relay.

7.4.1 Simulation Parameters

We consider a source that encodes frames of 1024 information bits by means of an $(1, 13/15)_8$ RSCC turbo code that is punctured to a rate of $2/3$. After encoding, the coded bits are mapped on M_1-PSK symbols which are broadcast in the first time slot. The quantization at the relay is performed using $\log_2(M_1) + 1$ bits, yielding $M_2 = 2M_1$.

At the destination side, pilot-based estimates of the source-destination, source-relay and relay-destination channels need to be calculated. The pilot-based estimates of the source-destination channel parameters are obtained using (7.10) and (7.11), while those of the source-relay and relay-destination channels are obtained iteratively as described in section 7.3.2.2 using 5 EM iterations.

For obtaining the code-aided estimates, 8 EM iterations are used. In order to reduce the computational complexity at the destination, the EM iterations and turbo decoding iterations are merged as explained in section 3.1.2.3. Using this technique, the increase in complexity induced by the code-aided estimation process is minimal. While the calculation of the pilot-based estimates also requires multiple EM iterations, the complexity increase induced by the latter is limited as these iterations are performed on a very limited number of pilot symbols and do not require channel code decoding.

The relay is located halfway between the source and the destination, unless stated otherwise. The path loss exponent equals 4 and the distance between the source and the destination is considered unity. For a given E_b/N_0 ratio, the symbol energy transmitted by the source and relay is computed using (7.1), assuming that $E_0 = E_r$. All noise variances are assumed to be equal ($N_0 = N_1 = N_2$) but will be estimated separately. A factor ξ equal to 0.95 is used for averaging the noise variance estimates. For $M_1 = 2$, $M_1 = 4$ and $M_1 = 8$, a number of 12, 6 and 4 pilot symbols, respectively, are added to the data symbol frames, unless stated otherwise. This approach ensures that the estimation overhead uses the same percentage of the total transmit energy, independent of the constellation size. In systems in which the channel parameters are assumed to be known, no pilot symbols are transmitted and thus no transmit energy is used for the transmission of pilot symbols.

7.4.2 Pilot-based Estimation

7.4.2.1 Optimization of α

At the relay, $\lceil \alpha K_p \rceil$ pilot symbols received from the source are quantized and forwarded to the destination. The relay also generates and sends to

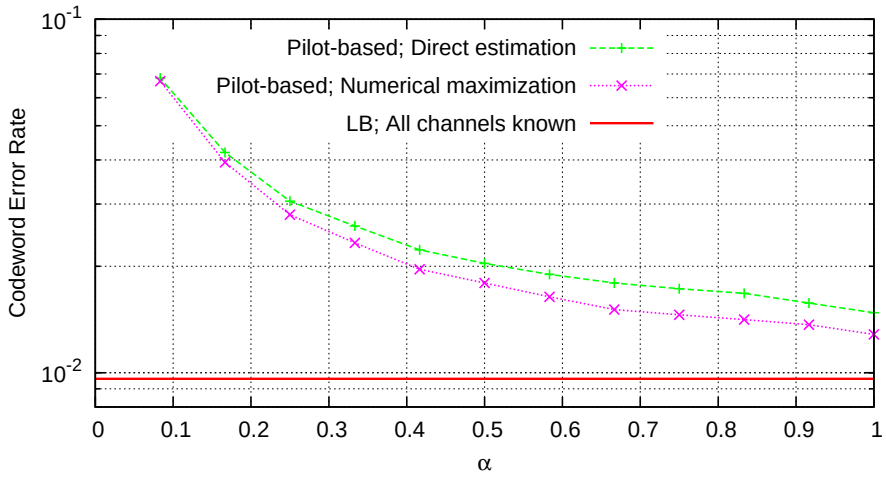

Figure 7.2: WER performance for $M_1 = 4$ at $E_b/N_0 = 9$ dB as a function of α.

the destination $\lfloor (1-\alpha)K_p \rfloor$ pilot symbols of its own for estimating the relay-destination channel. The optimal value of the parameter α can be determined by plotting the WER performance resulting from the pilot-based estimates as a function of α. This WER performance is displayed in Fig. 7.2 for a QPSK-mapped system ($M_1 = 4$) at an E_b/N_0 ratio of 9 dB. The source-relay channel is estimated by numerically maximizing (7.20) as explained in section 7.3.2.2, referred to as numerical maximization, and by directly estimating the transition probabilities as explained in section 7.3.4.1, referred to as direct estimation. The figure also shows an LB on the WER performance, corresponding to a system where the destination knows all channel parameters.

We observe that the minimum WER is achieved for $\alpha = 1$, which corresponds to the case where the relay sends to the destination a quantized version of all K_p pilot symbols from the source, but no pilot symbols of its own. This can be explained by noting from (7.18) and (7.19) that the pilot-based estimation of the relay-destination channel exploits both $\boldsymbol{r}_{2p}$ and $\boldsymbol{r}_{2p^\dagger}$ (corresponding to a total of K_p pilot symbols), whereas only $\boldsymbol{r}_{2p^\dagger}$ (corresponding to $\lceil \alpha K_p \rceil$ pilot symbols) is used for estimating the source-relay channel (see (7.57) and (7.58)); hence, taking $\alpha = 1$ yields the largest number of useful pilot symbols for both the source-relay and relay-destination channel estimation. Note that $\alpha = 1$ further simplifies the relay operation, as no relay specific pilot symbols must be generated. In the sequel, we take $\alpha = 1$. Although this optimal value has been obtained for an E_b/N_0 ratio of 9 dB, we have verified (results not shown) its optimality for other E_b/N_0 ratios.

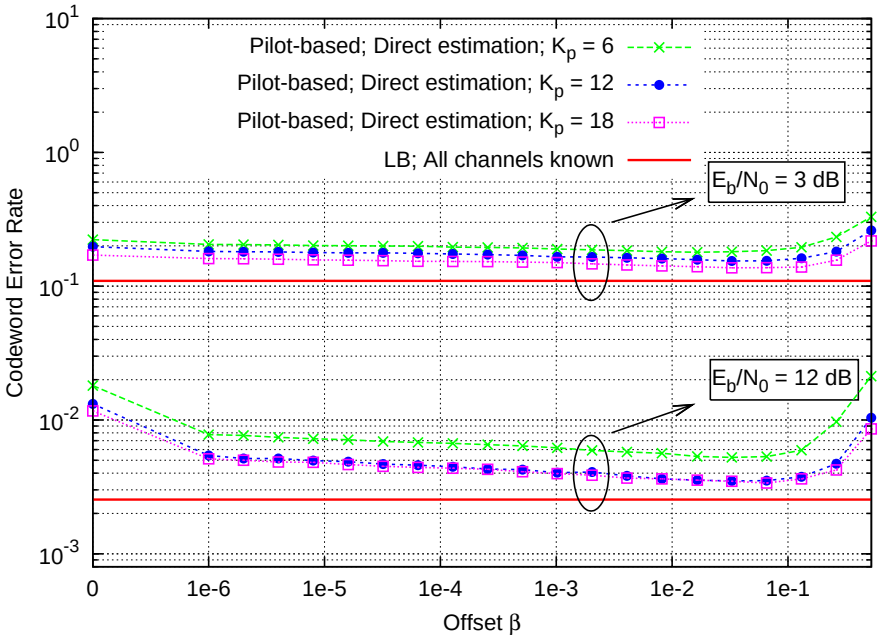

Figure 7.3: WER performance for $M_1 = 2$ at an E_b/N_0 ratio of 3 dB and 12 dB for different offset values.

When taking a value of $\alpha = 1$, the initializations (7.23) and (7.24) of the channel gain estimate and the noise variance estimate related to the relay-destination channel cannot be used. Instead, the channel gain estimate is initialized using an arbitrary value, e.g.,

$$\hat{h}_2^{(0)} = {d_2}^{-n/2}, \tag{7.40}$$

while the noise variance estimate is initialized with the averaged value computed in the previous frame. As substituting (h_1, h_2) by $(h_1\chi_{M_2}(q), h_2\chi_{M_2}(-q))$ with $q \in \{0, 1, ..., M_1 - 1\}$ does not alter the statistics of $\boldsymbol{r}_2$ when $\alpha = 1$, the absence of pilot symbols generated by the relay gives rise to a phase ambiguity of a multiple of $2\pi/M_2$ in $\hat{h_2}$ and a corresponding cyclic shift of the source-relay channel transition probabilities (either estimated directly or computed from the estimated source-relay channel parameters). This however does not affect the WER performance, because the phase ambiguity and the cyclic shift compensate each other.

7.4.2.2 Optimization of β

Fig. 7.3 shows the WER performance as a function of the offset parameter β from (7.37), for a BPSK-mapped ($M_1 = 2$) system at an E_b/N_0 ratio of 3 dB

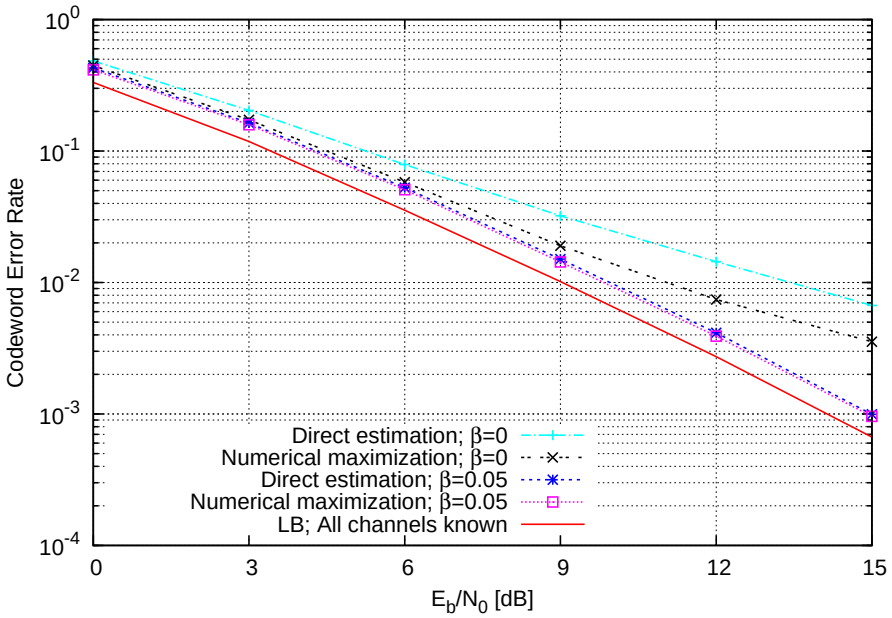

Figure 7.4: WER performance for $M_1 = 2$ using pilot-based estimation techniques.

and 12 dB and K_p = 6, 12, 18. The figure shows that a suitable value of β lies around 0.05 and depends only weakly on the E_b/N_0 ratio and the number of pilot symbols. At high E_b/N_0 ratios, however, the value of β has a more pronounced effect, as the situation depicted in Fig. 7.10 of Appendix 7.9 is more likely to occur. Adding too much offset degrades WER performance for all analyzed cases, due to the excessive flattening of the transition probability distribution. In the sequel, we take $\beta = 0.05$, unless specified otherwise.

7.4.2.3 WER Analysis

The WER performance resulting from the different pilot-based estimation methods is displayed in Fig. 7.4 for a system using BPSK-mapping ($M_1 = 2$). All channel parameters, including the noise variances of the source-destination and relay-destination channels are estimated. The transition probabilities (either estimated directly or computed from the estimated source-relay channel parameters) are modified according to (7.37) using $\beta = 0$ (no modification) and $\beta = 0.05$.

As mentioned in section 7.3.2.2, the numerical maximization and direct

estimation methods yield a poor WER performance when used without an offset. This is especially the case at high SNR values, where the offset has a greater impact, as illustrated in section 7.4.2.2. When using an offset, the WER performance drastically improves. Because the numerical maximization method makes use of the a-priori available shape of the source-relay channel distribution, given by (5.12), it yields a slightly better WER performance compared to the direct estimation method which does not make use of this information. The direct estimation method can however be used in situations where the channel distribution is either unknown or too complicated, and does not suffer from the computational complexity (2-dimensional search) associated with the numerical maximization. As will be shown in the next subsection, the performance gap between the direct estimation method and the numerical maximization method completely disappears when code-aided refinement is used.

7.4.3 Code-aided Estimation

The pilot-based estimates obtained in section 7.3.2 can be refined using the code-aided EM algorithm, as discussed in section 7.3.3. The effect of this refinement on the WER and MSE performance will be studied in this section.

7.4.3.1 WER Analysis

Fig. 7.5 shows the WER performance of an 8-PSK-mapped ($M_1 = 8$) system of which the estimates are refined using a code-aided EM approach. The performance of both the numerical maximization and the direct estimation method is investigated. An offset parameter β equal to 0.05 is applied to the initial transition probability estimates, after convergence of the pilot-based EM algorithm. After applying the offset, the resulting transition probabilities are used to decode the received information when no code-aided refinement is used or to initialize the code-aided EM algorithm when code-aided refinement is applied. After convergence of the code-aided EM algorithm, no offset is applied to the resulting transition probabilities estimate. We have verified (results not shown) that the use of an offset does not improve the performance of the latter.

As mentioned in subsection 7.3.3.1, it is possible to initialize the code-aided EM algorithm using pilot-based estimates of the source-relay and relay-destination channel parameters that have not been iteratively refined, obtained using (7.22) and (7.23), respectively, for $\alpha < 1$ and (7.22) and (7.40), respectively, for $\alpha = 1$. This initialization method is denoted direct initialization and the corresponding WER performance is also shown on Fig. 7.5.

The figure shows that the use of the code-aided EM algorithm drastically improves the WER performance. While the direct estimation method has a

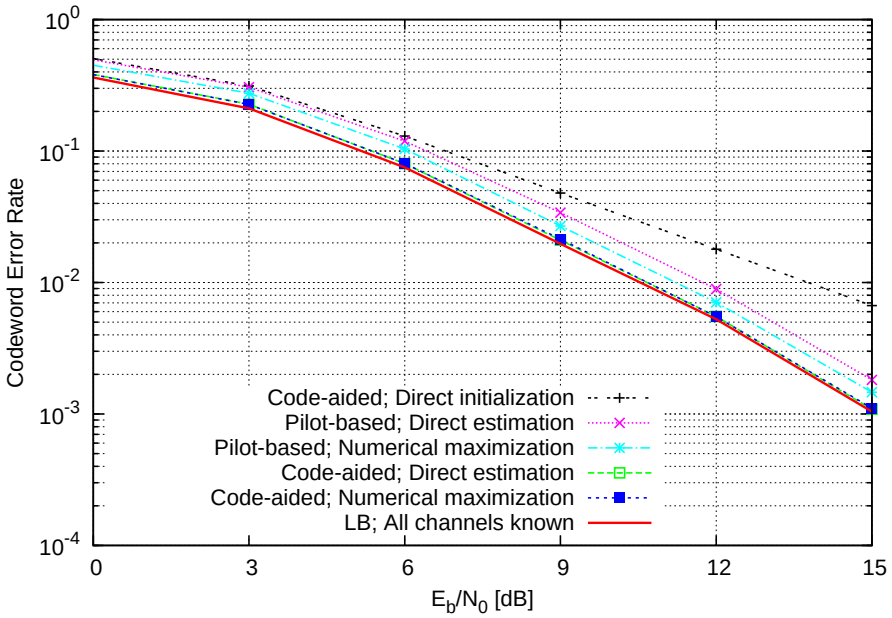

Figure 7.5: WER performance for $M_1 = 8$ using code-aided estimation techniques.

worse WER performance compared to the numerical maximization method for the pilot-based estimates, both methods have a similar WER performance when using a code-aided approach. Due to the large number of symbols available in a code-aided situation, the direct estimation method can reliably determine the source-relay channel transition probabilities, even without exploiting the relation (5.12) between transition probabilities and source-relay channel parameters.

When using the direct initialization method, the code-aided EM algorithm fails to converge when the source-destination channel is in fading, as the received data symbols cannot be reliably decoded using the poor initial source-relay and relay-destination channel estimates. Due to the limited number of pilot symbols as compared to the number of data symbols, the channel estimates that are updated each EM iteration will mostly be based on the (erroneously) decoded data symbols. Consequently, the WER is largely determined by the state of the source-destination channel and the benefits of cooperative communication are mostly lost, explaining the poor WER performance.

In order to study the performance of the proposed algorithms for a relay

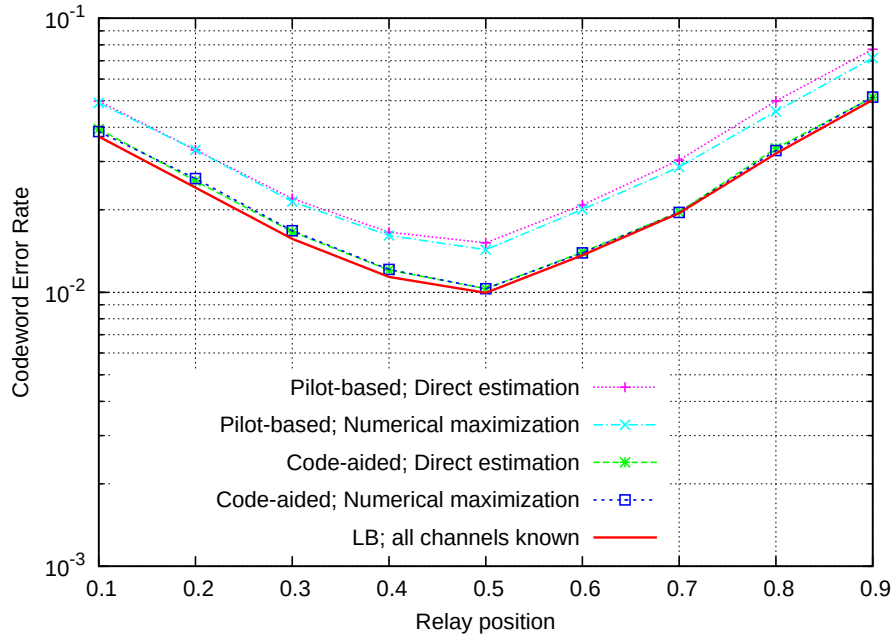

Figure 7.6: WER performance for different relay positions using $M_1 = 2$ and $E_b/N_0 = 9$ dB.

that is not located halfway between the source and the destination, Fig. 7.6 is introduced. The figure shows the WER performance of a BPSK-mapped system which operates at an E_b/N_0 ratio equal to 9dB. The relay position is varied on a line connecting the source and the destination, with the x-axis of Fig. 7.6 representing the distance between the source and the relay. The distance between the source and the destination is considered unity. The figure shows that the proposed estimation algorithms perform adequately for all analyzed relay positions. The best WER performance is achieved when the relay is located halfway between the source and the destination, as is to be expected considering the path loss exponent.

7.4.3.2 MSE Analysis

The estimation performance can also be analyzed by investigating the MSE values related to the different channel estimates. These MSE values are displayed in Fig. 7.7 for $\hat{h_0}$, Fig. 7.8 for $\hat{h_2}$ and Fig. 7.9 for the source-relay channel transition probabilities estimate. A BPSK mapping ($M_1 = 2$) constellation is used at the source. The direct estimation technique described in section 7.3.4 is used to obtain an estimate of the source-relay channel transition probabilities.

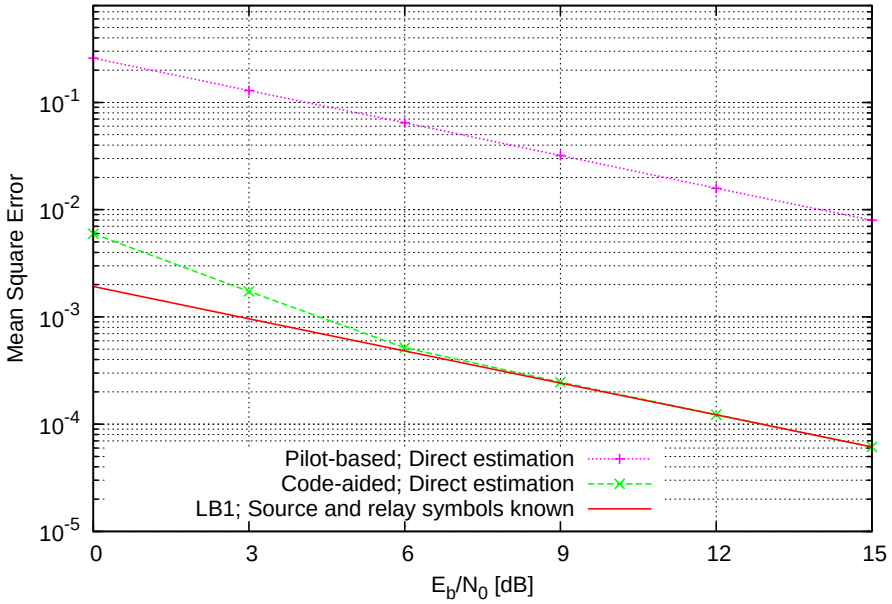

Figure 7.7: Mean Square Error related to the estimation of the source-destination channel gain h_0 of a system using $M_1 = 2$.

The MSE corresponding to the latter is obtained by computing the Euclidian distance between the vectors of the estimated transition probabilities and the actual ones

$$\begin{aligned}&\mathrm{MSE}_{\boldsymbol{\Phi}}\\ &= \sum_{q=0}^{M_2-1} \left(P\left[c_r = \chi_{M_2}(q) \,\middle|\, c_0 = 1, \widehat{\boldsymbol{\Phi}}\right] - P\left[c_r = \chi_{M_2}(q) \,\middle|\, c_0 = 1, \phi_{h_1}, \gamma\right]\right)^2.\end{aligned} \tag{7.41}$$

Because of the phase ambiguity on the source-relay and relay-destination channels, the estimates of these channels need to be compensated in order to obtain meaningfull MSE values. This is achieved by applying x cyclic shifts to the estimated transition probability vector $\widehat{\boldsymbol{\Phi}}$ and by multiplying $\hat{h_2}$ with $\chi_{M_2}(-x)$, with

$$x = \arg\min_{\tilde{x}} \left| \boldsymbol{u}_r \chi_{M_2}(\tilde{x}) - \boldsymbol{c}_r \right| \tag{7.42}$$

and $\boldsymbol{u}_r$ defined by (7.67). Two LB's are also displayed on the aforementioned figures. The first LB (LB1) corresponds to the situation in which the destination is assumed to know the symbols sent by both the source and the relay

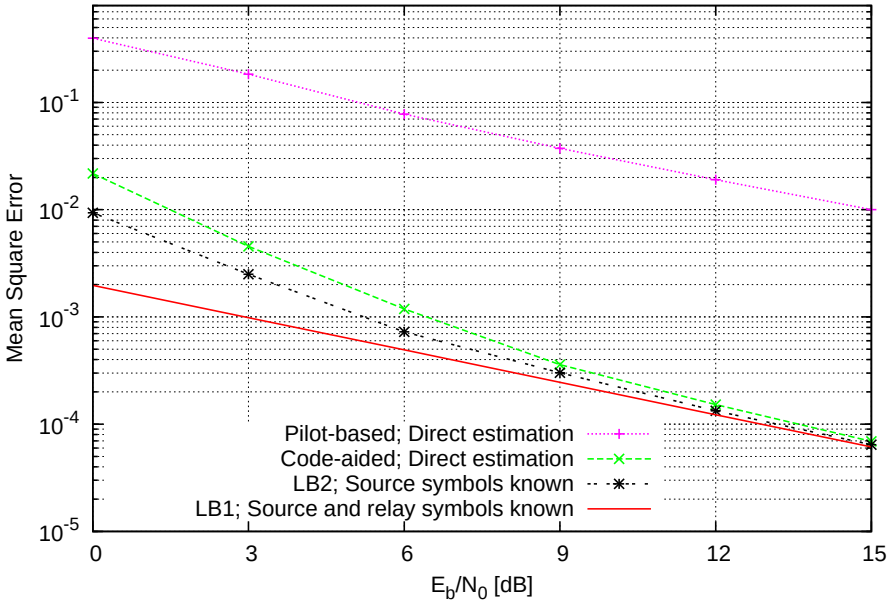

Figure 7.8: Mean Square Error related to the estimation of the relay-destination channel gain h_2 of a system using $M_1 = 2$.

when calculating the channel estimates. This LB has been described in section 7.3.5.2. The second LB (LB2) corresponds to the situation in which the destination is only assumed to know the symbols sent by the source, whereas the a posteriori expectation of the symbols sent by the relay is computed using (7.67), yielding a tighter LB.

As shown by Fig. 7.7, the MSE of the code-aided estimate of h_0 quickly approaches LB2 (which coincides with LB1 because only $\boldsymbol{r}_0$ is involved in the estimation of h_0) for increasing E_b/N_0, implying that, for moderate to high SNR values, the a posteriori expectation of the symbols sent by the source are close to the actual symbols. This is also the case in Fig. 7.8, which shows the MSE related to the channel coefficient estimate of the relay-destination channel. For increasing SNR values, the a posteriori expectation of the symbols sent by the relay, given by (7.67), gets closer to the actual relay symbols, and LB2 approaches LB1.

The MSE related to the estimation of the source-relay channel transition probabilities is shown in Fig. 7.9. The source-relay channel transition probabilities estimate is inaccurate when the relay-destination channel is in fading,

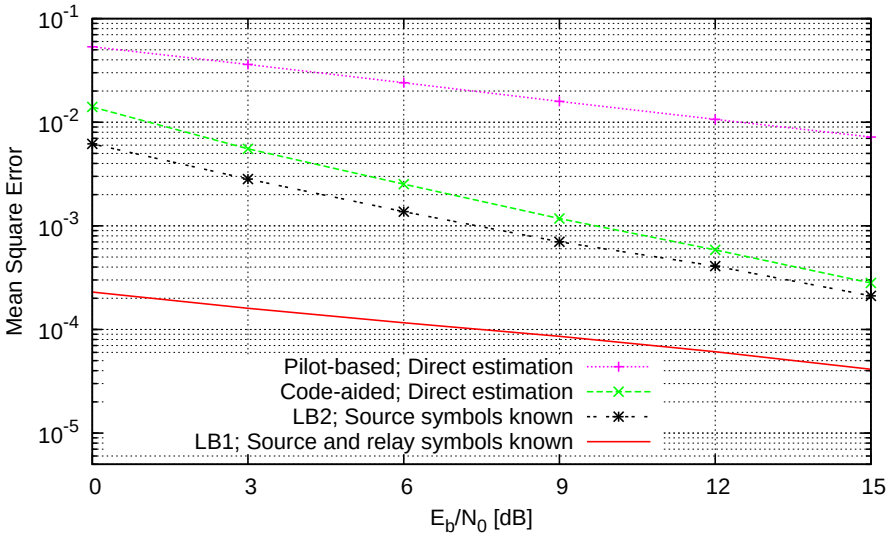

Figure 7.9: Mean Square Error related to the estimation of the source-relay channel transition probabilities of a system using $M_1 = 2$.

as in this case it is very difficult to determine the symbols sent by the relay. However, when this phenomenon occurs, the relay path is not used when decoding the received information symbols, so the WER performance is barely affected as compared to the case where the transition probabilities are known to the destination.

7.4.4 Comparison Between Coherent and Non-coherent Quantization

In Table 7.1, a comparison is made between the WER performance of the system model described in this chapter and the one described in chapter 6. In the first system model, the relay quantizes the received signal without knowing the state of the source-relay channel. This is denoted as non-coherent quantization. When using the QF protocol described in chapter 6, the relay estimates and compensates for the source-relay channel before quantizing the received signal. This is denoted as coherent quantization. The relay quantizes the received information using $\log_2(M_1) + 1$ and $\log_2(M_1)$ bits when using non-coherent and coherent quantization, respectively. A QPSK constellation ($M_1 = 4$) is used at the source in both system models and when non-coherent quantization is used, the direct estimation method is utilized to estimate the source-relay channel, as this method yields the lowest computational com-

Table 7.1: E_b/N_0 ratio needed to achieve a WER of 0.01.

Coherent quantization	E_b/N_0 (dB)	Difference
Reference system	9.03	0
LB; Source and relay symbols known	9.29	+ 0.26
Code-aided	9.32	+ 0.29
Pilot-based	9.91	+ 0.88

Non-coherent quantization	E_b/N_0 (dB)	Difference
Reference system	8.93	0
LB; Source and relay symbols known	8.98	+ 0.05
Code-aided	9.01	+ 0.08
Pilot-based	10.06	+ 1.13

plexity. Table 7.1 shows the performance of the reference system (all channel parameters known), the WER LB corresponding to channel estimation under the assumption that all source and relay symbols are known, and the WER for pilot-based estimation and code-aided estimation. Due to the different quantization schemes used, both reference systems have a different WER performance. Therefore, the performance of the different estimation methods is evaluated by investigating the extra energy (expressed in terms of E_b/N_0), as compared to the reference system, needed to achieve a given WER.

The results show that while the degradation associated with the pilot-based estimates is smaller for coherent quantization, the opposite holds when considering the code-aided estimation and the LB. When non-coherent quantization is used, the source-relay channel estimate is refined using the EM algorithm without increasing the computational complexity at the relay. In the case of coherent quantization, the source-relay channel parameter estimation is performed at the relay, and is based on pilot symbols only (no refinement by means of EM algorithm) in order not to increase the complexity at the relay. Hence, non-coherent quantization yields more accurate channel estimates and a better WER performance.

In comparison to the coherent quantization system from chapter 6, using non-coherent quantization shifts the burden of estimating the source-relay channel from the relay to the destination. In doing so, the complexity of the relay terminal is unaffected by the estimation process. At the destination, the estimation of the source-relay channel requires little additional effort, as the a posteriori probabilities used to calculate the elements of the vector Γ used in (7.29) and (7.36) are also used for estimating the source-destination and relay-destination channel parameters. When estimating the source-relay channel using a 2-dimensional search, the value of the transition probabilities for different values of ϕ_{h_1} and γ can be calculated beforehand and stored in memory.

This search can be avoided altogether by using the direct estimation method, which yields a significant decrease in complexity, while having essentially the same WER performance when code-aided refinement is used.

7.5 Conclusions

In this chapter, estimation methods were discussed for a QF system in which all channel parameters are estimated at the destination, keeping the relay complexity low. Furthermore, as shown in section 7.4.2.1, the best WER performance is achieved when the relay quantizes and forwards to the destination all pilot symbols received from the source, without the addition of supplementary, relay-generated, pilot symbols. This further lowers the complexity of the relay, as the latter does not need to distinguish anymore between data and pilot symbols.

In addition to not increasing the complexity at the relay terminal, the estimation algorithms derived in this chapter also exhibit a very good WER performance. By refining the pilot-based estimates using a code-aided EM algorithm, the loss in WER performance compared to a system with known channel parameters can be made very small. In an attempt to decrease the computational complexity at the destination, an algorithm is proposed to directly estimate the source-relay channel transition probabilities instead of the physical parameters of the source-relay channel, the latter requiring a two dimensional search. The excellent WER performance and low relay complexity make the results obtained in this chapter very suitable for the application in sensor networks, where the relay terminals have limited hardware resources.

7.6 Appendix: Pilot-based Estimation of ϕ_{h_1}, γ, h_2 and N_2

Pilot-based estimates of the relay path channel parameters are obtained iteratively using the EM algorithm. At each iteration i, the following Q-function is calculated:

$$Q\left(\boldsymbol{h}_r, \hat{\boldsymbol{h}}_r^{(i-1)}\right) = \mathbb{E}_{\boldsymbol{c}_{rp^\dagger}}\left[\ln p(\boldsymbol{r}_{2p}, \boldsymbol{c}_{rp^\dagger} \mid \boldsymbol{c}_{rp^\diamond}, \boldsymbol{c}_{0p}, \boldsymbol{h}_r) \,\middle|\, \boldsymbol{r}_{2p}, \hat{\boldsymbol{h}}_r^{(i-1)}\right], \tag{7.43}$$

which is then maximized with respect to $\boldsymbol{h}_r$ in order to update the channel estimates, yielding

$$\hat{\boldsymbol{h}}_r^{(i)} = \arg\max_{\boldsymbol{h}_r} Q\left(\boldsymbol{h}_r, \hat{\boldsymbol{h}}_r^{(i-1)}\right). \tag{7.44}$$

By conditioning on $\boldsymbol{c}_{rp^\dagger}$, (7.43) can be written as

$$\begin{aligned} Q\left(\boldsymbol{h}_r, \hat{\boldsymbol{h}}_r^{(i-1)}\right) = {} & \mathbb{E}_{\boldsymbol{c}_{rp^\dagger}}\left[\ln p(\boldsymbol{r}_{2p} \mid \boldsymbol{c}_{rp}, h_2, N_2) \,\middle|\, \boldsymbol{r}_{2p}, \hat{\boldsymbol{h}}_r^{(i-1)}\right] \\ & + \mathbb{E}_{\boldsymbol{c}_{rp^\dagger}}\left[\ln p(\boldsymbol{c}_{rp^\dagger} \mid \boldsymbol{c}_{0p}, \phi_{h_1}, \gamma) \,\middle|\, \boldsymbol{r}_{2p}, \hat{\boldsymbol{h}}_r^{(i-1)}\right]. \end{aligned} \tag{7.45}$$

As the first term in (7.45) only depends on the relay-destination channel parameters, while the second term in (7.45) only depends on the source-relay channel parameters, maximization problem (7.44) transforms to

$$(\hat{h_2}^{(i)}, \hat{N_2}^{(i)}) = \arg\max_{(h_2, N_2)} \mathbb{E}_{\boldsymbol{c}_{rp^\dagger}}\left[\ln p(\boldsymbol{r}_{2p} \mid \boldsymbol{c}_{rp}, h_2, N_2) \,\middle|\, \boldsymbol{r}_{2p}, \hat{\boldsymbol{h}}_r^{(i-1)}\right] \tag{7.46}$$

$$\left(\hat{\phi_{h_1}}^{(i)}, \hat{\gamma}^{(i)}\right) = \arg\max_{(\phi_{h_1}, \gamma)} \mathbb{E}_{\boldsymbol{c}_{rp^\dagger}}\left[\ln p(\boldsymbol{c}_{rp^\dagger} \mid \boldsymbol{c}_{0p}, \phi_{h_1}, \gamma) \,\middle|\, \boldsymbol{r}_{2p}, \hat{\boldsymbol{h}}_r^{(i-1)}\right]. \tag{7.47}$$

Taking into consideration (7.4), maximization problem (7.46) can be written as

$$\begin{aligned} & (\hat{h_2}^{(i)}, \hat{N_2}^{(i)}) \\ & \quad = \arg\min_{(h_2, N_2)} \mathbb{E}_{\boldsymbol{c}_{rp^\dagger}}\left[K_p \ln(\pi N_2) + \frac{\left|\boldsymbol{r}_{2p} - \sqrt{E_r} h_2 \boldsymbol{c}_{rp}\right|^2}{N_2} \,\middle|\, \boldsymbol{r}_{2p}, \hat{\boldsymbol{h}}_r^{(i-1)}\right]. \end{aligned} \tag{7.48}$$

The maximization of (7.48) with respect to h_2 for a given N_2 yields the following maximization problem for $\hat{h_2}^{(i)}(N_2)$:

$$\hat{h_2}^{(i)}(N_2) = \arg\min_{h_2} \mathbb{E}_{\boldsymbol{c}_{rp^\dagger}}\left[\left|\boldsymbol{r}_{2p} - \sqrt{E_r} h_2 \boldsymbol{c}_{rp}\right|^2 \,\middle|\, \boldsymbol{r}_{2p}, \hat{\boldsymbol{h}}_r^{(i-1)}\right]. \tag{7.49}$$

Identification between (7.49) and (6.68) yields

$$\hat{h_2}^{(i)} = \frac{\boldsymbol{r}_{2p}\left(\boldsymbol{c}_{rp^\diamond}, \boldsymbol{u}_{rp^\dagger}^{(i)}\right)^H}{K_p \sqrt{E_r}}, \tag{7.50}$$

with

$$\begin{aligned}\boldsymbol{u}_{rp^\dagger}^{(i)} &= \mathbb{E}_{\boldsymbol{c}_{rp^\dagger}}\left[\boldsymbol{c}_{rp^\dagger} \mid \boldsymbol{r}_{2p}, \hat{\boldsymbol{h}}_r^{(i-1)}\right] \\ &= \sum_{\boldsymbol{c}_{rp^\dagger}} \boldsymbol{c}_{rp^\dagger} p\left(\boldsymbol{c}_{rp^\dagger} \mid \boldsymbol{r}_{2p^\dagger}, \hat{\boldsymbol{h}}_r^{(i-1)}\right),\end{aligned} \tag{7.51}$$

The value $\hat{h_2}^{(i)}$, which is independent of N_2, can now be used in (7.48) to obtain an estimate of N_2:

$$\hat{N_2}^{(i)} = \frac{\mathbb{E}_{\boldsymbol{c}_{rp^\dagger}}\left[\left|\boldsymbol{r}_{2p} - \sqrt{E_r}\hat{h_2}^{(i)}\boldsymbol{c}_{rp}\right|^2 \middle| \boldsymbol{r}_{2p}, \hat{\boldsymbol{h}}_r^{(i-1)}\right]}{K_p}. \tag{7.52}$$

Using the definition of $\boldsymbol{u}_{rp^\dagger}^{(i)}$ from (7.51), (7.52) can be written as

$$\hat{N_2}^{(i)} = \frac{\left|\boldsymbol{r}_{2p} - \sqrt{E_r}\hat{h_2}^{(i)}\left(\boldsymbol{c}_{rp^\diamond}, \boldsymbol{u}_{rp^\dagger}^{(i)}\right)\right|^2 + E_r\left|\hat{h_2}^{(i)}\right|^2\left(\lceil \alpha K_p \rceil - \boldsymbol{u}_{rp^\dagger}^{(i)}\left(\boldsymbol{u}_{rp^\dagger}^{(i)}\right)^H\right)}{K_p}, \tag{7.53}$$

concluding the estimation of the relay-destination channel parameters.

In order to obtain an estimate of the source-relay channel parameters ϕ_{h_1} and γ, the maximization problem in (7.47) needs to be solved. Evaluating (7.47) on a symbol-by-symbol basis yields

$$\begin{aligned}\left(\hat{\phi_{h_1}}^{(i)}, \hat{\gamma}^{(i)}\right) &= \arg\max_{(\phi_{h_1},\gamma)} \sum_{\boldsymbol{c}_{rp^\dagger}} \ln p(\boldsymbol{c}_{rp^\dagger} \mid \boldsymbol{c}_{0p}, \phi_{h_1}, \gamma) p\left(\boldsymbol{c}_{rp^\dagger} \middle| \boldsymbol{r}_{2p}, \hat{\boldsymbol{h}}_r^{(i-1)}\right) \\ &= \arg\max_{(\phi_{h_1},\gamma)} \sum_{\boldsymbol{c}_{rp^\dagger}} \sum_{k=1}^{\lceil \alpha K_p \rceil} \ln p(c_{rp^\dagger}(k) \mid c_{0p}(k), \phi_{h_1}, \gamma) p\left(c_{rp^\dagger}(k) \middle| r_{2p^\dagger}(k), \hat{\boldsymbol{h}}_r^{(i-1)}\right).\end{aligned} \tag{7.54}$$

By summing over each quantization interval instead of summing over all possible combinations of $\boldsymbol{c}_{rp^\dagger}$, (7.54) can be written as

$$\begin{aligned}&\left(\hat{\phi_{h_1}}^{(i)}, \hat{\gamma}^{(i)}\right) \\ &= \arg\max_{(\phi_{h_1},\gamma)} \sum_{k=1}^{\lceil \alpha K_p \rceil} \sum_{q=0}^{M_2-1} \ln P\left[c_{rp^\dagger}(k) = \chi_{M_2}(q) \mid c_{0p}(k) = \chi_{M_1}(m), \phi_{h_1}, \gamma\right] \\ &\qquad .P\left[c_{rp^\dagger}(k) = \chi_{M_2}(q) \middle| r_{2p^\dagger}(k), \hat{\boldsymbol{h}}_r^{(i-1)}\right].\end{aligned} \tag{7.55}$$

The maximization problem in (7.55) can be rearranged by taking into account the circular symmetry at the relay, expressed as

$$P\left[c_{rp^\dagger}(k) = \chi_{M_2}(q) \,\middle|\, c_{0p}(k) = \chi_{M_1}(0), \phi_{h_1}, \gamma\right] = P\left[c_{rp^\dagger}(k) = \chi_{M_2}\left(q + \frac{M_2 m}{M_1}\right) \,\middle|\, c_{0p}(k) = \chi_{M_1}(m), \phi_{h_1}, \gamma\right]. \quad (7.56)$$

with $m \in \{0, 1, ..., M_1 - 1\}$. Using (7.56) and the fact that, for a given q and m, the first factor from (7.55) does not depend on the symbol position k, (7.55) can be written as

$$\left(\hat{\phi_{h_1}}^{(i)}, \hat{\gamma}^{(i)}\right) = \arg \max_{(\phi_{h_1}, \gamma)} \sum_{q=0}^{M_2-1} \ln P\left[c_{rp^\dagger} = \chi_{M_2}(q) \,|\, c_{0p} = 1, \phi_{h_1}, \gamma\right] \Gamma^{(i)}(q), \quad (7.57)$$

with

$$\Gamma^{(i)}(q) = \sum_{k=1}^{\lceil \alpha K_p \rceil} \sum_{m=0}^{M_1-1} P\left[c_{rp^\dagger}(k) = \chi_{M_2}\left(q + \frac{M_2 m}{M_1}\right) \,\middle|\, r_{2p^\dagger}(k), \hat{\boldsymbol{h}}_r^{(i-1)}\right] \mathbb{I}_k\left[c_{0p} = \chi_{M_1}(m)\right]. \quad (7.58)$$

The function $\mathbb{I}\left[c_{0p}(k) = \chi_{M_1}(m)\right]$ is defined as

$$\mathbb{I}\left[x = y\right] = \begin{cases} 1 & \text{if} \quad x = y \\ 0 & \text{otherwise} \end{cases}. \quad (7.59)$$

After the elements of the vector $\boldsymbol{\Gamma}^{(i)}$ have been calculated, the values of ϕ_{h_1} and γ that maximize (7.57) can be obtained using numerical maximization techniques.

7.7 Appendix: Maximization of $Q\left(\boldsymbol{h}, \hat{\boldsymbol{h}}^{(i-1)}\right)$

At each code-aided EM iteration i, new estimates of the channel parameters h_0, ϕ_{h_1} , γ and h_2 are calculated by selecting the value of $\boldsymbol{h}$ that maximizes the function $Q(\boldsymbol{h}, \hat{\boldsymbol{h}}^{(i-1)})$, defined by (7.25). Using (5.8), this function can be written as

$$\begin{aligned} Q\left(\boldsymbol{h}, \hat{\boldsymbol{h}}^{(k-1)}\right) &= \mathbb{E}_{\boldsymbol{c}_0}\left[\ln p(\boldsymbol{r}_0 \,|\, \boldsymbol{c}_0, h_0) \,\middle|\, \boldsymbol{r}_d, \hat{\boldsymbol{h}}^{(i-1)}\right] \\ &+ \mathbb{E}_{\boldsymbol{c}_r}\left[\ln p(\boldsymbol{r}_2 \,|\, \boldsymbol{c}_r, h_2) \,\middle|\, \boldsymbol{r}_d, \hat{\boldsymbol{h}}^{(i-1)}\right] \\ &+ \mathbb{E}_{\boldsymbol{c}_0, \boldsymbol{c}_r}\left[\ln p(\boldsymbol{c}_r \,|\, \boldsymbol{c}_0, \phi_{h_1}, \gamma) \,\middle|\, \boldsymbol{r}_d, \hat{\boldsymbol{h}}^{(i-1)}\right]. \end{aligned} \quad (7.60)$$

As each term only depends on a disjoint set of the channel parameters, the maximization problem transforms into

$$\hat{h_0}^{(i)} = \arg\max_{h_0} \mathbb{E}_{\boldsymbol{c}_0}\left[\ln p(\boldsymbol{r}_0 \mid \boldsymbol{c}_0, h_0) \,\middle|\, \boldsymbol{r}_d, \hat{\boldsymbol{h}}^{(i-1)}\right] \tag{7.61}$$

$$\hat{h_2}^{(i)} = \arg\max_{h_2} \mathbb{E}_{\boldsymbol{c}_r}\left[\ln p(\boldsymbol{r}_2 \mid \boldsymbol{c}_r, h_2) \,\middle|\, \boldsymbol{r}_d, \hat{\boldsymbol{h}}^{(i-1)}\right] \tag{7.62}$$

$$\left(\hat{\phi_{h_1}}^{(i)}, \hat{\gamma}^{(i)}\right) = \arg\max_{(\phi_{h_1}, \gamma)} \mathbb{E}_{\boldsymbol{c}_0, \boldsymbol{c}_r}\left[\ln p(\boldsymbol{c}_r \mid \boldsymbol{c}_0, \phi_{h_1}, \gamma) \,\middle|\, \boldsymbol{r}_d, \hat{\boldsymbol{h}}^{(i-1)}\right]. \tag{7.63}$$

Identification between (7.61) and (6.66) and between (7.62) and (6.67) yields the following values for $\hat{h_0}^{(i)}$ and $\hat{h_2}^{(i)}$, respectively

$$\hat{h_0}^{(i)} = \frac{\boldsymbol{r}_0 \left(\boldsymbol{u}_0^{(i)}\right)^H}{(K_p + K)\sqrt{E_0}} \tag{7.64}$$

$$\hat{h_2}^{(i)} = \frac{\boldsymbol{r}_2 \left(\boldsymbol{u}_r^{(i)}\right)^H}{(K_p + K)\sqrt{E_r}}, \tag{7.65}$$

with

$$\boldsymbol{u}_0^{(i)} = \sum_{\boldsymbol{c}_0} \boldsymbol{c}_0 p\left(\boldsymbol{c}_0 \,\middle|\, \boldsymbol{r}_d, \hat{\boldsymbol{h}}^{(i-1)}\right) \tag{7.66}$$

$$\boldsymbol{u}_r^{(i)} = \sum_{\boldsymbol{c}_0, \boldsymbol{c}_r} \boldsymbol{c}_r p\left(\boldsymbol{c}_0, \boldsymbol{c}_r \,\middle|\, \boldsymbol{r}_d, \hat{\boldsymbol{h}}^{(i-1)}\right). \tag{7.67}$$

The k-th component of $\boldsymbol{u}_0^{(i)}$ and $\boldsymbol{u}_r^{(i)}$ can be expressed as

$$u_0^{(i)}(k) = \sum_{c_0(k)} c_0(k) p\left(c_0(k) \,\middle|\, \boldsymbol{r}_d, \hat{\boldsymbol{h}}^{(i-1)}\right) \tag{7.68}$$

$$\begin{aligned} u_r^{(i)}(k) &= \sum_{c_0(k), c_r(k)} c_r(k) p\left(c_0(k), c_r(k) \,\middle|\, \boldsymbol{r}_d, \hat{\boldsymbol{h}}^{(i-1)}\right) \\ &= \sum_{c_0(k), c_r(k)} c_r(k) p\left(c_r(k) \,\middle|\, c_0(k), \boldsymbol{r}_d, \hat{\boldsymbol{h}}^{(i-1)}\right) p\left(c_0(k) \,\middle|\, \boldsymbol{r}_d, \hat{\boldsymbol{h}}^{(i-1)}\right). \end{aligned} \tag{7.69}$$

The source-relay channel estimates are obtained by evaluating (7.63) on a symbol-by-symbol basis and summing over each quantization interval and mapper symbol instead of summing over all possible combinations of $\boldsymbol{c}_0$ and $\boldsymbol{c}_r$, transforming (7.63) into

$$\begin{aligned} &\left(\hat{\phi_{h_1}}^{(i)}, \hat{\gamma}^{(i)}\right) \\ &= \arg\max_{(\phi_{h_1}, \gamma)} \sum_{k=1}^{\lceil \alpha K_p \rceil + K} \sum_{q=0}^{M_2-1} \sum_{m=0}^{M_1-1} \ln P\left[c_r(k) = \chi_{M_2}(q) \,\middle|\, c_0(k) = \chi_{M_1}(m), \phi_{h_1}, \gamma\right] \\ &\qquad .P\left[c_r(k) = \chi_{M_2}(q), c_0(k) = \chi_{M_1}(m) \,\middle|\, \boldsymbol{r}_d, \hat{\boldsymbol{h}}^{(i-1)}\right]. \end{aligned} \tag{7.70}$$

Taking into account the circular symmetry at the relay, defined by (7.56), and using a similar approach as was used in section 7.6 yields

$$\left(\hat{\phi_{h_1}}^{(i)}, \hat{\gamma}^{(i)}\right) = \arg \max_{(\phi_{h_1}, \gamma)} \sum_{q=0}^{M_2-1} \ln P\left[c_r = \chi_{M_2}(q) \,\middle|\, c_0 = 1, \phi_{h_1}, \gamma\right] \Gamma_c^{(i)}(q), \tag{7.71}$$

with

$$\begin{aligned}\Gamma_c^{(i)}(q) &\\ = \sum_{k=1}^{\lceil \alpha K_p \rceil + K} \sum_{m=0}^{M-1} & P\left[c_r(k) = \chi_{M_2}\left(q + \frac{M_2 m}{M_1}\right) \,\middle|\, c_0(k) = \chi_{M_1}(m), \boldsymbol{r}_d, \hat{\boldsymbol{h}}^{(i-1)}\right] \\ & .P\left[c_0(k) = \chi_{M_1}(m) \,\middle|\, \boldsymbol{r}_d, \hat{\boldsymbol{h}}^{(i-1)}\right].\end{aligned} \tag{7.72}$$

7.8 Appendix: Pilot-based Direct Estimation of the Transition Probabilities

When directly estimating the transition probabilities, the following equation needs to be solved

$$\widehat{\boldsymbol{\Phi}}^{(i)} = \arg\max_{\boldsymbol{\Phi}} \sum_{q=0}^{M_2-1} \ln P\left[c_{rp^\dagger} = \chi_{M_2}(q) \,\middle|\, c_{0p} = 1, \boldsymbol{\Phi}\right] \Gamma^{(i)}(q), \tag{7.73}$$

with $\Gamma^{(i)}(q)$ defined by (7.58). This maximization problem needs to be solved under the constraints $\sum_{q=0}^{M_2-1} \widehat{\Phi}^{(i)}(q) = 1$ (normalization) and $0 \leq \widehat{\Phi}^{(i)}(q) \leq 1$ for all q. By only considering the normalization constraint and ignoring the remaining inequality constraints, (7.73) can be solved using Lagrange multipliers. Afterwards, it will be verified that the resulting solution also satisfies the inequality constraints. The stationary points of the Lagrange function are found using the following equation

$$0 = \nabla_{\widehat{\boldsymbol{\Phi}}^{(i)}, \lambda} \left[\sum_{q=0}^{M_2-1} \Gamma^{(i)}(q) \ln \widehat{\Phi}^{(i)}(q) + \lambda \left(\sum_{\tilde{q}=0}^{M_2-1} \widehat{\Phi}^{(i)}(\tilde{q}) - 1 \right) \right]. \tag{7.74}$$

This can be transformed into a set of equations, yielding

$$\begin{cases} 0 = & \frac{\Gamma^{(i)}(q)}{\widehat{\Phi}^{(i)}(q)} + \lambda, \quad q \in \{0, 1, .., M_2 - 1\} \\ 0 = & \sum_{\tilde{q}=0}^{M_2-1} \widehat{\Phi}^{(i)}(\tilde{q}) - 1. \end{cases} \tag{7.75}$$

Solving (7.75) yields the following closed-form solution for the elements of $\boldsymbol{\Phi}$

$$\widehat{\Phi}^{(i)}(q) = \frac{\Gamma^{(i)}(q)}{\sum_{\tilde{q}=0}^{M_2-1} \Gamma^{(i)}(\tilde{q})}. \tag{7.76}$$

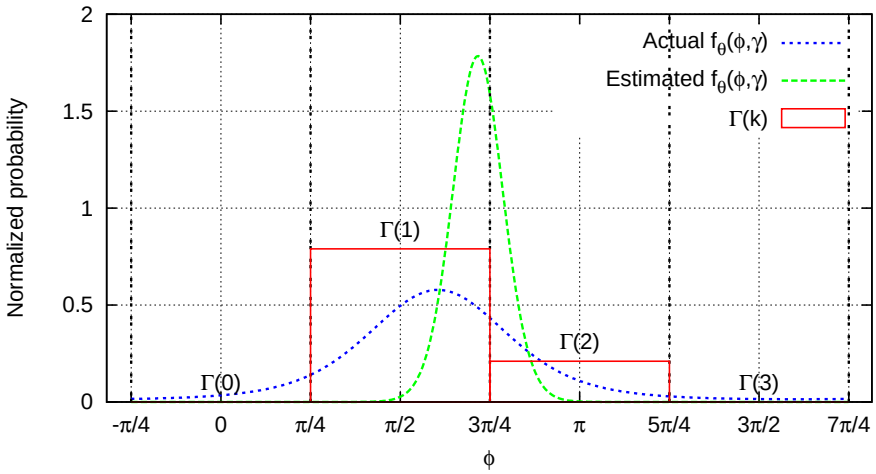

Figure 7.10: Example illustrating the ML estimation of the source-relay channel.

Noting from (7.58) that $\Gamma^{(i)}(q) \geq 0$, it can easily be verified that $0 \leq \widehat{\Phi}^{(i)}(q) \leq 1$ for all q.

7.9 Appendix: Source-relay Channel Transition Probabilities Offset

To understand the poor error performance of the pilot-based source-relay channel estimates derived in sections 7.3.2.2 and 7.3.4.1, consider the example illustrated in Fig. 7.10. The dotted line represents the function f_Θ from (5.12), evaluated using the true channel parameters (i.e. $\phi_{h_1} = \arg(h_1)$, $\gamma = |h_1|^2/N_1$). Integrating this function between the quantization borders (vertical dotted lines) yields the distribution of the symbols $c_r(k)$ sent by the relay, conditioned on the value of the symbols $c_0(k)$ sent by the source. In this example, 10 random BPSK pilot symbols ($M_1 = 2$) were sent by the source. The corresponding samples were quantized at the relay using 2 bits ($M_2 = 4$). After quantization, $\arg(c_{rp^\dagger}(k)) - \arg(c_{0p}(k))$ equals $\pi/2$ and π for 8 and 2 pilot symbols, respectively. Because of the limited number of pilot symbols, the angle differences of 0 and $3\pi/2$ have not occurred.

When calculating an estimate of the source-relay channel using (7.20) or (7.35), the value of the elements of $\mathbf{\Gamma}^{(i)}$ from (7.58) is needed. To rid this example of the complexity of an iterative algorithm, it is assumed that the destination directly observes the symbols $c_{rp^\dagger}(k)$ sent by the relay, i.e., $r_{2p^\dagger}(k) =$

$c_{rp^\dagger}(k)$. The elements of Γ computed under this assumption are also displayed on Fig. 7.10 by means of a normalized histogram (i.e. $\sum_{q=0}^{3}\Gamma(q)=1$), yielding $\Gamma(0)=0$, $\Gamma(1)=0.8$, $\Gamma(2)=0.2$ and $\Gamma(3)=0$. Using these values, the destination estimates ϕ_{h_1} and γ using (7.20). The dashed line represents the function f_Θ evaluated using these estimates. As shown by the illustration, the resulting distribution is significantly narrower than the distribution f_Θ that corresponds to the correct ϕ_{h_1} and γ. Therefore, when integrating the former distribution over the quantization intervals, the estimated conditional probability of the first and last quantization interval will be close to zero.

If subsequently for a BPSK data symbol $c_0(k)$, we have that $\arg(c_r(k)) - arg(c_0(k)) = 0$, the decoder will fail to correctly decode this symbol, even if the source-destination path provides useful information about this symbol. Because of the extremely low estimated probability of the occurrence of $\arg(c_r(k)) - arg(c_0(k)) = 0$, the decoder will consider this event highly unlikely, and will (erroneously) decide the opposite BPSK symbol was sent. One method to overcome this problem is to add an offset to the distribution $P\left[c_{rp^\dagger}=\chi_{M_2}(q)\,\middle|\,c_{0p}=1,\hat{\phi}_{h_1},\hat{\gamma}\right]$, so that very small values of $\Gamma(q)$ are excluded. This is achieved by adding a small offset value equal to $\frac{\beta}{M_2}$ to each element of the transition probability vector. After normalization, this yields

$$P_{\text{comp}}\left[c_{rp^\dagger}=\chi_{M_2}(q)\,\middle|\,c_{0p}=1\right]=\frac{P\left[c_{rp^\dagger}=\chi_{M_2}(q)\,\middle|\,c_{0p}=1\right]+\frac{\beta}{M_2}}{1+\beta}. \quad (7.77)$$

The transition probabilities $P\left[c_r=\chi_{M_2}(q)\,\middle|\,c_{rp^\dagger}=1\right]$ are to be determined using either (7.20) or (7.35).

8

Destination-side Estimation with a Carrier Frequency Mismatch

8.1 Introduction

In chapter 6, a system is discussed in which the source-relay channel is estimated at the relay, while in chapter 7, the source-relay channel is estimated at the destination, shifting the estimation burden from the relay to the destination. Both systems exhibit an excellent WER performance, with the second system having a reduced relay complexity. The communication channels in both chapters were modelled as flat Rayleigh fading channels with AWGN, with no carrier frequency mismatch present. This implies a perfect synchronization between the oscillators at the receiving and transmitting side.

Furthermore, it assumes the absence of Doppler shift, caused by the relative motion between the transmitting and receiving terminal. While these assumptions hold in some situations, a more realistic channel model includes a carrier frequency mismatch, and the corresponding carrier frequency offset needs to be estimated along with the complex channel gains and noise variances.

Carrier frequency offset estimation has been discussed in [79], [80] for SISO systems, with a computationally efficient estimation method which obtains near optimum performance being proposed in [80]. In [81], a pilot symbol based ML estimator is presented for the estimation of the carrier frequency offset in a MIMO system having flat-fading channels, while in [82], a data-aided approach is presented for the joint estimation of channel gain and the carrier frequency offset. Furthermore, [82] presents a computational efficient approach which reduces the complexity at the estimation terminal while maintaining a good estimation accuracy. Carrier frequency estimation for cooperative systems is discussed in [83], where an algorithm is presented for the joint estimation of the timing and frequency offset in an AF cooperative system. In the proposed algorithm, the relay is required to make an estimate of the timing and carrier frequency offset of the source-relay channel, raising its complexity.

In the chapter at hand, carrier frequency estimation is discussed for the QF protocol from chapter 7, in which all parameters are estimated at the destination. While it would be theoretically possible to derive carrier frequency estimation algorithms for the QF system described in chapter 6, in which the source-relay channel gain is estimated at the relay and compensated for before quantizing the symbols received from the source, the practical implementation poses some important difficulties. In order to obtain an accurate frequency offset estimate, the distance between pilot symbols needs to be maximized, meaning that the pilot symbols need to be spread evenly within the frame. Consequently, the whole frame needs to be received before an estimate of the carrier frequency offset can be made. If one wants to compensate for the carrier frequency offset before quantizing the received data samples, the latter need to be stored unquantized until the whole frame has been received and an estimate of the frequency offset can be computed to be used for the compensation. This would require the storage of analog values, which would defeat the whole purpose of using QF in the first place. Therefore, in this chapter, the carrier frequency offset of the source-relay channel will be estimated at the destination, along with the other channel parameters, keeping the complexity at the relay terminal low, as all estimation operations are performed at the destination terminal.

Due to the carrier frequency offset, the estimation methods from chapter

7 cannot be directly applied here, because this would yield a high increase in computational complexity as explained in section 8.3. In order to provide a solution to this problem, a new algorithm will be derived in this chapter for directly estimating the source-relay channel transition probabilities, taking into account the frequency offset. Furthermore, a whole new approach for estimating the relay path channel parameters is proposed and its strengths and weaknesses are discussed.

The outline of this chapter is as follows. In section 8.2, the system model is introduced, whereafter the detection at the destination is discussed in section 8.3, where the two methods for estimating the relay path channel parameters are also introduced. The actual estimation algorithms are derived in sections 8.4 and 8.5, whereafter the WER and MSE performance is analyzed in section 8.6. Finally, conclusions are drawn in section 8.7.

8.2 System Description

Throughout this chapter, the one-relay system model depicted in Fig. 5.1 is used. The relay operates in half-duplex mode and TDMA is used for signal separation. All channels, namely the source-destination, source-relay and relay-destination channels are considered flat Rayleigh fading channels with AWGN and introducing a carrier frequency offset. The source-destination, source-relay and relay-destination channel coefficients are denoted h_0, h_1 and h_2, respectively, while the source-destination, source-relay and relay-destination frequency offsets, normalized to the symbol interval, are denoted ν_0, ν_1 and ν_2, respectively. Considering this model, the symbol-wise output of the different channels can be written as

$$\begin{aligned} r_0(k) &= \sqrt{E_0} h_0 \exp\left(j2\pi k\nu_0\right) c_0(k) + n_0(k) \\ r_1(k) &= \sqrt{E_0} h_1 \exp\left(j2\pi k\nu_1\right) c_0(k) + n_1(k) \\ r_2(k) &= \sqrt{E_r} h_2 \exp\left(j2\pi k\nu_2\right) c_r(k) + n_2(k), \end{aligned} \tag{8.1}$$

with $\boldsymbol{c}_0$ being the vector consisting of $K_p + K$ symbols sent by the source and $\boldsymbol{c}_r$ being a vector consisting of $K + K_p$ symbols sent by the relay that correspond to the quantized elements of $\boldsymbol{r}_1$. The channel coefficients h_i and frequency offsets ν_i are constant during a timeslot. All channel coefficients have a zero mean circular symmetric complex gaussian (ZMCSCG) distribution with variance $N_{h_i} = 1/{d_i}^n$, with d_i the distance between the two terminals involved and n the path loss exponent; this implies a channel gain normalization yielding $\mathbb{E}[|h_i|^2] = 1$ for $d_i = 1$ with $i \in \{0,1,2\}$. The normalized carrier frequency offsets ν_i, $i \in \{0,1,2\}$, are uniformly distributed within the interval $\left[-\frac{1}{4(K_p+K)}, \frac{1}{4(K_p+K)}\right]$, yielding a maximum rotation of $\mp\pi/2$ between the first

and the last symbol of a frame. The elements of the noise vector $\boldsymbol{n}_i$ are ZM-CSCG distributed with variance N_i. The quantization process at the relay is not altered by the introduction of a carrier frequency offset and is discussed in section 5.2.

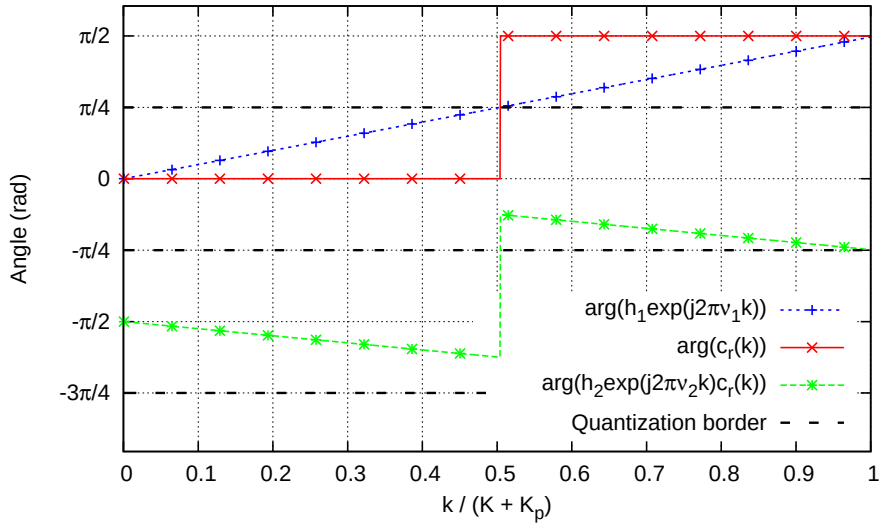

Figure 8.1: Illustration of the quantization process in the presence of a carrier frequency offset.

A graphical aid to gain insight into the quantization process is displayed in Fig. 8.1. The figure shows the transmission of a frame consisting of all ones ($c_0(k) = 1, \forall k$) over the relay path. The channel gains are initialized as $h_1 = 1$ and $h_2 = exp(\frac{-j\pi}{2})$, while the carrier frequency offsets are initialized as $\nu_1 = \frac{1}{4(K+K_p)}$ and $\nu_1 = -\frac{1}{8(K+K_p)}$, yielding a rotation between the first and last symbol of the frame of $\pi/2$ and $-\pi/4$ for the source-relay and relay-destination channel, respectively. At the relay, a 2 bit quantization scheme ($M_2 = 4$) is used. To improve clarity, it is assumed that there is no noise present on the source-relay and relay-destination channels ($N_1 = N_2 = 0$). The dotted blue line in Fig. 8.1 shows the angle of the symbols received by the relay, which is given by $\arg(r_1(k)) = \arg\left(h_1 \exp\left(j2\pi k\nu_1\right)\right)$. These symbols are subsequently quantized using 2 bits ($M_2 = 4$). Studying the angle of the symbols outputted by the relay, contained in $\boldsymbol{c}_r$, one can see a jump of $\pi/2$ at $k = \frac{K+K_p}{2}$, which is caused by the fact that $r_1(k)$ passes a quantization border at $k = \frac{K+K_p}{2}$. The symbols $\boldsymbol{c}_r$ are transmitted to the destination in the second time slot through the relay-destination channel,

where they are received as $\boldsymbol{r}_2$. The angle of the received symbols, given by $\arg(r_2(k)) = \arg\left(h_2 \exp\left(j2\pi k \nu_2 c_r(k)\right)\right)$, is also plotted on Fig. 8.1, showing the effect of ν_2 and h_2 on the symbols $\boldsymbol{c}_r$.

In order to aid in the estimation process, K_p pilot symbols, grouped in the vector $\boldsymbol{c}_{0p}$, are transmitted by the source along with the K data symbols and are received at the destination as $\boldsymbol{r}_{0p}$. As was the case in chapter 7, the relay will quantize a portion $\lceil \alpha K_p \rceil$ of these pilot symbols, grouped in the vector $\boldsymbol{c}_{rp^\dagger}$ and received at the destination as $\boldsymbol{r}_{2p^\dagger}$, and use the remaining $\lfloor (1-\alpha) K_p \rfloor$ pilot symbol slots, represented by the vector $\boldsymbol{c}_{rp^\diamond}$ and received at the destination as $\boldsymbol{r}_{2p^\diamond}$, to transmit pilot symbols of its own. The vector $\boldsymbol{c}_{rp} = (\boldsymbol{c}_{rp^\diamond}, \boldsymbol{c}_{rp^\dagger})$, received at the destination as $\boldsymbol{r}_{2p} = (\boldsymbol{r}_{2p^\diamond}, \boldsymbol{r}_{2p^\dagger})$, groups all pilot symbols sent by the relay.

In order to improve the accuracy of the carrier frequency offset estimate, the pilot symbols are spread uniformly throughout the frame and the distance between the pilot symbols is maximized. As a result, the position k of the $\tilde{k}$-th pilot symbol within a complete frame consisting of $K + K_p$ symbols is determined by the function $\psi(\tilde{k})$, yielding

$$k = \psi(\tilde{k}) = \left\lfloor (\tilde{k} - 1) \frac{K + K_p - 1}{K_p - 1} \right\rfloor + 1, \quad \tilde{k} \in \{1, 2, ..., K_p\}. \tag{8.2}$$

Similarly, the positions of the $\lceil \alpha K_p \rceil$ elements of $\boldsymbol{c}_{rp^\dagger}$ within the pilot symbol vector $\boldsymbol{c}_{rp}$ are also chosen so that the distance between two elements of $\boldsymbol{c}_{rp^\dagger}$ is maximized. The position $\tilde{k}$ in the vector $\boldsymbol{c}_{rp}$ of the $\ddot{k}$-th element of $\boldsymbol{c}_{rp^\dagger}$ is determined by the function $\varphi(\ddot{k})$, defined as

$$\tilde{k} = \varphi(\ddot{k}) = \left\lfloor (\ddot{k} - 1) \frac{K_p - 1}{\lceil \alpha K_p \rceil - 1} \right\rfloor + 1, \quad \ddot{k} \in \{1, 2, ... \lceil \alpha K_p \rceil\}. \tag{8.3}$$

8.3 Detection

The calculation of the symbol likelihoods, needed at the destination to decode the received information, proceeds similar to section 7.2. Introducing $\boldsymbol{h} = (h_0, h_1, h_2)$, $\boldsymbol{\nu} = (\nu_0, \nu_1, \nu_2)$ and $\boldsymbol{N} = (N_0, N_1, N_2)$, the likelihoods of the source symbols based on the observation vectors $\boldsymbol{r}_0$ and $\boldsymbol{r}_2$ can be written as

$$\begin{aligned} p(\boldsymbol{r}_0, \boldsymbol{r}_2 \mid \boldsymbol{c}_0, \boldsymbol{h}, \boldsymbol{\nu}, \boldsymbol{N}) = & \prod_{k=1}^{K} p(r_0(k) \mid c_0(k), h_0, \nu_0, N_0) \\ & \cdot \sum_{c_r(k)} p(r_2(k) \mid c_r(k), h_2, \nu_2, N_2) p(c_r(k) \mid c_0(k), h_1, \nu_1, N_1), \end{aligned} \tag{8.4}$$

with

$$p(r_0(k) \mid c_0(k), h_0, \nu_0, N_0) = \frac{1}{\pi N_0} \exp\left(-\frac{|r_0(k) - \sqrt{E_0}\exp(j2\pi k\nu_0)h_0 c_0(k)|^2}{N_0}\right) \tag{8.5}$$

$$p(r_2(k) \mid c_r(k), h_2, \nu_2, N_2) = \frac{1}{\pi N_2} \exp\left(-\frac{|r_2(k) - \sqrt{E_r}\exp(j2\pi k\nu_2)h_2 c_r(k)|^2}{N_2}\right) \tag{8.6}$$

$$p(c_r(k) \mid c_0(k), h_1, \nu_1, N_1) = \int_{\phi^l_{c_r(k)}}^{\phi^u_{c_r(k)}} f_\Theta\left(\theta - \arg(c_0(k)h_1) - 2\pi k\nu_1; \frac{E_0|h_1|^2}{N_1}\right) \mathrm{d}\theta. \tag{8.7}$$

The integration in (8.7) is carried out over the quantization interval that corresponds to the value of $c_r(k)$ in the summation (8.4). The corresponding integral must be computed for all M_2 values of $c_r(k)$ and all M_1 values of $c_0(k)$. Using circular symmetry at the relay, the aforementioned integral can be computed for $c_0(k) = \chi_{M_1}(0)$ and the values for $c_0(k) = \chi_{M_1}(m)$ with $m \in \{0, 1, ..., M_1 - 1\}$ can be obtained using relationship (7.56). However, due to the presence of the frequency offset ν_1 in the argument of $f_\Theta(.)$ in (8.7), the integral in (8.7) for a given $c_r(k)$, $c_0(k)$ and source-relay channel parameters, depends on the symbol index k within a frame. Therefore, the evaluation of the likelihood function (8.4) for given channel parameters would require that the integral in (8.7) be computed numerically, for all M_2 values of $c_r(k)$ and for each of the $K_p + K$ symbol indices.

In chapter 7, where the same problem is considered in the absence of frequency offsets, estimation and detection algorithms have been derived based on (8.4). In the case of zero frequency offsets, the integral in (8.7) for given $c_r(k)$, $c_0(k)$ and source-relay channel parameters becomes independent of the symbol index k, yielding an acceptable computational complexity. However, straightforward extension of the algorithms from chapter 7 to accommodate nonzero frequency offsets would drastically increase the computational complexity, as the integral (8.7) becomes a function of the symbol index k. Therefore, in this chapter, two methods are proposed for avoiding the high computational complexity associated with the evaluation of (8.7) for nonzero frequency offsets. These methods are discussed in the next two subsections.

8.3.1 Method 1: Direct Estimation of the Transition Probabilities

The first method involves using the estimation techniques described in section 7.3.4 to directly estimate the source-relay transition probabilities, instead of estimating the values of h_1, ν_1 and N_1 and using these estimates to evaluate the

integral in (8.7). In doing so, the numerical evaluation of (8.7) can be avoided. To this purpose, the 3-dimensional array $\overline{\mathbf{\Phi}}$ is introduced, the elements of which are defined as

$$\overline{\Phi}(q,m,k) = P\left[c_r(k) = \chi_{M_2}(q) \,\middle|\, c_0(k) = \chi_{M_1}(m)\right] \tag{8.8}$$

with $q \in \{0,1,...,M_2-1\}$, $m \in \{0,1,...,M_1-1\}$ and $k \in \{1,2,...,K_p+K\}$. Using circular symmetry of the constellations received and transmitted by the relay, the elements of $\overline{\mathbf{\Phi}}$ can be related to the matrix $\mathbf{\Phi}$:

$$\overline{\Phi}(q,m,k) = \Phi\left(q + \frac{M_2 m}{M_1}, k\right), \tag{8.9}$$

with

$$\Phi(q,k) = P\left[c_r(k) = \chi_{M_2}(q) \,\middle|\, c_0(k) = 1\right]. \tag{8.10}$$

When comparing (8.10) to (7.32), one notices that, due to the frequency offset, the source-relay channel transition probabilities are different for each symbol index k. The estimation particularities arising from the non-zero carrier frequency offset are further investigated in section 8.4, where estimates are derived for the different channel parameters.

8.3.2 Method 2: Assumption of AF

A different approach to avoid the numeric integration in (8.7) is to write the symbols transmitted by the relay as

$$c_r(k) = \frac{r_1(k)}{\sqrt{E_0}|h_1|} + n_q(k), \tag{8.11}$$

with n_q being a term representing the distortion caused by the quantization operation at the relay. To rid ourselves of the burden of having to calculate the statistics of $n_q(k)$, we will simply assume that $n_q(k) = 0$, implying that the relay performed an AF operation on the received symbols, amplifying them by a factor equal to $\sqrt{E_r}/(\sqrt{E_0}|h_1|)$. Under this assumption, (8.11) and (8.1) yield

$$r_2(k) = \sqrt{E_r} h_3 \exp(j2\pi k\nu_3)\, c_0(k) + n_3(k), \tag{8.12}$$

with

$$n_3(k) = \frac{\sqrt{E_r} h_2}{\sqrt{E_0}|h_1|} \exp(j2\pi k\nu_2)\, n_1(k) + n_2(k) \tag{8.13}$$

$$h_3 = \frac{h_1 h_2}{|h_1|} \tag{8.14}$$

$$\nu_3 = \nu_1 + \nu_2. \tag{8.15}$$

Using (8.12) and noting that the weighted sum of two Gaussians is also a Gaussian, the corresponding likelihood function associated with the observation $r_2(k)$ can be written as

$$p(r_2(k)|c_0(k), h_3, \nu_3, N_3) = \frac{1}{\pi N_3} \exp\left(-\frac{\left| r_2(k) - \sqrt{E_r} h_3 \exp\left(j2\pi k \nu_3\right) c_0(k) \right|^2}{N_3} \right), \tag{8.16}$$

with N_3 the variance of the elements in $\boldsymbol{n}_3$. Estimates for the different channel parameters, using the assumption outlined in this subsection, are derived in section 8.5.

8.4 Direct Estimation of the Source-Relay Transition Probabilities

When using the first estimation method, the unknown channel parameters h_0, ν_0, N_0, h_2, ν_2 and N_2 need to be estimated, along with the elements of the matrix $\boldsymbol{\Phi}$, containing the source-relay channel transition probabilities. Both pilot-based and code-aided estimation are discussed in the next subsections.

8.4.1 Pilot-based Estimation

In this subsection, the estimation of the various channel parameters, using the pilot symbols transmitted by the source and relay, is outlined. Because the source-relay transition probabilities, grouped in the matrix $\boldsymbol{\Phi}$, are different for each symbol index k, only the elements of $\boldsymbol{\Phi}$ corresponding to the positions of the pilot symbols $\boldsymbol{c}_{rp^\dagger}$ can be estimated. These elements are grouped into the matrix $\boldsymbol{\Phi}_p$, which is a subset of $\boldsymbol{\Phi}$. Once the elements of $\boldsymbol{\Phi}_p$ are estimated, the results will be interpolated to obtain an estimate of $\boldsymbol{\Phi}$.

Introducing $\boldsymbol{x}_0 = (h_0, \nu_0, N_0)$ and $\boldsymbol{x}_2 = (h_2, \nu_2, N_2)$, the pilot-based estimates are obtained by solving the following equation

$$(\hat{\boldsymbol{x}_0}, \hat{\boldsymbol{x}_2}, \widehat{\boldsymbol{\Phi}_p}) = \arg \max_{(\boldsymbol{x}_0, \boldsymbol{x}_2, \boldsymbol{\Phi}_p)} p(\boldsymbol{r}_{0p}, \boldsymbol{r}_{2p} \mid \boldsymbol{c}_{0p}, \boldsymbol{x}_0, \boldsymbol{x}_2, \boldsymbol{\Phi}_p) \tag{8.17}$$

Using (8.4), (8.17) can be written as

$$\hat{\boldsymbol{x}_0} = \arg \max_{\boldsymbol{x}_0} p(\boldsymbol{r}_{0p} \mid \boldsymbol{c}_{0p}, \boldsymbol{x}_0) \tag{8.18}$$

$$(\hat{\boldsymbol{x}_2}, \widehat{\boldsymbol{\Phi}_p}) = \arg \max_{(\boldsymbol{x}_2, \boldsymbol{\Phi}_p)} p(\boldsymbol{r}_{2p} \mid \boldsymbol{c}_{0p}, \boldsymbol{x}_2, \boldsymbol{\Phi}_p), \tag{8.19}$$

with $\boldsymbol{r}_{0p}$ and $\boldsymbol{r}_{2p}$ denoting the part of $\boldsymbol{r}_0$ and $\boldsymbol{r}_2$ that corresponds to the pilot symbol postions transmitted by the source and relay, respectively.

8.4.1.1 Direct Path

Pilot-based estimates of the direct path channel parameters h_0, ν_0 and N_0 are obtained by solving equation (8.18). As shown in Appendix 8.8, the following values satisfy (8.18):

$$\hat{\nu_0} = \frac{(K_p - 1)}{(K + K_p - 1)} \frac{\sum_{m=1}^{K_p} m|R_{0p}(m)| \arg(R_{0p}(m))}{2\pi \sum_{m=1}^{K_p} m^2 |R_{0p}(m)|} \tag{8.20}$$

$$\hat{h_0} = \frac{\sum_{\tilde{k}=1}^{K_p} r_{0p}(\tilde{k}) c_{0p}^*(\tilde{k}) \exp\left(-j2\pi\psi(\tilde{k})\hat{\nu_0}\right)}{K_p\sqrt{E_0}} \tag{8.21}$$

$$\hat{N_0} = \frac{\sum_{\tilde{k}=1}^{K_p} |r_{0p}(\tilde{k}) - \sqrt{E_0}\exp(j2\pi\psi(\tilde{k})\hat{\nu_0})\hat{h_0}c_{0p}(\tilde{k})|^2}{K_p}, \tag{8.22}$$

with

$$R_{0p}(m) = \frac{\sum_{\tilde{k}=1}^{K_p} r_{0p}^*(\tilde{k}-m) r_{0p}(\tilde{k}) c_{0p}^*(\tilde{k}) c_{0p}(\tilde{k}-m)}{K_p}. \tag{8.23}$$

and with the function $\psi(.)$ defined in (8.2).

8.4.1.2 Relay Path

Pilot-based estimates of the relay-destination and source-relay channel parameters, grouped in the vector $\boldsymbol{x}_2$ and the matrix $\boldsymbol{\Phi}_p$, respectively, are obtained iteratively using the EM algorithm as described in section 7.3.2.2. The quantized version of $\lceil \alpha K_p \rceil$ elements of $\boldsymbol{r}_{1p}$, contained in $\boldsymbol{c}_{rp^\dagger}$, are considered to be nuisance parameters. At each EM iteration i, the following equations need to be solved in order to update the estimates of $\boldsymbol{x}_2$ and $\boldsymbol{\Phi}_p$:

$$\hat{\boldsymbol{x}_2}^{(i)} = \arg\max_{\boldsymbol{x}_2} \mathbb{E}_{\boldsymbol{c}_{rp^\dagger}} \left[\ln p(\boldsymbol{r}_{2p} \mid \boldsymbol{c}_{rp}, \boldsymbol{x}_2) \,\middle|\, \boldsymbol{r}_{2p}, \hat{\boldsymbol{x}}_2^{(i-1)}, \widehat{\boldsymbol{\Phi}_p}^{(i-1)} \right] \tag{8.24}$$

$$\widehat{\boldsymbol{\Phi}_p}^{(i)} = \arg\max_{\boldsymbol{\Phi}_p} \mathbb{E}_{\boldsymbol{c}_{rp^\dagger}} \left[\ln p(\boldsymbol{c}_{rp^\dagger} \mid \boldsymbol{c}_{0p}, \boldsymbol{\Phi}_p) \,\middle|\, \boldsymbol{r}_{2p}, \hat{\boldsymbol{x}}_2^{(i-1)}, \widehat{\boldsymbol{\Phi}_p}^{(i-1)} \right]. \tag{8.25}$$

Combining the results obtained in Appendix 7.6 and Appendix 8.8, the following estimates are obtained for the relay-destination channel parameters:

$$\hat{\nu_2}^{(i)} = \frac{(K_p - 1)}{(K + K_p - 1)} \frac{\sum_{m=1}^{K_p} m |R_{2p}^{(i)}(m)| \arg(R_{2p}^{(i)}(m))}{2\pi \sum_{m=1}^{K_p} m^2 |R_{2p}^{(i)}(m)|} \tag{8.26}$$

$$\hat{h_2}^{(i)} = \frac{\sum_{\tilde{k}=1}^{K_p} r_{2p}(\tilde{k}) \left(u_{rp}^{(i)}(\tilde{k})\right)^* \exp\left(-j2\pi\psi(\tilde{k})\hat{\nu_2}^{(i)}\right)}{K_p\sqrt{E_r}} \tag{8.27}$$

$$\begin{aligned}\hat{N_2}^{(i)} = \frac{1}{K_p}\left(\sum_{\tilde{k}=1}^{K_p}\left|r_{2p}(\tilde{k}) - \sqrt{E_r}\exp\left(j2\pi\psi(\tilde{k})\hat{\nu_2}^{(i)}\right)\hat{h_2}^{(i)}u_{rp}^{(i)}(\tilde{k})\right|^2\right) \\ + \frac{1}{K_p}\left(E_r\left|\hat{h_2}^{(i)}\right|^2\left(K_p - \boldsymbol{u}_{rp}^{(i)}\left(\boldsymbol{u}_{rp}^{(i)}\right)^H\right)\right),\end{aligned} \tag{8.28}$$

with

$$R_{2p}^{(i)}(m) = \frac{\sum_{\tilde{k}=1}^{K_p} r_{2p}^*(\tilde{k}-m) r_{2p}(\tilde{k}) \left(u_{rp}^{(i)}(\tilde{k})\right)^* u_{rp}^{(i)}(\tilde{k}-m)}{K_p}. \tag{8.29}$$

The elements of $\boldsymbol{u}_{rp}$ are equal to

$$\begin{aligned}u_{rp}(\tilde{k}) = \sum_{c_{rp}(\tilde{k})} c_{rp}(\tilde{k}) p\left(c_{rp}(\tilde{k}) \mid r_{2p}(\tilde{k}), \hat{\boldsymbol{x}}_2^{(i-1)}, \widehat{\boldsymbol{\Phi}_p}^{(i-1)}\right) \\ \text{for } \tilde{k} \in \{\tilde{k} \mid \tilde{k} = \varphi(\ddot{k}),\ \ddot{k} = 1, 2, ..., \lceil \alpha K_p \rceil\}\end{aligned} \tag{8.30}$$

and

$$u_{rp}(\tilde{k}) = c_{rp^\diamond}(\tilde{k}) \quad \text{for } \tilde{k} \in \{1, 2, ..., K_p\} \setminus \{\tilde{k} \mid \tilde{k} = \varphi(\ddot{k}),\ \ddot{k} = 1, 2, ..., \lceil \alpha K_p \rceil\}. \tag{8.31}$$

The conditional distribution $p\left(c_{rp}(\tilde{k}) \mid r_{2p}(k), \hat{\boldsymbol{x}}_2^{(i-1)}, \widehat{\boldsymbol{\Phi}_p}^{(i-1)}\right)$ can be further evaluated using the same approach as was used in (7.21). The function $\varphi(.)$ is defined in (8.3). No averaging between frames is performed on the noise variance estimates N_0 and N_2, as was done in section 6.3.1.3 of chapter 6. Instead, the noise variance estimates will be refined using the code-aided EM algorithm.

An estimate of the source-relay transition probabilities is obtained by solving (8.25). This can be accomplished using the techniques from Appendix 7.6, yielding

$$\widehat{\Phi}_p^{(i)}(q, \ddot{k}) = \frac{\Gamma^{(i)}(q, \ddot{k})}{\sum_{\tilde{q}=0}^{M_2-1} \Gamma^{(i)}(\tilde{q}, \ddot{k})}, \tag{8.32}$$

with

$$\Gamma^{(i)}(q,\ddot{k}) = \sum_{m=0}^{M_1-1} P\left[c_{rp^\dagger}(\ddot{k}) = \chi_{M_2}\left(q + \frac{M_2 m}{M_1}\right) \,\middle|\, r_{2p^\dagger}(\ddot{k}), \hat{\mathbf{x}}_2^{(i-1)}, \widehat{\mathbf{\Phi}_p}^{(i-1)}\right] .\mathbb{I}_{\ddot{k}}\left[c_{0p}(\ddot{k}) = \chi_{M_1}(m)\right], \tag{8.33}$$

with $\mathbb{I}[.]$ defined in (7.59). The estimate of $\Phi_p^{(i)}(q,\ddot{k})$ thus obtained is based on only one sample (the $\ddot{k}$-th element of $\boldsymbol{c}_{rp^\dagger}$) and is highly inaccurate, as will be shown in section 8.6.2.2. The accuracy can be improved by noting the correlation between the source-relay channel transition probabilities at adjacent symbol positions. Indeed, due to the carrier frequency offset, the source-relay channel transition probabilities will be different of each symbol position, but the difference between probabilities at adjacent symbol positions is small as the maximum rotation caused by the frequency offset is considered to be limited to $\mp\pi/2$ between the first and last symbol of a frame. Therefore, a better approach is to also use the adjacent symbol positions when calculating an estimate of $\Phi_p^{(i)}(q,\ddot{k})$, yielding

$$\widehat{\Phi}_p^{(i)}(q,\ddot{k}) = \frac{\sum_{l\in\boldsymbol{\eta}_p(\ddot{k})}\Gamma^{(i)}(q,l)}{\sum_{\tilde{q}=0}^{M_2-1}\sum_{l\in\boldsymbol{\eta}_p(\ddot{k})}\Gamma^{(i)}(\tilde{q},l)}, \tag{8.34}$$

with the set $\boldsymbol{\eta_p}(\ddot{k})$ defined as

$$\boldsymbol{\eta}_p(\ddot{k}) = \left\{ l\in\mathbb{N} \,\middle|\, \max\left(1,\ddot{k} - \left\lceil\frac{W_p}{2}\right\rceil\right) < l \le \min\left(\ddot{k} + \left\lfloor\frac{W_p}{2}\right\rfloor, \lceil\alpha K_p\rceil\right)\right\}. \tag{8.35}$$

The optimal window size W_p is determined in section 8.6.2.2.

The pilot-based EM algorithm is initialized by assuming that all the source-relay channel transition probabilities are equal and by using in (8.26), (8.27) and (8.28) only the observations $\boldsymbol{r}_{2p^\diamond}$ that correspond to the relay's own pilot symbols $\boldsymbol{c}_{rp^\diamond}$. When the relay does not transmit any pilot symbols of its own ($\alpha = 1$), the pilot-based EM algorithm is initialized using $\hat{v_2}^{(0)} = 0$ and $\hat{h_2}^{(0)} = 1$. The noise variance estimate $\hat{N_2}^{(0)}$ is initialized using the pilot-based noise variance estimate obtained in the previous frame.

After convergence of the EM algorithm, the elements of $\mathbf{\Phi}$ are calculated from $\widehat{\mathbf{\Phi}_p}$ by means of linear interpolation, yielding

$$\widehat{\Phi}(q,k) = \frac{\varphi(\ddot{k}+1)-k}{\varphi(\ddot{k}+1)-\varphi(\ddot{k})}\widehat{\Phi}_p(q,\ddot{k}) + \frac{k-\varphi(\ddot{k})}{\varphi(\ddot{k}+1)-\varphi(\ddot{k})}\widehat{\Phi}_p(q,\ddot{k}+1), \quad \text{for} \quad \varphi(\ddot{k}) \le k < \varphi(\ddot{k}+1). \tag{8.36}$$

Subsequently, an offset β is applied to the elements of $\mathbf{\Phi}$, as described in section 7.3.5.1.

8.4.2 Code-aided Estimation

The accuracy of the pilot-based estimates obtained in the previous subsection can be improved by means of a code-aided EM approach. All channel parameters, including the noise variance estimates $\hat{N}_0$ and $\hat{N}_2$, are refined using the EM algorithm. Using the results from section 7.3.3 and section 8.4.1, and introducing $\boldsymbol{x}_d = (\nu_0, h_0, N_0, \nu_2, h_2, N_2, \mathbf{\Phi})$ and $E_2 = E_r$, the following expressions are obtained for updating the elements of $\boldsymbol{x}_d$ in the i-th EM iteration:

$$\hat{\nu_n}^{(i)} = \frac{\sum_{m=1}^{K+K_p} m|R_n^{(i)}(m)| \arg(R_n^{(i)}(m))}{2\pi \sum_{m=1}^{K+K_p} m^2 |R_n^{(i)}(m)|} \tag{8.37}$$

$$\hat{h_n}^{(i)} = \frac{\sum_{k=1}^{K+K_p} r_n(k) \left(u_n^{(i)}(k)\right)^* \exp\left(-j2\pi k \hat{\nu_n}^{(i)}\right)}{(K+K_p)\sqrt{E_n}} \tag{8.38}$$

$$\begin{aligned}\hat{N_n}^{(i)} = \frac{1}{K+K_p} \left(\sum_{k=1}^{K+K_p} \left| r_n(k) - \sqrt{E_n} \exp\left(j2\pi k \hat{\nu_n}^{(i)}\right) \hat{h_n}^{(i)} u_n^{(i)}(k) \right|^2 \right) \\ + \frac{1}{K+K_p} \left(E_n \left| \hat{h_n}^{(i)} \right|^2 \left(K + K_p - \boldsymbol{u}_n^{(i)} \left(\boldsymbol{u}_n^{(i)}\right)^H \right) \right)\end{aligned} \tag{8.39}$$

with $n \in \{0, 2\}$ and

$$R_n^{(i)}(m) = \frac{\sum_{k=1}^{K+K_p} r_n^*(k-m) r_n(k) \left(u_n^{(i)}(k)\right)^* u_n^{(i)}(k-m)}{K+K_p} \tag{8.40}$$

and

$$u_0^{(i)}(k) = \sum_{c_0(k)} c_0(k) p\left(c_0(k) \mid \boldsymbol{r}_0, \boldsymbol{r}_2, \hat{\boldsymbol{x}}_d^{(i-1)}\right) \tag{8.41}$$

$$u_2^{(i)}(k) = u_r^{(i)}(k) = \sum_{c_0(k), c_r(k)} c_r(k) p\left(c_r(k), c_0(k) \mid \boldsymbol{r}_0, \boldsymbol{r}_2, \hat{\boldsymbol{x}}_d^{(i-1)}\right), \tag{8.42}$$

denoting the a posteriori expectation of the source symbol $c_0(k)$ and the relay symbol $c_r(k)$, respectively. Taking into account the correlation between the source-relay transition probabilities at adjacent symbol positions as explained at the end of section 8.4.1.2, the estimates of the elements of $\mathbf{\Phi}$ obtained in the i-th EM iteration are equal to

$$\hat{\Phi}^{(i)}(q,k) = \frac{\sum_{l \in \boldsymbol{\eta}(k)} \Gamma_c^{(i)}(q,l)}{\sum_{\tilde{q}=0}^{M_2-1} \sum_{l \in \boldsymbol{\eta}(k)} \Gamma_c^{(i)}(\tilde{q},l)} \tag{8.43}$$

with

$$\boldsymbol{\eta}(k) = \left\{ l \in \mathbb{N} \;\middle|\; \max\left(1, k - \left\lceil \frac{W}{2} \right\rceil\right) < l \leq \min\left(k + \left\lfloor \frac{W}{2} \right\rfloor, K + \lceil \alpha K_p \rceil\right) \right\} \tag{8.44}$$

and

$$\begin{aligned} &\Gamma_c^{(i)}(q,k) \\ &= \sum_{m=0}^{M-1} P\left[c_r(k) = \chi_{M_2}\left(q + \frac{M_2 m}{M_1}\right) \;\middle|\; c_0(k) = \chi_{M_1}(m), \boldsymbol{r}_0, \boldsymbol{r}_2, \hat{\boldsymbol{x}}_d^{(i-1)}\right] \\ &\qquad .P\left[c_0(k) = \chi_{M_1}(m) \;\middle|\; \boldsymbol{r}_0, \boldsymbol{r}_2, \hat{\boldsymbol{x}}_d^{(i-1)}\right]. \end{aligned} \tag{8.45}$$

The elements of $\boldsymbol{u}_0^{(i)}$, $\boldsymbol{u}_r^{(i)}$ and $\boldsymbol{\Gamma}_c^{(i)}$ can be expressed in terms of the probabilities $p\left(c_0(k) \;\middle|\; \boldsymbol{r}_0, \boldsymbol{r}_2, \hat{\boldsymbol{x}}_d^{(i-1)}\right)$ and $p\left(c_r(k) \;\middle|\; c_0(k), \boldsymbol{r}_0, \boldsymbol{r}_2, \hat{\boldsymbol{x}}_d^{(i-1)}\right)$, which are evaluated as explained in section 7.3.3. The optimal window size W is determined in section 8.6.2.2.

8.5 Estimation Using the AF Approximation

When using the AF approximation, the symbol likelihoods contain the channel parameters h_0, ν_0 and N_0 corresponding to the direct channel (see section 8.3) and the parameters h_3, ν_3 and N_3 corresponding to the relay path (see section 8.3.2). These parameters are estimated at the destination using pilot symbols sent by the source. Because the relay-destination channel no longer needs to be estimated separately, the relay will not send any pilot symbols of its own ($\alpha = 1$). After the pilot-based estimates have been computed, they are refined using a code-aided EM algorithm.

8.5.1 Pilot-based Estimation

Introducing $\boldsymbol{x}_3 = (h_3, \nu_3, N_3)$, the pilot-based estimates are obtained by solving the following equation

$$(\hat{\boldsymbol{x}_0}, \hat{\boldsymbol{x}_3}) = \arg\max_{(\boldsymbol{x}_0, \boldsymbol{x}_3)} p(\boldsymbol{r}_{0p}, \boldsymbol{r}_{2p} \mid \boldsymbol{c}_{0p}, \boldsymbol{x}_0, \boldsymbol{x}_3) \tag{8.46}$$

Taking into account the orthogonality between the direct path and the relay path, (8.46) can be written as

$$\hat{\boldsymbol{x}_0} = \arg\max_{\boldsymbol{x}_0} p(\boldsymbol{r}_{0p} \mid \boldsymbol{c}_{0p}, \boldsymbol{x}_0) \tag{8.47}$$

$$\hat{\boldsymbol{x}_3} = \arg\max_{\boldsymbol{x}_3} p(\boldsymbol{r}_{2p} \mid \boldsymbol{c}_{0p}, \boldsymbol{x}_3) \tag{8.48}$$

Considering that (8.47) is identical to (8.18), the elements of $\hat{\boldsymbol{x}_0}$ are given by (8.21), (8.20) and (8.22). By noting the similarity between the distribution $p(r_2(k)|c_0(k), h_3, \nu_3, N_3)$, given by (8.16), and $p(r_0(k)|c_0(k), h_0, \nu_0, N_0)$, given by (8.5), the elements of $\hat{\boldsymbol{x}_3}$ are found to be equal to:

$$\hat{\nu_3} = \frac{(K_p - 1)}{(K + K_p - 1)} \frac{\sum_{m=1}^{K_p} m|R_{3p}(m)| \arg(R_{3p}(m))}{2\pi \sum_{m=1}^{K_p} m^2 |R_{3p}(m)|} \tag{8.49}$$

$$\hat{h_3} = \frac{\sum_{\tilde{k}=1}^{K_p} r_{2p}(\tilde{k}) c_{0p}^*(\tilde{k}) \exp\left(-j2\pi\psi(\tilde{k})\hat{\nu_3}\right)}{K_p \sqrt{E_r}} \tag{8.50}$$

$$\hat{N_3} = \frac{\sum_{\tilde{k}=1}^{K_p} \left| r_{2p}(\tilde{k}) - \sqrt{E_r} \exp(j2\pi\psi(\tilde{k})\hat{\nu_3})\hat{h_3} c_{0p}(\tilde{k}) \right|^2}{K_p}, \tag{8.51}$$

with

$$R_{3p}(m) = \frac{\sum_{\tilde{k}=1}^{K_p} r_{2p}^*(\tilde{k} - m) r_{2p}(\tilde{k}) c_{0p}^*(\tilde{k}) c_{0p}(\tilde{k} - m)}{K_p}. \tag{8.52}$$

8.5.2 Code-aided Estimation

The pilot-based estimates can again be refined using a code-aided EM algorithm, in which the symbols transmitted by the source are considered to be nuisance parameters. All pilot-based estimates, including the noise variances, are refined using the code-aided EM algorithm. Introducing $\boldsymbol{r}_d = (\boldsymbol{r}_0, \boldsymbol{r}_2)$, the estimates calculated in the i-th EM iteration are obtained by solving the following maximization problem:

$$(\hat{\boldsymbol{x}_0}^{(i)}, \hat{\boldsymbol{x}_3}^{(i)}) = \arg \max_{(\boldsymbol{x}_0, \boldsymbol{x}_3)} Q\left(\boldsymbol{x}_0, \boldsymbol{x}_3, \hat{\boldsymbol{x}_0}^{(i-1)}, \hat{\boldsymbol{x}_3}^{(i-1)}\right), \tag{8.53}$$

with

$$Q\left(\boldsymbol{x}_0, \boldsymbol{x}_3, \hat{\boldsymbol{x}_0}^{(i-1)}, \hat{\boldsymbol{x}_3}^{(i-1)}\right) = \mathbb{E}_{\boldsymbol{c}_0}\left[\ln p(\boldsymbol{r}_d|\boldsymbol{c}_0, \boldsymbol{x}_0, \boldsymbol{x}_3) \mid \boldsymbol{r}_d, \hat{\boldsymbol{x}_0}^{(i-1)}, \hat{\boldsymbol{x}_3}^{(i-1)}\right]. \tag{8.54}$$

The estimates $\hat{\boldsymbol{x}_0}^{(0)}$ and $\hat{\boldsymbol{x}_3}^{(0)}$, used to initialize the iterative process, correspond to the pilot-based estimates obtained in the previous subsection. Using the techniques from section 8.4.2 and section 8.5.1, and using the convenient notation $\boldsymbol{r}_3 = \boldsymbol{r}_2$ and $E_3 = E_r$, the following estimates are found to satisfy

(8.53):

$$\hat{\nu_n}^{(i)} = \frac{\sum_{m=1}^{K_p+K} m|R_n^{(i)}(m)| \arg(R_n^{(i)}(m))}{2\pi \sum_{m=1}^{K_p+K} m^2 |R_n^{(i)}(m)|} \tag{8.55}$$

$$\hat{h_n}^{(i)} = \frac{\sum_{k=1}^{K_p+K} r_n(k) \left(u_0^{(i)}(k)\right)^* \exp\left(-j2\pi k \hat{\nu_n}^{(i)}\right)}{\sqrt{E_n}(K_p+K)} \tag{8.56}$$

$$\begin{aligned}\hat{N_n}^{(i)} = &\frac{1}{K_p+K}\left(\sum_{k=1}^{K_p+K}\left|r_n(k) - \sqrt{E_n}\exp\left(j2\pi k\hat{\nu_n}^{(i)}\right)\hat{h_n}^{(i)}u_0^{(i)}(k)\right|^2\right) \\ &+ \frac{1}{K_p+K}\left(E_n\left|\hat{h_n}^{(i)}\right|^2\left(K_p+K-\boldsymbol{u}_0^{(i)}\left(\boldsymbol{u}_0^{(i)}\right)^H\right)\right),\end{aligned} \tag{8.57}$$

with $n \in \{0,3\}$ and

$$R_n^{(i)}(m) = \frac{\sum_{k=1}^{K+K_p} r_n^*(k-m) r_n(k) \left(u_0^{(i)}(k)\right)^* u_0^{(i)}(k-m)}{K+K_p}. \tag{8.58}$$

The elements of the a posteriori source symbol expectations $\boldsymbol{u}_0^{(i)}$ are calculated according to (8.41), in which $\hat{\boldsymbol{x}}_d^{(i-1)}$ is replaced by $\left(\hat{\boldsymbol{x}_0}^{(i-1)}, \hat{\boldsymbol{x}_3}^{(i-1)}\right)$.

8.6 Performance Evaluation.

The performance of the proposed estimation algorithms is analyzed using computer simulations. First, the simulation parameters are introduced in section 8.6.1, whereafter the design parameters (α, W_p and W) of the direct estimation method from section 8.4 are optimized in section 8.6.2. The WER resulting from the two estimation methods is discussed in section 8.6.3, whereafter the MSE of the estimates is analyzed in section 8.6.4.

8.6.1 Simulation Parameters

At the source, 1024 information symbols are coded into 1536 coded symbols using an $(1, 13/15)_8$ RSCC turbo code that is punctured to a rate of $2/3$. After encoding, the coded bits are mapped on M_1-PSK symbols, which are quantized at the relay using $\log_2(M_1)+1$ bits, yielding $M_2 = 2M_1$. The relay is located halfway between source and destination. The path loss exponent equals 4 and the distance between source and destination is considered unity. All noise variances are assumed to be equal ($N_0 = N_1 = N_2$) but will be estimated separately. For a given E_b/N_0 ratio, the symbol energy transmitted by the source and relay is computed using (7.1), assuming that $E_0 = E_r$.

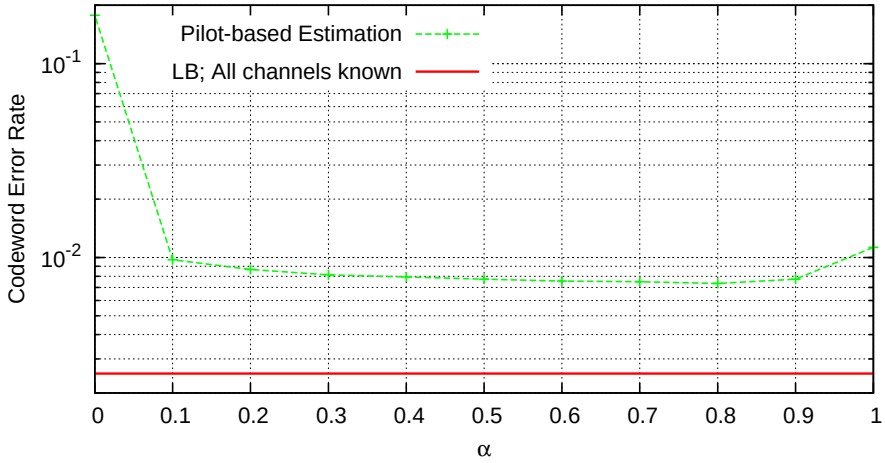

Figure 8.2: WER performance for $M_1 = 2$ at $E_b/N_0 = 9$ dB as a function of α.

For $M_1 = 2$, $M_1 = 4$ and $M_1 = 8$, a number of 24, 12 and 8 pilot symbols, respectively, are added to the data symbol frames, unless stated otherwise. This approach ensures that the estimation overhead uses the same percentage of the total transmit energy, independent of the constellation size. The power loss arising from the estimation overhead can be calculated using (7.1) and equals 0.067 dB. In the reference system in which the channel parameters are assumed to be known, no pilot symbols are transmitted and there is no loss stemming from the estimation overhead. When using the direct estimation method, 8 EM iterations are used to obtain the pilot-based estimates of the relay path channel parameters. For both the direct estimation method and the AF approximation method, 12 code-aided EM iterations are used at the destination to refine the pilot-based estimates.

8.6.2 Optimization of the Design Parameters of the Direct Estimation Method

8.6.2.1 Optimization of α

Due to the carrier frequency offset, the optimal value of α, used to determine the fraction of pilot symbols that the relay quantizes and forwards to the destination, could be different from the optimal value determined in chapter 7, in which no frequency offset is present. The WER performance is displayed as a function of α in Fig. 8.2 for a BPSK-mapped system ($M_1 = 2$) at an E_b/N_0 ratio of 9 dB. The window size parameter W_p is set equal to $2\lceil \alpha K_p/4 \rceil$.

We observe a poor WER performance of $\alpha = 0$ and $\alpha = 1$, whereas the optimal value of α is situated around $\alpha = 0.8$. The poor performance for $\alpha = 0$ is explained by noting that when $\alpha = 0$, the relay does not quantize any pilot symbols from the source and only sends to the destination pilot symbols of its own, making it impossible to make an estimate of the source-relay channel parameters. In order to explain the results for $\alpha = 1$, in which case the relay does not send pilot symbols of its own, we first introduce the vector $\boldsymbol{\Xi}$, the elements of which are defined as

$$\Xi(\tilde{k}) = \arg\left(\sum_{q=0}^{M_2-1} \chi_{M_2}(q) h_2 \exp\left(j2\pi\nu_2\psi(\tilde{k})\right) \times P\left[c_{rp}(\tilde{k}) = \chi_{M_2}(q) | c_{0p}(\tilde{k}) = 1, h_1, \nu_1, N_1\right] \right). \quad (8.59)$$

In doing so, the value of $\Xi(\tilde{k})$ represents the expected total phase rotation at symbol position $\tilde{k}$, induced by the relay path (the cascade of the source-relay channel, the quantization operation at the relay and the relay-destination channel). We further introduce the vector $\widehat{\boldsymbol{\Xi}}$, which is also defined using (8.59), in which the actual channel parameters are replaced with their corresponding pilot-based estimates. In the upper half of Fig. 8.3, the elements of $\boldsymbol{\Xi}$ and $\widehat{\boldsymbol{\Xi}}$ are plotted together with the actual phase rotation experienced by the pilot symbols received from the relay path in a random frame. The lower half of Fig. 8.3 displays the phase difference between the pilot symbols transmitted by the source and the quantized version of these pilot symbols transmitted by the relay. The figure also shows the phase difference between the vectors $\boldsymbol{c}_{0p}$ and $\boldsymbol{u}_{rp}$. The latter, being defined by (8.30), represents the expected value of the symbols transmitted by the relay and is obtained after the last pilot-based EM iteration.

When $\alpha = 1$, one can see from the lower half of Fig. 8.3 that the calculated expected value of the symbols transmitted by the relay does not correspond to the actual symbols transmitted. When $\alpha = 1$, the pilot-based EM algorithm is initialized using arbitrary values, as explained in section 8.4.1.2. This inaccurate initialization, together with the fact that the source-relay transition probabilities have to be estimated for each pilot symbol position $\tilde{k}$, have made the pilot-based EM algorithm converge to a wrong local optimum. Instead of correctly estimating a positive carrier positive frequency offset on h_2 and a jump in quantization intervals at $\tilde{k} = 16$, the pilot-based EM algorithm yielded a negative carrier frequency offset on h_2 and no quantization interval jump. This is also reflected by studying the curves corresponding to $\widehat{\boldsymbol{\Xi}}; \alpha = 1$ and $\boldsymbol{\Xi}$, shown in the upper half of Fig. 8.3. As a result, there is a greater probability (as compared to the case in which $\alpha = 0.8$) of a decoding error occurring when the obtained pilot-based estimates are used to decode the re-

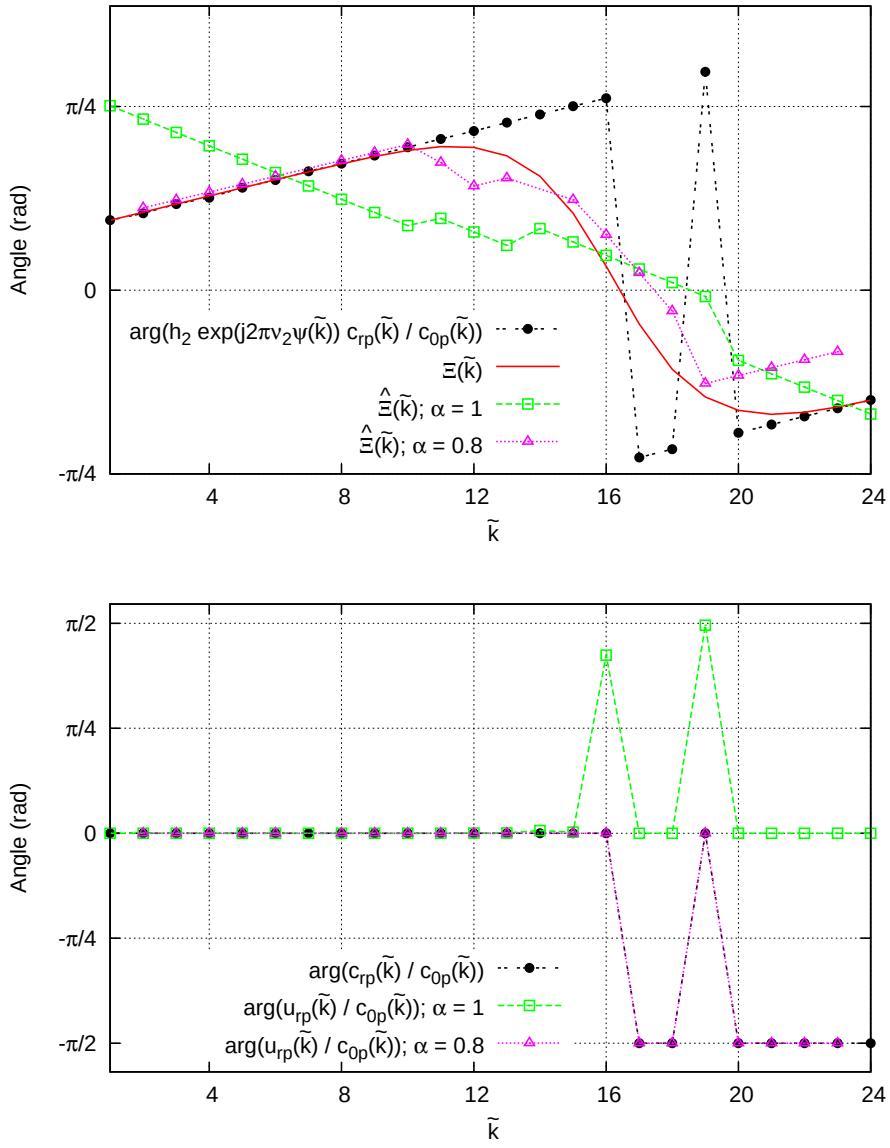

Figure 8.3: Metrics obtained from a random frame with $M_1 = 2$.

ceived information in the first code-aided EM iteration. In chapter 7 where no carrier frequency offset is present, the source-relay transition probabilities are the same for each symbol within the frame, preventing this effect from occurring and yielding an optimal value of $\alpha = 1$.

When $\alpha = 0.8$, the pilot symbols generated by the relay (and known to the destination) force the pilot-based EM algorithm to converge to the correct extremum, yielding a smaller difference between $\widehat{\Xi}; \alpha = 0.8$ and Ξ, and decreasing the possibility of a decoding error, accounting for the better WER performance. In the remainder of this chapter, a value of $\alpha = 0.8$ will be used, unless stated otherwise.

8.6.2.2 Optimization of W_p and W

The optimal value of the window size parameters W_p and W is determined by plotting the WER as a function of the normalized window size W_{norm}, defined as the window size divided by the total number of symbols available to the estimator, yielding $W_{\text{norm}} = W_p / \lceil \alpha K_p \rceil$ for the pilot-based estimation and $W_{\text{norm}} = W/(K + \lceil \alpha K_p \rceil)$ for the code-aided estimation. This WER is plotted in Fig. 8.4, in which the E_b/N_0 ratio is set equal to 9 dB and BPSK mapping is used at the source ($M_1 = 2$). The figure shows that a value of $W_{\text{norm}} = 0.5$ (equivalent to $W_p = 10$) yields the best WER performance when using pilot-based estimation, and a value of $W_{\text{norm}} = 0.16$ (equivalent to $W = 250$) is optimal when using code-aided estimation. The dependency of the WER on the value of W_{norm} is explained by noting that when W_{norm} is too small, not enough symbols are used for the calculation of the source-relay transition probabilities at each symbol position, yielding inaccurate estimates. When the value of W_{norm} is too large, too much averaging is used, making it difficult to observe the effects caused by the source-relay channel carrier frequency offset. In the remainder of this chapter, W_p and W will be set equal to $0.5\lceil \alpha K_p \rceil$ and $0.16(K + \lceil \alpha K_p \rceil)$, respectively.

8.6.3 WER Analysis

The WER performance of the proposed estimation methods is shown in Fig. 8.5, Fig. 8.6 and Fig. 8.7 for BPSK ($M_1 = 2$), QPSK ($M_1 = 4$) and 8-PSK ($M_1 = 8$) mapping, respectively. The figures all display the WER performance of both the direct estimation and AF approximation method. The pilot-based WER performance is obtained by decoding the received information using the pilot-based estimates, while the code-aided WER performance is obtained by first refining the pilot-based estimates using the code-aided EM algorithm, and using the refined estimates to decode the received information. The figures also display the performance of a reference system in which all channel parameters are assumed to be known and no pilot symbols are transmitted.

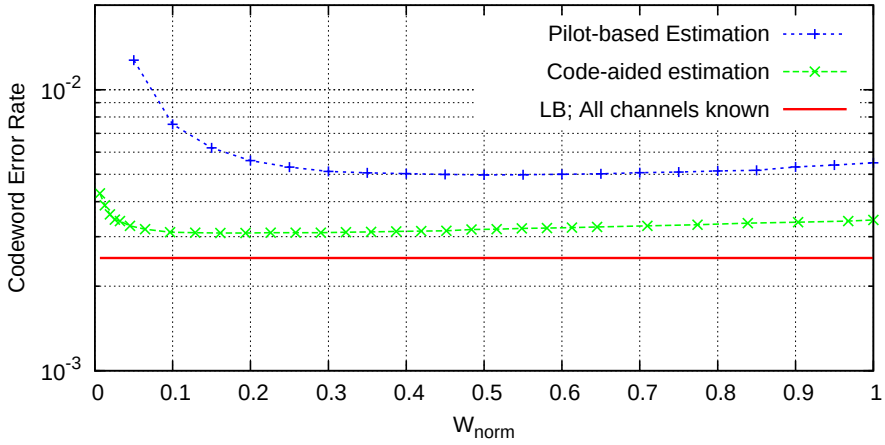

Figure 8.4: WER performance as function of the normalized window size for $M_1 = 2$ at $E_b/N_0 = 9$ dB.

In the reference system, the source-relay transition probabilities are calculated by numerically integrating (8.7) for each symbol index k.

Fig. 8.5 shows that for $M_1 = 2$, when using only pilot-based estimates, the AF approximation method performs better as compared to the direct estimation method. When the code-aided EM algorithm is used, the direct estimation method performs slightly better as compared to the AF approximation method. Both methods yield a WER performance that is very close to that of the reference system.

When the source mapping constellation is increased, the number of quantization interval also increases, as $M_2 = 2M_1$. As a result, more transition probabilities need to be estimated. Additionally, the number of pilot symbols also decreases as M_1 is increased, in order to ensure that the estimation overhead uses the same percentage of the total transmit energy, independent of the constellation size. As a result, the WER of the direct estimation method using pilot-based estimates deteriorates with increasing M_1, as can be seen by comparing Fig. 8.5 ($M_1 = 2$) to Fig. 8.6 ($M_1 = 4$) and Fig. 8.7 ($M_1 = 8$). This deterioration in WER performance also degrades the performance of the code-aided approach, as the large number of decoding errors resulting from the pilot-based estimates make it impossible to accurately determine the a posteriori probabilities of the source symbols, which are required in the first iteration of the code-aided EM approach. This is especially the case for $M_1 = 8$, where the pilot-based estimation method yields a very poor WER

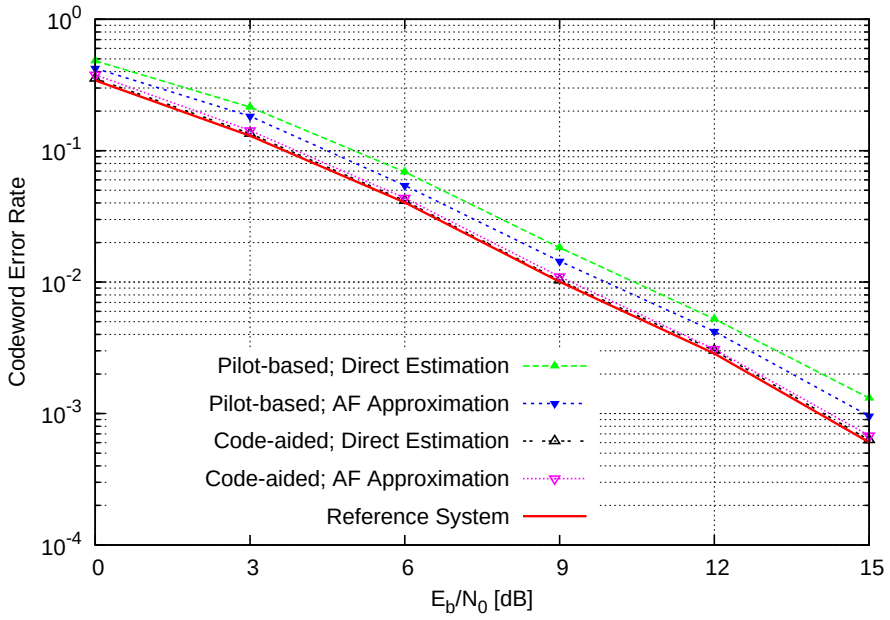

Figure 8.5: WER performance as function of the E_b/N_0 ratio for $M_1 = 2$.

performance.

The AF approximation does not suffer from this effect, as no transition probabilities need to be estimated. On the contrary, when the number of quantization intervals is increased, the average quantization noise n_q from (8.11) decreases ($n_q \to 0$ when $M_2 \to \infty$). As a result, the AF approximation yields better results for large M_1 (and M_2) values, while the direct estimation method yields better results for small M_1 (and M_2) values.

8.6.4 MSE Analysis

In this subsection the MSE performance of the different estimation methods is studied. The MSE related to the estimation of h_0 and ν_0 is displayed in Fig. 8.8 and Fig. 8.9, respectively, for a system using the AF approximation method with $M_1 = 2$. Similar results are obtained when the direct estimation method is used. The figures also show the EM lower bound, which is obtained by considering the symbols transmitted by the source to be known to the destination when calculating the estimates of h_0 and ν_0. This corresponds to a situation in which $\boldsymbol{u}_0 = \boldsymbol{c}_0$. The figures show that there is a large gap in MSE between the pilot-based estimates of h_0 and ν_0 and the EM lower bound. This

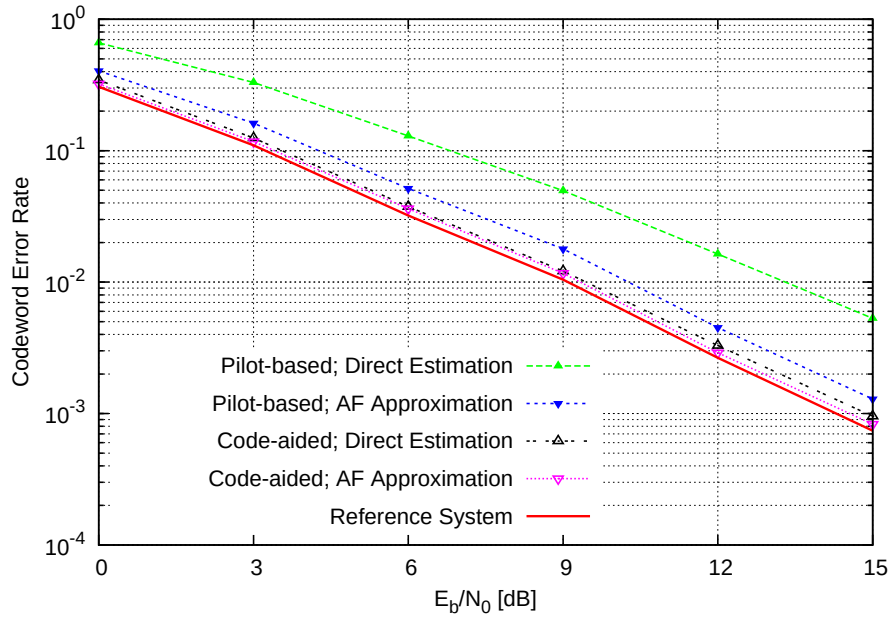

Figure 8.6: WER performance as function of the E_b/N_0 ratio for $M_1 = 4$.

gap is greatly reduced when using a code-aided approach, especially at high SNR, when the MSE of the code-aided estimates coincides with that of the EM lower bound.

In order to be able to compare the relay path channel estimates of the direct estimation method to those of the AF approximation method, we need a metric for the quality of these estimates that can be used for both approaches. For a system in which the channel parameters are known, we introduced the total phase rotation per symbol $\Xi(k)$ in (8.59). When estimating the relay path channel parameters using the direct estimation method, we can replace the true channel parameters in (8.59) with their corresponding estimates, thus obtaining $\widehat{\Xi}(k)$. When using the AF approximation, we define the total phase rotation per symbol as

$$\widetilde{\Xi}(k) = \arg(\hat{h}_3 \exp(2\pi\hat{\nu}_3 k)). \tag{8.60}$$

Using the aforementioned definitions, we define the squared error (SE) related to the relay path channel estimation as

$$\mathrm{SE}_{\mathrm{DE}} = \frac{\sum_{k=1}^{K+\lceil \alpha K_p \rceil} \left(\widehat{\Xi}(k) - \Xi(k)\right)^2}{K + \lceil \alpha K_p \rceil}, \tag{8.61}$$

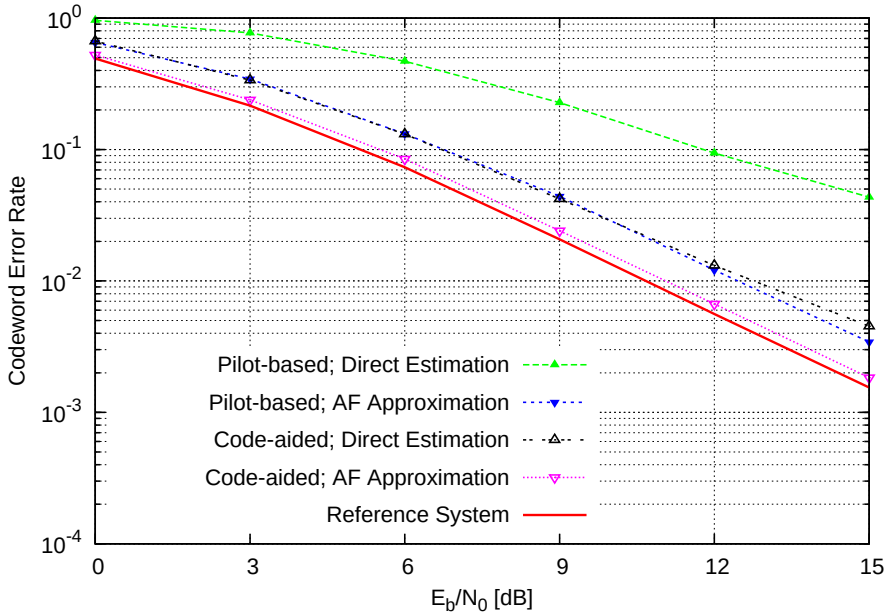

Figure 8.7: WER performance as function of the E_b/N_0 ratio for $M_1 = 8$.

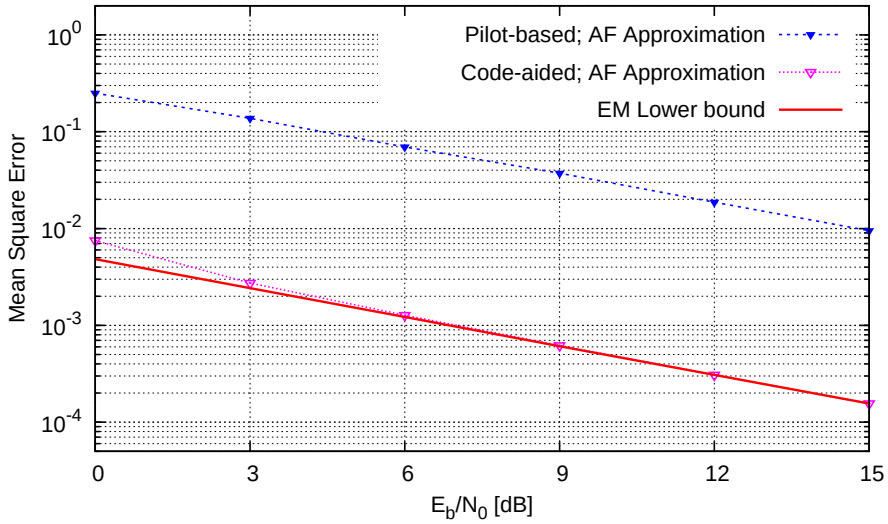

Figure 8.8: MSE of $\hat{h_0}$ as function of the E_b/N_0 ratio for $M_1 = 2$ and using the AF approximation method.

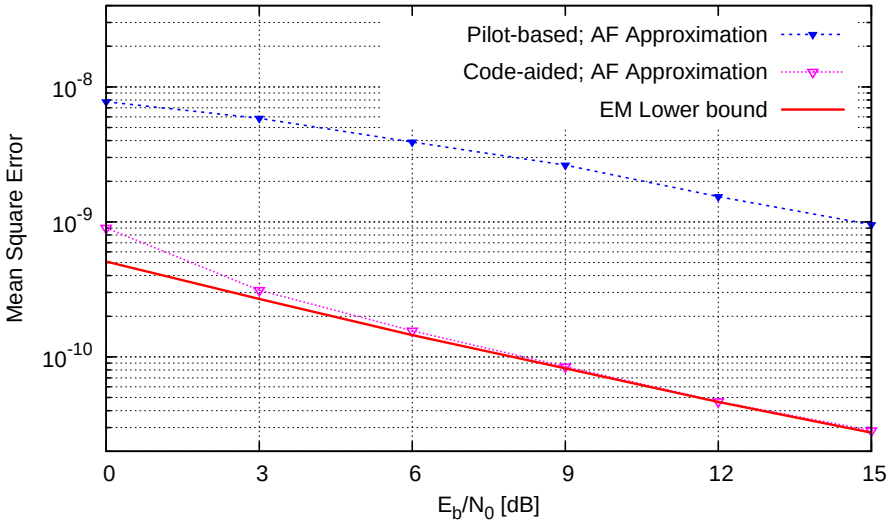

Figure 8.9: MSE of $\hat{v_0}$ as function of the E_b/N_0 ratio for $M_1 = 2$ and using the AF approximation method.

for the direct estimation method and as

$$\mathrm{SE}_{\mathrm{AF}} = \frac{\sum_{k=1}^{K+K_p} \left(\widetilde{\Xi}(k) - \Xi(k)\right)^2}{K + K_p}, \tag{8.62}$$

for the AF approximation method. By averaging (8.61) and (8.62) over all transmitted frames, we obtain the MSE values $\mathrm{MSE}_{\mathrm{DE}}$ and $\mathrm{MSE}_{\mathrm{AF}}$, respectively, which are plotted as function of the E_b/N_0 ratio in Fig. 8.10 for $M_1 = 2$ and Fig. 8.11 for $M_1 = 8$. The EM lower bound for the system using the AF approximation is obtained by assuming the symbols transmitted by the source to be known to the destination when calculating the relay path channel estimates, which are subsequently used in (8.60) and (8.62) to determine the MSE performance of the EM lower bound. In the direct estimation system, the EM lower bound is obtained by assuming the destination knows both the symbols transmitted by the source and those transmitted by the relay when calculating the relevant channel estimates, which are subsequently used in (8.59) and (8.61).

To help us interpret the results from Fig. 8.10 and Fig. 8.11, Fig. 8.12 is introduced, in which it is assumed that there is no noise on the relay-destination link ($N_2 = 0$). Fig. 8.12 thus displays the actual rotation experienced by the symbols received from the relay path, together with the values of $\Xi(k)$, $\widehat{\Xi}(k)$

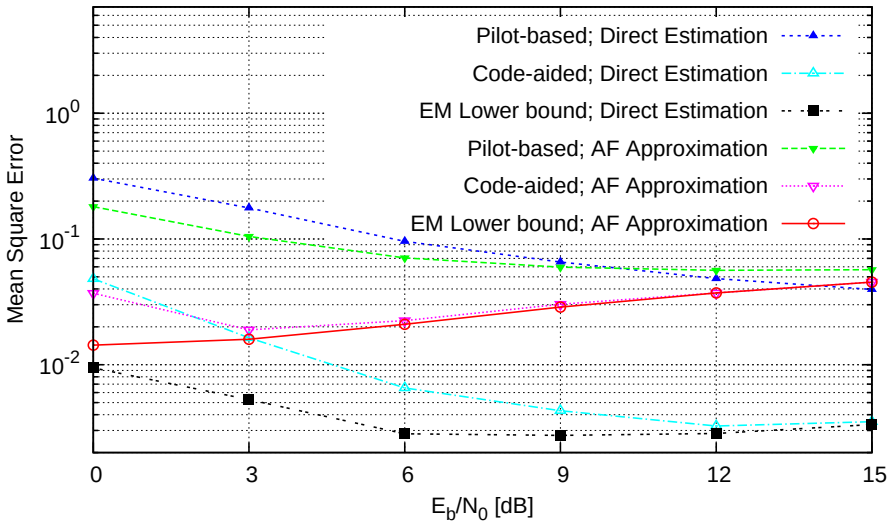

Figure 8.10: Value of MSE_{DE} and MSE_{AF} as function of the E_b/N_0 ratio for $M_1 = 2$.

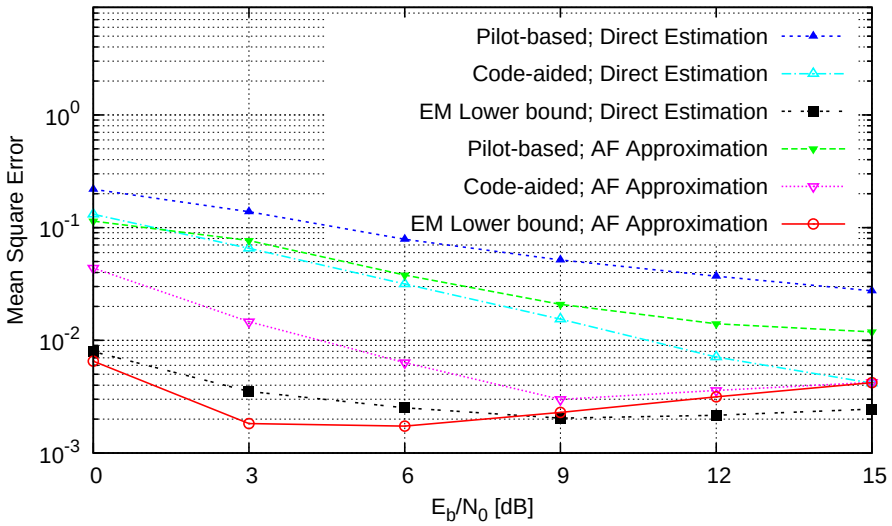

Figure 8.11: Value of MSE_{DE} and MSE_{AF} as function of the E_b/N_0 ratio for $M_1 = 8$.

and $\widetilde{\Xi}(k)$ at a low (top graph) and high (bottom graph) SNR on the source-relay link, for a particular frame. The values of $\widehat{\Xi}(k)$ and $\widetilde{\Xi}(k)$ are calculated using the estimates from the EM lower bound (source and relay symbols known). The MSE corresponding to the EM lower bound of the direct estimation method and the AF approximation method can be interpreted as the average (over the symbol index k) square distance between $\Xi(k)$ and $\widehat{\Xi}(k)$, and between $\Xi(k)$ and $\widetilde{\Xi}(k)$, respectively.

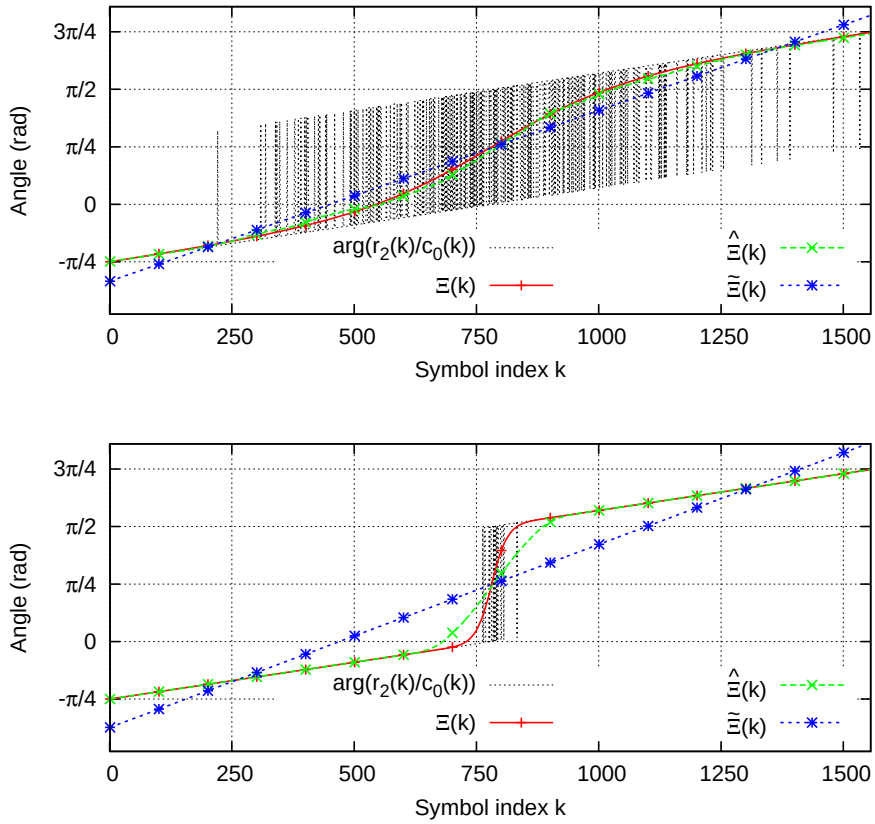

Figure 8.12: Value of $\Xi(k)$, $\widehat{\Xi}(k)$ and $\widetilde{\Xi}(k)$ for a low (top) and high (bottom) SNR on the source-relay link with $M_1 = 2$.

Using the aforementioned figures, the following observations can be made regarding the MSE of the relay path channel parameters:

• When the E_b/N_0 ratio is increased, the a posteriori probabilities of the symbols transmitted by the source and the relay are determined more accurately, and the MSE of the code-aided EM algorithm will approach that of the

EM lower bound, for both the direct estimation and the AF approximation method.

• The MSE of the EM lower bound in the AF approximation approach increases with increasing SNR for $M_1 = 2$. This can be explained by first noting that in the AF approximation, we have assumed that $n_q(k) = 0$ in (8.11). Because the error caused by this assumption does not depend on the E_b/N_0 ratio, the AF approximation will exhibit an error floor. This error floor is lower for higher values of M_2, as the quantization distortion decreases when the number of quantization intervals is increased. Secondly, by studying Fig. 8.12, one notices that for low SNR ratios (top graph) on the source-relay link, $\widetilde{\Xi}(k)$ is a better approximation for $\Xi(k)$ as compared to the situation in which the source-relay SNR is high (bottom graph). When the SNR on the source-relay link is low, the noise-induced jumps between quantization intervals will yield a more gradual transition of $\Xi(k)$ between two quantization intervals. Because $\widetilde{\Xi}(k)$ is essentially a linear approximation of $\Xi(k)$, it will better fit these gradual transitions as compared to a steep step that occurs when the SNR on the source-relay link is high.

• The MSE of the EM lower bound of the direct estimation method also slightly increases at high E_b/N_0 ratios, an effect that can also be explained with the aid of Fig. 8.12. As can be seen on the bottom graph of the aforementioned figure, $\widehat{\Xi}(k)$ is unable to accurately approximate steep changes in $\Xi(k)$, which occur at high source-relay SNR ratios. This is because, when using the direct estimation method, samples from adjacent symbol positions are used for calculating the transition probabilities at a certain symbols position k, a process which is controlled by the window size parameter W. The larger the value of W, the slower the changes of $\widehat{\Xi}(k)$.

8.7 Conclusions

In this chapter, channel parameter estimation in the presence of a frequency offset is discussed. Two estimation methods are proposed, both avoiding a computationally complex numerical integration which is required to decode the received information. By estimating all channel parameters at the destination, the relay complexity is also kept low. By studying the WER performance of the proposed estimation algorithms, it is determined which algorithm should be used for a given value of M_1 (and M_2), yielding excellent WER performances for all simulated constellation sizes. By also studying the MSE values, more insight is gained into the process of estimating channel parameters using quantized data in the presence of a carrier frequency offset.

8.8 Appendix: Pilot-based Estimation of h_0, ν_0 and N_0

Pilot-based estimates of h_0, ν_0, N_0, grouped in the vector $\boldsymbol{x}_0$, are obtained by solving the following equation

$$\hat{\boldsymbol{x}_0} = \arg\max_{\boldsymbol{x}_0} p(\boldsymbol{r}_{0p} \mid \boldsymbol{c}_{0p}, \boldsymbol{x}_0). \tag{8.63}$$

Using (8.5), (8.63) can be written as

$$\hat{\boldsymbol{x}_0} = \arg\max_{\boldsymbol{x}_0} \prod_{\tilde{k}=1}^{K_p} \frac{1}{\pi N_0} \exp\left(-\frac{|r_{0p}(\tilde{k}) - \sqrt{E_0}\exp(j2\pi\psi(\tilde{k})\nu_0)h_0 c_{0p}(\tilde{k})|^2}{N_0} \right), \tag{8.64}$$

with the function $\psi(.)$ defined in (8.2). By discarding terms and factors that do not depend on h_0 and ν_0, we can solve (8.64) for ν_0 and h_0 as function of N_0, yielding

$$\left(\hat{h_0}(N_0), \hat{\nu_0}(N_0)\right) = \arg\min_{h_0,\nu_0} \sum_{\tilde{k}=1}^{K_p} \left| r_{0p}(\tilde{k}) - \sqrt{E_0}\exp(j2\pi\psi(\tilde{k})\nu_0)h_0 c_{0p}(\tilde{k}) \right|^2 \tag{8.65}$$

A computationally efficient solution to this problem has been obtained in [82] for MIMO systems. Applying this solution to the system at hand yields the following estimates for the carrier frequency offset ν_0 and the channel coefficient h_0

$$\hat{\nu_0} = \frac{(K_p - 1)}{(K + K_p - 1)} \frac{\sum_{m=1}^{K_p} m|R_{0p}(m)| \arg(R_{0p}(m))}{2\pi \sum_{m=1}^{K_p} m^2 |R_{0p}(m)|} \tag{8.66}$$

$$\hat{h_0} = \frac{\sum_{\tilde{k}=1}^{K_p} r_{0p}(\tilde{k}) c_{0p}^*(\tilde{k}) \exp\left(-j2\pi\psi(\tilde{k})\hat{\nu_0}\right)}{K_p\sqrt{E_0}}, \tag{8.67}$$

with

$$R_{0p}(m) = \frac{\sum_{\tilde{k}=1}^{K_p} r_{0p}^*(\tilde{k}-m) r_{0p}(\tilde{k}) c_{0p}^*(\tilde{k}) c_{0p}(\tilde{k}-m)}{K_p}. \tag{8.68}$$

By using (8.66) and (8.67) in (8.64) and taking into account that the estimates obtained for ν_0 and h_0 do not depend on N_0, an equation for $\hat{N_0}$ can be obtained:

$$\hat{N_0} = \arg\max_{\boldsymbol{x}_0} \prod_{\tilde{k}=1}^{K_p} \frac{1}{\pi N_0} \exp\left(-\frac{|r_{0p}(\tilde{k}) - \sqrt{E_0}\exp(j2\pi\psi(\tilde{k})\hat{\nu_0})\hat{h_0} c_{0p}(\tilde{k})|^2}{N_0} \right). \tag{8.69}$$

Identification between (8.69) and (6.57) yields

$$\hat{N_0} = \frac{\sum_{\tilde{k}=1}^{K_p} |r_{0p}(\tilde{k}) - \sqrt{E_0}\exp(j2\pi\psi(\tilde{k})\hat{\nu_0})\hat{h_0}c_{0p}(\tilde{k})|^2}{K_p}, \tag{8.70}$$

concluding the pilot-based estimation of the source-destination channel parameters.

9

Two-way Relaying

9.1 Introduction

In a classical cooperative communication system, only unidirectional communication is considered: one transmitting terminal communicates to one receiving terminal with the help of a relaying terminal. Many practical applications however require bidirectional communication, in which two terminals both send and receive information to/from each other. Using a classical (one-way) cooperative system in this situation would yield a poor spectral efficiency, as this would require four orthogonal channels, i.e., the two transmitting terminals need one channel each, and the relay transmits over two channels the data received from the first and second terminal, respectively. The spectral efficiency can be improved using a two-way relaying system, in which the relay uses a single channel to simultaneously assists in the information transfer from the first to the second terminal and from the second to the first terminal,

so that in total only three orthogonal channels are required.

As for one-way cooperative systems, a variety of forwarding protocols have been developed for two-way systems, including, but not limited to, network coding [84, 85], Amplify and Forward (AF) [86], Decode and Forward (DF) [86, 87] and Compress and Forward (CF) [88]. While many of these protocols achieve satisfactory results regarding outage probability and WER, they also impose a (large) burden upon the relay in terms of computational complexity and/or storage space requirements. The DF strategy requires the relay to decode the received data. In the AF protocol the relay needs to store the analog signals awaiting retransmission, requiring a high-precision analog-to-digital conversion (i.e., many quantization bits per sample) and, therefore, a large memory to store the samples.

Two-way QF protocols have been studied in [90] and [89]. In [90], the capacity of a two-way relaying channel is maximized using an information theoretical approach. Channel symmetry is assumed, i.e. both users' channel qualities need to be the same, both in the uplink and downlink. In [89], a two-way QF relaying scheme using space-time block coding (STBC) is proposed. The two transmitting nodes use STBC to simultaneously transmit their signals to the relay, where they are estimated using minimum mean square error ordered successive interference cancellation (MMSE-OSIC). The main drawback of the proposed system is the MMSE-OSIC algorithm that needs to be executed at the relay, inevitably raising its complexity. Furthermore, the relay is required to have multiple antennas, which also raises its hardware cost. Both [89] and [90] also assume there is no direct link between the two user terminals, making it impossible to exploit cooperative diversity.

These hardware requirements can limit the usefulness of existing two-way relaying strategies in applications requiring a low relay complexity, such as sensor networks and battery powered devices. Therefore, in the current chapter, a low-complexity two-way relaying strategy is presented, based on the QF protocol from chapter 5. The main goal is to keep the relay complexity to a minimum by shifting as much operations as possible to the user terminals, where typically there is more processing power available. The proposed relaying strategy exploits cooperative diversity, by assuming there is a direct path between the user terminals. Additionally, efficient estimation algorithms are developed for the estimation of the unknown channel parameters, based on the results from chapter 7. As was the case in the aforementioned chapter, all estimation is performed at the destination terminals, with no additional calculations needed at the relay, hence maintaining the low complexity of the latter.

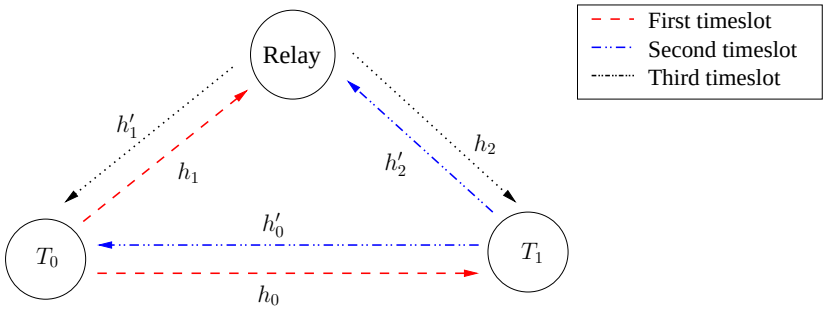

Figure 9.1: Timeslot assignment.

The remainder of this chapter is organized as follows: The system model is outlined in section 9.2, whereafter the proposed quantization scheme is presented in section 9.3. In section 9.3.3, the receiver structure is obtained and in section 9.4, the estimation algorithm is discussed. The WER performance of the proposed algorithms is analyzed using Monte Carlo [96] simulations in section 9.5. Finally, conclusions are drawn in section 9.6.

9.2 System Description

A cooperative two-way relaying scheme is analyzed consisting of two terminals exchanging information, denoted T_0 and T_1, and one assisting relay, denoted R. At both T_0 and T_1, the information to be transmitted is divided into frames of K coded bits, which are obtained by encoding the information bits by means of a channel encoder. The terminals T_0, T_1 and R transmit in turn using time-division multiple access (TDMA), as depicted in Fig. 9.1. At T_1 (T_0), the signals received from the relay and from T_0 (T_1) are combined in order to retrieve the information sent by T_0 (T_1).

All channels are modelled as flat Rayleigh fading channels with additive white Gaussian noise. We denote the complex-valued channel gains between T_0 and T_1, between T_0 and R and between R and T_1 as h_0, h_1 and h_2, respectively. The gains of the reciprocal channels are denoted h_0', h_1' and h_2', respectively, as also shown in Fig. 9.1. In order to keep the discussion general, no assumptions are made on the relation between the fading gains of reciprocal channels. Denoting by $\boldsymbol{c}_0$, $\boldsymbol{c}_1$ and $\boldsymbol{c}_r$ the PSK symbol sequences sent by T_0 (first slot), T_1 (second slot) and R (third slot), respectively, the channel outputs

for the information transfer from T_0 to T_1 are equal to

$$\boldsymbol{r}_0 = \sqrt{E_0} h_0 \boldsymbol{c}_0 + \boldsymbol{n}_0 \tag{9.1}$$

$$\boldsymbol{r}_1 = \sqrt{E_0} h_1 \boldsymbol{c}_0 + \boldsymbol{n}_1 \tag{9.2}$$

$$\boldsymbol{r}_2 = \sqrt{E_r} h_2 \boldsymbol{c}_r + \boldsymbol{n}_2, \tag{9.3}$$

where $\boldsymbol{r}_0$, $\boldsymbol{r}_1$ and $\boldsymbol{r}_2$ denote the signals received by T_1 (first slot), R (first slot) and T_1 (third slot), respectively. Similarly, the channel outputs for the information transfer from T_1 to T_0 are equal to

$$\boldsymbol{r}'_0 = \sqrt{E_1} h'_0 \boldsymbol{c}_1 + \boldsymbol{n}'_0 \tag{9.4}$$

$$\boldsymbol{r}'_1 = \sqrt{E_r} h'_1 \boldsymbol{c}_r + \boldsymbol{n}'_1 \tag{9.5}$$

$$\boldsymbol{r}'_2 = \sqrt{E_1} h'_2 \boldsymbol{c}_1 + \boldsymbol{n}'_2, \tag{9.6}$$

Assuming the normalization condition $|\boldsymbol{c}_0|^2 = |\boldsymbol{c}_1|^2 = |\boldsymbol{c}_r|^2 = K$, the quantities E_0, E_1 and E_r denote the transmitted energy per symbol at T_0, T_1 and R, respectively. All channel coefficients are considered to be constant during a frame and have a zero mean circular symmetric complex gaussian (ZMCSCG) distribution with variances $N_{h_x} = 1/{d_x}^{n_{loss}}$, with $N_{h_x} = N_{h'_x}$ and $x \in \{0, 1, 2\}$. The quantity d_x represents the distance between the two considered terminals, while n_{loss} denotes the path loss exponent. The components of the noise vectors $\boldsymbol{n}_x$ and $\boldsymbol{n}'_x$ are also ZMCSCG distributed with variances N_x and N'_x, respectively, with $x \in \{0, 1, 2\}$.

9.3 Two-way Relaying

In the following subsections, the operation performed at the relay is discussed, assuming that the symbols transmitted by T_0 and T_1 belong to a M_1-PSK constellation, with M_1 the constellation size. This operation results in the symbol vector $\boldsymbol{c}_r$ transmitted by the relay in the third slot. An AF two-way relaying strategy, to be used for benchmarking the performance of the proposed QF system, is briefly discussed first.

9.3.1 Amplify and Forward

In a two-way relaying AF system, the relay simply adds the signals received from T_0 and T_1 and transmits a scaled version of the resulting sum. This yields the following expression for $\boldsymbol{c}_r$:

$$\begin{aligned} \boldsymbol{c}_r &= \beta \left(\boldsymbol{r}_1 + \boldsymbol{r}'_2 \right) \\ &= \beta \left(\sqrt{E_0} h_1 \boldsymbol{c}_0 + \sqrt{E_1} h'_2 \boldsymbol{c}_1 \right) + \beta \left(\boldsymbol{n}_1 + \boldsymbol{n}'_2 \right). \end{aligned} \tag{9.7}$$

In order to satisfy the normalization constraint $\mathbb{E}[|c_r|^2] = K$, the gain β is chosen as

$$\beta = \frac{1}{\sqrt{E_0|h_1|^2 + E_1|h_2'|^2 + N_1 + N_2'}}. \tag{9.8}$$

Note that the relay in a two-way AF system needs to know the squared channel magnitudes $|h_1|^2$ and $|h_2'|^2$.

9.3.2 Quantize and Forward

A straight-forward implementation of a two-way QF relaying system that is similar to the AF relaying system would involve the coarse quantization of the sum of the signals received in the first and second time slot from T_0 and T_1, respectively, and the broadcasting of these quantized samples in the third slot. While the initial purpose of quantization is to avoid the storage of analog samples, this approach however would require the relay to store the analog samples received from T_0 in the first slot, until the data from T_1 is received in the second slot and the two can be added and quantized. Instead, a quantization scheme that does not necessitate the storage of analog values is proposed, where the relay separately quantizes the signals received in the first and second slot, and then properly combines the quantized values. This involves the following operations, which do not require any channel knowledge at the relay.

9.3.2.1 Quantization

In the first and second slot, the phase of the samples received from T_0 and T_1, respectively, is quantized uniformly using $\log_2 M_2$ bits. When taking $M_2 \geq 2M_1$, this approach has shown to yield a performance close to that of AF for one-way relaying systems, as shown in chapter 5. The uniform quantization, with $\log_2 M_2$ bits, of the phases of the signals $r_1(k)$ and $r_2'(k)$ received by the relay, yields the quantized phases $2\pi q_1(k)/M_2$ and $2\pi q_2'(k)/M_2$, respectively, where

$$q_1(k) = f_q(r_1(k)) \tag{9.9}$$
$$q_2'(k) = f_q(r_2'(k)), \tag{9.10}$$

with the function $f_Q(x) \in \{0, 1, ..., M_2 - 1\}$ defined in (5.3). In order to be able to exploit circular symmetry at the relay, we impose that M_2 is a multiple of M_1.

9.3.2.2 Addition

The quantized phases of $r_1(k)$ and $r_2'(k)$ are added modulo-M_2, and the resulting sum determines the symbol $c_r(k)$ to be sent by the relay in the third

slot. Using the mapping function $\chi_{M_2}(q)$ defined in (5.5), the symbols sent by the relay can be written as

$$c_r(k) = \chi_{M_2}((q_1(k) + q_2'(k)) \bmod M_2). \tag{9.11}$$

9.3.2.3 Relay Complexity

In the proposed quantization scheme, the storage and processing requirements at the relay are kept low. For each frame, only the vectors $\boldsymbol{q}_1$ and $\boldsymbol{q}_2'$ need to be stored at the relay; the memory requirements are low, because the components of $\boldsymbol{q}_1$ and $\boldsymbol{q}_2'$ are represented by only $\log_2 M_2$ bits. The memory usage can further be lowered in a practical implementation by storing the elements of $\boldsymbol{q}_1$ obtained in the first slot, performing the modulo M_2 addition element-wise in the second slot as the values of $\boldsymbol{q}_2'$ become available by quantizing the incoming signal $\boldsymbol{r}_2'$, and storing the result of the addition back in $\boldsymbol{q}_1$. The latter is then mapped on M_2-PSK symbols and broadcast in the third slot.

The number of computations the relay needs to perform is also limited. The quantization operation has a low complexity, as only the phase of the incoming signals is quantized, neglecting the amplitude. This complexity is further lowered by only considering uniform quantization. The modulo-M_2 addition of the resulting quantization intervals involves the addition of two integers with a limited range and is thus easily implemented in hardware. Channel parameter estimation does not add to the computational burden of the relay, because all channel parameters are estimated at the destination terminals.

9.3.3 Detection

At T_1 (T_0), the signals received from the relay and from T_0 (T_1) need to be combined in order to optimally retrieve the information bits sent by T_0 (T_1). In this section we will focus on the calculation of the likelihoods of the received symbols at T_1, which are used by the channel decoder at T_1 to detect the information bits transmitted by T_0. Similar expressions are obtained for the symbol likelihoods at T_0, used to detect the information transmitted by T_1. Introducing $\boldsymbol{h} = (h_0, h_1, h_2)$ and $\boldsymbol{N} = (N_0, N_1, N_2)$, the symbol likelihoods at T_1 are given by

$$p(\boldsymbol{r}_0, \boldsymbol{r}_2 | \boldsymbol{c}_0, \boldsymbol{h}, \boldsymbol{N}, h_2', N_2' ; \boldsymbol{c}_1) = p(\boldsymbol{r}_0 | \boldsymbol{c}_0, h_0, N_0) p(\boldsymbol{r}_2 | \boldsymbol{c}_0, h_1, h_2, h_2', N_1, N_2, N_2' ; \boldsymbol{c}_1), \tag{9.12}$$

As T_1 knows the symbols $\boldsymbol{c}_1$, (9.12) denotes the likelihood of $\boldsymbol{c}_0$ based on the observations $\boldsymbol{r}_0$ and $\boldsymbol{r}_2$, and $\boldsymbol{c}_1$ is to be considered as a known parameter. Evaluating (9.12) on a symbol-by-symbol basis and conditioning on the symbols

sent by the relay yields

$$p(\boldsymbol{r}_0, \boldsymbol{r}_2 | \boldsymbol{c}_0, \boldsymbol{h}, \boldsymbol{N}, h_2' \,;\, \boldsymbol{c}_1) = \prod_{k=1}^{K} p(r_0(k)|c_0(k), h_0, N_0) \times \sum_{c_r(k)} p(r_2(k)|c_r(k), h_2, N_2) p(c_r(k)|c_0(k), h_1, h_2', N_1, N_2' \,;\, c_1(k)), \quad (9.13)$$

with

$$p(r_0(k)|c_0(k), h_0, N_0) = \frac{1}{\pi N_0} \exp\left(-\frac{|r_0(k) - \sqrt{E_0} h_0 c_0(k)|^2}{N_0} \right) \quad (9.14)$$

$$p(r_2(k)|c_r(k), h_2, N_2) = \frac{1}{\pi N_2} \exp\left(-\frac{|r_2(k) - \sqrt{E_r} h_2 c_r(k)|^2}{N_2} \right). \quad (9.15)$$

To determine the factor $p(c_r(k)|c_0(k), h_1, h_2', N_1 \,;\, c_1(k))$ in (9.13), further on referred to as the transition probabilities, one has to take into account that due to the modulo M_2 addition, there are multiple combinations of $q_1(k)$ and $q_2'(k)$ that all give rise to the same relay symbol $c_r(k)$. This yields the following expression for the transition probabilities:

$$P[c_r(k) = \chi_{M_2}(q)|c_0(k), h_1, h_2', N_1, N_2' \,;\, c_1(k)] = \sum_{\tilde{q}=0}^{M_2-1} P[q_2'(k) = \tilde{q}|h_2', N_2' \,;\, c_1(k)] P[q_1(k) = (q - \tilde{q}) \bmod M_2 | h_1, N_1, c_0(k)]. \quad (9.16)$$

Using the function f_Θ from (5.12), the probabilities $p(q_2'(k)|h_2', N_2' \,;\, c_1(k))$ and $p(q_1(k)|h_1, N_1, c_0(k))$ to be used in (9.16) can be written as

$$p(q_2'(k)|h_2', N_2' \,;\, c_1(k)) = \int_{\frac{2\pi(q_2'(k)-\frac{1}{2})}{M_2}}^{\frac{2\pi(q_2'(k)+\frac{1}{2})}{M_2}} f_\Theta\left(\theta - (\arg(c_1(k) h_2') \,;\, \frac{E_1 |h_2'|^2}{N_2'} \right) \mathrm{d}\theta \quad (9.17)$$

$$p(q_1(k)|h_1, N_1, c_0(k)) = \int_{\frac{2\pi(q_1(k)-\frac{1}{2})}{M_2}}^{\frac{2\pi(q_1(k)+\frac{1}{2})}{M_2}} f_\Theta\left(\theta - (\arg(c_0(k) h_1) \,;\, \frac{E_0 |h_1|^2}{N_1} \right) \mathrm{d}\theta, \quad (9.18)$$

which completes the calculation of the symbol likelihoods.

9.4 Estimation

The likelihoods calculated in the previous section depend on the specific realization of the channel coefficients h_0, h_1, h_2, and h_2' (for the likelihoods calculated at T_0) and h_0', h_1', h_2' and h_1 (for the likelihoods at T_1). As these

parameters change between frames and are not a-priori known, they need to be estimated before the data decoding can be performed. In addition, the noise variances N_0, N_1, N_2 and N_2' also need to be estimated. In the remainder of this section, we will focus on the channel estimation at T_1 in order to decode the data sent by T_0. Similar expressions are obtained for the channel estimation at T_0.

The parameters that need to be estimated can be divided into two groups: the ones that are directly observed by T_1 (these are h_0, h_2, N_0 and N_2) and the ones that are not (these are h_1, h_2', N_1 and N_2'). The main difficulty is estimating the parameters that are not directly observed. In order to keep the complexity at the relay terminal low, we deliberately choose not to perform any relay-side estimation. However, due to the quantization performed at the relay, it is quite difficult to estimate the parameters that are not directly observed at T_1. Fortunately, this problem can be circumvented by directly estimating the transition probabilities used in (9.13), so that we no longer need to estimate h_1, h_2', N_1 and N_2'. Indeed, in chapter 7, it was shown that the source-relay transition probabilities can be estimated at the destination in a one-way quantize and forward system. Accurate results were obtained by first estimating the transition probabilities using pilot symbols transmitted by the source, and then iteratively refining these pilot-based estimates by also using the a posteriori probabilities of the unknown data symbols in the estimation process.

In the one-way relaying system described in chapter 7, the transition probabilities only depend on the symbols transmitted by T_0 and on the channel between T_0 and R. However, in the two-way system at hand, they also depend on the symbols sent by T_1 and on the channel between T_1 and R, which makes the estimation more complex. In order to be able to apply the results from chapter 7 to the considered two-way system, we first group the transition probabilities from (9.16) into the three-dimensional array $\overline{\mathbf{\Phi}}$, of which the elements are defined as

$$\overline{\Phi}(q,m,n) = P[c_r = \chi_{M_2}(q) | c_0 = \chi_{M_1}(m), h_1, h_2', N_1, N_2' \,;\, c_1 = \chi_{M_1}(n)). \quad (9.19)$$

The symbol index k is omitted from (9.19) because, due to the slow fading nature of communication channels, the elements of $\overline{\mathbf{\Phi}}$ do not depend on the position within a frame. Note that $\overline{\mathbf{\Phi}}$ contains a total of $M_2 \times M_1 \times M_1$ elements, all of which need to be estimated. For higher order mapping constellations, it can be a problem to estimate all elements of $\overline{\mathbf{\Phi}}$ individually, as this would require very long frames and a vast number of pilot symbols. Fortunately, the number of elements from $\overline{\mathbf{\Phi}}$ which actually need to be estimated can be reduced to only M_2 by exploiting the inherent circular symmetry of $\overline{\mathbf{\Phi}}$. Indeed, defining $\Phi(q) = \overline{\Phi}(q,0,0)$ with $q = 0, 1, ..., M_2 - 1$ it can be easily be shown

from (9.16), (9.17) and (9.18) that

$$\overline{\Phi}(q,m,n) = \Phi\left(\left(q - \frac{M_2(m+n)}{M_1}\right) \bmod M_2\right), \tag{9.20}$$

indicating that, for given m and n, the elements $\{\overline{\Phi}(q,m,n),\ q = 0,1,...,M_2 - 1\}$ are obtained as a cyclic shift of the vector $\mathbf{\Phi} = (\Phi(0),...,\Phi(M_2-1))$ over $(m+n)\frac{M_2}{M_1}$ positions.

In order to assist the estimation of the unknown parameters, both T_0 and T_1 transmit pilot symbols which are known to both terminals. These pilot symbols are quantized at the relay using the same quantization method as was used for the data symbols. The relay does not send any pilot symbols of its own. Hence, the relay operation does not need to distinguish between data symbols and pilot symbols. Using the pilot symbols, an initial estimate of the various channel parameters is obtained at T_1. These pilot-based estimates are then iteratively refined using code-aided estimation that exploits also the presence of the unknown data symbols contained in $\boldsymbol{r}_0$ and $\boldsymbol{r}_2$. This process is discussed in the next subsections.

9.4.1 Pilot-based Estimation

Because the 3-dimensional transition probability array $\overline{\mathbf{\Phi}}$ has been reduced to the one-dimensional vector $\mathbf{\Phi}$, the results from chapter 7 can be used. The pilot-based estimates of h_0 and N_0 are given by (7.10) and (7.11), respectively. The estimates of N_2, h_2 and $\mathbf{\Phi}$ are obtained iteratively using the EM algorithm as described in sections 7.3.2.2 and 7.3.4.1, using equations (7.18), (7.19) and (7.35) to update the estimates of h_2, N_2 and $\mathbf{\Phi}$, respectively. The elements of the vectors $\boldsymbol{u}_{rp^\dagger}^{(i)}$ and $\mathbf{\Gamma}^{(i)}$, used in (7.18), (7.19) and (7.35), are equal to

$$u_{rp^\dagger}^{(i)}(k) = \sum_{c_{rp}(k)} c_{rp}(k)\, p\left(c_{rp}(k) \mid r_{2p}(k), \hat{h_2}^{(i-1)}, \hat{N_2}^{(i-1)}, \widehat{\mathbf{\Phi}}^{(i-1)};\, c_{0p}(k), c_{1p}(k)\right) \tag{9.21}$$

$$\Gamma_p^{(i)}(q) = \sum_{k=1}^{K_p} P\left[c_{rp}(k) = \chi_{M_2}\left(q + \frac{M_2(m_{0p}+n_{0p})}{M_1}\right) \,\middle|\, r_{2p}(k), \hat{h_2}^{(i-1)}, \hat{N_2}^{(i-1)}, \widehat{\mathbf{\Phi}}^{(i-1)};\, c_{0p}(k), c_{1p}(k)\right] \tag{9.22}$$

where $m_{0p}(k)$ and $n_{0p}(k)$ are the integers in the interval $\{0,1,...,M_1-1\}$ that satisfy the relation $c_{0p}(k) = \chi_{M_1}(m_{0p}(k))$ and $c_{1p}(k) = \chi_{M_1}(n_{0p}(k))$, respectively. The initial conditions for the pilot-based EM algorithm are set to $\hat{h}_2^{(0)} = 1$ and $\widehat{\mathbf{\Phi}}^{(0)}(q) = 1/M_2$, $\forall q$. The noise variance estimates are averaged

over consecutive frames, as explained in section 6.3.1.3, and will not be refined using the code-aided EM algorithm. The noise variance estimate $\hat{N_2}^{(0)}$ is set equal to the thus obtained average of N_2.

9.4.2 Code-aided Estimation

At T_1, the channel coefficients h_0 and h_2, and the transition probabilities $\mathbf{\Phi}$ are refined using a code-aided EM algorithm. Using the results from sections 7.3.3 and 7.3.4.2, and introducing $\boldsymbol{h}_d = (h_0, h_2, \mathbf{\Phi})$, the following estimates are obtained in the i-th EM iteration for the aforementioned channel parameters:

$$\hat{h_0}^{(i)} = \frac{\boldsymbol{r}_0 \left(\boldsymbol{u}_0^{(i)}\right)^H}{(K+K_p)\sqrt{E_0}} \tag{9.23}$$

$$\hat{h_2}^{(i)} = \frac{\boldsymbol{r}_2 \left(\boldsymbol{u}_r^{(i)}\right)^H}{(K+K_p)\sqrt{E_r}} \tag{9.24}$$

$$\hat{\Phi}^{(i)}(q) = \frac{\Gamma_c^{(i)}(q)}{\sum_{\tilde{q}=0}^{M_2-1} \Gamma^{(i)}(\tilde{q})}, \tag{9.25}$$

with

$$u_0^{(i)}(k) = \sum_{m=0}^{M_1-1} \chi_{M_1}(m) F_{m,n_0(k)}^{(i)}(k) \tag{9.26}$$

$$u_r^{(i)}(k) = \sum_{q=0}^{M_2-1} \sum_{m=0}^{M_1-1} \chi_{M_2}(q) F_{m,n_0(k)}^{(i)}(k) P\left[c_r(k) = \chi_{M_2}(q) \middle| c_0(k), \boldsymbol{r}_2, \hat{\boldsymbol{h}_d}^{(i-1)}; c_1(k)\right] \tag{9.27}$$

$$\begin{aligned}\Gamma^{(i)}(q) = &\sum_{k=1}^{K+K_p} \sum_{m=0}^{M_1-1} F_{m,n_0(k)}^{(i)}(k) \\ &\times P\left[c_r(k) = \chi_{M_2}\left(q + \frac{M_2(m+n_0)}{M_1}\right) \middle| c_0(k) = \chi_{M_1}(m), \boldsymbol{r}_2, \hat{\boldsymbol{h}_d}^{(i-1)}; c_1(k)\right],\end{aligned} \tag{9.28}$$

where $n_0(k)$ is the integer in the interval $\{0, 1, ..., M_1 - 1\}$ that satisfies the relation $c_1(k) = \chi_{M_1}(n_0(k))$, and $F_{m,n_0(k)}^{(i)}(k)$ is a short-hand notation for the a posteriori probability of the symbol $c_0(k)$ based on the estimate $\hat{\boldsymbol{h}_d}^{(i-1)}$, i.e.,

$$F_{m,n}^{(i)}(k) = P\left[c_0(k) = \chi_{M_1}(m) \,\middle|\, \boldsymbol{r}_0, \boldsymbol{r}_2, \hat{\boldsymbol{h}_d}^{(i-1)}; c_1(k) = \chi_{M_1}(n)\right]. \tag{9.29}$$

These a posteriori probabilities are provided by the channel decoder at T_1.

9.5 Performance Evaluation.

The WER performance of the proposed protocol is investigated using Monte Carlo simulations. In section 9.5.1, the simulation parameters are discussed, whereafter the WER performance of a system with known channel parameters is discussed in section 9.5.2. Finally, The WER performance of a system with estimated parameters is discussed in section 9.5.3.

9.5.1 Simulation Parameters

We consider frames of 1024 information bits, which are encoded by means of an $(1, 13/15)_8$ RSCC turbo code that is punctured to a rate of $2/3$, yielding a total of 1536 coded bits which are then mapped on BPSK symbols ($M_1 = 2$). At the relay, 2 bit quantization of the phase of the received samples is used, yielding transmitted relay symbols belonging to a QPSK constellation ($M_2 = 4$). The path loss exponent equals 4 and the distance between T_0 and T_1 is considered unity. All symbol energies are considered to be equal ($E_0 = E_1 = E_r$) and all noise variances are also assumed to be equal ($N_0 = N_0' = N_1 = N_1' = N_2 = N_2'$), but will be estimated separately. In the remainder of this section, performance metrics related to the information transfer from T_0 to T_1 are considered. Results for the communication in the opposite direction are obtained by simply interchanging the positions of T_0 and T_1.

In order to assist the estimation process, 24 pilot symbols are added to the data frames at both T_0 and T_1. The pilot symbols added by T_0 do not need to equal those added by T_1, but both pilot symbol sequences need to be known to both terminals. When the channel parameters are considered to be known, no pilot symbols are added. The pilot-based estimates of the transition probabilities and of h_2 are computed using 5 EM iterations, while the code-aided refining is executed using 8 EM iterations.

9.5.2 Channels and Transition Probabilities Known

In this subsection, the WER performance of the proposed two-way relaying system is analyzed under the assumption that the relevant channels, noise variances and transition probabilities are known at the receiving terminal. This WER performance is compared to that of a non-cooperative system and a classical one-way relaying system. For a fair comparison, we require the three systems to operate at the same spectral efficiency R_b/R_s, with R_b and R_s denoting the average information bitrate and the symbol rate, respectively. This is achieved by dimensioning the systems as indicated in Fig. 9.2:

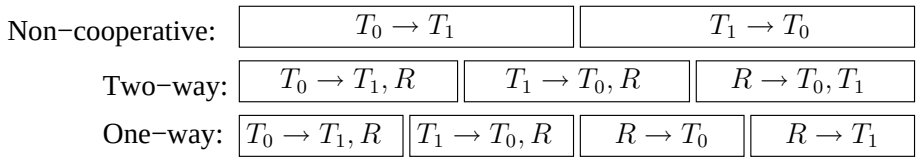

Figure 9.2: Timeslot assignment for the one-way and two-way relaying systems.

• In the two-way relay system, we use three slots to send 1024 information bits in each direction (2048 information bits in total), yielding a total transmission time of $2048/R_b$ and a duration of $2048/(3R_b)$ per slot. As stated in section 9.5.1, the turbo code is punctured to a rate of $2/3$, yielding 1536 coded bits (1536 BPSK symbols) in the first slot and in the second slot, and 1536 QPSK symbols in the third slot (i.e., $3 \times 1536 = 4608$ symbols in total). The resulting spectral efficiency is $R_b/R_s = 4/9$ information bits per channel use.

• In the non-cooperative system, there are only two slots as no relay is involved in the communication process. Each slot has a duration of $1024/R_b$, which is $3/2$ times the slot duration of the two-way relay system. The spectral efficiency of $R_b/R_s = 4/9$ is obtained by puncturing the turbo code to a rate of $4/9$ (instead of $6/9$ for the two-way relaying systems), yielding 2304 coded bits (2304 BPSK symbols) per slot (i.e., $2 \times 2304 = 4608$ symbols in total).

• In the one-way relay system, the relay uses two slots, to forward the information from T_0 to T_1 and from T_1 to T_0, requiring a total of four slots, each of duration $512/R_b$. The turbo code is punctured to a rate of $8/9$ (instead of $6/9$ for the two-way relaying systems), yielding 1152 coded bits (1152 BPSK symbols) in the first and the third slot and 1152 QPSK symbols in the second and in the fourth slot (i.e., $4 \times 1152 = 4608$ symbols in total), again resulting in a spectral efficiency of $R_b/R_s = 4/9$.

Also note that, while the above three communication systems yield the same spectral efficiency, the relay in a one-way relaying system needs to transmit more symbols (and thus consume more energy) as compared to the relay in a two-way relaying system. Indeed, in a one-way relaying system, the relay is active during two slots, transmitting a total of 2034 symbols. In a two-way relaying system, the relay is active during only one slot, transmitting a total of 1536 symbols. This favors the two-way relaying system in applications where low relay energy consumption is required, such as battery-powered sensor networks and on-body relaying networks.

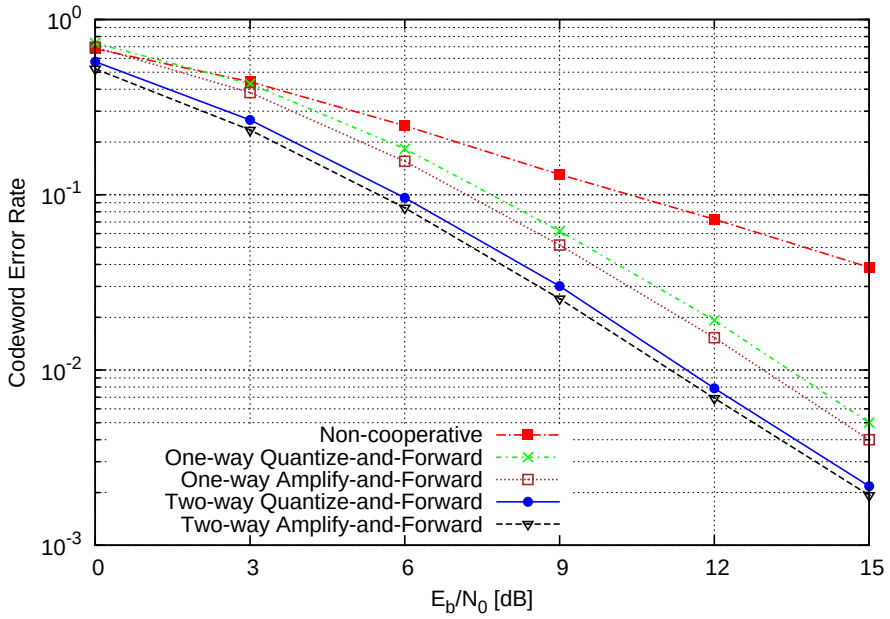

Figure 9.3: WER of a one-way and a two-way QF and AF protocol, along with the WER of a non-cooperative system. The relay position is uniformly distributed on a line connecting T_0 and T_1.

The WER performance of the considered relaying protocols is shown in Fig. 9.3 as a function of the E_b/N_0 ratio. The quantity E_b is used to represent the energy needed to transmit (and relay) 1 information bit from T_0 to T_1. The relay position is varied uniformly on a line connecting T_0 and T_1 (i.e. in each frame a random relay position is selected). The figure shows that the proposed two-way QF system achieves a good WER performance that is only slightly worse than for the two-way AF system. Both two-way systems outperform their one-way counterparts and due to the increased diversity, all the cooperative systems clearly outperform the non-cooperative system.

In Fig. 9.4, the position of the relay is varied on a line connecting T_0 and T_1, while the E_b/N_0 ratio is kept fixed at 9 dB. The resulting WER values are shown as a function of the normalized distance between T_0 and the relay. In order to better understand the WER behavior of the two-way protocols shown in Fig. 9.4, the WER performance of a two-way AF and QF system in which the relay ignores the signal from T_1 is also shown. These configurations will be referred to as non-interfering AF and non-interfering QF, respectively. Because the relay ignores the contribution from T_1, the sole contribution in the

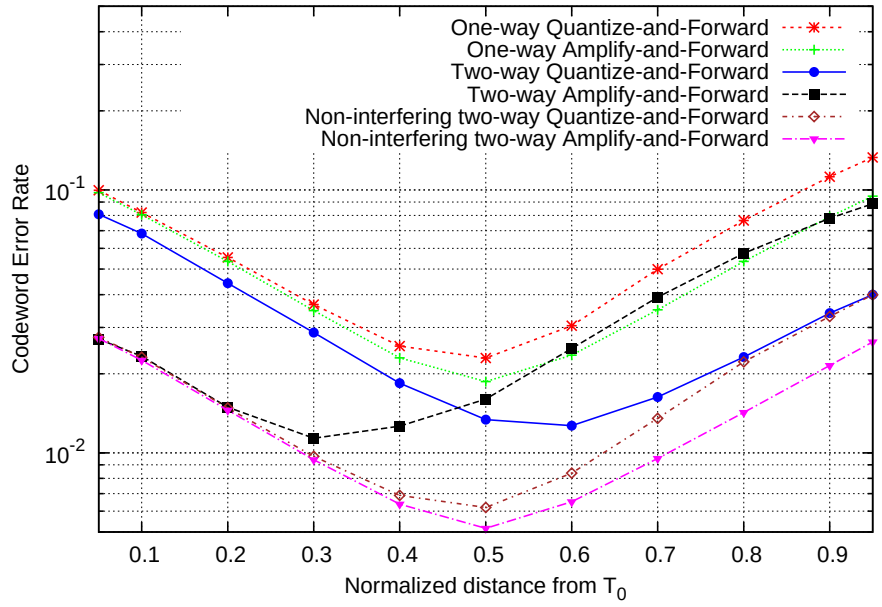

Figure 9.4: WER of a one-way and a two-way QF and AF protocol, along with the WER of a non-interfering two-way QF and AF system as function of the normalized distance between transmitting terminal and relay for a fixed E_b/N_0 ratio of 9dB.

signal transmitted by the relay stems from T_0. In the non-interfering QF (AF) system, the first and third slot support a one-way QF (AF) protocol between T_0 and T_1 in which the relay only assists T_0, while the second slot supports a single-diversity information transfer from T_1 to T_0. The following observations can be made from the aforementioned figure:

• In the one-way AF protocol, the WER curve is symmetrical w.r.t. the relay position. Assuming that $E_0|h_1|^2 \gg N_1$ and taking into account the operation of the AF relay, it can easily be verified that signal received from the relay is characterized by an instantaneous SNR given by

$$\text{SNR} = \left(\frac{N_1}{E_0|h_1|^2} + \frac{N_2}{E_r|h_2|^2} \right)^{-1}. \tag{9.30}$$

Because $N_1/E_0 = N_2/E_r$, as specified in the beginning of this section, (9.30) is symmetrical with respect to $|h_1|^2$ and $|h_2|^2$, implying the symmetry of the WER curve.

• Due to the coarse quantization at the relay, the one-way QF protocol is outperformed by one-way AF. The degradation of the former w.r.t. the latter is negligible when the relay is located close to T_0, but increases when their distance gets larger, because of the decreasing SNR on the h_1 channel.

• In the two-way AF protocol, the relay transmits a scaled version of the sum of the signals received from T_0 and T_1, such that the sum signal has a given energy per symbol interval. As the resulting contribution from T_0 to the transmitted relay symbols is smaller than in the case of non-interfering AF (in which the contribution from T_0 is the sole contribution), two-way AF is outperformed by non-interfering AF. The degradation of the two-way AF system w.r.t. the non-interfering AF system decreases when the relay moves in the direction of T_0, because in the former system the weight of the signal from T_0 to the transmitted relay signal increases. When the relay is very close to T_0, the signal from T_1 has a negligible contribution to the relay symbols, so the WER performance of the two-way AF system approaches that of the non-interfering AF system.

• In the two-way QF protocol, the symbols transmitted by the relay depend on the phases of the noisy signals received from T_0 and T_1, but not on their amplitudes. As the transmitted relay symbols are function of the noise on both the h_1 and h_2' channels, they are less reliable than in the non-interfering QF system; therefore, non-interfering QF outperforms two-way QF. The degradation of the two-way QF system w.r.t. the non-interfering QF system decreases when the relay gets closer to T_1, because of the increasing SNR on the h_2' channel. When the distance between the relay and T_1 is very small, the noise on the h_2' channel can be ignored, yielding the same situation, and thus the same WER performance, as the non-interfering QF system.

The WER plots from Fig. 9.4 show that, depending on the position of the relay with respect to T_0 and T_1, two-way QF clearly outperforms two-way AF and vice versa. When sufficient relay resources are available to support a two-way AF protocol, the results from Fig. 9.4 can be used to determine which protocol is best suited to yield the lowest WER (on average) for the information transfer from T_0 to T_1 for a given relay position. Of course, for the same relay position, the selected protocol may not be optimal for the information transfer from T_1 to T_0, so trade-offs will have to be made. When we have the freedom to select the position of the relay, we achieve maximum fairness (information transfer from T_1 to T_0 and from T_0 to T_1 yield the same WER) when the relay is located halfway between T_0 and T_1; for this relay position, the two-way QF system slightly outperforms the two-way AF system when $E_b/N_0 = 9$ dB.

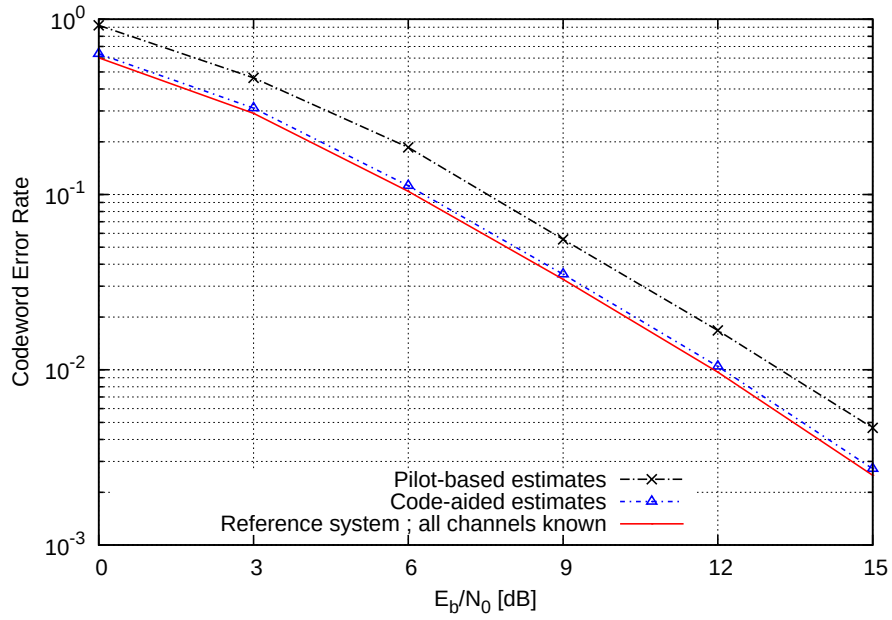

Figure 9.5: WER performance of a two-way QF system with estimated channel parameters. The relay position is uniformly distributed on a line connecting T_0 and T_1.

9.5.3 Channels and Transition Probabilities Estimated

Figure 9.5 shows the WER performance of the proposed QF system in which the relevant channel gains, noise variances and transition probabilities are estimated by the destination terminal. The performance of a system in which only pilot-based estimates are used is plotted, together with that of a system in which the pilot-based estimates are refined using the code-aided EM algorithm. The WER performance of a system in which the channel parameters are considered to be known is also displayed. We observe that pilot-based estimation yields a significant degradation with respect to the reference system in which all channel parameters are assumed to be known. This degradation is however almost completely mitigated using the code-aided approach. These results prove that the proposed two-way relaying QF system is suitable to be used in real-life systems, because efficient estimation of the unknown channel parameters can be achieved.

9.6 Conclusions

In this chapter, an implementation has been proposed for a two-way QF relaying system. The computational complexity at the relay has been kept low, in order to make the proposed algorithm suitable for relaying networks with hardware constraints at the relay, such as sensor networks. After presenting a closed-form expression for the symbol likelihoods at the receivers, the estimation of the unknown channel parameters was discussed. In order to keep the relay complexity low, all parameters are estimated at the destination, requiring no additional operations from the relay. The performance of the proposed algorithms for a relay position that is uniformly distributed between the transmitting and receiving terminal was subsequently evaluated using Monte Carlo simulations. It was shown that the considered two-way QF system clearly outperforms both one-way systems and non-cooperative ones. It was further shown that the WER degradation with respect to a two-way AF system, which has a much higher relay-side complexity, is very low within the full SNR range. In order to gain more insight into the proposed algorithm, the effect of the relay position was also investigated and the results explained. Finally, it was shown that the proposed estimation algorithms yield only a negligible degradation in WER as compared to an (unrealistic) system in which all channel parameters are assumed to be known, making the presented QF protocol and estimation algorithms suitable to be used in real-life cooperative networks that require a low relay-side complexity.

10

Future Work

In the chapter at hand, two interesting topics for future work are investigated. First, in section 10.1, the Cramer-Rao bound is discussed, which is a fundamental lower bound on the MSE of an unbiased estimate. Besides giving a general expression for the CRB, the CRB is calculated for the system from chapter 7, providing more insight in the estimation algorithms from the aforementioned chapter. Secondly, in section 10.2, a QF system for the multiple-access relay channel (MARC) is presented, in which two source terminals transmit information to one destination terminal with the aid of a single relay.

10.1 Cramer-Rao Bounds

In this dissertation, various methods have been presented for estimating the unknown channel parameters for a QF cooperative system. By comparing the WER of a system in which the channel parameters are known to that of a sys-

tem with estimated channel parameters, we have shown that the estimation algorithms obtained perform in a satisfactory manner. Another way to study the quality of an estimate is to compare the MSE of the considered estimate to the CRB. As explained in section 2.1.1.3, the CRB is a lower bound on the MSE that an (unbiased) estimate can achieve. It can therefore be of interest to compare the MSE of the estimates obtained in the previous chapters to their CRBs.

In this section, it is outlined how to obtain the CRBs for a system in which all channels are estimated at the destination and in which there is no carrier frequency offset, such as the systems described in chapters 7 and 9. To make the obtained expressions applicable to a broad spectrum of problems, the only assumption made is that the cascade of the source-relay channel and the operation at the relay can be characterized by a finite set of transition probabilities, as is the case for the systems from chapter 7 and chapter 9. The obtained results can also easily be extended to include a carrier frequency offset, which is a matter of future work. Because the CRB is difficult to evaluate in some cases, the modified Cramer-Rao bound (MCRB), which is a looser but mathematically less complex bound, is also considered. The results presented in this chapter have been published in [91], where the reader is referred to for a more in depth analysis.

This section is organized as follows. In section 10.1.1 the system model is introduced. In section 10.1.2 it is outlined how the CRB is obtained, whereafter the MCRB is derived in section 10.1.3. In section 10.1.4, the CRB and MCRB are calculated using numerical methods for the estimates from the one-way QF system from chapter 7. It is a matter of future work to also apply the expressions from this chapter to the two-way QF system from chapter 9.

10.1.1 System Model

We consider a cooperative network consisting of a source transmitting information to a destination with the help of one relay. The communication over the relay path can either be one-way, as is the case in chapter 7, or two-way, as is the case in chapter 9. In both cases, the cascade of the source-relay channel and the quantization operation can be abstracted to be a discrete-valued channel with M_1 inputs and M_2 outputs, as explained in sections 7.3.4 and 9.4 for a one-way and a two-way QF system, respectively. As also shown in the aforementioned sections, this discrete-valued channel is fully characterized by M_2 transition probabilities, grouped in the vector $\mathbf{\Phi}$, which needs to be estimated at the destination, together with the source-destination and relay-destination channel coefficients, denoted as h_0 and h_2, respectively.

10.1.2 The Cramer-Rao Bound

For obtaining the CRB, the unknown channel parameters are first grouped into the real-valued vector $\boldsymbol{\theta}$, which is given by

$$\boldsymbol{\theta} = (\Re(h_0), \Im(h_0), \boldsymbol{\Phi_t}, \Re(h_2), \Im(h_2)), \tag{10.1}$$

with $\boldsymbol{\Phi_t} = (\Phi(0), \Phi(1), \cdots, \Phi(M_2-2))$. Note that $\Phi(M_2-1)$ is not contained in $\boldsymbol{\theta}$, because it is not an independent parameter ($\Phi(M_2-1) = 1 - \Phi(0) - \ldots - \Phi(M_2-2)$). In order to obtain the CRB, the Fisher information matrix (FIM) $\boldsymbol{J}$ needs to be computed, the elements of which are defined as [92]

$$\boldsymbol{J}(i,j) = \mathbb{E}_{\boldsymbol{r}}\left[\frac{\partial}{\partial\theta(i)} \ln p(\boldsymbol{r}\,;\,\boldsymbol{\theta}) \frac{\partial}{\partial\theta(j)} \ln p(\boldsymbol{r}\,;\,\boldsymbol{\theta})\right], \tag{10.2}$$

with $\boldsymbol{r} = (\boldsymbol{r}_0, \boldsymbol{r}_2)$. The reader is referred to [91] for details concerning the computation of the FIM, where it is shown that order to evaluate (10.2), the a posteriori probabilities $p(c_0(k) \,|\, \boldsymbol{r}\,;\,\boldsymbol{\theta})$ of the source symbols are needed. These depend on the structure of the channel code and are obtained at the destination using a soft decoder that operates on $\boldsymbol{r}$. Note that (10.2) depends on the specific realization of $\boldsymbol{\theta}$. In order to obtain a LB that is independent of $\boldsymbol{\theta}$, the obtained expressions need to be averaged over $\boldsymbol{\theta}$.

Once the elements of the FIM have been computed, it can be shown [91] that the MSE related to the estimation of h_0 satisfies

$$\mathbb{E}_{\boldsymbol{r}}\left[|h_0 - \hat{h_0}|^2\right] \geq \left(\boldsymbol{u}\boldsymbol{J}^{-1}\boldsymbol{u}^H\right) = \mathrm{CRB}_{h_0}, \tag{10.3}$$

with $\boldsymbol{u} = (1, j, \boldsymbol{0}_{M_2+1})$ and $\boldsymbol{0}_{M_2+1}$ being a row vector of M_2+1 elements which are all equal to 0. Similarly, a LB on the MSE arising from the estimation of h_2 is found to be equal to:

$$\mathbb{E}_{\boldsymbol{r}}\left[|h_2 - \hat{h_2}|^2\right] \geq \left(\boldsymbol{w}\boldsymbol{J}^{-1}\boldsymbol{w}^H\right) = \mathrm{CRB}_{h_2}, \tag{10.4}$$

with $\boldsymbol{w} = (\boldsymbol{0}_{M_2+1}, 1, j)$. Considering that $\Phi(q) = \theta(q+2), \forall q \in \{0, 1, ..., M_2 - 2\}$ and that $\Phi(M_2-1) = 1 - \theta(2) - \theta(3) - ... - \theta(M_2)$, the CRB on the MSE arising from the estimation of $\boldsymbol{\Phi}$ is given by

$$\mathbb{E}_{\boldsymbol{r}}\left[(\boldsymbol{\Phi} - \hat{\boldsymbol{\Phi}})(\boldsymbol{\Phi} - \hat{\boldsymbol{\Phi}})^H\right] \geq \mathrm{Tr}\left(\boldsymbol{V}\boldsymbol{J}^{-1}\boldsymbol{V}^H\right) = \mathrm{CRB}_{\boldsymbol{\Phi}}, \tag{10.5}$$

with

$$\boldsymbol{V} = \begin{bmatrix} 0 & 0 & & & 0 & 0 \\ 0 & 0 & \mathbf{I}_{M_2-1} & & 0 & 0 \\ 0 & 0 & -1 & -1 & 0 & 0 \end{bmatrix}, \tag{10.6}$$

and $\mathbf{I}_{M_2-1}$ representing the identity matrix of size $M_2 - 1$.

10.1.3 The Modified Cramer-Rao Bound

As explained in the previous subsection, the calculation of the elements of the FIM involves the computation of the a posteriori probabilities of the source symbols, making it difficult to obtain a closed form expression for the CRB. Therefore, when using non-trivial channel codes, the CRB needs to be obtained using numerical simulation methods that are quite time-consuming. In order to avoid the computational complexity associated with the CRB, we also consider the modified CRB (MCRB) [93–95], which does not need the a posteriori probabilities of the source symbols (the MCRB assumes the source symbols are known by the receiver). The MCRB is a looser bound compared to the CRB; the CRB approaches the MCRB at high signal to noise ratios, where $p(c_0(k) \mid \boldsymbol{r}, \boldsymbol{\theta}) \approx 1$ for $c_0(k)$ equal to the symbol actually transmitted. Due to the less complex mathematics of the MCRB, simulation times are greatly reduced and in some cases closed-formed expressions can be found, as explained in [91]. The MCRB is obtained by substituting in (10.3), (10.4) and (10.5) the inverse of the FIM with the inverse of the modified Fisher information matrix (MFIM), the elements of which are defined as

$$\boldsymbol{J}_M(i,j) = \mathbb{E}_{\boldsymbol{c}_0}\left[\mathbb{E}_{\boldsymbol{r}\,|\,\boldsymbol{c}_0}\left[\frac{\partial}{\partial\theta(i)}\ln p(\boldsymbol{r}\mid \boldsymbol{c}_0\,;\,\boldsymbol{\theta})\frac{\partial}{\partial\theta(j)}\ln p(\boldsymbol{r}\mid \boldsymbol{c}_0\,;\,\boldsymbol{\theta})\right]\right]. \tag{10.7}$$

It follows from the circular symmetry expressed in (7.56) that

$$p(r(k)\mid c_0(k) = \chi_{M_1}(m)\,;\,\boldsymbol{\theta})\Big|_{r(k)=y} = p(r(k)\mid c_0(k) = \chi_{M_1}(0)\,;\,\boldsymbol{\theta})\Big|_{r(k)=y\chi^*_{M_1}(m)}, \tag{10.8}$$

so that in (10.7) the conditional expectation $\mathbb{E}_{\boldsymbol{r}\,|\,\boldsymbol{c}_0}[.]$ does not depend on the particular realization of $\boldsymbol{c}_0$. Hence, the outer expectation in (10.7) can be omitted, yielding

$$\boldsymbol{J}_M(i,j) = \mathbb{E}_{\boldsymbol{r}\,|\,\boldsymbol{c}_0}\left[\frac{\partial}{\partial\theta(i)}\ln p(\boldsymbol{r}\mid \boldsymbol{c}_0\,;\,\boldsymbol{\theta})\frac{\partial}{\partial\theta(j)}\ln p(\boldsymbol{r}\mid \boldsymbol{c}_0\,;\,\boldsymbol{\theta})\right]. \tag{10.9}$$

As shown in [91], $\boldsymbol{J}_M$ is a block-diagonal matrix equal to

$$\boldsymbol{J}_M = \begin{bmatrix} \boldsymbol{J}_{M,SD} & 0 \\ 0 & \boldsymbol{J}_{M,SRD} \end{bmatrix}, \tag{10.10}$$

where $\boldsymbol{J}_{M,SD}$ and $\boldsymbol{J}_{M,SRD}$ are the MFIMs related to the estimation of the source-destination channel parameters and the source-relay-destination channel parameters, respectively. Because of the block-diagonal nature of $\boldsymbol{J}_M$, the source-destination channel parameters are decoupled from the source-relay-destination channel parameters: the MCRB corresponding to the source-destination (the source-relay-destination) channel parameters does not depend on whether or not the parameters of the source-relay-destination (the source-destination) channel are known.

10.1.4 Numerical Results

In this section, the value of the CRB and MCRB is obtained for the channel parameters from the one-way QF system described in chapter 7. The reader is referred to the aforementioned chapter for a detailed description of the different communication channels and parameters involved.

10.1.4.1 System Parameters

The instantaneous SNRs on the source-destination, source-relay and relay-destination channels are equal to $\gamma_0 = E_0|h_0|^2/N_0$, $\gamma_1 = E_0|h_1|^2/N_1$ and $\gamma_2 = E_r|h_2|^2/N_2$, respectively; the corresponding average SNRs are $N_{h_0}E_0/N_0$, $N_{h_1}E_0/N_1$ and $N_{h_2}E_r/N_2$, respectively. The source, relay and destination terminals are located at the vertices of an equilateral triangle with normalized edge length, i.e., $d_0 = d_1 = d_2 = 1$, yielding $\mathbb{E}[|h_n|^2] = 1$ for $n = 0, 1, 2$. All noise variances are taken equal (i.e., $N_0 = N_1 = N_2$) and the source and relay symbols are assumed to have the same energy (i.e., $E_0 = E_r$). The source broadcasts BPSK symbols (i.e., $M_1 = 2$), which are quantized at the relay to QPSK symbols (i.e., $M_2 = 4$). For the calculation of the CRB, channel encoding is performed using a $(1, 13/15)_8$ RSCC turbo code that is punctured to a rate of $2/3$. A frame contains 1024 information bits, which corresponds to 1536 data symbols after channel encoding and BPSK mapping. In addition to these BPSK data symbols, 12 pilot symbols are added to each frame, to help the destination to obtain estimates for the various channel parameters; this yields a total frame size of $K = 1548$ BPSK symbols.

The CRB for a given realization of $\boldsymbol{\theta}$ is obtained by performing the averaging in (10.2) by means of a Monte Carlo [96] simulation involving $N = 5000$ independent realizations of $\boldsymbol{r}$; this corresponds to the generation of $2K \cdot N \approx 1.5 \cdot 10^7$ scalar observations. Subsequently, 10^4 realizations of $\boldsymbol{\theta}$ are used to average the CRB over $\boldsymbol{\theta}$. The calculation of the MCRB for a given realization of $\boldsymbol{\theta}$ is performed using Monte Carlo simulation with importance sampling (IS), as explained in [91, 97]. In doing so, only 5000 scalar observations need to be generated in order to compute the conditional average over r_2. When compared to the $1.5 \cdot 10^7$ iterations required for the CRB where no IS is used, IS reduces the simulation time by a factor of 3000. After averaging over r_2, 10^4 realizations of $\boldsymbol{\theta}$ are used to average the MCRB over $\boldsymbol{\theta}$. In order to evaluate the tightness of the obtained LBs, we also provide MSE results from the estimation algorithm from chapter 7, where pilot-based estimates of the various channel parameters are refined using the Expectation-Maximization (EM) algorithm.

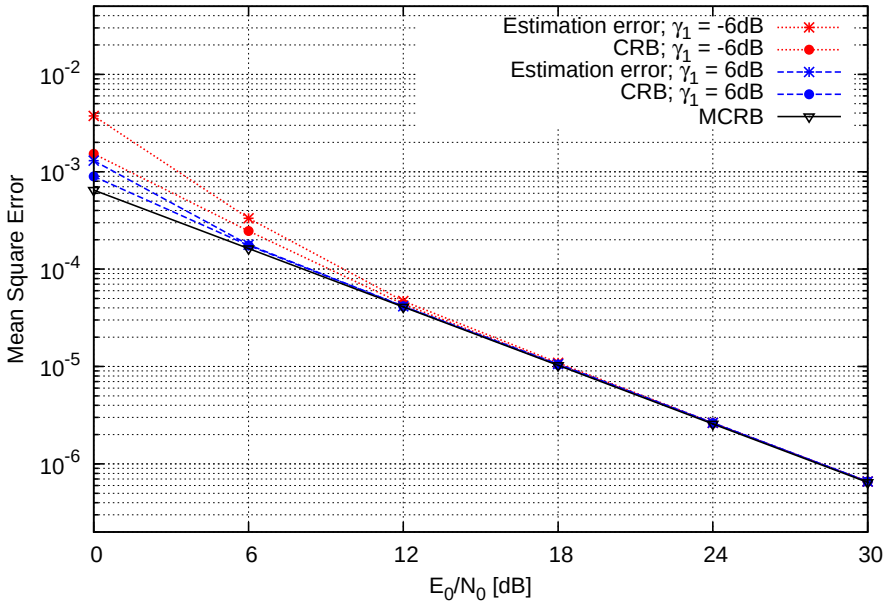

Figure 10.1: MSE of $\hat{h_0}$ as a function of the E_0/N_0 ratio for various values of γ_1.

10.1.4.2 Estimation of the Source-Destination Channel

The MSE of the source-destination channel coefficient is analyzed as a function of E_0/N_0, while keeping the instantaneous SNR on the source-relay channel, represented by γ_1, fixed. We set E_r/N_2 equal to E_0/N_0. Fig. 10.1 shows the MSE resulting from the EM algorithm, the CRB and the MCRB related to the estimation of h_0 for various values of γ_1. The MCRB is independent of γ_1, as was pointed out in section 10.1.3. However, the CRB is affected by the value of γ_1, because γ_1 determines the transition probabilities $\mathbf{\Phi}$, which in turn impact the a posteriori source symbol probabilities that are used in the computation of the CRB. As the figure shows, the state of the source-relay channel, represented by γ_1, has only little impact on the MSE of the source-destination channel coefficient. As expected, this effect further diminishes at high SNR ratios, where the CRB approaches the MCRB.

10.1.4.3 Estimation of the Source-Relay Channel

We consider the bounds on the MSE of the equivalent source-relay channel transition probabilities $\mathbf{\Phi}$, as a function of E_0/N_1, with the source-destination channel being characterized by $E_0/N_0 = E_0/N_1$. We take fixed values for

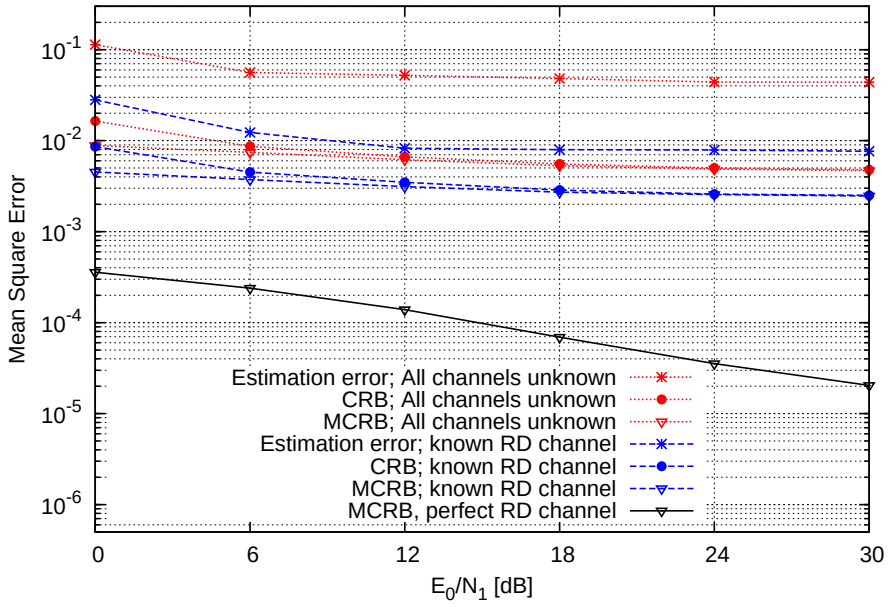

Figure 10.2: MSE of $\hat{\mathbf{\Phi}}$ as a function of the E_0/N_1 ratio for $\gamma_2 = -6\,\text{dB}$.

γ_2, the instantaneous SNR of the relay-destination channel. Figure 10.2, 10.3 and 10.4 show the CRB, the MCRB and the MSE resulting from the EM algorithm, for various γ_2. In order to evaluate the impact of an imperfect relay-destination channel estimate $\hat{h_2}$ on the estimation performance of the source-relay channel transition probabilities $\mathbf{\Phi}$, the aforementioned figures also show the results corresponding to the estimation of $\mathbf{\Phi}$ when h_2 is known to the destination. As a LB on the obtained results, the MCRB corresponding to the case of a perfect relay-destination channel is also plotted (in which case the destination is assumed to directly observe the relay output).

Several key observations can be made from the aforementioned figures. At high γ_2 values, shown in Fig. 10.4, the CRB converges to the MCRB for moderate and high E_0/N_1 when all channels are unknown and, at high E_0/N_1, both the CRB and MCRB converge to the MCRB corresponding to a perfect relay-destination channel. Assuming the relay-destination channel is known to the destination when estimating the source-relay channel yields only a slight decrease in MSE. Fig. 10.4 also shows that at high γ_2 values, the CRB is a tight LB on the MSE of the actual estimation algorithm.

For lower γ_2 (see Figs. 10.2 and 10.3), the CRB still approaches the MCRB

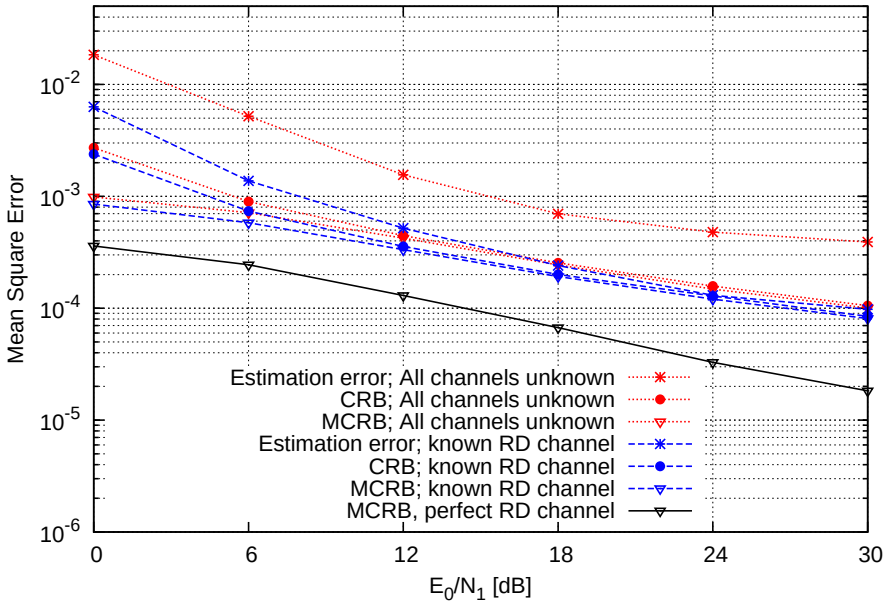

Figure 10.3: MSE of $\hat{\mathbf{\Phi}}$ as a function of the E_0/N_1 ratio for $\gamma_2 = 0\,\text{dB}$.

at high E_0/N_1 when all channels are unknown, but there remains a substantial (especially at very low γ_2 values) gap in MSE as compared to the case where the relay-destination channel is known to the destination; a still larger gap occurs as compared to the case of a perfect relay-destination channel. The former gap is caused by the poor accuracy of $\hat{h_2}$ at low γ_2, which in turn deteriorates the estimate of $\mathbf{\Phi}$, even at large E_0/N_1; this indicates a considerable coupling between the estimates $\hat{h_2}$ and $\hat{\mathbf{\Phi}}$. The difference in MSE between the cases of known relay-destination channel and perfect relay-destination channel is caused by the noise on the relay-destination channel, and therefore increases with decreasing γ_2.

Next, we observe a MSE floor that occurs at high E_0/N_1 when γ_2 is low. This phenomenon is explained by calculating the MCRB corresponding to the estimation of the source-relay channel transition probabilities at the high SNR limit, yielding Fig. 10.5, in which the high E_0/N_1 limit of the MCRB related to estimating $\mathbf{\Phi}$ is plotted as a function of γ_2. As the figure shows, the value of the MSE floor observed on Fig. 10.2 and Fig. 10.3 is determined by the instantaneous relay-destination channel quality γ_2. The figure also shows that this MSE floor drops very steeply when $\gamma_2 > 0\,\text{dB}$, explaining the apparent absence of an MSE floor on Fig. 10.4.

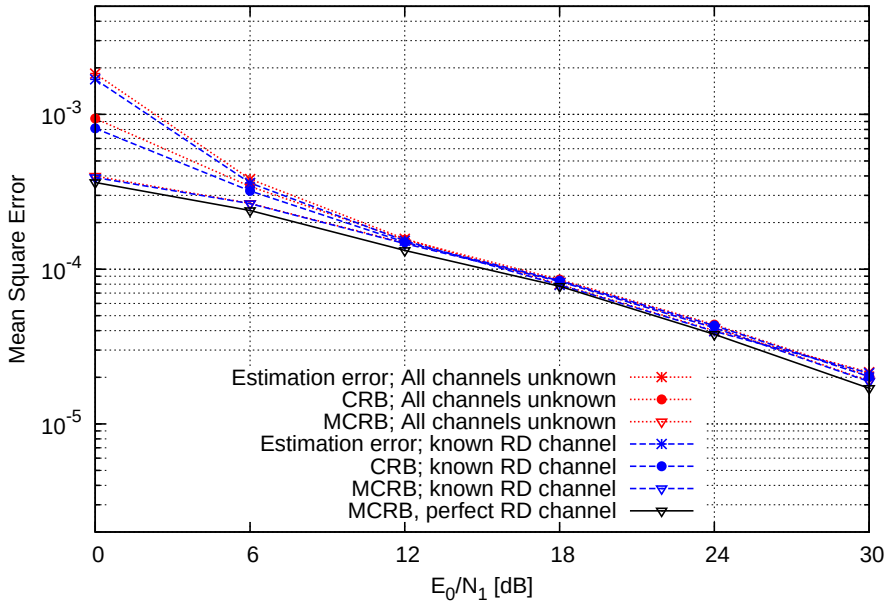

Figure 10.4: MSE of $\hat{\mathbf{\Phi}}$ as a function of the E_0/N_1 ratio for $\gamma_2 = 6$ dB.

Fig. 10.2-10.4 indicate that the MSE resulting from the EM algorithm does not approach the CRB at low values of γ_2. This is due to the fact that the estimation scheme described in chapter 7 fails to obtain accurate estimates for the source-relay transition probabilities at low γ_2, accounting for the gap between the MSE of the EM algorithm and the (M)CRB. It should be noted that the inability to accurately estimate the source-relay transition probabilities at low γ_2 has only a minor effect on the error performance of the decoder at the destination, as observed in section 7.4.3.1 from chapter 7. Indeed, at low γ_2, the decoder basically ignores the signal $\boldsymbol{r}_2$ received from the relay, and exploits only the source-destination signal $\boldsymbol{r}_0$; in this case, the error performance of the decoder is essentially independent of the quality of the source-relay channel estimate.

10.1.4.4 Estimation of the Relay-Destination Channel

The MSE resulting from the estimation of the relay-destination channel coefficient is shown in Figs. 10.6 - 10.8 as a function of E_r/N_2. We take $E_0/N_0 = E_r/N_2$, while keeping a fixed value for γ_1, the instantaneous SNR on the source-relay channel. As a reference, the figures also show the results for a

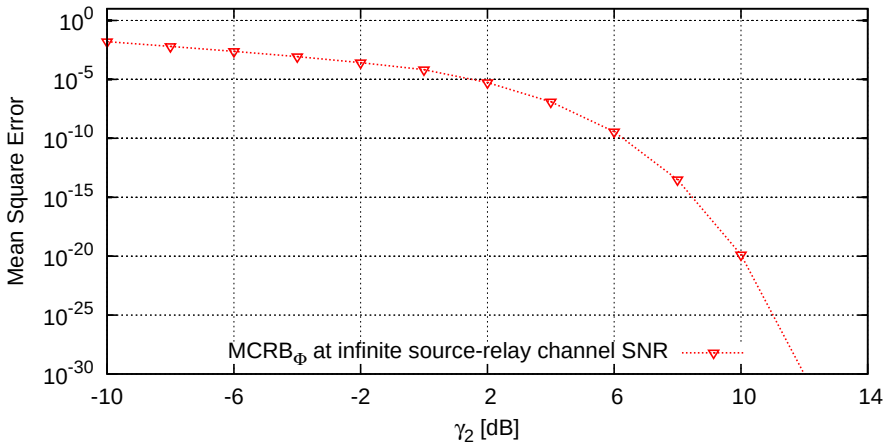

Figure 10.5: MCRB$_{\mathbf{\Phi}}$ at infinite source-relay channel SNR as function of the instantaneous relay-destination channel SNR.

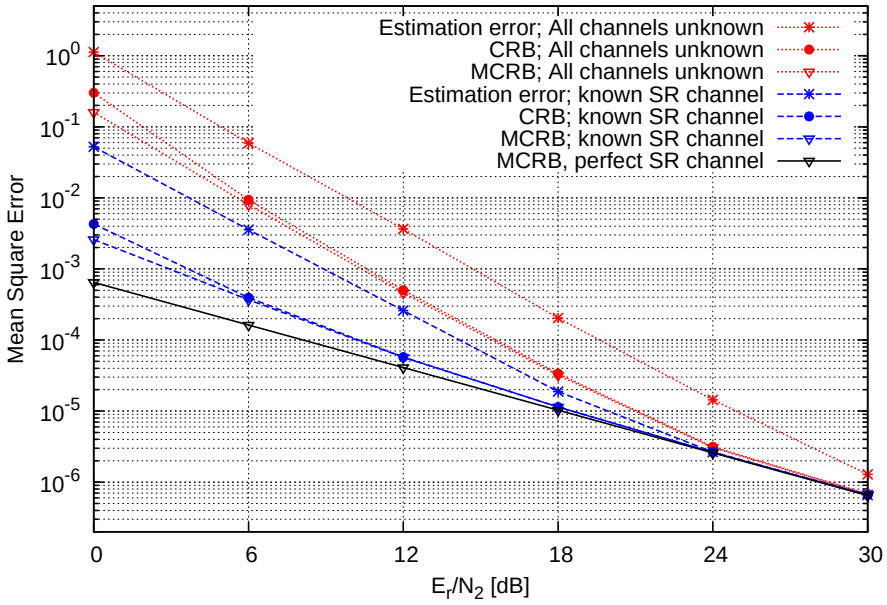

Figure 10.6: MSE of $\hat{h_2}$ as a function of the E_r/N_2 ratio for $\gamma_1 = -6\,\text{dB}$.

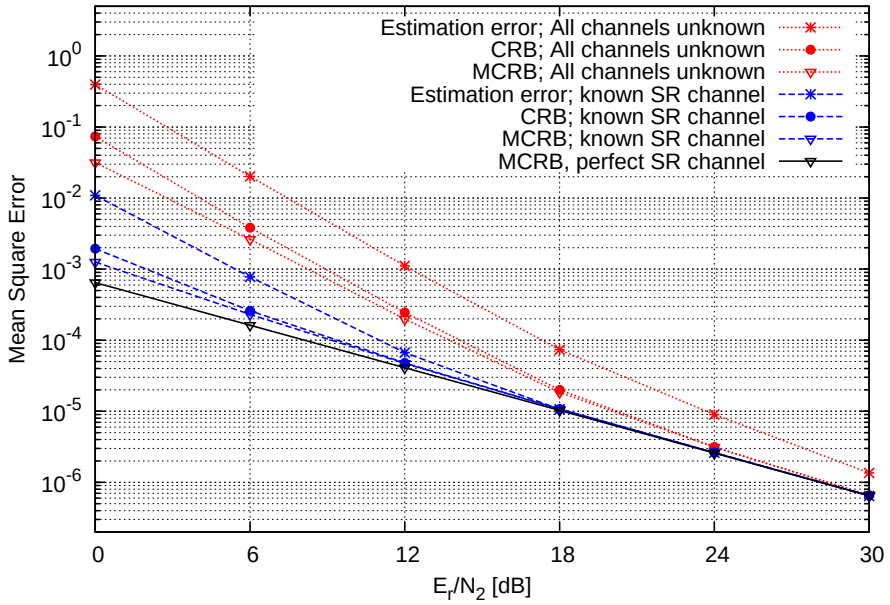

Figure 10.7: MSE of $\hat{h_2}$ as a function of the E_r/N_2 ratio for $\gamma_1 = 0\,\text{dB}$.

known source-relay channel (i.e., $\hat{\mathbf{\Phi}} = \mathbf{\Phi}$) and for a perfect source-relay channel (in which case the relay symbols are deterministically determined by the source symbols).

As the aforementioned figures show, the CRB converges to the MCRB at high E_r/N_2, and this irrespective of γ_1. Unlike the LBs associated with the estimation of the source-relay channel transition probabilities, the CRB and MCRB of the relay-destination channel coefficient do not exhibit an MSE floor and, for any γ_1, both converge to the (M)CRB corresponding to a known source-relay channel ($\hat{\mathbf{\Phi}} = \mathbf{\Phi}$), and also to the MCRB corresponding to a perfect source-relay channel. Hence, seen from an estimation point of view, it is advantageous to place the relay terminal close to the destination, as this enables the latter to obtain a good estimate of both the source-relay channel (due to a high average γ_2 value) and the relay-destination channel (due to the robustness of the estimate of h_2 with respect to low γ_1 values).

Comparison of the results obtained in this subsection to the bounds obtained for the source-destination channel from section 10.1.4.2 indicates that due to the presence of the source-relay link, the relay-destination channel is more difficult to accurately estimate. This effect diminishes as the source-relay channel quality is increased and especially if the source-relay channel is as-

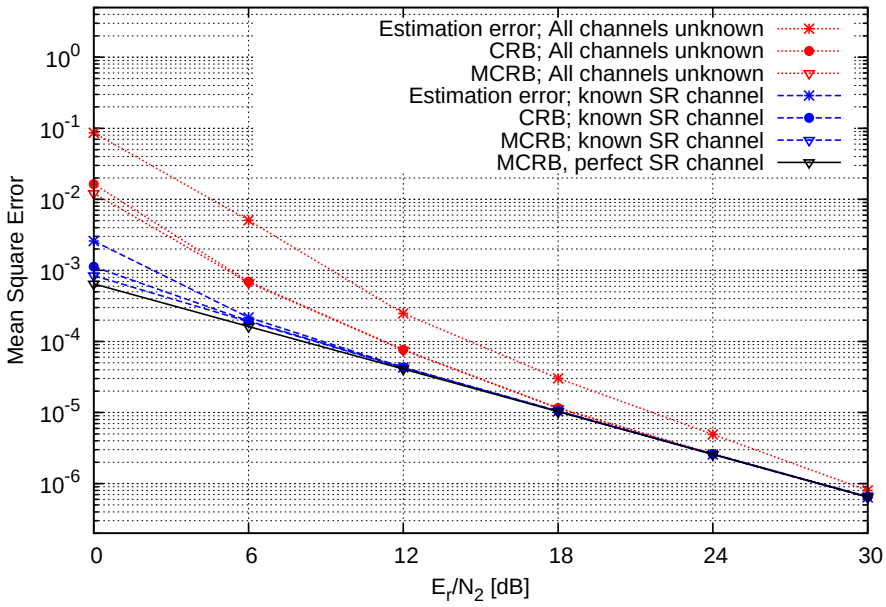

Figure 10.8: MSE of $\hat{h_2}$ as a function of the E_r/N_2 ratio for $\gamma_1 = 6$ dB.

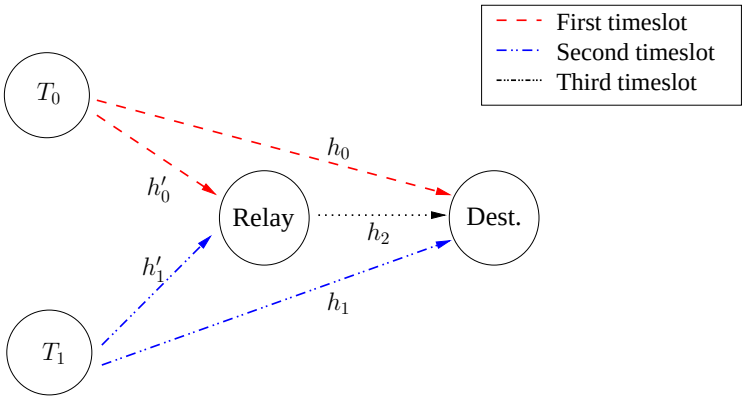

Figure 10.9: Timeslot assignment.

sumed to be known. In the case of a perfect source-relay channel, the MCRB related to the estimation of the relay-destination channel corresponds to that of the source-destination channel, as is to be expected.

10.2 Multiple Access Relay Channel

In the multiple access relay channel (MARC), two terminals, denoted T_0 and T_1, communicate to a single destination, denoted D. A single relay, denoted R assists both terminals simultaneously, as shown in the timing diagram in Fig. 10.9. In the first and second timeslot, T_0 and T_1, respectively, transmit their information, which is received by both the relay and the destination. The relay processes the information received from the two sources and transmits the result to the destination in the third timeslot. At the destination, the signal received from the relay is combined with the signals received from T_0 and T_1, in order to retrieve the information bits sent by T_0 and T_1. The outline of this section is as follows: In section 10.2.1, the system model is introduced, whereafter the decoding process at the destination is discussed in section 10.2.2. The different operations that the relay can perform on the received information are outlined in section 10.2.3. Finally, numerical results are presented in section 10.2.4.

10.2.1 System Model

The symbols transmitted by T_0, T_1 and the relay are denoted by the vectors $\boldsymbol{c}_0$, $\boldsymbol{c}_1$ and $\boldsymbol{c}_r$, respectively. It is assumed that T_0 and T_1 transmit BPSK symbols. It is a matter of future work to extend this to higher constellations. The

communication channels are modelled as flat Rayleigh fading channels with additive white Gaussian noise and without a carrier frequency mismatch. The complex-valued channel gains between T_0 and D and between T_1 and D are denoted by h_0 and h_1, respectively, while the channel gains between T_0 and R and between T_1 and R are denoted by h'_0 and h'_1, respectively. The channel gain between R and D is denoted by h_2. The signals received at D from T_0, T_1 and R are denoted by the vectors $\boldsymbol{r}_0$, $\boldsymbol{r}_1$ and $\boldsymbol{r}_2$, respectively, while the signals received at R from T_0 and T_1 are denoted by $\boldsymbol{r}'_0$ and $\boldsymbol{r}'_1$, respectively. Considering the channel model, these received signals can be written as:

$$\boldsymbol{r}_0 = \sqrt{E_0} h_0 \boldsymbol{c}_0 + \boldsymbol{n}_0 \tag{10.11}$$

$$\boldsymbol{r}'_0 = \sqrt{E_0} h'_0 \boldsymbol{c}_0 + \boldsymbol{n}'_0 \tag{10.12}$$

$$\boldsymbol{r}_1 = \sqrt{E_1} h_1 \boldsymbol{c}_1 + \boldsymbol{n}_1 \tag{10.13}$$

$$\boldsymbol{r}'_1 = \sqrt{E_1} h'_1 \boldsymbol{c}_1 + \boldsymbol{n}'_1 \tag{10.14}$$

$$\boldsymbol{r}_2 = \sqrt{E_r} h_2 \boldsymbol{c}_r + \boldsymbol{n}_2. \tag{10.15}$$

Assuming the normalization condition $|\boldsymbol{c}_0|^2 = |\boldsymbol{c}_1|^2 = |\boldsymbol{c}_r|^2 = K$, the quantities E_0, E_1 and E_r denote the transmitted energy per symbol at T_0, T_1 and R, respectively. All channel coefficients are considered to be constant during a frame and have a zero mean circular symmetric complex Gaussian (ZMCSCG) distribution with variances $N_{h_x} = 1/{d_x}^{n_{loss}}$, $N_{h'_x} = 1/{d'_x}^{n_{loss}}$ and $N_{h_2} = 1/{d_2}^{n_{loss}}$, with $x \in \{0,1\}$. The quantities d_x and d'_x represent the distance between the two considered terminals, while n_{loss} denotes the path loss exponent. The components of the noise vectors $\boldsymbol{n}_x$, $\boldsymbol{n}'_x$ and $\boldsymbol{n}_2$ are also ZMCSCG distributed with variances N_x, N'_x and N_2 respectively, with $x \in \{0,1\}$.

10.2.2 Detection

At the destination, the observations from T_0, T_1 and R, represented by $\boldsymbol{r}_0$, $\boldsymbol{r}_1$ and $\boldsymbol{r}_2$, respectively, need to be combined in order to retrieve the information bits sent by T_0 and T_1. An elegant solution to this problem is obtained by representing the structure of the destination terminal using a factor graph, as shown in Fig. 10.10. Before proceding with reading this section, a reader who is unfamiliar with factor graphs is strongly encouraged to consult the works from [17–19], in order to familiarize himself/herself with factor graphs and the sum-product algorithm. The decoding proceeds using the sum-product algorithm as follows, with the messages being represented by log-likelihood ratios (LLRs) :

• In a first step, the messages from the lower code block to the lower equality node are assumed to have an uniform distribution, so that the LLRs from the equality node to the $\boldsymbol{c}_1^{(3)}$-branch are computed using only the observation

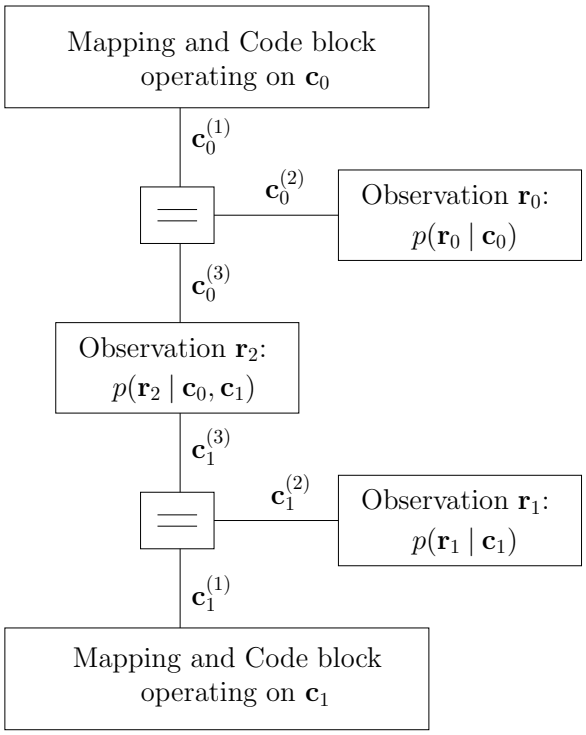

Figure 10.10: Factor graph representation of the operations at the destination terminal.

r_1 .

• Using the messages from the $c_1^{(3)}$-branch and the observation r_2, the messages to the $c_0^{(3)}$-branch are computed.

• At the upper equality node, the messages from the $c_0^{(3)}$-branch are combined with those from the node corresponding to the observation r_0, yielding the messages on the $c_0^{(1)}$-branch to the upper code block.

• In order to obtain the messages from the upper code block to the $c_0^{(1)}$-branch, the message passing algorithm is applied within the upper code block. This corresponds to performing one decoding iteration, in case of a iteratively decoded channel code, or performing a full decoding, in case of a non-iteratively decoded channel code.

• The algorithm propagates downwards in a similar way, until the lower

code block is reached. After applying the message passing algorithm to the lower code block, the messages from the latter to the $c_1^{(1)}$-branch are updated and the whole process repeats. The algorithm is ended after a fixed number of iterations, whereafter the information bits transmitted by T_0 and T_1 can be retrieved from the upper and lower code blocks.

10.2.3 Relay Operations

Three different quantization schemes are proposed for the relay, which are discussed separately below. Afterwards, their WER performance is analyzed using numerical simulations in section 10.2.4.

10.2.3.1 QF; Modulo-4 Addition

The first relaying operation is strongly based on the two-way relaying QF system described in section 9.3.2: the signals from T_0 and T_1 are quantized separately using 2 bits, as described in section 9.3.2.1, whereafter the quantization intervals are added modulo-4, as described in section 9.3.2.2. The resulting sum determines the symbol sent by the relay, which belongs to a QPSK constellation.

10.2.3.2 QF; 16-QAM Gray

In the second relaying operation, the signals received from T_0 and T_1 are again quantized separately using 2 bits. The quantized version of the signal $\boldsymbol{r}_0'$ and $\boldsymbol{r}_1'$ is denoted by the vector $\boldsymbol{q}_0$ and $\boldsymbol{q}_1$, respectively, of which the k-th element is equal to

$$q_0(k) = f_q(r_0'(k)) \tag{10.16}$$

$$q_1(k) = f_q(r_1'(k)), \tag{10.17}$$

with the function $f_Q(x) \in \{0, 1, 2, 3\}$ defined in (5.3). For each symbol index k, the resulting $(q_0(k), q_1(k))$-pair is subsequently mapped on a 16-QAM symbol, as shown on the left side of Fig. 10.11. Note that the proposed mapping method closely resembles a Gray code: adjacent constellation points in the 16-QAM constellation correspond to $(q_0(k), q_1(k))$-pairs that differ as little as possible from each other.

10.2.3.3 QF; 16-QAM Anti-Gray

This relaying operation closely resembles the one described in the previous subsection. The signals from T_0 and T_1 are quantized separately, and the resulting $(q_0(k), q_1(k))$-pairs are again mapped on 16-QAM symbols. As opposed to the system described in section 10.2.3.2, where adjacent constellation

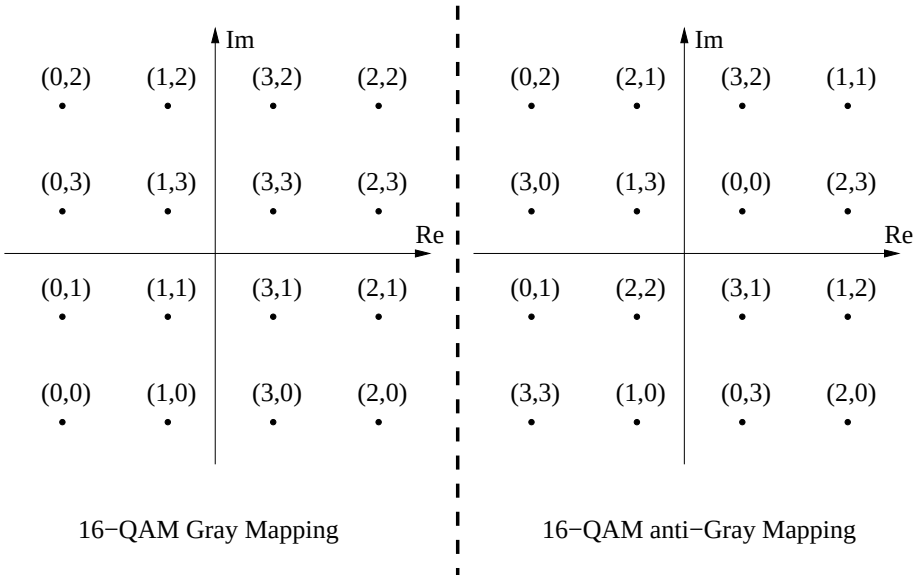

Figure 10.11: Relay mapping methods: 16-QAM Gray and 16-QAM anti-Gray.

points correspond to $(q_0(k), q_1(k))$-pairs that differ as little as possible from each other, in the system at hand it is strived to maximize the distance between similar $(q_0(k), q_1(k))$-pairs, yielding the mapping strategy shown on the right side of Fig. 10.11.

10.2.4 Numerical Results

In this section, the WER performance of the previously discussed relaying strategies is analyzed using Monte-Carlo simulations.

10.2.4.1 Simulation Parameters

Both T_0 and T_1 transmit frames of 1024 information bits, which are encoded by means of an $(1, 13/15)_8$ RSCC turbo code that is punctured to a rate of $2/3$, yielding a total of 1536 coded bits which are then mapped on BPSK symbols. The path loss exponent equals 4 and the terminals are distributed in a plane as shown in Fig. 10.12. The distances between T_0 and R, between T_1 and R and between R and D are assumed to be equal to 0.5, making the distances between T_0 and D and between T_1 and D equal to $\frac{\sqrt{2+\sqrt{2}}}{2} \approx 0.9238$. All symbol energies are considered to be equal ($E_0 = E_1 = E_r$) and all noise variances are also assumed to be equal ($N_0 = N_0' = N_1 = N_1' = N_2$). The results in this section will only consider the information transfer from T_0 to

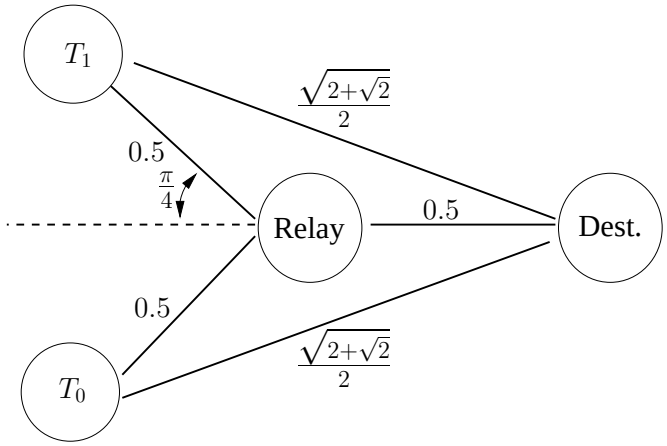

Figure 10.12: Spatial distribution of the various terminals.

D. Similar results are obtained for the information transfer from T_1 to D, owing to the interchangeability of T_0 and T_1.

10.2.4.2 WER Performance

The WER performance of the different relaying strategies is shown as a function of the E_b/N_0 ratio in Fig. 10.13. The quantity E_b is defined similarly as in chapter 9 and denotes the energy needed to transmit (and relay) one bit of information from T_0 to D. In the non-cooperative system, only two timeslots are used and the number of parity bits is increased as described in section 9.5.1. The following observations can be made by studying Fig. 10.13:

• Due to the increased diversity, all cooperative systems outperform the non-cooperative one.

• The 16-QAM systems outperform the modulo-4 addition system. This is due to the fact that, in the 16-QAM systems, the observation from the relay remains useful, even when either the T_0-R or T_1-R channel is in deep fading. Take for example the 16-QAM Gray mapping strategy, and assume that the channel between T_1 and R is in a deep fading state. As a result of the latter, all $q_1(k)$ values are equally probable, because the quantization interval in which the k-th symbol coming from T_1 is quantized, is mainly determined by noise. Even so, the destination can use the real part of the signal transmitted by the relay to retrieve the value of $q_0(k)$. This is not the case in the modulo-4 addition system, where a deep fading state on one of the source-relay channels renders the relay observation useless.

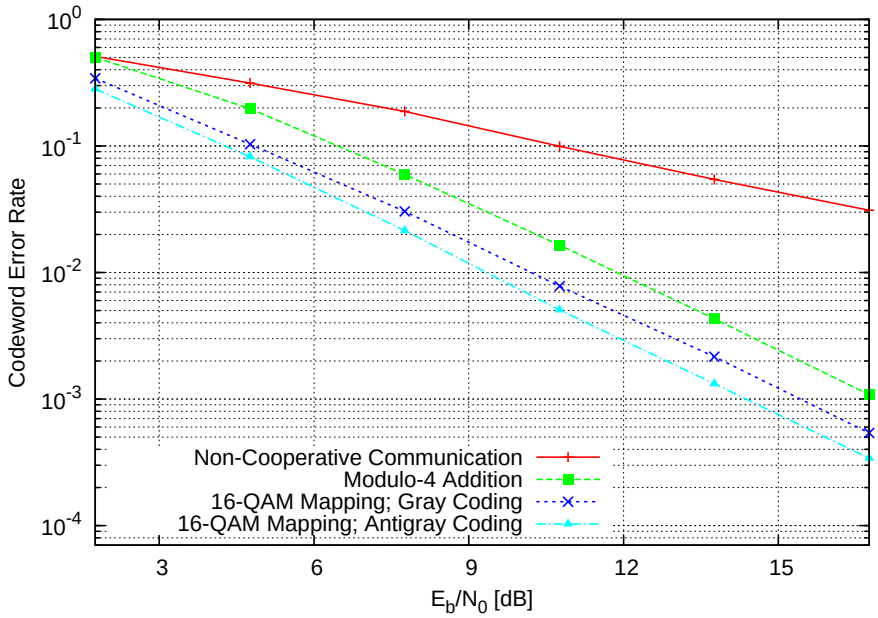

Figure 10.13: WER performance of the various relaying strategies as a function of the E_b/N_0 ratio.

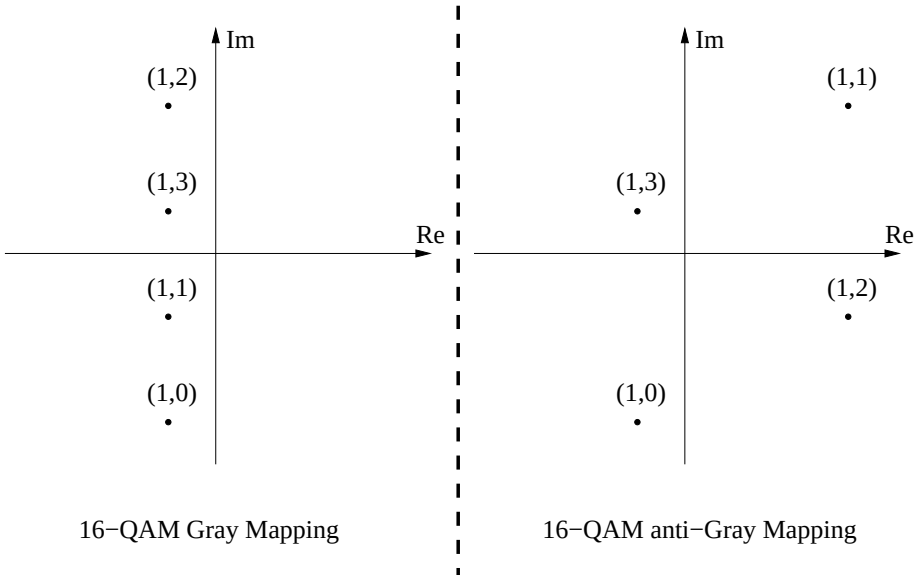

Figure 10.14: 16-QAM Gray and 16-QAM anti-Gray constellations, given that $q_0(k) = 1$.

• The anti-Gray mapping system outperforms the Gray mapping system. This can be explained by considering the situation where the destination is sure about the symbols transmitted by T_0, but not on those transmitted by T_1, or vice-versa. Assume for example that the destination knows the symbol $c_0(k)$, and that it knows that the latter was quantized in the second quantization interval, so that $q_0(k) = 1$. Eliminating from Fig. 10.11 all constellation points which seem improbable to the destination yields Fig. 10.14. Note that in the anti-Gray constellation, the remaining constellation points are spaced further apart as compared to the Gray constellation, so that the destination will better be able to discriminate the symbol transmitted by the relay, and thus determine the value of $q_1(k)$.

10.2.5 Conclusions

In this section, we have presented a MARC system using QF cooperative communication. Three different quantization schemes were proposed, and their performance was analyzed using numerical simulations. While the latter show promising results, work still needs to be done to investigate the deployment feasibility of the proposed protocols in real-life systems. This includes the development of estimation algorithms for all channel parameters

involved, as well as investigating how the proposed quantization schemes can be scaled if higher mapping constellations are used at T_0 and T_1.

11 Conclusions

In this thesis, we investigated various methods for estimating the channel parameters in a quantize and forward (QF) cooperative system. By browsing through the available literature on cooperative systems, a QF protocol having a low relay-side complexity was selected as a starting point for this work. In a first phase, this protocol was slightly modified to allow the relay to calculate an estimate of the source-relay channel, and compensate for the effects of the aforementioned channel at the relay terminal itself. In doing so, the destination no longer needs to know the source-relay channel, making the estimation of the latter less complex. Numerical results have shown that the estimation algorithms designed for this system perform adequately, having only a small performance loss as compared to a system in which the channel parameters are assumed to be known.

A major drawback of estimating the source-relay channel at the relay are the increased number of operations that the latter needs to perform. Therefore, in a second phase, an algorithm was designed to estimate the source-relay channel at the destination. Modelling the cascade of the source-relay channel and the quantization operation as a discrete-valued channel yields an

elegant estimation algorithm, which allows estimating the source-relay channel at the destination, without needing to use numerical maximization techniques. An additional benefit of estimating the source-relay channel at the destination is that the EM-algorithm can be used to refine the source-relay channel estimate. As a result, the system in which the source-relay channel is estimated at the destination outperforms the one in which the source-relay channel is estimated at the relay.

In the two estimation methods previously discussed, the communication channels were modelled as flat Rayleigh fading channels with AWGN, with no carrier frequency mismatch present. In order to extend the results to a more general channel model, we also investigated the channel parameter estimation in the presence of a carrier frequency mismatch. Because each symbol now experiences a different channel rotation, the available estimation algorithms could not be used. Therefore, we have proposed two novel estimation methods to estimate all channel parameters, including the carrier frequency offsets, at the destination terminal. We have shown that one algorithm is the better when sparse source mapping constellations are used (BPSK), while the other algorithm is the better with larger source mapping constellations (QPSK and 8-PSK). As a result, a suitable algorithm is available for all the considered mapping constellations.

In a classic cooperative system, one source communicates to one destination with the aid of one relay. In order to improve the spectral efficiency, two-way relaying systems were introduced, in which two sources communicate with one another, simultaneously assisted by only one relay. In order to make two-way relaying systems suitable for implementation in low complexity relays, we have proposed a novel QF protocol for the two-way relaying channel. The proposed protocol features a low relay-side complexity and can be used in conjunction with half-duplex relay devices. Furthermore, we have developed channel estimation algorithms for the proposed protocol. Using numerical simulations, we have shown that the proposed protocol has an excellent WER performance and that the developed estimation algorithms perform adequately.

Because cooperative communication systems have a vast number of facets, no work on the topic is ever complete. Therefore, we have proposed two interesting paths for future work. First, the foundations were laid for the calculation of the Cramer-Rao bound. A general expression was given which can be used to calculate the Cramer-Rao bound for all the parameters estimated in this work. Secondly, QF systems were proposed for the multiple-access relay channel (MARC). When all the channel parameters are assumed to be known to the destination, it was shown that the proposed QF protocols for the MARC

offer promising WER performance results. Future work on the topic is needed to design estimation algorithms for the various channel parameters involved, and to evaluate the scalability of the proposed systems.

11.1 Publications

The work in this thesis yielded the following A1 journal publications:

• [98] I. Avram, N. Aerts, D. Duyck and M. Moeneclaey *A novel quantize-and-forward cooperative system : Channel Estimation and M-PSK Detection Performance.* EURASIP Journal on Wireless Communications and Networking, vol. 2010, WOS 000282979600001, 11 pages

• [99] I. Avram, N. Aerts, H. Bruneel and M. Moeneclaey *Quantize and Forward Cooperative Communication: Channel Parameter Estimation.* IEEE Trans. on Wireless Commun., Vol. 11, no. 3, pp. 1167-1179, March 2012

• [100] N. Aerts, I. Avram and M. Moeneclaey *Low-complexity a posteriori probability approximation in EM-based channel estimation for trellis-coded systems.* EURASIP Journal on Wireless Communications and Networking, vol. 2014, WOS 000347402300001, 7 pages

• [53] N. Aerts, I. Avram, J. Van Hecke, H. Bruneel and M. Moeneclaey *Iterative SAGE-Based Channel Estimation in a Block Fading Amplify-and-Forward Relaying Network.* IEEE Transactions on Wireless Communications, vol. 13, no. 4, pp. 1742-1753, Apr. 2014

• [101] I. Avram, N. Aerts and M. Moeneclaey *Low-complexity quantize-and-forward cooperative communication using two-way relaying.* EURASIP Journal on Wireless Communications and Networking, vol. 2014, WOS 000345753700001, 16 pages

• [102] N. Aerts, I. Avram and M. Moeneclaey *Exploiting a priori information for iterative channel estimation in block-fading amplify-and-forward cooperative networks.* EURASIP Journal on Wireless Communications and Networking, vol. 2014, WOS 000350809800001, 16 pages

• [91] I. Avram, N. Aerts and M. Moeneclaey *Lower Bounds on the Estimation Performance in Low Complexity Quantize-and-Foward Cooperative Systems.* EURASIP Journal on Wireless Communications and Networking, vol. 2015, DOI: 10.1186/s13638-015-0461-8, 14 pages

Additionally, the following papers were published in the proceedings of the hereafter mentioned international conferences:

• [103] I. Avram, N. Aerts and M. Moeneclaey *A Novel Quantize-and-Forward Cooperative System: Channel Parameter Estimation Techniques.* Future Network & Mobile Summit 2010, Florence, Italy, 16-18 Jun. 2010

• [57] N. Aerts, I. Avram and M. Moeneclaey *The Cramer-Rao Bound for Channel Estimation in Block Fading Amplify-and-Forward Relaying Networks* IEEE 11th International Symposium on Spread Spectrum Techniques and Applications (ISITA), pp. 12-16, 17-20 Oct. 2010, Taichung, Taiwan

• [52] N. Aerts, I. Avram, D. Duck and M. Moeneclaey *EM Based Channel Estimation in an Amplify-and-Forward Relaying Network.* IEEE 21th International Symposium on Personal Indoor and Mobile Radio Communications (PIMRC), pp. 724-729, 26 - 29 Sep. 2010, Istanbul, Turkey

• [54] N. Aerts, I. Avram and M. Moeneclaey *Maximum-Likelihood Channel Estimation in Block Fading Amplify-and-Forward Relaying Networks* IEEE 12th International Symposium on Signal Processing Advances in Wireless Communications (SPAWC), pp. 221-225, 26-29 Jun. 2011, San Francisco, CA

• [104] I. Avram and M. Moeneclaey *Quantize and forward cooperative communication : joint channel and frequency offset estimation.* IEEE International Symposium on Personal, Indoor, and Mobile Radio Communications (PIMRC), pp. 845 - 850, 09-12 Sep. 2012, Sydney, Australia

• [105] I. Avram, M. Moeneclaey *The Modified Cramer-Rao Bound for Channel Estimation in Quantize-and-Forward Cooperative Systems.* WCNC 2013, Shanghai, China, 7-10 Apr. 2013.

Bibliography

[1] H. Van Trees *Detection, Estimation, and Modulation Theory: Part I.* John Wiley and Sons, 2001

[2] S. Kay *Fundamentals of Statistical Signal Processing, Volume 1: Estimation Theory.* Prentice Hall 1993

[3] S. Kay *Fundamentals of Statistical Signal Processing, Volume 2: Detection Theory.* Prentice Hall 1998

[4] A. Papoulis *Probability, Random Variables, and Stochastic Processes.* McGraw-Hill 1984

[5] T.K. Moon *The expectation-maximization algorithm.* IEEE Signal Processing Magazine, vol. 13, no. 6, pp. 47 - 60, Nov. 1996

[6] H.J. Landau *Sampling, data transmission, and the Nyquist rate.* Proceedings of the IEEE, vol. 55, no. 10, pp. 1701 - 1706, Oct. 1967

[7] R.M. Gray and D.L. Neuhoff *Quantization.* IEEE Transactions on Information Theory, vol. 44, no. 6, pp. 2325 - 2383, Oct. 1998

[8] J. Max *Quantizing for minimum distortion.* IRE Transactions on Information Theory, vol. 6, no. 1, pp. 7 - 12, Mar. 1960

[9] Khalid Sayood *Introduction to Data Compression.* Morgan Kaufmann Publishers Inc, Fourth Edition, Dec. 2005

[10] S. Lin and D. Costello *Error Control Coding.* Pearson Education Inc., second edition, 2004

[11] S. Lin, T. Kasami, T. Fujiwara and M. Fossorier *Trellises and Trellis-Based Decoding Algorithms for Linear Block Codes.* Kluwer Academic Publishers Inc., Volume I, 1998

[12] J.K. Wolf *Efficient maximum likelihood decoding of linear block codes using a trellis.* IEEE Transactions on Information Theory, vol. 24, no. 1, pp. 76 - 80, Jan. 1978

[13] L. Bahl, J. Cocke, F. Jelinek, and J. Raviv, *Optimal decoding of linear codes for minimizing symbol error rate.* IEEE Transactions on Information Theory, vol. 20, no. 2, pp. 284 - 287, Mar. 1974

[14] G.D. Forney Jr. *The viterbi algorithm.* Proceedings of the IEEE, vol. 61, no. 3, pp. 268 - 278, Mar. 1973

[15] A. J. Viterbi *Convolutional codes and their performance in communication systems.* IEEE Transactions on Information Theory, vol. 19, no. 5, pp. 751–772, Oct. 1971.

[16] C. Berrou, A. Glavieux and P. Thitimajshima *Near Shannon limit error-correcting coding and decoding: Turbo-codes.* IEEE International Conference on Communications, vol. 2, pp. 1064 - 1070, 23-26 May 1993, Geneva, Switzerland

[17] F.R. Kschischang *Codes defined on graphs.* IEEE Communications Magazine, vol. 41, no. 8, pp. 118 - 125, Aug. 2003

[18] F.R. Kschischang, B.J. Frey and H.-A. Loeliger *Factor Graphs and the Sum-Product Algorithm.* IEEE Transactions on Information Theory, vol. 47, no. 2, pp. 498 - 519, Feb. 2001

[19] H. Wymeersch *Iterative Receiver Design.* Cambridge University Press, 2007

[20] E. N. Gilbert *Gray codes and paths on the N-cube.* Bell System Technical Journal, vol. 37, no. 3, pp. 815 - 826, May 1958

[21] B. Sklar *Rayleigh fading channels in mobile digital communication systems .I. Characterization.* IEEE Communications Magazine, vol. 35 , no. 7, pp. 90 - 100, Jul. 1997

[22] S.H. Lin *Statistical Behavior of a Fading Signal.* The Bell System Technical Journal, vol. 50 , no. 10, pp. 3211 - 3270, Dec. 1971

[23] K.A. Norton, P.L. Rice, H.B. Janes and A.P. Barsis *The Rate of Fading in Propagation through a Turbulent Atmosphere.* Proceedings of the IRE, vol. 43, no. 10, pp. 1341 - 1353, Oct. 1955

[24] P.D. Shaft *On the Relationship Between Scintillation Index and Rician Fading.* IEEE Transactions on Communications, vol. 22, no. 5, pp. 731 - 732, May 1974

[25] G.G. Messier and J.A. Hartwell *An Empirical model for Nonstationary Ricean Fading.* IEEE Transactions on Vehicular Technology, vol. 58 , no. 1, pp. 14 - 20, Jan. 2009

[26] Y. Karasawa and H. Iwai *Formulation of Spatial Correlation Statistics in Nakagami–Rice Fading Environments.* IEEE Transactions on Antennas and Propagation, vol. 48 , no. 1, pp. 12 - 18, Jan. 2000

[27] G.K Karagiannidis, N.C Sagias and P.T. Mathiopoulos *N*Nakagami: A Novel Stochastic Model for Cascaded Fading Channels.* IEEE Transactions on Communications, vol. 55 , no. 8, pp. 1453 - 1458, Aug. 2007

[28] J. Capetanakis *Generalized TDMA: The Multi-Accessing Tree Protocol.* IEEE Transactions on Communications, vol. 27, no. 10, pp. 1476 - 1484, Oct. 1979

[29] H.G. Myung, L. Junsung Lim and D. Goodman *Single carrier FDMA for uplink wireless transmission.* IEEE Vehicular Technology Magazine, vol. 1, no. 3, pp. 30 - 38, Sep. 2006

[30] R.L. Pickholtz, D.L. Schilling and L.B. Milstein *Theory of Spread-Spectrum Communications - A Tutorial.* IEEE Transactions on Communications, vol. 30, no. 5, pp. 855 - 884, May 1982

[31] K.S. Gilhousen, I.M. Jacobs, R. Padovani, A.J. Viterbi, L.A. Weaver and C.E. Wheatley *On the capacity of a cellular CDMA system.* IEEE Transactions on Vehicular Technology, vol. 40, no. 2, pp. 303 - 312, May 1991

[32] N. Noels, C. Herzet, A. Dejonghe, V. Lottici, H. Steendam, M. Moeneclaey, M Luise and L. Vandendorpe *Turbo-synchronization: an EM algorithm approach.* IEEE International Conference on Communications, pp. 191 - 195, May 2003, Anchorage, Turkey

[33] C.E. Shannon *Communication in the Presence of Noise.* Proceedings of the IRE, vol. 37, no. 1, pp. 10 - 21 , Jan. 1949

[34] J. Proakis, M. Salehi *Digital Communications.* McGraw-Hill, 5th edition, 2007

[35] W.C.Y. Lee *Estimate of channel capacity in Rayleigh fading environment.* IEEE Transactions on Vehicular Technology, vol. 39, no. 3, pp. 187 - 189, Aug. 1990

[36] E. Biglieri, J. Proakis and S. Shamai *Fading channels: information-theoretic and communications aspects.* IEEE Transactions on Information Theory, vol.44, no. 6, pp. 2619 - 2692, Oct. 1998

[37] W. Zhengdao and G.B. Giannakis *A simple and general parameterization quantifying performance in fading channels.* IEEE Transactions on Communications, vol. 51, no. 8, pp. 1389 - 1398, Aug. 2003 Cited by: Papers (411) | Patents (6)

[38] J.H. Winters *On the Capacity of Radio Communication Systems with Diversity in a Rayleigh Fading Environment.* IEEE Journal on Selected Areas in Communications, vol. 5, no. 5, pp. 871 - 878, Jun. 1987

[39] J.H. Winters, J. Salz and R.D. Gitlin *The impact of antenna diversity on the capacity of wireless communication systems.* IEEE Transactions on Communications, vol. 42, no. 234, pp. 1740 - 1751, Feb./Mar./Apr. 1994

[40] G. J. Foschini and M. J. Gans *On limits of wireless communications in a fading environment when using multiple antennas.* Wireless Personal Communications, vol. 6, no. 3, pp. 311-335, Mar. 1998

[41] G. Foschini *Layered space time architecture for wireless communication in a fading environment when using multi-element antennas.* Bell Labs. Tech., vol. 1, no. 2, pp. 41-59, 1996

[42] L.J. Cimini *Analysis and Simulation of a Digital Mobile Channel Using Orthogonal Frequency Division Multiplexing.* IEEE Transactions on Communications, vol. 33, no. 7, pp. 665 - 675, Jul. 1985

[43] J.N. Laneman, D.N.C. Tse and W.G. Wornell *Cooperative diversity in wireless networks: Efficient protocols and outage behavior.* IEEE Transactions on Information Theory, vol. 50, no. 12, pp. 3062 - 3080, Dec. 2004

[44] T. Cover and A.E. Gamal *Capacity theorems for the relay channel.* IEEE Transactions on Information Theory, vol. 25, no. 5, pp. 572 - 584, Sep. 1979

[45] A. Sendonaris, E. Erkip and B. Aazhang *User cooperation diversity. Part I. System description.* IEEE Transactions on Communications, vol. 51, no. 11, pp. 1927 - 1938, Nov. 2003

[46] A. Sendonaris, E. Erkip and B. Aazhang *User cooperation diversity. Part II. Implementation aspects and performance analysis.* IEEE Transactions on Communications, vol. 51, no. 11, pp. 1939 - 1948, Nov. 2003

[47] R.U. Nabar, H. Bolcskei and F.w. Kneubuhler *Fading relay channels: performance limits and space-time signal design.* IEEE Journal on Selected Areas in Communications, vol. 22, no. 6, pp. 1099 - 1109, Aug. 2004

[48] O. Amin, B. Gedik and M. Uysal *Channel estimation for amplify-and-forward relaying: Cascaded against disintegrated estimators.* IET Communications, vol. 4, no. 10, pp. 1207 - 1216, Jul. 2010

[49] G. Feifei, C. Tao and A. Nallanathan *On channel estimation and optimal training design for amplify and forward relay networks.* IEEE Transactions on Wireless Communications, vol. 7, no. 5, pp. 1907 - 1916 , May 2008

[50] C. S. Patel and G. L. Stüber *Channel Estimation for Amplify and Forward Relay Based Cooperation Diversity Systems.* IEEE Trans. on Wireless Commun., vol. 6, no. 6, pp. 2348-2356, Jun. 2007

[51] N. Aerts, I. Avram and M. Moeneclaey *Pilot-based ML estimation in Amplify-and-Forward cooperative networks.* IEEE Wireless Communications and Networking Conference (WCNC), pp. 1044-1048, 1-4 Apr. 2012, Paris, France

[52] N. Aerts, I. Avram, D. Duck and M. Moeneclaey *EM Based Channel Estimation in an Amplify-and-Forward Relaying Network.* IEEE 21th International Symposium on Personal Indoor and Mobile Radio Communications (PIMRC), pp. 724-729, 26 - 29 Sep. 2010, Istanbul, Turkey

[53] N. Aerts, I. Avram, J. Van Hecke, H. Bruneel and M. Moeneclaey *Iterative SAGE-Based Channel Estimation in a Block Fading Amplify-and-Forward Relaying Network.* IEEE Transactions on Wireless Communications, vol. 13, no. 4, pp. 1742-1753, Apr. 2014

[54] N. Aerts, I. Avram and M. Moeneclaey *Maximum-Likelihood Channel Estimation in Block Fading Amplify-and-Forward Relaying Networks* IEEE 12th International Symposium on Signal Processing Advances in Wireless Communications (SPAWC), pp. 221-225, 26-29 Jun. 2011, San Francisco, CA

[55] B. Gedik and M. Uysal *Impact of Imperfect Channel Estimation on the Performance of Amplify-and-Forward Relaying.* IEEE Trans. on Wireless Commun., vol. 8, no. 3, p. 1468-1479, Mar. 2009

[56] S. Bharadwaj and N.B. Mehta *Performance Analysis of Fixed Gain Amplify-and-Forward Relaying with Time-Efficient Cascaded Channel Estimation.* IEEE Global Telecommunications Conference (GLOBECOM 2011), pp. 1 - 5, 5-9 Dec. 2011, Houston, TX

[57] N. Aerts, I. Avram and M. Moeneclaey *The Cramer-Rao Bound for Channel Estimation in Block Fading Amplify-and-Forward Relaying Networks* IEEE

11th International Symposium on Spread Spectrum Techniques and Applications (ISITA), pp. 12-16, 17-20 Oct. 2010, Taichung, Taiwan

[58] J. Luo, R.S. Blum, L.J. Cimini, L.J. Greenstein and A.M. Haimovich *Decode-and-Forward Cooperative Diversity with Power Allocation in Wireless Networks.* IEEE Transactions on Wireless Communications, vol. 6, no. 3, pp. 793 - 799, Mar. 2007

[59] S.S. Ikki and M.H. Ahmed *Performance analysis of adaptive decode-and-forward cooperative diversity networks with best-relay selection.* IEEE Transactions on Communications, vol. 58, no. 1, pp. 68 - 72, Jan. 2010

[60] Y. Zhihang and I.M. Kim *Diversity order analysis of the decode-and-forward cooperative networks with relay selection.* IEEE Transactions on Wireless Communications, vol. 7, no. 5, pp. 1792 - 1799, May 2008

[61] N.C. Beaulieu and J. Hu *A closed-form expression for the outage probability of decode-and-forward relaying in dissimilar Rayleigh fading channels.* IEEE Communications Letters, vol. 10, no. 12, pp. 813 - 815, Dec. 2006

[62] L. In-Ho and K. Dongwoo *BER analysis for decode-and-forward relaying in dissimilar Rayleigh fading channels.* IEEE Communications Letters, vol. 11, no. 1, pp. 52 - 54, Jan. 2007

[63] M.R. Souryal and B.R. Vojcic *Performance of Amplify-and-Forward and Decode-and-Forward Relaying in Rayleigh Fading with Turbo Codes.* IEEE International Conference on Acoustics, Speech and Signal Processing (ICASSP), May 15-19 2006, Toulouse, France

[64] T.Q. Duong and H.J. Zepernick *On the Performance Gain of Hybrid Decode-Amplify-Forward Cooperative Communications.* EURASIP Journal on Wireless Communications and Networks, vol. 2009, Article ID 479463, 10 pages, 2009

[65] S. Bouanen, H. Boujemaa and W. Ajib *Threshold-based Adaptive Decode-Amplify-Forward relaying protocol for cooperative systems.* Wireless Communications and Mobile Computing Conference (IWCMC), pp. 725- 730, 4-8 Jul. 2011, Istanbul, Turkey

[66] G. Feifei, C. Tao and A. Nallanathan *Optimal Training Design for Channel Estimation in Decode-and-Forward Relay Networks With Individual and Total Power Constraints.* IEEE Transactions on Signal Processing, vol. 56, no. 12, pp. 5937 - 5949, Dec. 2008

[67] D. Qingxiong Deng, R.G. Machado and A.G. Klein *Adaptive channel estimation in decode and forward relay networks.* 46th Annual Conference on Information Sciences and Systems (CISS), pp. 1 - 6, 21 - 23 Mar. 2012, Princeton, NJ, USA

[68] H. Junhong and C. Xujun Chen *Performance of decode-and-forward cooperative communications with channel estimation errors over Rayleigh fading channels.* 2nd International Conference on Future Computer and Communication (ICFCC), pp. V1:164 - V1:167, 21-24 May 2010, Wuhan, China

[69] H. Ruiyuan and L. Li *Exploiting Slepian-Wolf codes in wireless user cooperation.* IEEE 6th Workshop on Signal Processing Advances in Wireless Communications, pp. 275 - 279, 5-8 Jun. 2005, New York, NY, USA

[70] D. Slepian and J.K. Wolf *Noiseless coding of correlated information sources.* IEEE Transactions on Information Theory, vol. 19, no. 4, pp. 471 - 480, Jul. 1973

[71] H. Ruiyuan and J. Li *Practical Compress-Forward in User Cooperation: Wyner-Ziv Cooperation.* IEEE International Symposium on Information Theory, pp. 489 - 493, 6-12 Jul. 2006, Seattle, WA, USA

[72] A. Wyner and J. Ziv *The rate-distortion function for source coding with side information at the decoder.* IEEE Trans. on Information Theory, vol. 22, no. 1, pp. 1-10, Jan. 1976.

[73] W. Xiugang and X. Liang-Liang *On the Optimal Compressions in the Compress-and-Forward Relay Schemes.* IEEE Transactions on Information Theory, vol. 59, no. 5, pp. 2613 - 2628, May 2013

[74] G. Kramer, M. Gastpar and P. Gupta *Cooperative Strategies and Capacity Theorems for Relay Networks.* IEEE Transactions on Information Theory, vol. 51, no. 9, pp. 3037 - 3063, Sep. 2005

[75] Y. W. Hong, W. J. Huang, F. H. Chiu, and C. C. J. Kuo *Cooperative Communications in Resource-Constrained Wireless Networks.* IEEE Signal Processing Magazine, vol. 24, no. 3, pp. 47 - 57, May 2007

[76] D.T. Tran, S. Sumei and E. Kurniawan *A Low-Complexity Practical Quantize-and-Forward Scheme for Two-Hop Relay Systems.* IEEE 75th Vehicular Technology Conference (VTC Spring), pp. 1-5, 6-9 May 2012, Yokohama, Japan

[77] D.A. Huffman *A Method for the Construction of Minimum-Redundancy Codes.* Proceedings of the IRE, vol. 40, no. 9, pp. 1098 - 1101, Sep. 1952

[78] M. Souryal and H. You *Quantize-and-Forward Relaying with M-ary Phase Shift Keying.* IEEE Wireless Communications and Networking Conference 2008, pp. 42-47, 31 Mar. - 3 Apr. 2008, Las Vegas, NV

[79] M. Luise and R. Reggiannini *Carrier frequency recovery in all-digital modems for burst-mode transmissions.* IEEE Trans. Commun., vol. 43, pp. 1169-1178, Feb./Mar./Apr. 1995

[80] M. P. Fitz *Further results in the Fast Estimation of a Single Frequency.* IEEE Trans. Commun., vol. 42, pp. 862-864, Feb./Mar./Apr. 1994

[81] O. Bessonand and P. Stoica *On parameter estimation of MIMO flat-fading channels with frequency offsets.* IEEE Trans. on Signal Proc., vol. 51, no. 3, pp. 602-616, Mar. 2003

[82] F. Simoens and M. Moeneclaey *Reduced Complexity Data-Aided and Code-Aided Frequency Offset Estimation for Flat-Fading MIMO Channels.* IEEE Trans. on Wireless Commun., vol. 5, no. 6, pp. 1558-1567, Jun. 2006

[83] C. Shen, G. Deng, J. Zhang and M. Liu *Channel Estimation for Amplify-and-Forward Relay Networks with Both Time and Frequency Offsets.* Conference on Vehicular Technology (VTC Fall), 2-5 Sept. 2013, Las Vegas, NV

[84] P. Larsson, N. Johansson, and K. Sunell *Coded bi-directional relaying.* IEEE Vehicular Technology Conference, (VTC 2oo6-Spring), vol. 2, pp. 851-855, May 2006, Melbourne, Australia

[85] P. Popovski and H. Yomo *Physical network coding in two-way wireless relay channels* IEEE International Conference on Communications, pp. 707-712, June 2007, Glasgow, Ireland

[86] B. Rankov and A. Wittneben *Spectral efficient protocols for half-duplex fading relay channels.* IEEE J.Sel.Areas Commun. vol. 25, pp. 379-389, Feb. 2007.

[87] S. Bagheri, F. Verde, D. Darsena, and A. Scaglione *Randomized decode-and-forward strategies for two-way relay networks.* IEEE Trans. Wireless Commun., vol. 10, no. 12, pp. 4214-4225, Dec. 2011.

[88] P. Zhong and M. Vu *Compress-Forward without Wyner-Ziv Binning for the One-Way and Two-Way Relay Channels* Proc. Allerton Conference on Communication, Control, Computing and Urbana-Champaign, IL, USA, Sep. 2011, pp. 426-433.

[89] R.M. Legnain, R.H.M. Hafez, I.D. Marand and A.M. Legnain *Two-way quantize-and-forward relaying with STBC.* Proc. IEEE Canadian Conference on Electrical & Computer Engineering (CCECE), pp. 1-5, Apr.-May 2012, Montreal, Canada

[90] M. Heindlmaier, O. Iscan and C. Rosanka *Scalar Quantize-and-Forward for symmetric half-duplex Two-Way Relay Channels.* Proc. IEEE International Symposium on Information Theory (ISIT), pp. 1322 - 1326, Jul. 2013, Istanbul, Turkey

[91] I. Avram, N. Aerts and M. Moeneclaey *Lower Bounds on the Estimation Performance in Low Complexity Quantize-and-Foward Cooperative Systems.* EURASIP Journal on Wireless Communications and Networking, vol. 2015, DOI: 10.1186/s13638-015-0461-8, 14 pages

[92] C. R. Rao *Information and the Accuracy Attainable in the Estimation of Statistical Parameters.* Bulletin of Cal. Math. Soc., vol. 37, no. 3, pp. 81-91, 1945

[93] M. Moeneclaey *On the true and the modified Cramer-Rao bounds for the estimation of a scalar parameter in the presence of nuisance parameters* IEEE Transactions on Communications, vol. 46, no. 11, pp. 1536 - 1544, Nov. 1998

[94] A. D. Andrea, U. Mengali, and R. Reggiannini *The modified Cramer-Rao bound and its application to synchronization problems.* IEEE Trans. Commun., vol. 42, pp. 1391-1399, Feb.-Apr. 1994.

[95] F. Gini, R. Reggiannini and U. Mengali *The modified Cramer-Rao bound in vector parameter estimation.* IEEE Transactions on Communications, vol. 46, no. 1, pp. 52 - 60, Jan. 1998 Cited by: Papers (74)

[96] R. Y. Rubinstein and D. P. Kroese *Simulation and the Monte Carlo Method.* Wiley Series in Probability and Statistics, Second Edition, 2007

[97] J. M. Hammersley and D. C. Handscomb *Monte Carlo Methods.* Methuen & Co., London, and John Wiley & Sons, New York, 1964

[98] I. Avram, N. Aerts, D. Duyck and M. Moeneclaey *A novel quantize-and-forward cooperative system : Channel Estimation and M-PSK Detection Performance.* EURASIP Journal on Wireless Communications and Networking, vol. 2010, WOS 000282979600001, 11 pages

[99] I. Avram, N. Aerts, H. Bruneel and M. Moeneclaey *Quantize and Forward Cooperative Communication: Channel Parameter Estimation.* IEEE Trans. on Wireless Commun., Vol. 11, no. 3, pp. 1167-1179, March 2012

[100] N. Aerts, I. Avram and M. Moeneclaey *Low-complexity a posteriori probability approximation in EM-based channel estimation for trellis-coded systems.* EURASIP Journal on Wireless Communications and Networking, vol. 2014, WOS 000347402300001, 7 pages

[101] I. Avram, N. Aerts and M. Moeneclaey *Low-complexity quantize-and-forward cooperative communication using two-way relaying.* EURASIP Journal on Wireless Communications and Networking, vol. 2014, WOS 000345753700001, 16 pages

[102] N. Aerts, I. Avram and M. Moeneclaey *Exploiting a priori information for iterative channel estimation in block-fading amplify-and-forward cooperative networks.* EURASIP Journal on Wireless Communications and Networking, vol. 2014, WOS 000345753700001, 16 pages

[103] I. Avram, N. Aerts and M. Moeneclaey *A Novel Quantize-and-Forward Cooperative System: Channel Parameter Estimation Techniques.* Future Network & Mobile Summit 2010, Florence, Italy, 16-18 Jun. 2010

[104] I. Avram and M. Moeneclaey *Quantize and forward cooperative communication : joint channel and frequency offset estimation.* IEEE International Symposium on Personal, Indoor, and Mobile Radio Communications (PIMRC), pp. 845 - 850, 09-12 Sep. 2012, Sydney, Australia

[105] I. Avram, M. Moeneclaey *The Modified Cramer-Rao Bound for Channel Estimation in Quantize-and-Forward Cooperative Systems.* WCNC 2013, Shanghai, China, 7-10 Apr. 2013.